LEADING EDGE STALL

A thesis submitted to the University of Manchester
for the degree of Doctor of Philosophy
in the Faculty of Engineering and Physical Sciences

2011

Kwan Yee Chan

School of Mathematics

Contents

Word count: 69399

List of Tables

List of Figures

The University of Manchester

Kwan Yee Chan
Doctor of Philosophy
Leading Edge Stall
September 8, 2011

An airfoil is placed in a high Reynolds number but subsonic fluid flow and is subject to very slow perturbations of its angle of attack compared to the time scale of the flow. Asymptotic solutions for the Navier-Stokes equations are obtained for the boundary layer and interaction region flow structure on the airfoil. The viscous-inviscid interaction between the boundary layer and external inviscid flow is on a time scale sufficiently large such that the induced pressure gradient from the displacement of the boundary layer from the surface is negligible. Numerical solutions are found for the solvability condition from the method of matched asymptotic expansions, which ensures flow structure consistency. A short bubble of reversed recirculating flow forms on the surface of the airfoil. As time progresses, the angle of attack approaches a critical angle for a skin friction singularity and nonlinear breakdown. Discontinuous skin friction solutions are obtained for a second interactive stage equation. An eruption process from the bubble thickens the boundary layer and terminates the second interactive stage, resulting in a vortex, or eddy, spanning the boundary layer. The ejection of the vortex from the surface is the process of leading edge stall.

Declaration

No portion of the work referred to in this thesis has been submitted in support of an application for another degree or qualification of this or any other university or other institute of learning.

Copyright Statement

i. The author of this thesis (including any appendices and/or schedules to this thesis) owns certain copyright or related rights in it (the "Copyright") and s/he has given The University of Manchester certain rights to use such Copyright, including for administrative purposes.

ii. Copies of this thesis, either in full or in extracts and whether in hard or electronic copy, may be made only in accordance with the Copyright, Designs and Patents Act 1988 (as amended) and regulations issued under it or, where appropriate, in accordance with licensing agreements which the University has from time to time. This page must form part of any such copies made.

iii. The ownership of certain Copyright, patents, designs, trade marks and other intellectual property (the "Intellectual Property") and any reproductions of copyright works in the thesis, for example graphs and tables ("Reproductions"), which may be described in this thesis, may not be owned by the author and may be owned by third parties. Such Intellectual Property and Reproductions cannot and must not be made available for use without the prior written permission of the owner(s) of the relevant Intellectual Property and/or Reproductions.

iv. Further information on the conditions under which disclosure, publication and commercialisation of this thesis, the Copyright and any Intellectual Property and/or Reproductions described in it may take place is available in the University IP Policy (see `http://www.campus.manchester.ac.uk/medialibrary/policies/intellectual-property.pdf`), in any relevant Thesis restriction

declarations deposited in the University Library, The University Librarys regulations (see `http://www.manchester.ac.uk/library/aboutus/regulations`) and in The Universitys policy on presentation of Theses.

Acknowledgements

Thank you:

Prof. Jitesh S. B. Gajjar

Prof. Anatoly I. Ruban

The University of Manchester

Engineering and Physical Sciences Research Council

Dr Dmitry Yumashev

My mother & my father

P. A. V.

Chapter 1

Introduction

Flow separation from the surface of a solid body and the flow that develops as a result of this separation is an intriguing and complex phenomenon of fluid dynamics. Its occurrence is known to be potentially dangerous. Detached fluid flow from the surface of an airfoil limits its lift force and can lead to stalling during flight.[1] Hence, understanding the theoretical basis and properties of flow separation, and predicting whether it will occur or not, is desirable.

1.1 A Brief Introduction to the Thesis

High speed and low viscosity fluid flow separation from a surface of a solid body, like all phenomenon of fluid dynamics, is governed by the Navier-Stokes equations. A historical account follows of the introduction of the boundary layer and the methods used to find solutions to the equations.

The introduction of the Prandtl (1904) boundary layer and the Prandtl (1935) hierarchical principal of constructing asymptotic expansion solutions leads to the Goldstein (1948) singularity; self-induced separation, in which there is an induced pressure gradient by the displacement effect of the boundary layer; the triple-deck

[1] See Jones (1933), Jones (1934) and Tani (1964).

interaction region structure about a point of zero skin friction on the surface; viscous-inviscid interaction between the boundary layer and the external part of the flow; and bubbles of reversed recirculating flow.

In application to flight, the solid body is a thin airfoil. The angle of attack of the airfoil, its range of values and its rate of change are important factors because they affect the pitch, roll and yaw of an aircraft. The range of angle of attack is assumed small. If the angle of attack of the airfoil is such that the fluid is attached to its surface then the angle can be incrementally increased so that the steady attached flow is forced to gradually detach from the surface. The resulting flow separation is called marginal separation. A solvability condition resulting from the method of matched asymptotic expansions between the regions of the triple-deck must be satisfied for the flow structure to be consistent.

Marginal separation can be extended to quasi-steady and unsteady flows where the angle of attack is increasing with time such that steady flow is now over a downstream-moving surface. (See Figure 1.1.) The solvability condition is an unsteady, nonlinear, partial integro-differential equation which relates skin (surface) friction on the airfoil to the angle of attack. It requires numerical solution and several types of flow configuration are described depending on the far away boundary conditions and the initial distribution. After a finite time, a critical limit of angle of attack is reached where a nonlinear breakdown singularity occurs, leading to Smith (1982a) dynamic stall on the leading edge of the airfoil.

The thesis aims to bridge the work on marginal separation with that on steady flow over a downstream-moving surface, unsteady marginal separation and dynamic stall. In particular, the focus is on the quasi-steady flow structure which develops over a very large time scale when there are very slow perturbations to the otherwise steady stream functions. The slow perturbations are from a slow change in angle of attack over a small range as it gradually approaches the critical angle where stream function solutions become complex and nonlinear breakdown occurs. The time scale is sufficiently large such that the induced pressure gradient by the displaced boundary

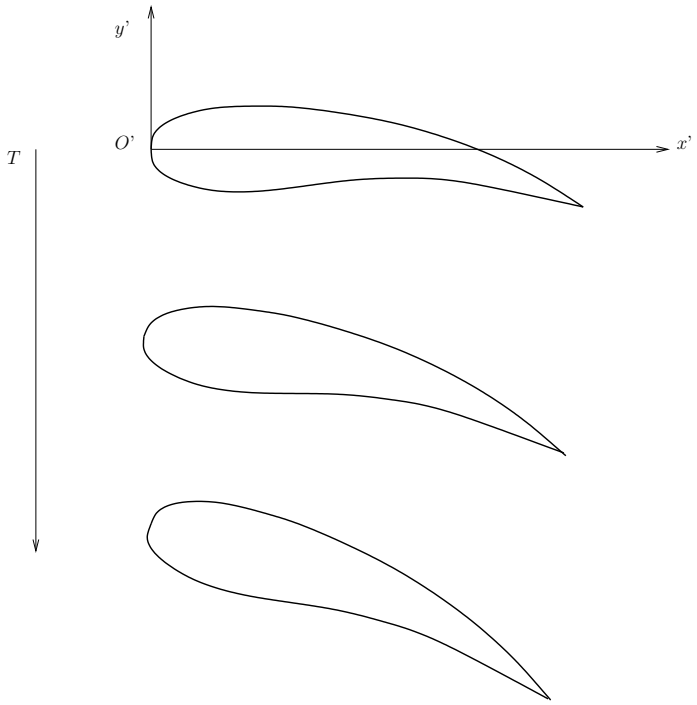

Figure 1.1: The airfoil with a very slow change of angle of attack causing a downstream movement of the surface on a very large time scale. The range of angle of attack is small but exaggerated here.

layer is of relatively small order of magnitude compared to the unsteady or viscous forces acting on the boundary layer. The quasi-steady nature of the problem complicates the definition of what is separated flow. The criterion for a point of separation differ for steady and unsteady scenarios and will be defined further in this introduction. Most of the thesis will focus about a point of zero skin friction because it is unambiguous, instead of a point of separation.

The analytical process begins in Chapter 2 which firstly outlines the work carried out by van Dyke (1956) in describing subsonic air flow in the external region (outside of the boundary layer) about a thin steady airfoil with its parabolic nose to a uniform stream. The van Dyke analysis enables the introduction of an airfoil asymmetry parameter for the asymptotic series expansion of the stream function solutions. The stream function solutions for the Navier-Stokes equations are the concatenation of the steady flow solutions and their time-dependent perturbations which incorporate the slow change in angle of attack. The unsteady, nonlinear Navier-Stokes equations are non-dimensionalised to introduce the non-dimensional Reynolds number. The

Reynolds number is the ratio of the orders of magnitude of inertial and viscous forces. The flow in the boundary layer is then characterised by a limit process of when the Reynolds number tends to infinity.

Substituting the asymptotic expansion of the stream function into the Navier-Stokes equations, the triple-deck regions about the point of zero skin friction can be constructed by the hierarchical process. Boundary value problems are derived for each term of the stream function for say, the viscous sublayer of the boundary layer. The solutions lead to a stream function series expansion for the main boundary layer by the method of matched asymptotic expansions.

The analysis fails when either attempts to match the boundary layer solutions upstream of the point of zero skin friction with those downstream come to a contradiction as in Goldstein's singularity, or when the perturbations in the asymptotic expansions becomes the same order of magnitude as the steady flow and hence are no longer negligible. There is another region about the point of zero skin friction with a new limit process. The interaction region is introduced in Chapter 3 and the same hierarchical process in Chapter 2 is used to determine stream function solutions there. The stream function solutions and triple-deck structure are consistent by the method of matched asymptotic expansions if a solvability condition is satisfied.

Chapter 4 is on the construction of the initial-boundary value problem for the solvability condition and its numerical solution, based on the methods set out by Smith & Elliott (1985). Several types of initial flow configuration, from the Smith & Elliott attached flow steady state solution to a bubble of reversed flow, lead to unbounded growth in skin friction after some finite time. With the numerical solutions, stream function and velocity contours can be found. Analytical solutions are difficult if not impossible to find.

Chapter 5 follows from the evidence of a skin friction singularity and is the analysis as the nonlinear breakdown is approached. The unbounded skin friction can be modelled as a discontinuous wave in the fluid. The discontinuous wave is theorised to travel along the surface in a second interactive region. Depending on the travelling

speed of the wave, the triple-deck structure either remains intact and moves with the point of zero skin friction, or is destroyed. A boundary value problem is solved to describe the flow there.

Descriptions of the numerical algorithms for the solvability condition problem, the algorithms for the second interactive stage problem, and their tests are given in Sections 4.3, 4.4 and 5.3. The tests are for satisfaction of boundary conditions; convergence; domain and grid size independence.

Chapter 6 describes the end of the second interactive stage based on the Elliott & Smith (1987) dynamic stall. As the angle of attack increases, the flow continues to develop with time. After a finite time, the second interactive stage transforms into a third interactive stage where a vortex spans the boundary layer and is eventually ejected. The third interactive stage is beyond the scope of the thesis since it is characteristic of fully unsteady flow.

Summaries and conclusions from the boundary layer analysis (Chapter 2) to the leading edge stall (Chapter 6) are given in Chapter 7.

1.2 The Navier-Stokes Equations

The Navier-Stokes equations are derived in Appendix A. The Navier-Stokes equations for incompressible, Newtonian fluids, in the two-dimensional Cartesian coordinate system (x, y) with time t, are:

$$\frac{\partial u}{\partial t} + u\frac{\partial u}{\partial x} + v\frac{\partial u}{\partial y} = f_x - \frac{1}{\rho}\frac{\partial p}{\partial x} + \nu\left(\frac{\partial^2 u}{\partial x^2} + \frac{\partial^2 u}{\partial y^2}\right),$$

$$\frac{\partial v}{\partial t} + u\frac{\partial v}{\partial x} + v\frac{\partial v}{\partial y} = f_y - \frac{1}{\rho}\frac{\partial p}{\partial y} + \nu\left(\frac{\partial^2 v}{\partial x^2} + \frac{\partial^2 v}{\partial y^2}\right),$$

$$\frac{\partial u}{\partial x} + \frac{\partial v}{\partial y} = 0\,.$$

The variables are the tangential and normal velocity components u and v; body forces f_x, f_y; pressure p; density ρ; constant kinetic viscosity $\nu = \frac{\mu}{\rho}$; and constant

dynamic viscosity μ. Each of the terms of the equations represent the forces of the fluid dynamics system. Using the first, x-momentum equation as an example, the unsteady forces are represented by the term $\frac{\partial u}{\partial t}$; the inertial forces by $u\frac{\partial u}{\partial x}+v\frac{\partial u}{\partial y}$; body forces by f_x; pressure forces by $\frac{1}{\rho}\frac{\partial p}{\partial x}$; and viscous forces by $\nu\left(\frac{\partial^2 u}{\partial x^2}+\frac{\partial^2 u}{\partial y^2}\right)$.

For simplicity, the body forces f_x and f_y in the airfoil problem, such as gravity, are neglected. The governing equations of the airfoil problem are:

$$\frac{\partial u}{\partial t}+u\frac{\partial u}{\partial x}+v\frac{\partial u}{\partial y}=\nu\left(\frac{\partial^2 u}{\partial x^2}+\frac{\partial^2 u}{\partial y^2}\right)-\frac{1}{\rho}\frac{\partial p}{\partial x}\,,$$

$$\frac{\partial v}{\partial t}+u\frac{\partial v}{\partial x}+v\frac{\partial v}{\partial y}=\nu\left(\frac{\partial^2 v}{\partial x^2}+\frac{\partial^2 v}{\partial y^2}\right)-\frac{1}{\rho}\frac{\partial p}{\partial y}\,,$$

$$\frac{\partial u}{\partial x}+\frac{\partial v}{\partial y}=0\,.$$

The equations may be non-dimensionalised using the variables: $x=L\tilde{x}$, $y=L\tilde{y}$, $t=\frac{L}{U_\infty}\tilde{t}$, $u=U_\infty\tilde{u}$, $v=U_\infty\tilde{v}$, $p=\rho U_\infty^2\tilde{p}$, where L is the length of the airfoil chord and U_∞ is the unperturbed flow speed far away from the airfoil at infinity. The non-dimensionalised equations (after removing the tilde notation) are:

$$\frac{\partial u}{\partial t}+u\frac{\partial u}{\partial x}+v\frac{\partial u}{\partial y}=\frac{1}{\mathrm{Re}}\left(\frac{\partial^2 u}{\partial x^2}+\frac{\partial^2 u}{\partial y^2}\right)-\frac{\partial p}{\partial x}\,, \tag{1.1}$$

$$\frac{\partial v}{\partial t}+u\frac{\partial v}{\partial x}+v\frac{\partial v}{\partial y}=\frac{1}{\mathrm{Re}}\left(\frac{\partial^2 v}{\partial x^2}+\frac{\partial^2 v}{\partial y^2}\right)-\frac{\partial p}{\partial y}\,, \tag{1.2}$$

$$\frac{\partial u}{\partial x}+\frac{\partial v}{\partial y}=0\,. \tag{1.3}$$

The Reynolds number

$$\mathrm{Re}=\frac{U_\infty L}{\nu}\,,$$

is the remaining parameter. Flow at high Reynolds number concerns most natural gas and liquid flows where there is relatively small kinetic viscosity ν compared to unperturbed speed U_∞ or length scale L. Mathematically, it is a ratio of the orders of magnitude of inertial and viscous forces. Where fluid flow is of high speed and low

viscosity, the limit as $\mathrm{Re} \to \infty$ is taken.

By the mass continuity equation (1.3), the velocity components u, v are written in terms of the stream function ψ where

$$u = \frac{\partial \psi}{\partial y}\,, \qquad v = -\frac{\partial \psi}{\partial x}\,. \tag{1.4}$$

The Navier-Stokes equations (1.1), (1.2) and (1.3) and the required two boundary conditions and one initial condition is the basic set of equations of which the solution describes fluid flow. There are some exact analytical solutions[2] but where there is none, the problem can be solved using the hierarchical boundary layer theory introduced in the twentieth century, and the principle of matched asymptotic expansion solutions.

1.3 Laminar Self-Induced Separation

A history of fluid dynamics in relation to flight has been written by Anderson (1997) and Anderson (2008) and an introduction to the asymptotic solution of the Navier-Stokes equations is presented by Sychev, Ruban, Sychev & Korolev (1998a).

In the early twentieth century, Prandtl (1904) proposed the concept of the *laminar boundary layer* (as opposed to *turbulent* flow) to describe separation of high Reynolds number fluid flow from the surface of solid body. Prandtl theorised that the effects of surface skin friction are experienced only in a thin viscous boundary layer near the surface and that the fluid particles adjacent to the surface adhered to it.[3] Outside the boundary layer, the external flow is essentially inviscid. If the type of external flow promotes an *adverse* positive pressure gradient in the direction of flow then the result is flow separation. The fluid particles with their kinetic energy dissipated in a region where the pressure is increasing are lifted off the surface at a point of separation

[2] See for example, Poiseuille flow through a circular pipe, as discussed in Batchelor (2000a).

[3] Details on the development of the boundary layer with an aerodynamic background and with regards to vorticity is given by Lighthill (1963).

$x = x_s$ where skin friction has been driven to zero. The point of zero skin friction coincides with the point of separation for steady cases. This is the Prandtl criterion for flow separation.

Taking the limit as $\mathrm{Re} \to \infty$ results in a very small viscosity coefficient of the highest order derivative of the Navier-Stokes equations (1.1), (1.2) such that the Euler system of equations:

$$\frac{\partial u}{\partial t} + u\frac{\partial u}{\partial x} + v\frac{\partial u}{\partial y} = -\frac{\partial p}{\partial x}\,,$$

$$\frac{\partial v}{\partial t} + u\frac{\partial v}{\partial x} + v\frac{\partial v}{\partial y} = -\frac{\partial p}{\partial y}$$

are obtained (for negligible body forces f_x and f_y). Hence, the two boundary conditions required for the equations cannot both be satisfied and so, the problem becomes singular. The Euler equations do not account for frictional, viscous effects and so apply to the external flow. Prandtl's boundary layer allows for viscous forces and so the Navier-Stokes equations apply there. Nevertheless, Prandtl's theory does not account for flow beyond the point of separation because of the adverse pressure gradient ahead of it.

A solution to the Navier-Stokes equations was proposed by Goldstein (1930) for steady, incompressible fluid flow in the boundary layer upstream of the point of separation $x = x_s$, where $x < x_s$ is considered the upstream region before separation takes place and $x > x_s$ is considered the downstream region. The solutions for velocity and pressure are asymptotic series expansions and are formulated assuming there is a constant adverse pressure gradient in a finite neighbourhood of the point of separation. Prandtl (1935) goes on to show the hierarchical principal of constructing asymptotic expansions according to the external flow and the boundary layer regions, and the iterative procedure of building the regions alternately whilst refining the solutions term by term.[4]

Goldstein (1948), knowing the work by Landau & Lifshitz (1944), carried out a rigorous analysis of the boundary layer close to the point of separation (which for

[4]See van Dyke (1975) for example.

convenience is chosen as the origin of coordinates $x_s = 0$) and immediately ahead of it using the method of matched asymptotic expansions. There is unbounded growth of the transverse velocity component v inversely proportional to $|\Delta x|^{\frac{1}{2}} = |x - x_s|^{\frac{1}{2}}$ whilst the pressure gradient ratio $\frac{\Delta p}{\Delta x}$ is inversely proportional to $(\Delta x)^{\frac{1}{3}}$. Numerical analysis by Howarth (1938) and Hartree (1939) indicated singular behaviour of the solution at the point of separation. Goldstein found that the boundary layer immediately upstream of the point of separation is in fact divided into a main boundary layer (region 2 in Figure 1.2) and a viscous sublayer (region 3) adjacent to the surface. The viscous sublayer ensures the fluid velocity is dissipated to zero on the surface whilst decreasing in thickness according to the rule $Y \to (-x)^{\frac{1}{4}}$ as $x \to -0$. However, the viscous sublayer stream function solution grows exponentially as its normal coordinate $Y \to \infty$. The viscous sublayer solution cannot match the external region solution, hence there is a main boundary layer in between.

Goldstein showed that the solutions cannot be constructed past the point of separation. There is a contradiction in the terms of the asymptotic expansions as $x \to +0$ which results in the downstream solution for the viscous sublayer being imaginary. Beyond the point of separation, it would seem the boundary layer ceases to exist because of the prescribed adverse pressure gradient and in the wake, the entire Navier-Stokes equations come into action. Goldstein's singularity implies that Prandtl's boundary layer hypothesis is not valid in the vicinity of the point of separation and so cannot be a complete account of the flow structure.[5] Indeed, Lighthill (1951) renders a uniformly valid fluid speed on the aerofoil (with leading edge of radius of curvature ρ_L) surface but only if a part singular like x^{-1} is subtracted and the remainder is multiplied by $\left[\frac{x}{\left(x+\frac{1}{2}\rho_L\right)}\right]$.

Logarithmic term and singular term modifications were introduced into Goldstein's asymptotic expansions by Stewartson (1958) and Messiter & Enlow (1973). Each term is singular at the point of separation and it is suggested that the boundary layer must somehow adjust itself so that these terms cannot appear. The numerical

[5]The evidence of Goldstein's singularity is expanded upon in Section 2.3.4.

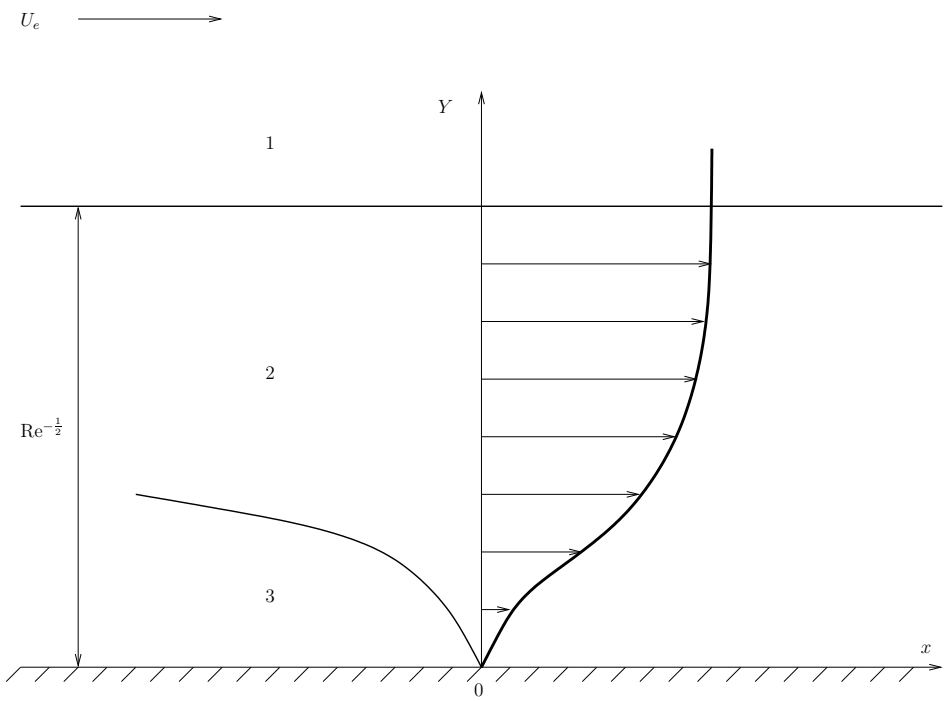

Figure 1.2: Goldstein's main boundary layer 2 and viscous sublayer 3 of combined thickness $O(\mathrm{Re}^{\frac{1}{2}})$ about a point of separation $x_s = 0$. The external inviscid flow 1 has velocity $U_e(x)$.

analysis by Catherall & Mangler (1966) supports this assumption. There is an interaction of the boundary layer with the external flow such that the pressure gradient redistributes along the boundary layer in a way to lead to separation. This process is called *self-induced* separation. Catherall & Mangler prescribe displacement thickness, that is the displacement of the streamlines by the viscous sublayer, as a regular function of distance along the surface, leaving the pressure gradient to be calculated from the consequent solution.[6] The numerical solutions are marched through the point of separation, in the absence of Goldstein's singularity, into a region of reversed recirculating flow. Solutions for self-induced separation were also formulated (for supersonic flow) by Neiland (1969) and Stewartson & Williams (1969).[7]

The situation where a redistribution of pressure gradient removes Goldstein's singularity such that there is a smooth transition of boundary layer into a separation region was considered by Stewartson (1970). Stewartson continues Goldstein's

[6]For example, Lighthill (1958) calculates the displacement thickness of the boundary layer to a first approximation at any point of the surface from the velocity profile.

[7]Lighthill (1953) illustrates some differences between separation of subsonic and supersonic flows.

boundary layers (regions 2 and 3 in Figure 1.3) and external flow (region 1) into the *triple-deck* structure about the point of separation called the *interaction region*. However, Stewartson only confirmed the unavoidability of Goldstein's singularity because the solutions in the neighbouring regions on either side of the singularity failed to match. Like Goldstein, the solutions become complex past the point of separation unless eigenvalues in the solution are chosen correctly. The eigenvalues are found *in situ* in Section 2.3.4.

In the interaction region, pressure perturbations and boundary layer displacement are no longer negligible compared to the flow. The terms of the asymptotic series solutions in the layers outside the interaction region become the same order of magnitude. The interaction region and boundary layer regions downstream of the point of separation are the continuations of the external flow, boundary layer and viscous sublayer upstream. Hence, the flow structure is of three tiers. (See Figure 1.3.) There is a boundary layer of thickness $O(\mathrm{Re}^{-\frac{1}{2}})$ which is divided into the main boundary layer 2 and $2'$ (upstream and downstream of the interaction region respectively) and the viscous sublayer adjacent to the surface 3 and $3'$. The triple-deck interaction region consists of the upper layer (region I) analogous to the external inviscid region 1; the middle layer (region II) from the main boundary layer; and the lower layer (region III) from the viscous sublayer. The proportions of the regions in terms of the Reynolds number are established *in situ* from the balance of forces in the Navier-Stokes equations and with interaction region analysis in Chapter 3. The whole structure is consistent if a solution can be found to a partial integro-differential equation called the *solvability condition* (*fundamental equation*) particular to subsonic flow involving $A(x)$, where $A(x)$ is directly proportional to skin friction. The classical two-tier, boundary layer and external inviscid flow structure, still holds for the majority of the flow field far away from the region of separation.

Laminar self-induced separation is also reviewed by Sychev (1972). There exists a triple-deck interaction region of the point of separation where there is a large

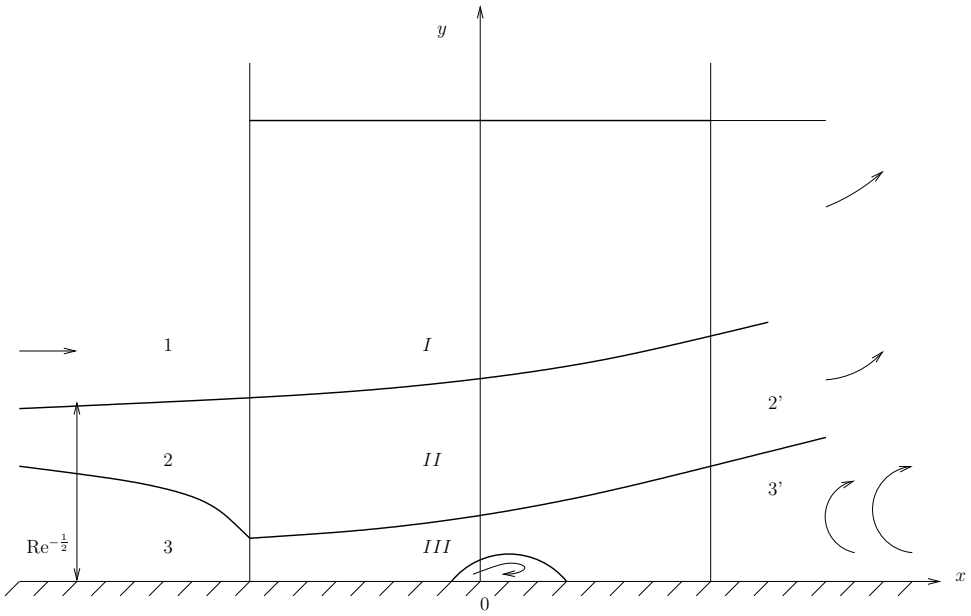

Figure 1.3: The triple-deck interaction region for steady subsonic flow: I, II, III; viscous sublayer: 3, 3'; external inviscid region: 1; main boundary layer: 2, 2'. There is a bubble about the point of separation $x_s = 0$.

self-induced pressure gradient. The fluid velocity being relatively slow in the viscous sublayer compared to the rest of the boundary layer is sensitive to pressure fluctuations. Any deceleration of fluid particles from an adverse pressure gradient causes the sublayer to become thicker such that streamlines are displaced from the surface. The displacement, or the slope of the streamlines, is transmitted through the main boundary layer to the external flow where the pressure perturbations feedback to the viscous sublayer to induce more displacement. The feedback is termed *viscous-inviscid interaction* and continues until the perturbations are so large that the streamline detaches from the wall. Upon detachment, a region of reversed recirculating flow is formed called the *separation bubble*. When the bubble erupts, there is a wake downstream of the point of separation.

1.4 Marginal Separation

Marginal separation at the leading edge of a thin airfoil is reviewed by Sychev, Ruban, Sychev & Korolev (1998b).

Goldstein's singularity is associated with strong boundary layer separation and its strength can be reduced by varying a parameter controlling the adverse pressure gradient acting on the layer. The parameter is the angle of attack (angle of incidence) of a slender airfoil with a parabolic leading edge.[8] When the attached flow on the airfoil is forced to gradually approach separation by increasing the angle of attack then the eventual detachment is called *marginal separation*.

In experimental observations,[9] the air flow around the airfoil is attached to the surface when the angle of attack is small and below a critical value. When the angle of attack is above the critical value (but within a small range), there is the formation of a closed region of recirculating flow, a so-called "short bubble". The length of the bubble does not usually exceed 1% of the airfoil chord and its presence has little effect upon the aerodynamic forces acting on the airfoil. With increase in angle of attack, the bubble eventually bursts to form either a so-called "long bubble" or a stagnation zone. (See Figure 1.4.) Accompanying the change in flow field is a decrease in lift and an increase in drag acting on the airfoil. In the application of flight, a sudden increase in drag acting on an airfoil performing a relatively slow oscillation through a large angle past the critical angle of attack can lead to stalling.[10]

Werle & Davis (1972) detail a numerical solution to the boundary layer problem consisting of Prandtl's classical equation (for the boundary layer normal coordinate Y):[11]

$$\frac{\partial \Psi}{\partial Y}\frac{\partial^2 \Psi}{\partial x \partial Y} - \frac{\partial \Psi}{\partial x}\frac{\partial^2 \Psi}{\partial Y^2} = \frac{\partial^3 \Psi}{\partial Y^3} - \frac{\partial p_e}{\partial x}\,;$$

the no-slip condition; a matching condition with the external inviscid region; an initial condition at the flow stagnation point O; and Bernoulli's equation for the external

[8] Stewartson, Smith & Kaups (1982) and Smith & Elliott (1985) respectively define a slender airfoil as having a thickness ratio less than $\mathrm{Re}^{-\frac{1}{16}}$ or a thickness to chord ratio comparable to a sufficiently small angle of attack.

[9] See for example, the review by Tani (1964).

[10] See Crabtree (1959) and Smith (1982a).

[11] A quasi-steady version of Prandtl's classical equation (2.14) is derived later from the Navier-Stokes equation (1.1) and streamfunction (1.4) in Chapter 2.

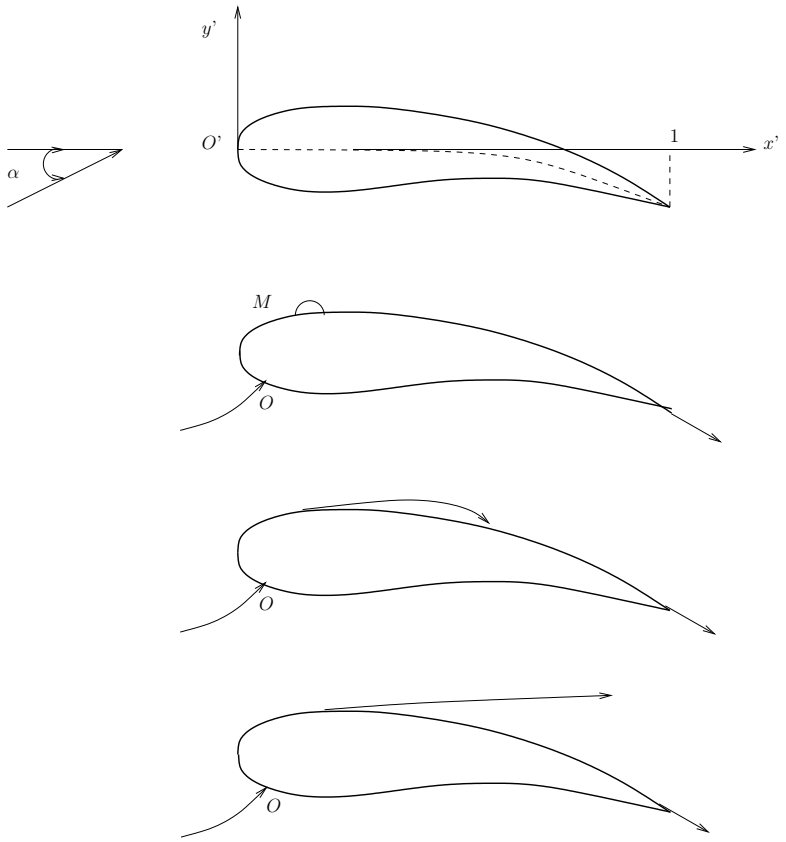

Figure 1.4: The flow around an airfoil at angle of attack α with a short bubble, a long bubble, and an extended separation zone (from top to bottom). There is a stagnation point at O.

flow:

$$\frac{\mathrm{d}p_e}{\mathrm{d}x} = -U_e \frac{\mathrm{d}U_e}{\mathrm{d}x} \,.$$

The solutions are in terms of the skin friction and an asymmetry parameter k of the parabolic nose. The parameter k is related to the angle of attack and similar to k related to the position of separation mentioned in Section 1.3. The results from Werle and Davies give support to the experimental observations.

The skin friction

$$\tau = \left. \frac{\partial^2 \Psi}{\partial Y^2} \right|_{Y=0}$$

is parabolic in shape with a positive minimum. The minimum value of the skin friction first vanishes for $k_0 = 1.1556$ at a critical angle of attack α_c and a point of separation occurs at $x = x_0$. When $k < k_0$, the skin friction remains positive for all x and has a minimum just beyond a point M where the pressure gradient is adverse.

(See Figure 1.4.) As $k \to k_0$ from below, the minimum value of skin friction decreases then vanishes for k_0 at x_0. If $k > k_0$, the point of separation $x = x_s$ shifts upstream of x_0. As $k > k_0$ is increased, x_s moves further upstream of x_0. The larger the difference in k from its critical value k_0, the greater the shift upstream in x_s from x_0. Moreover for $k > k_0$, a singularity occurs in the boundary layer solution ahead of the point of separation.

Two solutions are indicated by Goldstein (1948). The first solution arrives at Goldstein's singularity and the second solution describes an unrealistic case of no singularity but similar velocity distributions along the surface and thus similar separating boundary layer profiles.[12] There is another asymptotic expansion solution by Ruban (1981).[13] The stream function and pressure series solutions incorporate the asymmetry parameter k with a small change in k defined as $\Delta k = k - k_0 \to 0$. They are written as

$$\psi = \psi_0(x, y) + \Delta k \psi_1(x, y) + \dots \qquad p = p_0(x) + \Delta k p_1(x) + \dots$$

The third solution requires the existence of the interaction region and occurs at $k = k_0$. It has a singularity at the point of separation but at the same time can be extended continuously through this point.[14]

The stream function and pressure series expansions are used by Ruban (1982a) to construct an asymptotic theory of short separation regions for $|\Delta k| > 0$ and explains how the boundary layer extends through separation into a bubble along the leading edge of the airfoil. Ruban shows that a function $A(X)$, directly proportional to skin friction, satisfies the fundamental equation of marginal separation (for space X):

$$A^2 - X^2 + 2a = \lambda \int_X^\infty \frac{A''(\xi)}{(\xi - X)^{\frac{1}{2}}} \, \mathrm{d}\xi \,, \qquad \lambda = \frac{(-\frac{1}{4}!)}{\sqrt{2} \cdot (\frac{1}{4}!)} \,. \tag{1.5}$$

[12] Catherall & Mangler (1966)

[13] See also Stewartson (1970).

[14] One of the first complete solutions for the flow field without Goldstein's singularity is given by Smith & Daniels (1981).

The integral on the right hand side stems from the pressure-displacement relationship and the viscous-inviscid interaction between the viscous sublayer and the external inviscid region. The parameter a, like k, is a constant directly proportional to the departure of the angle of attack from its critical marginal value: $|\alpha - \alpha_c|$.

The boundary conditions are from matching with the singular branch of solutions of the boundary layer equation. Far away from the local interaction:

$$|A| \sim |X|\,, \qquad |X| \to \infty\,. \tag{1.6}$$

Ryzhov & Smith (1984) identify four subsonic cases from the boundary conditions (1.6). The boundary conditions most relevant to the thesis are the attached-to-attached (forward-forward) flow corresponding to

$$A \sim |X|\,, \qquad X \to \pm\infty\,; \tag{1.7}$$

and the separated-to-separated (reversed-reversed) flow corresponding to

$$A \sim -|X|\,, \qquad X \to \pm\infty\,. \tag{1.8}$$

The solution of (1.5) with (1.8) is discussed in Brown & Stewartson (1983). Classical marginal separation concerns the numerical solution of (1.5) with (1.7), as described by Stewartson et al. (1982) and given here.

To find solutions to the fundamental equation boundary value problem (1.5) and (1.7), then the parameter a is fixed and after a numerical solution is obtained, a is adjusted and the calculations repeated.

Recall that $A(X)$ is directly proportional to skin friction. Like skin friction, $A(X)$ is parabolic in shape with a minimum. As $a \to a_s$ from minus infinity, $A(X)$ and hence skin friction, is all positive which corresponds to attached flow. For the value $a_s = 1.14$, the skin friction minimum reaches zero and a point of separation occurs. As a increases to a critical value $a_c = 1.33$, an asymmetric closed zone of

recirculating flow grows in length and thickness, which coincides with negative skin friction. For $a > a_c$, there is only a complex solution.[15] The assumption is that the complex solution corresponds to short-bubble bursting and the formation of an extended separation zone.

Stewartson et al. (1982) developed marginal separation theory independently; confirmed Ruban's results but showed that the flow may assume various configurations since there is non-uniqueness of solution. Quasi-steady *hysteresis* is shown to occur when the roles of parameter a and $A(X = 0)$ are interchanged.[16] There is a lower branch of solutions as $a_c \to a_s$ which corresponds to either unseparated flow or a local zone of separation. Brown & Stewartson (1983) refine the numerical solution further to find for $0.60 < a < 0.68$, there is a loop on the lower branch and there are in fact four solutions. One solution is unseparated flow and the remaining three solutions correspond to local zones of separation with the primary difference between them being the length of the zone. The jump from one regime of flow to another is known from experiments as the process that accompanies short-bubble bursting. As $a \to +0$, where $a = 0$ is found to be a singular point on the lower branch, the point of separation approaches $x = 0$ and the reattachment point of the bubble recedes downstream to infinity.

1.5 Steady Flow on a Downstream-Moving Surface

The theory of unsteady separation is reviewed by Sychev, Ruban, Sychev & Korolev (1998c) and that of unsteady flows along moving walls by Sears & Telionis (1975).[17]

The appearance of Goldstein's singularity on the surface and thus vanishing skin

[15] Chernyshenko (1985)

[16] See also work by Kuryanov, Stolyarov & Steinberg (1979).

[17] Care must be taken over terminology when switching between discussions on steady flows and steady flows over downstream-moving surfaces. For example, Stewartson (1960) on the theory of unsteady laminar boundary layers uses the term "separation" to denote vanishing wall shear and "breakdown" to denote separation.

friction, or wall shear stress, is adopted as the most general definition of separation in the case of steady flow past fixed walls. However, "vanishing wall shear and accompanying flow reversal near the wall, do not, in general denote separation in any meaningful sense in unsteady flows."[18]

An example of unsteady flow is the Blasius (1908) problem of flow past a circular cylinder set into motion instantaneously from rest. At the first instant, the flow is potential and is described by the solution for unseparated steady flow past a cylinder with zero circulation. At the body surface, the no-slip condition is imposed. There arises the process of vorticity diffusion and convection which leads to the formation of a boundary layer.[19] At a certain instant, the point of zero skin friction starts moving upstream along the body surface from the rear stagnation point. The solution of the unsteady boundary layer equations is regular although a point of zero skin friction is located. At the point of vanishing wall shear, there is a region of reversed flow direction within the boundary layer.

In contrast to steady flow problems, the appearance of reverse flow does not lead to the violation of Prandtl's hierarchical concept. Unsteady effects make it possible for flow direction to reverse without the termination of the boundary layer and the beginning of a wake, which produces global effects such as drag or buffeting. Therefore, the appearance of a point of zero skin friction in an unsteady boundary layer is not to be identified with the occurrence of flow separation. The circumstance was first noted by Rott (1956), Sears (1956) and Moore (1958) when accounting the flows produced when two-dimensional stagnation point flow is combined with unsteady movement of the wall parallel to itself.

Prandtl's separation criterion to encompass both unsteady flow and flow moving past walls was generalised by Moore (1958). The criterion for unsteady separation is best illustrated by an analogy between steady boundary layer separation from the surface of a moving body and the separation of an unsteady boundary layer. Moore

[18]Rott (1956)
[19]Lighthill (1963)

considers a steady boundary layer flow over a body surface moving downstream with constant speed. Since the body surface moves, it entrains the nearest portion of fluid due to viscous forces. If the boundary layer develops an adverse pressure gradient then the fluid is decelerated and there will be a minimum point of zero shear stress within a region of the entrained fluid. The totality of these points forms a dividing line across the boundary layer: in one zone, the stress is positive; in the other zone, it is negative. Additionally, should the minimum of the longitudinal velocity component vanish at a point then there is a region of reversed flow beyond that point. Separation for a downstream-moving wall is defined to occur at a point where the shear stress and longitudinal velocity component vanish simultaneously.

The *Moore-Rott-Sears* (MRS) criterion generalises the Prandtl (1904) criterion. The point of zero shear stress and zero longitudinal velocity divisive of forward flow motion and reversed flow direction in the boundary layer is the MRS point of unsteady separation. In contrast to steady flow, the point of separation lies within the boundary layer as opposed to on the surface and hence the fluid breaks away from the layer. The MRS concept has been confirmed experimentally by Koromilas & Telionis (1980).

Transferring the vanishing wall shear from the wall to an interior point (x_0, y_0) of the boundary layer generalises the Goldstein (1948) model for steady separation for unsteady and moving-wall flows. The interior point of vanishing shear is in an "inner" flow region (of a separate limit process) within the boundary layer. Restrictions on the "inner" flow region to eliminate exponential terms in Goldstein's theory is found to not be necessary.[20]

Furthermore, unsteady flow involving moving separation at a fixed wall can be directly related to steady flow. The interior point $x_0(t)$ at the upstream end of a wake or bubble is a moving point, such that the moving wall frame of reference is $\chi = x_0(t) - x$. The velocity profiles can be transformed to a wall-fixed frame by a Galilean transformation, that is by adding or subtracting the appropriate constant velocities. If the point of separation moves with variable speed but its acceleration

[20]Brown (1965), c.f. Stewartson (1970), Section 1.3

is not large then this should not lead to qualitative changes in the flow structure in comparison with that of a point of separation moving with constant speed.

Like self-induced and marginal separation, solutions of the unsteady boundary layer equations are known to develop generic separation singularities in regions where the pressure gradient is prescribed and adverse. The first interactive stage, governed by the classical boundary layer equations, is where the solutions terminate in a singularity. As the boundary layer starts to separate from the surface, the external pressure distribution is altered though large-scale viscous-inviscid interaction just prior to the formation of the singularity. This is referred to as the *second interactive stage* by Cassel (2000). A numerical solution for the second interactive stage in unsteady boundary layer separation has been obtained by Cassel, Smith & Walker (1996). As an eruption develops, the boundary layer thickens and leads to the third interactive stage of vortex-sheet formation. The solutions of the Navier-Stokes equations for interaction in unsteady separation at large but finite Reynolds number, described by Cassel (2000), support a sequence of events for flow induced by a "thick-core" vortex.

Unsteady boundary layer separation is discussed by Sears & Telionis (1971). Boundary layer solution from a downstream-moving surface and subsequent singularity analysis is given by Elliott, Smith & Cowley (1983). Furthermore, boundary layer separation from a parabolic cylinder at an angle of incidence having a downstream-moving surface is analysed by Telionis & Werle (1973). There is evidence of breakdown of the boundary layer equations well downstream of vanishing wall shear.

1.6 Unsteady Marginal Separation & Dynamic Stall

Marginal separation theory can be extended to quasi-steady and unsteady fluid motion. Smith & Elliott (1985) consider the subcritical case where the angle of attack is static, like in classical marginal separation theory, but flow is allowed to develop on a very large time scale T compared to the boundary layer time scale t. The governing equation is the (normalised) unsteady fundamental equation for skin friction

parameter $A(X,T)$ and angle of attack parameter $2a = -1$:

$$A^2 - X^2 + 2a = \int_{-\infty}^{X} \frac{\partial A}{\partial T}(\xi, T)\, \frac{\mathrm{d}\xi}{(X-\xi)^{\frac{1}{4}}}\,. \tag{1.9}$$

The viscous-inviscid interaction integral on the right hand side of (1.5) is replaced by the unsteady effects integral on the right hand side of (1.9). The marginal separation and attached-to-attached flow motion case has the boundary conditions (1.7). Solutions can be obtained from various initial conditions. A steady state solution:

$$A = (X^2 + 1)^{\frac{1}{2}}$$

appears to be approached as time becomes large, if the initial condition is sufficiently smooth and close to the boundary conditions treated as a function of X:

$$A \sim |X|\,, \qquad \forall\, X\,. \tag{1.10}$$

In short, steady state streamlined flow can be preserved in some cases. Other initial conditions not sufficiently close to the boundary conditions function (1.10) lead to a singularity after a finite time.

Furthermore, Smith (1982a) introduces the concept of *dynamic stall* where there is a relatively slow oscillation of the airfoil through a large angle of attack. The change in angle of attack can cause the onset of the third interactive stage. Vortices form at the leading edge of the airfoil which then travel along the airfoil towards the trailing edge. When the vortices are eventually shed from the airfoil, the lift is reduced and stall occurs.

The flow motion far away from the region of separation is taken to vary slowly with time compared to the local interaction. The unsteady interaction region is of a triple-deck structure with length scale $x - x_s$ of order $\mathrm{Re}^{-\frac{1}{5}}$ whilst the time scale is initially long and of order $\mathrm{Re}^{-\frac{1}{20}}$. The unsteady flow response is initially a small deviation

from the steady separation profile but is governed by the fully unsteady equation of marginal separation, which is an unsteady, nonlinear, partial integro-differential equation for skin friction parameter $A(X,T)$:

$$A^2 - X^2 + 2a = \int_X^\infty \frac{\partial^2 A}{\partial \xi^2}(\xi, T)\, \frac{\mathrm{d}\xi}{(\xi - X)^{\frac{1}{2}}} - \int_{-\infty}^X \frac{\partial A}{\partial T}(\xi, T)\, \frac{\mathrm{d}\xi}{(X - \xi)^{\frac{1}{2}}}\,. \tag{1.11}$$

Its derivation is adapted from Stewartson (1970) and is determined by the solvability condition for the stream function, like the derivation of the steady fundamental equation of marginal separation (1.5).

Smith (1982a), Ruban (1982b), Ryzhov & Smith (1984) and Elliott & Smith (1987) study the Cauchy problem of (1.11) and the effect of instabilities. The main result is that the perturbations of the steady solution are not damped with time. The boundary layer displacement is progressively shifted upstream and increasing in thickness. There is local behaviour of reversed flow, which is faster than the initial response, on a shorter time scale of order $\mathrm{Re}^{-\frac{1}{7}}$. Eventually, the displacement becomes enormously accentuated and asymmetric. Accompanying the massive displacement and reversed flow is wave-like behaviour, multiple vortices and their shedding from the surface of the airfoil. Smith suggests a *finite-time nonlinear breakdown* is encountered as $T \to T_s$, when displacement becomes unbounded at a finite point of separation.

Furthermore, the dynamic stall process and nonlinear breakdown can occur in subcritical conditions, when the angle of attack is less than the critical angle for the steady fundamental equation (1.5). This is because any reversed flow encountered is unstable to short-wavelength disturbances.[21]

The next stage in dynamic stall due to unsteady marginal separation is studied by Elliott & Smith (1987). There is a new flow regime governed by a shortened length scale of order $\mathrm{Re}^{-\frac{2}{7}}$ and time scale of order $\mathrm{Re}^{-\frac{1}{7}}$ where the dimensions of the recirculating vortex becomes comparable to the original boundary layer thickness. The evolution of the vortex is a third interactive stage vortex-sheet problem.

[21] See Ruban (1982b) and Ryzhov & Smith (1984).

Recent Works

Work on marginal separation and steady flow over a moving surface has been extended (post-1990) to three-dimensional flows, flows over obstacles, local suction flows and/or all of the mentioned in order to control the flow, by Braun & Kluwick (2002), Braun & Kluwick (2004), Braun & Kluwick (2005) and Hackmüller & Kluwick (1990a), Hackmüller & Kluwick (1990b), and is reviewed by Braun (2006).

Detailed reviews on laminar separation flows including: compressible flows, flows with suction and injection of fluid, flows with severe pressure gradients, boundary layer interactions with shock waves, and wake studies are given by Brown & Stewartson (1969); boundary layer separation at supersonic speeds, supersonic ramp and base flows, incompressible trailing edge flows, and turbulent flows are given by Messiter (1979); high Reynolds number flows in channels and pipes by Smith (1982b); breakdown of boundary layers on moving surfaces in unsteady flow by Elliott et al. (1983); and boundary layer interaction theory on the trailing edge by Messiter (1983).

Work by Duck (1990) (and also Samad (2004)) extends the unsteady problem to include three-dimensional effects; McCroskey (1982) studies unsteady oscillating airfoils and their effects; Degani, Li & Walker (1996) (and also Stavrou (2004)) is concerned with an abruptly-started airfoil and goes on to suggest localised control measures such as suction to inhibit separation.

More recent work by Scheichl, Braun & Kluwick (2008) presents numerical computation of the solutions leading to the finite-time breakdown, displacement thickness and wall shear stress characteristics of the bubble bursting process.

Elliott & Smith (1987) on dynamic stall due to unsteady marginal separation ends with a vortex-sheet problem spanning the boundary layer. Numerical solutions of the Navier-Stokes equations for unsteady separation induced by a vortex are given by Obabko & Cassel (2002b). The vortices eventually merge before being lifted away from the surface. Obabko & Cassel (2002a) extends the problem to detachment of the dynamic-stall vortex above a moving surface where it is found that increasing the wall

speed close to a critical value can supress unsteady separation and the detachment of the vortex.

Another branch of research is the instability analysis of unsteady boundary layer separation. Further work on the instability of Navier-Stokes solutions of unsteady boundary layer separation has been done by Cassel et al. (1996); and on instability caused by the vortex ejection has been done by Obabko & Cassel (2005) and Cassel & Obabko (2010).

Objectives of the Thesis

The aim of the thesis is mentioned in Section 1.1 and is expanded upon here.

The thesis aims to bridge the work on marginal separation with that on steady flow over a downstream-moving surface, unsteady marginal separation and dynamic stall. In particular, the focus is on the quasi-steady flow structure about a point of zero skin friction which develops over a very large time scale when there are very slow perturbations to the otherwise steady stream functions. The slow perturbations are from a slow change in angle of attack causing a downstream movement of the surface only observable on the large time scale. (See Figure 1.1.) The angle of attack is over a small range and it gradually approaches the critical angle where stream function solutions become complex and nonlinear breakdown occurs. Furthermore, the time scale is sufficiently large such that the induced pressure gradient by the displaced boundary layer is of relatively small order of magnitude compared to the unsteady or viscous forces acting on the boundary layer. The induced pressure gradient is somewhat removed by the slow perturbations on the large time scale much like how the strength of Goldstein's singularity (and adverse pressure gradient) is reduced by marginal separation theory.

The unsteady equation of marginal separation and solvability condition to be solved is like (1.9) but the angle of attack parameter a is a function of the large time scale. If the large time scale approaches a smaller asymptotic scale where the induced pressure gradient is no longer negligible then the dynamic stall equation

(1.11) takes effect. If the induced pressure gradient is significant and the angle of attack is static (and subcritical) then the flow is governed by the classical marginal separation equation (1.5).

Chapter 2

Boundary Layer Analysis

To begin the boundary layer analysis, the external inviscid flow (region 1 in Figure 1.3) must be considered first.

2.1 The External Inviscid Flow Region

A rectangular coordinate system $O'x'y'$ (which is not to be confused with a system Oxy) is introduced, where the origin O' coincides with the apex of the leading edge of the airfoil and the axis $O'x'$ lies along the tangent to the mean line of the profile. (See Figure 1.4.) In the external inviscid flow region, x' and y' are of order unity.

The airfoil is thin and of relative thickness ϵ such that the classical thin airfoil theory applies. The thin airfoil theory states that the angle of attack is related to lift for inviscid incompressible flows and that the pressure gradient on the surface is also of order ϵ.[1] The nose of the airfoil is assumed parabolic in shape such that the surface can be described by the equations:

$$y' = \epsilon F_{\pm}(x')\,, \qquad 0 \leq x' \leq 1\,;$$
$$F_{\pm}(x') = \pm\sqrt{2x'} + \ldots \qquad x' \to 0\,,$$

where the positive and negative signs correspond to the top and underside of the

[1] Batchelor (2000b)

airfoil, respectively. (See Figure 2.1.) The angle of attack α is also of order ϵ, such that:

$$\alpha = \epsilon\alpha_* \,, \qquad \alpha_* = O(1) \,. \tag{2.1}$$

At the vicinity of the leading edge of the airfoil, the thin airfoil theory becomes invalid. A region where the variables $X' = \epsilon^{-2}x'$ and $Y' = \epsilon^{-2}y'$ are of order unity, and the airfoil contour is represented by the parabola $Y' = \pm\sqrt{2X'}$, should be analysed separately.

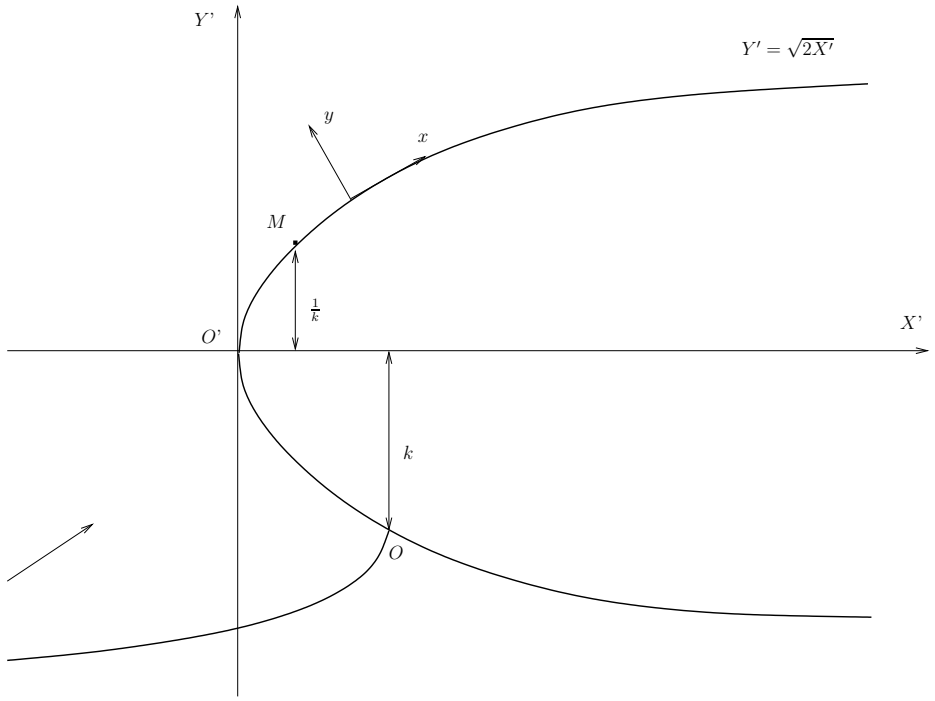

Figure 2.1: The parabolic nose of the airfoil with Cartesian coordinate system $O'X'Y'$ for the leading edge; and orthogonal curvilinear coordinate system Oxy for the boundary layer.

van Dyke (1956) determined that the tangential velocity component U_e of the free-stream flow at the vicinity of the leading edge can be written in the form:

$$U_e = \frac{Y' + k}{\sqrt{Y'^2 + 1}} \,, \tag{2.2}$$

where Y' is the distance from the axis of the parabola to the point at the surface

where the speed is to be calculated. The parameter k, where

$$k = \sqrt{2}\left(\alpha_* + \frac{1}{\pi}\int_0^1 \frac{G(x')}{\sqrt{x'(1-x')}}\,\mathrm{d}x'\right)\,, \tag{2.3}$$
$$G = -\frac{1}{2}\left(\frac{\mathrm{d}F_+}{dx'} + \frac{\mathrm{d}F_-}{dx'}\right)\,,$$

is a representation of the flow asymmetry near the leading edge in terms of the angle of attack α_* (2.1). The stagnation point is given by $Y' = -k$ and for example, when $k = 0$, the stagnation point is at the parabola vertex.

2.2 The Boundary Layer

The orthogonal curvilinear coordinate system Oxy (which is not to be confused with the external inviscid flow region Cartesian coordinate system $O'x'y'$), where x lies along the upper surface of the airfoil from stagnation point O and y is normal to the surface, is preferable when examining the boundary layer at the vicinity of the leading edge of the airfoil. (See Figure 2.1.)

The non-dimensionalised Navier-Stokes equations in two-dimensional orthogonal curvilinear coordinates x and y, are:

$$\frac{\partial u}{\partial t} + \frac{u}{h}\frac{\partial u}{\partial x} + v\frac{\partial u}{\partial y} + \frac{\kappa v u}{h} = \frac{1}{\mathrm{Re}}\frac{\partial}{\partial y}\left(\frac{1}{h}\left[\frac{\partial(hu)}{\partial y} - \frac{\partial v}{\partial x}\right]\right) - \frac{1}{h}\frac{\partial p}{\partial x}\,, \tag{2.4}$$

$$\frac{\partial v}{\partial t} + \frac{u}{h}\frac{\partial v}{\partial x} + v\frac{\partial v}{\partial y} + \frac{\kappa u^2}{h} = -\frac{1}{\mathrm{Re}}\frac{1}{h}\frac{\partial}{\partial x}\left(\frac{1}{h}\left[\frac{\partial(hu)}{\partial y} - \frac{\partial v}{\partial x}\right]\right) - \frac{\partial p}{\partial y}\,, \tag{2.5}$$

$$\frac{\partial u}{\partial x} + \frac{\partial(hv)}{\partial y} = 0\,, \tag{2.6}$$

where

$$h = 1 + \kappa(x)y\,.$$

The dimensionless curvature $\kappa(x)$ of the body surface is defined as positive for a

convex wall when the centre of curvature is located on the side $y < 0$.[2] Similarly, the stream function equations in two-dimensional orthogonal curvilinear coordinates x and y, are:

$$u = \frac{\partial \psi}{\partial y}\,, \qquad (1 + \kappa(x)y)v = -\frac{\partial \psi}{\partial x}\,. \tag{2.7}$$

To leading order, the equations in orthogonal curvilinear coordinates (2.4), (2.5), (2.6) and (2.7) return to the equations in Cartesian coordinates (1.1), (1.2), (1.3) and (1.4).

The boundary layer extends along the surface of the airfoil and hence the longitudinal coordinate x and velocity component u are of order unity. From the balance of inertial and viscous terms in the first, x-momentum equation (1.1):

$$u\frac{\partial u}{\partial x} + v\frac{\partial u}{\partial y} \sim \frac{1}{\mathrm{Re}}\left(\frac{\partial^2 u}{\partial x^2} + \frac{\partial^2 u}{\partial y^2}\right)\,.$$

Hence, to leading order, the thickness of the boundary layer is of order $\mathrm{Re}^{\frac{1}{2}}$ such that the normal coordinate to the surface is

$$Y = \mathrm{Re}^{\frac{1}{2}} y = O(1)\,; \tag{2.8}$$

the normal velocity component is

$$V = \mathrm{Re}^{\frac{1}{2}} v = O(1)\,; \tag{2.9}$$

and the stream function is:

$$\Psi = \mathrm{Re}^{\frac{1}{2}} \psi = O(1)\,. \tag{2.10}$$

As the air flow is of high speed and low viscosity, the limit as $\mathrm{Re} \to \infty$ may be taken. A viscous term: $\frac{\partial^2 u}{\partial x^2}$ cannot be balanced with the $O(1)$ terms. However, the term: $\frac{\partial^2 u}{\partial Y^2}$ is present and the x-momentum equation is not singular.

The conditions to be satisfied are:

[2] Rosenhead (1963)

1. the no-slip conditions on the surface:

$$\Psi = \frac{\partial \Psi}{\partial Y} = 0\,, \qquad Y = 0\,; \tag{2.11}$$

2. the condition of matching of the boundary layer with the external inviscid region. The stream function Ψ must not grow exponentially as $Y \to \infty$.

Only a local region of the point of zero skin friction $x = x_s$ is considered and so the variable:

$$s = x - x_s = O(1) \tag{2.12}$$

is introduced. It is noted that $(-s)$ is positive for the region upstream of the point of zero skin friction.

The Time Scale

The airfoil is subject to a very slow perturbation only observable on a very large time scale T compared to the external region time scale t, such that

$$T = \sigma^{-1} t = O(1)\,, \qquad \sigma \to \infty\,. \tag{2.13}$$

The perturbation is a slow change in angle of attack of the airfoil causing a downstream-movement of the surface. (See Figure 1.1.) The change in angle of attack is characterised by k (2.3), which is now a function of time T. (See Figure 2.1.) At the critical value $k = k_0$ is the first appearance of a point of zero skin friction $x = x_s$. The small variable:

$$\Delta k = k(T) - k_0 \to 0$$

is introduced to represent the small change in angle of attack. On the external region time scale t is steady flow over a fixed surface such that the no-slip conditions (2.11) apply. Meanwhile, on the boundary layer time scale T, there are slow and small $O(\Delta k)$ perturbations to the steady flow caused by the slow and small change in angle

of attack.

Taking the limits as Re $\to \infty$, $\sigma \to \infty$, $s = O(1)$ and $\Delta k \to 0$ in the boundary layer (regions 2 and 3 in Figure 1.3), the x-momentum equation to leading order becomes the boundary layer equation:

$$\frac{1}{\sigma}\frac{\partial^2\Psi}{\partial T\partial Y} + \frac{\partial\Psi}{\partial Y}\frac{\partial^2\Psi}{\partial x\partial Y} - \frac{\partial\Psi}{\partial x}\frac{\partial^2\Psi}{\partial Y^2} = \frac{\partial^3\Psi}{\partial Y^3} - \frac{\partial p_e}{\partial x}\,, \tag{2.14}$$

where p_e is the pressure at the outer edge of the boundary layer.

When the parameter k differs slightly from its critical value k_0, the asymptotic series expansion of the tangential velocity about $k = k_0$ in the external inviscid region is:

$$U_e(x,k) = U_e(x,k_0) + \Delta k\left.\frac{\partial U_e}{\partial k}\right|_{k=k_0} + \ldots$$

By Bernoulli's equation, there is a similar series expansion for pressure, that is

$$p_e = p_0(x,Y) + \Delta k p_1(x,Y,T) + \frac{\Delta k}{\sigma}p_2(x,Y,T) + \ldots$$

where $p_0(x,Y)$ is the pressure for flow over a static airfoil. The series expansion of the pressure gradient is

$$\frac{\partial p_e}{\partial x} = \lambda_0 + \lambda_1 s + \ldots \tag{2.15}$$

for s (2.12). The corresponding series expansion of the stream function $\Psi(x,Y,T)$ is defined as:

$$\Psi = \mathrm{Re}^{\frac{1}{2}}\psi = \Psi_0(x,Y) + \Delta k\Psi_1(x,Y,T) + \frac{\Delta k}{\sigma}\Psi_2(x,Y,T) + \ldots \tag{2.16}$$

The steady flow is represented by the term: $\Psi_0(x,Y)$. The flow perturbation is represented by the term: $\Delta k\Psi_1(x,Y,T)$. The unsteady perturbation effects on the flow are exhibited by the forcing term: $\frac{\Delta k}{\sigma}\Psi_2(x,Y,T)$.

To allow for quasi-steady flow, the constants arising from the stream function perturbation solutions $\Psi_1(x,Y,T)$ and $\Psi_2(x,Y,T)$ become functions of time T. Their

effects are only perceived on this large time scale and not on the external inviscid region time scale t.

2.3 $\Psi_0(x, Y)$ Solution

From the boundary layer equation (2.14), stream function (2.16) and pressure gradient (2.15) series expansions, and the no-slip conditions (2.11):

$$\left.\frac{\partial^3 \Psi_0}{\partial Y^3}\right|_{Y=0} = \frac{\mathrm{d}p_e}{\mathrm{d}x} = \lambda_0 \,.$$

At the point of zero skin friction, by definition:

$$\tau = \left.\frac{\partial^2 \Psi_0}{\partial Y^2}\right|_{Y=0} = 0 \,. \tag{2.17}$$

Hence, the leading term of the asymptotic representation of the stream function at the vicinity of the point of zero skin friction is

$$\Psi_0 = \frac{1}{6}\lambda_0 Y^3 + \ldots = O(Y^3) \,. \tag{2.18}$$

The length scales of the viscous flow region are determined by the stream function (2.18), and the balance of the orders of magnitude of viscous and inertia terms in the boundary layer equation (2.14):

$$\frac{\partial \Psi_0}{\partial Y}\frac{\partial^2 \Psi_0}{\partial x \partial Y} \sim \frac{\partial^3 \Psi_0}{\partial Y^3} \,.$$

Hence, the longitudinal scale decreases according to $Y = O[(-s)^{\frac{1}{4}}]$ as $s \to -0$ and a similarity variable of the viscous flow region can be defined as:

$$\eta = \frac{Y}{(-s)^{\frac{1}{4}}} = O(1) \,. \tag{2.19}$$

The stream function (2.18) becomes

$$\Psi_0 = (-s)^{-\frac{3}{4}} \frac{1}{6} \lambda_0 \eta^3 + \dots$$

The asymptotic expansion for the steady stream function $\Psi_0(x, Y)$ is sought in the form

$$\Psi_0 = (-s)^{\frac{3}{4}} \frac{1}{6} \lambda_0 \eta^3 + (-s)^{\alpha} f_{01}(\eta) + (-s)^{2\alpha - \frac{3}{4}} f_{02}(\eta) + \dots \tag{2.20}$$

where the second term is an eigenfunction with an unknown eigenvalue α and the third term is a forcing term arising from the square of the second term. The forcing term appears in the expansion due to the nonlinearity of the boundary layer equation (2.14). Substituting the expansion into the boundary layer equation and taking the limit as $s \to -0$, then differential equations for $f_{01}(\eta)$ and $f_{02}(\eta)$ are obtained.

2.3.1 $f_{01}(\eta)$ Solution

The $f_{01}(\eta)$ equation is

$$f_{01}''' - \frac{1}{8} \lambda_0 \eta^3 f_{01}'' + \frac{1}{2} \lambda_0 \left(\alpha + \frac{1}{4} \right) \eta^2 f_{01}' - \lambda_0 \alpha \eta f_{01} = 0 \tag{2.21}$$

with the no-slip conditions:

$$f_{01}(\eta) = f_{01}'(\eta) = 0\,, \qquad \eta = 0\,.$$

Three linearly independent solutions can be constructed for (2.21) in such a way that their Taylor series expansions about the point $\eta = 0$ start with either 1, η or η^2. However, only the solution starting with η^2 satisfies the no-slip conditions. Hence, a non-trivial solution of (2.21) for any eigenvalue α is

$$f_{01}(\eta) = \frac{1}{2} a_0 \eta^2\,. \tag{2.22}$$

The arbitrary constant a_0 depends on the external inviscid flow, U_e.

2.3.2 $f_{02}(\eta)$ Solution

The $f_{02}(\eta)$ equation is

$$f_{02}''' - \frac{1}{8}\lambda_0\eta^3 f_{02}'' + \lambda_0\left(\alpha - \frac{1}{4}\right)\eta^2 f_{02}' - \lambda_0\left(2\alpha - \frac{3}{4}\right)\eta f_{02} = \frac{1}{4}\left(1-2\alpha\right)a_0^2\eta^2 \quad (2.23)$$

with the no-slip conditions:

$$f_{02}(\eta) = f_{02}'(\eta) = 0\,, \qquad \eta = 0$$

and the matching condition with the external inviscid region. The solution should not grow exponentially as $\eta \to \infty$. The general solution is the linear concatenation of the contemporary solution for the homogeneous form of (2.23) and the particular solution. The contemporary solution for the homogeneous equation is

$$f_{02}^c(\eta) = \frac{1}{2}b_0\eta^2$$

from the same reasons as in Section 2.3.1, where b_0 is an arbitrary constant. A description of the Frobenius method to find the particular solution of an equation similar to (2.23) is described in Sections 2.6.1 and 2.6.2. The particular solution is

$$f_{02}^p(\eta) = \frac{1}{2}\frac{a_0^2}{\lambda_0}(\eta - h_\alpha(\eta))$$

where

$$h_\alpha(\eta) = \eta - \eta^2\int_0^\eta \eta_1^{-2}\left[{}_1F_1\left(1-2\alpha;\frac{5}{4};\frac{\lambda_0}{32}\eta_1^4\right) - 1\right]\,\mathrm{d}\eta_1 \quad (2.24)$$

and ${}_1F_1\left(1-2\alpha;\frac{5}{4};\frac{\lambda_0}{32}\eta^4\right)$ is a confluent hypergeometric function. The general solution is therefore

$$f_{02}(\eta) = \frac{1}{2}b_0\eta^2 + \frac{1}{2}\frac{a_0^2}{\lambda_0}(\eta - h_\alpha(\eta)) \quad (2.25)$$

with h_α (2.24).[3]

2.3.3 Confluent Hypergeometric Functions

The confluent hypergeometric function ${}_1F_1(a;b;z)$ is defined[4] throughout the entire complex plane z, as

$$ {}_1F_1(a;b;z) = \sum_{n=0}^{\infty} \frac{(a)_n}{(b)_n} \frac{z^n}{n!} \tag{2.26} $$

where the Pochhammer symbol $(a)_n$ is defined as:

$$ (a)_n = (a)(a+1)\dots(a+n-1)\,, \qquad (a)_0 = 1\,. \tag{2.27} $$

When $|z|$ is large and a and b are fixed, then

$$ \begin{aligned} {}_1F_1(a;b;z) = {} & e^{\pm i\pi a} z^{-a} \frac{\Gamma(b)}{\Gamma(b-a)} \left\{ \sum_{n=0}^{R-1} \frac{(a)_n (1+a-b)_n}{n!} (-z)^{-n} + O\left(|z|^{-R}\right) \right\} \\ & + e^z z^{a-b} \frac{\Gamma(b)}{\Gamma(a)} \left\{ \sum_{n=0}^{S-1} \frac{(b-a)_n (1-a)_n}{n!} z^{-n} + O\left(|z|^{-S}\right) \right\} \end{aligned} \tag{2.28} $$

where the upper sign is taken if $-\frac{1}{2}\pi < \arg z < \frac{3}{2}\pi$, the lower sign is $-\frac{3}{2}\pi < \arg z \leq -\frac{1}{2}\pi$. The Gamma function Γ is defined as

$$ \Gamma(b) = (b-1)! = \int_0^\infty t^{b-1} e^{-t}\, \mathrm{d}t\,, \qquad \Re(t) > 0\,. \tag{2.29} $$

The behaviour of the the general solution (2.25) can be determined as the point of zero skin friction is approached or when the outer edge of the boundary layer is approached, that is as $\eta \to \infty$. To match at the outer edge of the boundary layer, the general solution, and consequently the confluent hypergeometric function from (2.24), cannot grow exponentially as $\eta \to \infty$. When

$$ 1 - 2\alpha = -m\,, \qquad m = 0,\, 1,\, 2,\, \dots \tag{2.30} $$

[3] Sychev et al. (1998b)

[4] See, for example, Abramovich & Stegun (1972).

the confluent hypergeometric function from (2.24) reduces to a polynomial of degree m which grows like η^m as $\eta \to \infty$, according to:

$$ {}_1F_1\left(-m; \frac{5}{4}; \frac{\lambda_0}{32}\eta^4\right) = e^{-i\pi m}\frac{\Gamma\left(\frac{5}{4}\right)}{\Gamma\left(\frac{5}{4}+m\right)}\left(\frac{\lambda_0}{32}\eta^4\right)^m\left[1+O\left(-\frac{\lambda_0}{32}\eta^4\right)^{-1}\right]. $$

Nevertheless, regardless of how m and thus the eigenvalue α is chosen, the subsequent solution cannot match with the external inviscid region. Hence, the solution must be for a viscous sublayer (region 3 in Figure 2.2) which must match with a main boundary layer (region 2). Matching is only possible if (2.30) is true and hence, the eigenvalues are:

$$ \alpha = \frac{m+1}{2}, \qquad m = 0,\ 1,\ 2,\ \ldots \tag{2.31} $$

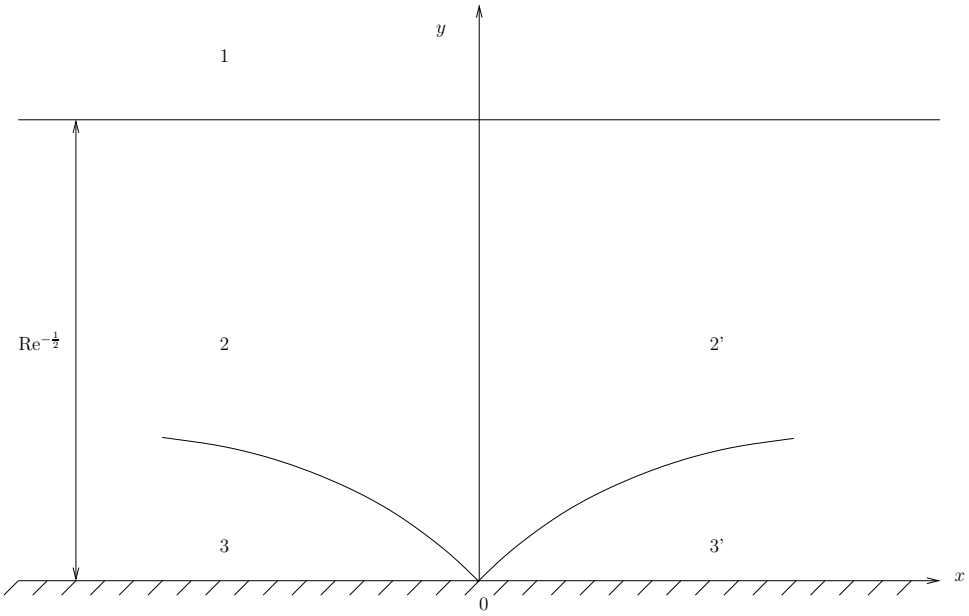

Figure 2.2: The flow structure consists of the external inviscid region 1; the viscous sublayers: 3 and 3', upstream and downstream of the point of zero skin friction $x = 0$; and the main boundary layers: 2 and 2'.

2.3.4 Goldstein's Singularity

The choice of eigenvalue α from (2.31) must be made carefully for the viscous sublayer (region 3) stream function (2.20).

For $\alpha = \frac{1}{2}$ $(m = 0)$, (2.20) becomes

$$\Psi_0 = (-s)^{\frac{3}{4}}\frac{1}{6}\lambda_0\eta^3 + (-s)^{\frac{1}{2}}f_{01}(\eta) + (-s)^{-\frac{1}{4}}f_{02}(\eta) + \dots$$

where each successive term is of a smaller order of magnitude then the preceding term. This does not make sense by definition of the asymptotic expansion.

For $\alpha = 1$ $(m = 1)$, (2.20) becomes

$$\Psi_0 = (-s)^{\frac{3}{4}}\frac{1}{6}\lambda_0\eta^3 + (-s)f_{01}(\eta) + (-s)^{\frac{5}{4}}f_{02}(\eta) + \dots \tag{2.32}$$

with $f_{01}(\eta)$ and $f_{02}(\eta)$ given by (2.22) and (2.25) respectively. In particular,

$$f_{01}(\eta) = \frac{1}{2}a_0\eta^2\,, \qquad f_{02}(\eta) = \frac{1}{2}b_0\eta^2 - \frac{1}{2\cdot 5!}a_0^2\eta^5 + \dots$$

The subsequent hierarchical analysis (as illustrated in Figure 2.3), for the viscous sublayer (region 3 in Figure 2.2) to the main boundary layer (region 2) and the regions 3' and 2' downstream of the point of zero skin friction, leads to a contradiction and Goldstein's singularity.[5]

To determine a solution for the main boundary layer (region 2) where $Y = O(1)$, a change of variables from η (2.19) to $(-s)^{-\frac{1}{4}}Y$ is made in the viscous sublayer (region 3) stream function Ψ_0 (2.32). Collecting terms of the same order of magnitude as $s \to -0$ then gives

$$\Psi_0 = \frac{1}{6}\lambda_0 Y^3 + (-s)^{\frac{1}{2}}\frac{1}{2}a_0 Y^2 + \dots$$

Hence, the series expansion solution for the main boundary layer (region 2) should be sought in the form

$$\Psi_0 = \Psi_{00}(Y) + (-s)^{\frac{1}{2}}\Psi_{01}(Y) + \dots \tag{2.33}$$

The solution should match with the outer edge of the viscous sublayer (region 3), of

[5]See Hartree (1939) and Goldstein (1948).

which the stream function components (2.32) when $\eta = (-s)^{-\frac{1}{4}}Y$, are:

$$\Psi_{00} = \frac{1}{6}\lambda_0 Y^3 - \frac{1}{2\cdot 5!}a_0^2 Y^5 + \dots\,, \qquad \Psi_{01} = \frac{1}{2}a_0 Y^2 + \dots\,, \qquad Y \to 0\,. \tag{2.34}$$

Substituting (2.33) into the boundary layer equation (2.14) and taking into account the conditions of matching (2.34), then

$$\Psi_{01} = \frac{a_0}{\lambda_0}\frac{\mathrm{d}\Psi_{00}}{\mathrm{d}Y}$$

and hence,

$$\Psi_0 = \Psi_{00}(Y) + (-s)^{\frac{1}{2}}\frac{a_0}{\lambda_0}\frac{\mathrm{d}\Psi_{00}}{\mathrm{d}Y} + \dots$$

The transverse velocity component

$$V = \mathrm{Re}^{\frac{1}{2}}v = (-s)^{-\frac{1}{2}}\frac{1}{2}\frac{a_0}{\lambda_0}\frac{\mathrm{d}\Psi_{00}}{\mathrm{d}Y} + \dots \tag{2.35}$$

exhibits singular behaviour as $s \to -0$, that is as the point of zero skin friction is approached from upstream. The skin friction:

$$\tau = \left.\frac{\partial^2\Psi}{\partial Y^2}\right|_{Y=0} = (-s)^{\frac{1}{2}}a_0 + \dots$$

The transverse velocity component $V = O[(-s)^{-\frac{1}{2}}]$ exhibits Goldstein's singularity. For a non-zero coefficient a_0, the solution cannot be extended beyond the point of zero skin friction. The argument for this is by contradiction.

Suppose that the solution can be extended continuously through the point of zero skin friction. By continuity of the boundary layer (region 2), the leading term of the series expansion for the boundary layer (region 2') downstream of the point of zero skin friction coincides with (2.33):

$$\Psi_0 = \Psi_{00}(Y) + \dots \qquad s \to +0\,. \tag{2.36}$$

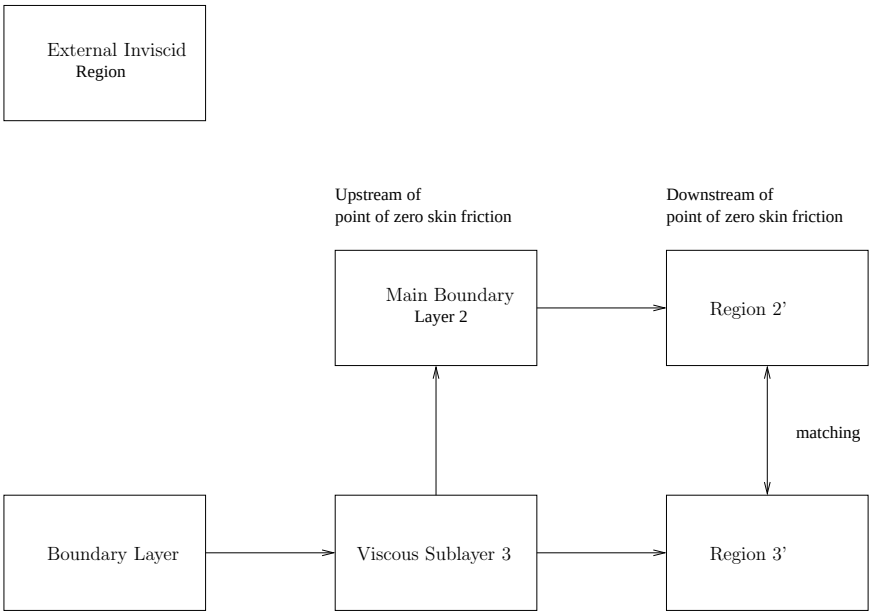

Figure 2.3: The hierarchical matching process to find solutions for the main boundary layer 2 and viscous sublayer 3 upstream of the point of zero skin friction, and the analogous regions 2' and 3' downstream.

This term should also match with (2.34).

The longitudinal velocity component $u = \frac{\partial \Psi}{\partial Y}$ is of order unity in the boundary layer. Balancing the orders of magnitude of the viscous and inertial forces in the boundary layer equation (2.14), then the thickness of the viscous sublayer (region 3') downstream of the point of zero skin friction is estimated as $Y = O(s^{\frac{1}{4}})$. Hence, the associated limit process is

$$\hat{\eta} = \frac{Y}{s^{\frac{1}{4}}} = O(1)\,, \qquad s \to +0\,. \tag{2.37}$$

The stream function solution for the viscous sublayer (region 3') is in the form:

$$\Psi_0 = s^{\frac{3}{4}}\frac{1}{6}\lambda_0\hat{\eta}^3 + s^{\hat{\alpha}}\hat{f}_{01}(\hat{\eta}) + s^{2\hat{\alpha}-\frac{3}{4}}\hat{f}_{02}(\hat{\eta}) + \ldots \tag{2.38}$$

where $\hat{\alpha}$ is an exponent to be found. The functions $\hat{f}_{01}(\hat{\eta})$ and $\hat{f}_{02}(\hat{\eta})$ are determined using the same Frobenius method (as described in Sections 2.6.1 and 2.6.2) for $f_{01}(\eta)$ and $f_{02}(\eta)$ in Sections 2.3.1 and 2.3.2 respectively. The expressions for $\hat{f}_{01}(\hat{\eta})$, $\hat{f}_{02}(\hat{\eta})$

are

$$\hat{f}_{01} = \frac{1}{2}\hat{a}_0\hat{\eta}^2\,,$$

$$\hat{f}_{02} = \frac{1}{2}\hat{b}_0\hat{\eta}^2 + \frac{1}{2}\frac{\hat{a}_0}{\lambda_0}(\hat{\eta}^2 - h_{\hat{\alpha}})\,,$$

where

$$h_{\hat{\alpha}} = \hat{\eta} - \hat{\eta}^2 \int_0^{\hat{\eta}} \hat{\eta}_1^{-2} \left[{}_1F_1\left(1 - 2\hat{\alpha}; \frac{5}{4}; -\frac{\lambda_0}{32}\hat{\eta}_1^4\right) - 1 \right] \mathrm{d}\hat{\eta}_1\,;$$

$\hat{a}_0$, $\hat{b}_0$ are arbitrary constants; and ${}_1F_1\left(1 - 2\hat{\alpha}; \frac{5}{4}; -\frac{\lambda_0}{32}\hat{\eta}^4\right)$ is a confluent hypergeometric function. The behaviour of the confluent hypergeometric function is described in Section 2.3.3.

As the outer edge of region 3' is approached from below and $\hat{\eta} \to \infty$, the hypergeometric function behaves like

$${}_1F_1\left(1 - 2\hat{\alpha}; \frac{5}{4}; -\frac{\lambda_0}{32}\hat{\eta}^4\right) = e^{-i\pi m}\frac{\Gamma\left(\frac{5}{4}\right)}{\Gamma\left(\frac{1}{4} + 2\hat{\alpha}\right)}\left(-\frac{\lambda_0}{32}\hat{\eta}^4\right)^{-1+2\hat{\alpha}}\left[1 + O\left(\frac{\lambda_0}{32}\eta^4\right)^{-1}\right]$$

and hence, the function:

$$\hat{f}_{02} = \frac{1}{2}\frac{\hat{a}_0^2}{\lambda_0}\frac{\Gamma\left(\frac{5}{4}\right)}{\Gamma\left(\frac{1}{4} + 2\hat{\alpha}\right)}\left(\frac{\lambda_0}{32}\right)^{-1+2\hat{\alpha}}\frac{\hat{\eta}^{8\hat{\alpha}-3}}{8\hat{\alpha} - 5} + \ldots$$

Therefore, the stream function (2.38) at the outer edge of region 3', with the change of variable from $\hat{\eta}$ (2.37) to $s^{-\frac{1}{4}}Y$, is

$$\Psi_0 = \frac{1}{6}\lambda_0 Y^3 + \frac{1}{2}\frac{\hat{a}_0^2}{\lambda_0}\frac{\Gamma\left(\frac{5}{4}\right)}{\Gamma\left(\frac{1}{4} + 2\hat{\alpha}\right)}\left(\frac{\lambda_0}{32}\right)^{-1+2\hat{\alpha}}\frac{Y^{8\hat{\alpha}-3}}{8\hat{\alpha} - 5} + \ldots \tag{2.39}$$

As the inner edge of region 2' is approached from above, the series expansion (2.36) by condition of matching (2.34) becomes:

$$\Psi_0 = \frac{1}{6}\lambda_0 Y^3 - \frac{1}{2 \cdot 5!}a_0^2 Y^5 + \ldots\,, \qquad Y \to 0\,. \tag{2.40}$$

According to the principle of matched asymptotic expansions, the expression

(2.34) for main boundary layer (region 2) upstream of the point of zero skin friction should match with the downstream (region 2') expression (2.40). Therefore,

$$\hat{\alpha} = 1$$

and the region 3' expression (2.39) becomes:

$$\Psi_0 = \frac{1}{6}\lambda_0 Y^3 + \frac{1}{2 \cdot 5!}\hat{a}_0^2 Y^5 + \dots \tag{2.41}$$

Crucially, matching the region 3' expression (2.41) with the region 2' expression (2.40) gives

$$\hat{a}_0^2 = -a_0^2 \,. \tag{2.42}$$

The constant a_0 is found from the process of solving the boundary layer equations with an initial upstream cross section $x = 0$ up to the point of zero skin friction. The constant (2.42) determines $\hat{a}_0$ for the solution downstream, which is imaginary. This means that a real solution ahead of the point of zero skin friction is impossible. A real solution is only obtained when $a_0 = 0$ and the first eigenfunction is absent. For $a_0 \neq 0$, the transverse velocity component (2.35) grows without bound as $s \to \pm 0$ and the boundary layer hypothesis ceases to be valid.

A triple-deck interaction region in the neighbourhood of the point of zero skin friction is created where the displacement of streamlines from the surface no longer has a negligible effect on the external flow and leads to a redistribution of pressure along the boundary layer. (See Figure 2.4.) The middle layer (region II) is analogous to the main boundary layer (region 2). If Goldstein's singularity is true then solutions for the interaction region cease to exist since the flow profile in region 2' must match with that of the interaction region II. A change in longitudinal velocity component u is small in high Reynolds number flow, that is

$$\Delta u \to 0 \,, \qquad \mathrm{Re} \to \infty$$

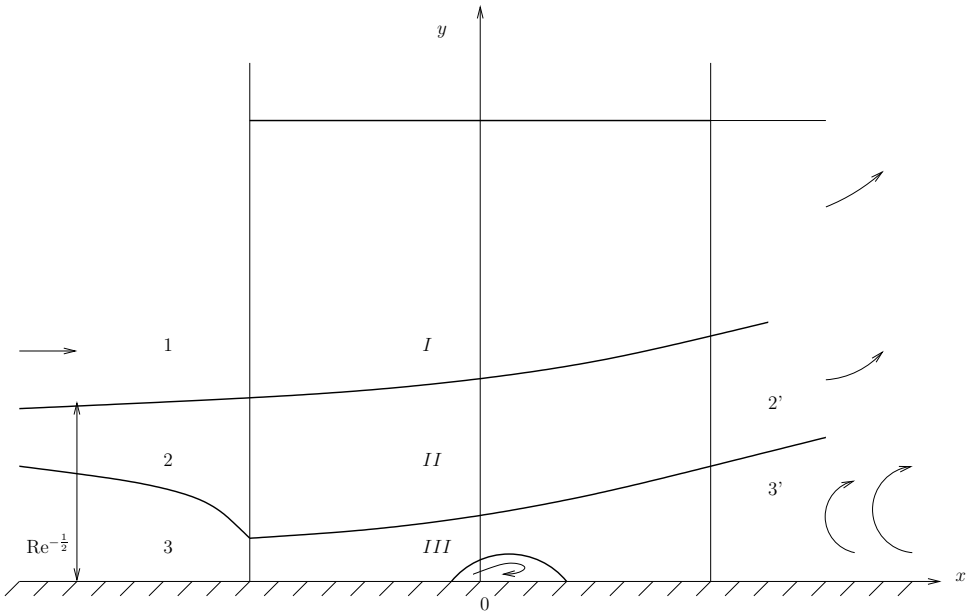

Figure 2.4: The triple-deck interaction region: I, II, III; viscous sublayer: 3, 3'; external inviscid region: 1; main boundary layer: 2, 2'.

and hence, the interaction region II does not alter the constant condition (2.42) for region 2'. Therefore, Goldstein's singularity is not removable by an adjustment of the pressure gradient and an imaginary solution remains when eigenvalue $\alpha = 1$.[6] Beyond Goldstein's singularity, it seems the boundary layer ceases to exist and the entire Navier-Stokes equations must be considered.

Other modes of flow are available with different choices of eigenvalue. The next eigenvalue is $\alpha = \frac{3}{2}$ $(m = 2)$ and corresponds with the marginal separation theory in the thesis.

[6]Stewartson (1970)

2.3.5 The Steady Airfoil General Solution

The eigenvalue is $\alpha = \frac{3}{2}$ and the steady stream function $\Psi_0(x, Y)$ in the viscous sublayer (region 3) is

$$\begin{aligned}\Psi_0 = {} & (-s)^{\frac{3}{4}}\frac{1}{6}\lambda_0\eta^3 + (-s)^{\frac{3}{2}}\frac{1}{2}a_0\eta^2 \\ & + (-s)^{\frac{7}{4}}\left[-\frac{1}{6}\lambda_1\eta^3 + \frac{2}{7!}\lambda_0\lambda_1\eta^7\right] \\ & + (-s)^{\frac{9}{4}}\left[\frac{1}{2}b_0\eta^2 - \frac{1}{5!}a_0^2\eta^5 + \frac{1}{8!}\lambda_0 a_0^2\eta^9\right] + \dots \end{aligned} \tag{2.43}$$

where the second term $(-s)^{\frac{3}{2}}\frac{1}{2}a_0\eta^2$ is the first eigenfunction; λ_0, λ_1 are the coefficients for the leading terms in expansion of the pressure gradient (2.15); and a_0, b_0 are constants.[7] The solution (2.43) can be extended continuously through the point of zero skin friction unlike the solution for eigenvalue $\alpha = 1$: (2.32), and the proof is by the following regional construction. (See Figure 2.3.)

By the same method as in the previous Section 2.3.4, the steady stream function (2.43) is written in the variables $\eta = (-s)^{-\frac{1}{4}}Y$ and hence, the stream function in the main boundary layer (region 2) is of the form:

$$\Psi_0 = \Psi_{00}(Y) + (-s)\Psi_{01}(Y) + \dots \qquad s \to -0\,, \tag{2.44}$$

which should match with (2.43) as $Y \to 0$. Substituting (2.44) into the boundary layer equation (2.14) and gathering the $O(1)$ terms then

$$-\Psi'_{00}\Psi'_{01} + \Psi_{01}\Psi''_{00} = -\lambda_0 + \Psi'''_{00}\,, \tag{2.45}$$

with the notation:

$$\Psi'_{00} = \frac{\mathrm{d}\Psi_{00}}{\mathrm{d}Y}\,, \qquad \Psi'''_{00} = \frac{\mathrm{d}^3\Psi_{00}}{\mathrm{d}Y^3}\,.$$

The region 2 Ψ_{01} equation (2.45), divided by $(\Psi'_{00})^2$ and integrated with respect to

[7] For an airfoil with a parabolic leading edge then $a_0 = 0.0085$ by Sychev et al. (1998b).

Y, becomes the solution:

$$\Psi_{01} = \Psi'_{00}\left[c_0 + \int_0^Y \frac{\lambda_0 - \Psi'''_{00}}{(\Psi'_{00})^2}\,\mathrm{d}Y\right] \tag{2.46}$$

where, from the condition of matching between (2.43) and (2.44), the constant of integration is

$$c_0 = \frac{a_0}{\lambda_0}\,; \tag{2.47}$$

and

$$\Psi_{00} = \frac{1}{6}\lambda_0 Y^3 + \frac{2}{7!}\lambda_0\lambda_1 Y^7 + \frac{1}{8!}\lambda_0 a_0^2 Y^9 + \ldots \qquad Y \to 0\,. \tag{2.48}$$

Next, the solutions ahead of the point of zero skin friction are constructed. By the previous method, the solution for region 2' (as shown in Figure 2.2) is sought in the form:

$$\Psi_0 = \Psi_{00}(Y) + s\hat{\Psi}_{01}(Y) + \ldots \qquad s \to +0\,. \tag{2.49}$$

The region 2' $\hat{\Psi}_{01}$ equation is obtained from substitution of (2.49) into the boundary layer equation, in a similar fashion for (2.45). Like (2.46), the equation is satisfied if

$$\hat{\Psi}_{01} = \Psi'_{00}\left[\hat{c}_0 + \int_0^Y \frac{\lambda_0 - \Psi'''_{00}}{(\Psi'_{00})^2}\,\mathrm{d}Y\right] \tag{2.50}$$

where

$$\hat{c}_0 = \frac{\hat{a}_0}{\lambda_0}\,.$$

Matching with the main boundary layer (region 2) implies Ψ_{00} (2.48) still applies.

Finally, the solution for region 3' is sought in the form:

$$\Psi_0 = s^{\frac{3}{4}}\frac{1}{6}\lambda_0\hat{\eta}^3 + s^{\frac{3}{4}}\hat{f}_{01}(\hat{\eta}) + s^{\frac{7}{4}}\hat{F}_{01}(\hat{\eta}) + s^{\frac{9}{4}}\hat{f}_{02}(\hat{\eta}) + \ldots \qquad s \to +0\,. \tag{2.51}$$

Substituting (2.51) into the boundary layer equation and taking into account the

no-slip conditions gives

$$\hat{f}_{01} = \frac{1}{2}\hat{a}_0\hat{\eta}^2\,,$$

$$\hat{F}_{01} = \frac{1}{6}\lambda_1\hat{\eta}^3 + \frac{2}{7!}\lambda_0\lambda_1\hat{\eta}^7\,,$$

$$\hat{f}_{02} = \frac{1}{2}\hat{b}_0\hat{\eta}^2 + \frac{1}{5!}\hat{a}_0^2\hat{\eta}^5 + \frac{1}{8!}\lambda_0\hat{a}_0^2\hat{\eta}^9\,.$$

The solutions for regions 2' (2.49) and 3' (2.51) can match because the constant relation

$$\hat{a}_0^2 = a_0^2 \tag{2.52}$$

is found to admit real solutions for these regions downstream of the point of zero skin friction.

One region 3' expression, given by $\hat{a}_0 = a_0$, is

$$\Psi_0 = \Psi_{00}(Y) + \Psi'_{00}\left[\frac{a_0}{\lambda_0}|s| + s\int_0^Y \frac{\Psi'''_{00} - \lambda_0}{(\Psi'_{00})^2}\,\mathrm{d}Y\right] + O(s^2)\,.$$

The angle of inclination θ of the streamlines in the boundary layer is given by

$$\mathrm{Re}^{\frac{1}{2}}\theta = -\frac{\frac{\partial\Psi_0}{\partial x}}{\frac{\partial\Psi_0}{\partial Y}} = -\frac{a_0}{\lambda_0}\mathrm{sign}(s) + \int_0^Y \frac{\Psi'''_{00} - \lambda_0}{(\Psi'_{00})^2}\,\mathrm{d}Y + O(s) \tag{2.53}$$

and undergoes a discontinuity when passing through the point of zero skin friction at $s = 0$. The skin friction behaves as

$$\tau = \left.\frac{\partial^2\Psi_0}{\partial Y^2}\right|_{Y=0} = a_0|s| + O\left(s^2\right)\,, \qquad s \to 0\,.$$

Hence, the $\hat{a}_0 = a_0$ expression is singular.

When $\hat{a}_0 = -a_0$, there is the region 3' solution:

$$\Psi_0 = \Psi_{00}(Y) + \Psi'_{00}\left[-\frac{a_0}{\lambda_0}s + s\int_0^Y \frac{\Psi'''_{00} - \lambda_0}{(\Psi'_{00})^2}\,\mathrm{d}Y\right] + O(s^2) \tag{2.54}$$

which can be continued smoothly through the point of zero skin friction. The skin friction behaves as

$$\tau = -a_0 s + O(s^2)\,, \qquad s \to 0$$

and becomes negative past the point of zero skin friction, when s becomes positive. This is evidence of a region of reverse flow downstream.[8] Again, matching with the viscous sublayer (region 3) implies Ψ_{00} (2.48) still applies.

2.4 $\Psi_1(x, Y, T)$ Solution

When $\Delta k \neq 0$ and the parameter k differs slightly from its critical value k_0, there are perturbations Ψ_1 to the steady flow Ψ_0. The Ψ_1 analysis is given in Sychev et al. (1998b).

Substituting the stream function series expansion (2.16) into the boundary layer equation (2.14) and collecting terms of order Δk then the Ψ_1 equation:

$$\frac{\partial\Psi_0}{\partial Y}\frac{\partial^2\Psi_1}{\partial x\partial Y} + \frac{\partial^2\Psi_0}{\partial x\partial Y}\frac{\partial\Psi_1}{\partial Y} - \frac{\partial\Psi_0}{\partial x}\frac{\partial^2\Psi_1}{\partial Y^2} - \frac{\partial^2\Psi_0}{\partial Y^2}\frac{\partial\Psi_1}{\partial x} = -\frac{\mathrm{d}p_1}{\mathrm{d}x} + \frac{\partial^3\Psi_1}{\partial Y^3} \tag{2.55}$$

is obtained. The solution is subject to the no-slip conditions:

$$\Psi_1 = \frac{\partial\Psi_1}{\partial Y} = 0\,, \qquad Y = 0$$

and the condition of no exponential growth as $Y \to \infty$.

The solutions for (2.55) in the viscous sublayer (region 3) and main boundary layer (region 2) are constructed, in that order, using the same methods as shown in Section 2.3. The region 3 Ψ_0 terms are from (2.43).

For the viscous sublayer (region 3), the perturbation Ψ_1 is sought in the form:

$$\Psi_1 = (-s)^{\beta} f_{11}(\eta) + (-s)^{\beta+\frac{1}{4}} f_{12}(\eta) + \ldots \qquad s \to -0 \tag{2.56}$$

[8] Ruban (1981)

where β is the eigenvalue to be found. Substituting (2.56) into (2.55) and solving using the Frobenius method then

$$f_{11} = \frac{1}{2} a_1 \eta^2 \,,$$

$$f_{12} = \frac{1}{2} b_1 \eta^2 + \frac{a_0 a_1}{\lambda_0} (\eta - h_\beta)$$

where

$$h_\beta = \eta - \eta^2 \int_0^\eta \eta_1^{-2} \left[{}_1F_1 \left(- \left(\beta + \frac{1}{2} \right) ; \frac{5}{4} ; \frac{\lambda_0}{32} \eta_1^4 \right) - 1 \right] \mathrm{d}\eta_1 \,.$$

The confluent hypergeometric function ${}_1F_1 \left(- \left(\beta + \frac{1}{2} \right) ; \frac{5}{4} ; \frac{\lambda_0}{32} \eta^4 \right)$ and hence h_β do not grow exponentially as $\eta \to \infty$ when

$$\beta = m - \frac{1}{2} \,, \qquad m = 0,\, 1,\, 2,\, \ldots$$

The function $h_\beta = \eta$ with the smallest eigenvalue $\beta = \frac{1}{2}$. Therefore, the Ψ_1 solution for the region 3 is

$$\Psi_1 = (-s)^{-\frac{1}{2}} \frac{1}{2} a_1 \eta^2 + (-s)^{\frac{1}{4}} \frac{1}{2} b_1 \eta^2 + \ldots \tag{2.57}$$

The arbitrary constants a_1 and b_1 are determined by conditions of matching with the outer edge of the boundary layer as $Y \to \infty$ and matching with the initial cross section as $x \to -\infty$.

Taking into account the viscous sublayer (region 3) solution (2.57), then by the method of matched asymptotic expansions, the main boundary layer (region 2) stream function is

$$\Psi_1 = (-s)^{-1} \frac{a_1}{\lambda_0} a_1 \frac{\mathrm{d}\Psi_{00}}{\mathrm{d}Y} + O\left[(-s)^{-\frac{1}{4}} \right] , \qquad s \to -0 \,. \tag{2.58}$$

The condition of matching (2.48) implies

$$\Psi_{00} = \frac{1}{6} \lambda_0 Y^3 + \frac{2}{7!} \lambda_0 \lambda_1 Y^7 + \frac{1}{8!} \lambda_0 a_0^2 Y^9 + \ldots \qquad Y \to 0 \,.$$

The solution (2.58) grows without bound as the point of zero skin friction is approached. Hence, a neighbourhood about the point must be analysed separately as the interaction region in Chapter 3.

2.5 $\Psi_0(x,Y,T)$ & $\Psi_1(x,Y,T)$ Solutions by Region

The stream function (2.16) solutions

$$\Psi = \mathrm{Re}^{\frac{1}{2}}\psi = \Psi_0(x,Y) + \Delta k\Psi_1(x,Y,T) + \frac{\Delta k}{\sigma}\Psi_2(x,Y,T) + \dots$$

by regions in Figure 2.5, are summarised.

1. The leading viscous sublayer (region 3) stream function components are Ψ_0 (2.43):

$$\begin{aligned}\Psi_0 = {} & (-s)^{\frac{3}{4}}\frac{1}{6}\lambda_0\eta^3 + (-s)^{\frac{3}{2}}\frac{1}{2}a_0\eta^2 \\ & + (-s)^{\frac{7}{4}}\left[-\frac{1}{6}\lambda_1\eta^3 + \frac{2}{7!}\lambda_0\lambda_1\eta^7\right] \\ & + (-s)^{\frac{9}{4}}\left[\frac{1}{2}b_0\eta^2 - \frac{1}{5!}a_0^2\eta^5 + \frac{1}{8!}\lambda_0 a_0^2\eta^9\right] + \dots\end{aligned}$$

   and Ψ_1 (2.57):

$$\Psi_1 = (-s)^{-\frac{1}{2}}\frac{1}{2}a_1\eta^2 + (-s)^{\frac{1}{4}}\frac{1}{2}b_1\eta^2 + \dots$$

   for similarity variable (2.19):

$$\eta = \frac{Y}{(-s)^{\frac{1}{4}}} = O(1)\,.$$

2. The leading main boundary layer (region 2) stream function components are Ψ_0 (2.44) and Ψ_1 (2.58). The Ψ_0 component is

$$\Psi_0 = \Psi_{00}(Y) + (-s)\Psi_{01}(Y) + \dots \qquad s \to -0$$

where from matching with the viscous sublayer (region 3), (2.48):

$$\Psi_{00} = \frac{1}{6}\lambda_0 Y^3 + \frac{2}{7!}\lambda_0\lambda_1 Y^7 + \frac{1}{8!}\lambda_0 a_0^2 Y^9 + \dots \qquad Y \to 0 \qquad (2.59)$$

and (2.46):

$$\Psi_{01} = \Psi'_{00}\left[\frac{a_0}{\lambda_0} + \int_0^Y \frac{\lambda_0 - \Psi'''_{00}}{(\Psi'_{00})^2}\,\mathrm{d}Y\right].$$

The Ψ_1 component is

$$\Psi_1 = (-s)^{-1}\frac{a_1}{\lambda_0}a_1\frac{\mathrm{d}\Psi_{00}}{\mathrm{d}Y} + O\left[(-s)^{-\frac{1}{4}}\right], \qquad s \to -0\,.$$

3. The leading region 2' stream function component is Ψ_0 (2.49):

$$\Psi_0 = \Psi_{00}(Y) + s\hat{\Psi}_{01}(Y) + \dots \qquad s \to +0\,.$$

where (2.50):

$$\hat{\Psi}_{01} = \Psi'_{00}\left[-\frac{a_0}{\lambda_0} + \int_0^Y \frac{\lambda_0 - \Psi'''_{00}}{(\Psi'_{00})^2}\,\mathrm{d}Y\right]$$

and matching with the main boundary layer (region 2) implies $\Psi_{00}(Y)$ is (2.59).

4. The leading region 3' stream function component is Ψ_0 (2.51):

$$\begin{aligned}\Psi_0 = {} & s^{\frac{3}{4}}\frac{1}{6}\lambda_0\hat{\eta}^3 + s^{\frac{3}{4}}\frac{1}{2}\hat{a}_0\hat{\eta}^2 \\ & + s^{\frac{7}{4}}\left[\frac{1}{6}\lambda_1\hat{\eta}^3 + \frac{2}{7!}\lambda_0\lambda_1\hat{\eta}^7\right] \\ & + s^{\frac{9}{4}}\left[\frac{1}{2}\hat{b}_0\hat{\eta}^2 + \frac{1}{5!}\hat{a}_0^2\hat{\eta}^5 + \frac{1}{8!}\lambda_0\hat{a}_0^2\hat{\eta}^9\right] + \dots \qquad s \to +0\end{aligned}$$

for similarity variable (2.37):

$$\hat{\eta} = \frac{Y}{s^{\frac{1}{4}}} = O(1)\,.$$

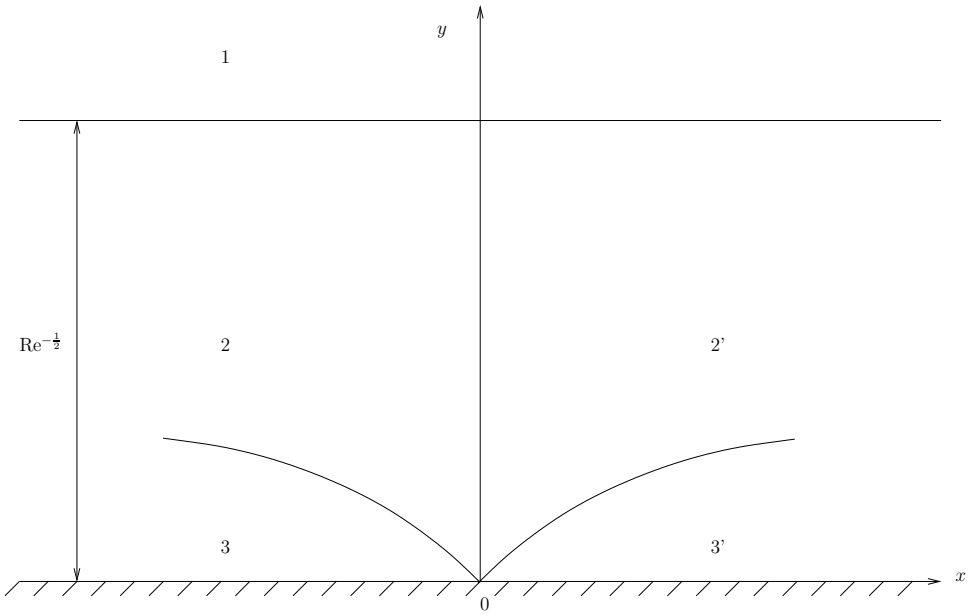

Figure 2.5: The flow structure consists of the external inviscid region 1; the viscous sublayers: 3 and 3', upstream and downstream of the point of zero skin friction $x = 0$; and the main boundary layers: 2 and 2'.

2.6 $\Psi_2(x, Y, T)$ Solution

To adapt the viscous sublayer (region 3) stream function so it allows slow perturbations of the airfoil on the large time scale T, any constants a_n and b_n for $n \geq 1$ of the perturbation components Ψ_1 and Ψ_2, will now become functions of time $a_n(T)$ and $b_n(T)$. The angle of attack α and asymmetry parameter k are also time-dependent such that (for example) $a_1(T)$ is related to k (2.3) and is of a small order of magnitude Δk.

Substituting the stream function (2.16) and pressure (2.15) series expansions into the boundary layer equation (2.14) and collecting terms of order $\frac{\Delta k}{\sigma}$ gives the Ψ_2 equation:

$$\frac{\partial^2 \Psi_1}{\partial T \partial Y} + \frac{\partial \Psi_0}{\partial Y}\frac{\partial^2 \Psi_2}{\partial x \partial Y} + \frac{\partial^2 \Psi_0}{\partial x \partial Y}\frac{\partial \Psi_2}{\partial Y} - \frac{\partial \Psi_0}{\partial x}\frac{\partial^2 \Psi_2}{\partial Y^2} - \frac{\partial^2 \Psi_0}{\partial Y^2}\frac{\partial \Psi_2}{\partial x} = \frac{\partial^3 \Psi_2}{\partial Y^3} - \frac{\partial p_2}{\partial x}\,.$$

Next, substituting for the region 3 terms Ψ_0 (2.43) and Ψ_1 (2.57) gives the Ψ_2 equation:

$$\begin{aligned}\frac{\partial^3\Psi_2}{\partial Y^3} &+ \frac{1}{2}\lambda_0(-s)^{\frac{1}{2}}\eta^2\frac{\partial^2\Psi_2}{\partial x\partial Y} - a_0(-s)^{\frac{1}{4}}\eta\frac{\partial\Psi_2}{\partial Y}\\ &+ \frac{1}{2}a_0(-s)^{\frac{1}{2}}\eta^2\frac{\partial^2\Psi_2}{\partial Y^2} - \lambda_0(-s)^{\frac{1}{4}}\eta\frac{\partial\Psi_2}{\partial x}\\ &= (-s)^{-\frac{3}{4}}\dot{a}_1\eta - \frac{\partial p_2}{\partial x}\,,\end{aligned} \tag{2.60}$$

with the notation:

$$\dot{a}_1(T) \equiv \frac{\mathrm{d}a}{\mathrm{d}T}\,.$$

The no-slip conditions:

$$\Psi_2 = \frac{\partial\Psi_2}{\partial Y} = 0\,, \qquad Y = 0 \tag{2.61}$$

and the condition of no exponential growth at the outer edge of the viscous sublayer apply. It is necessary to impose a condition at the initial cross section $x = 0$ but the specific form of this condition is unimportant for the analysis at this stage. Additionally, the pressure perturbation p_2 will not balance in the analysis, like the pressure term p_1 in the Ψ_1 analysis.

The asymptotic expansion for Ψ_2 is sought in a similar form to the series expansions (2.20) and (2.56) for Ψ_0 and Ψ_1, such that

$$\Psi_2 = (-s)^{\gamma} f_{21}(\eta, T) + (-s)^{\gamma+\frac{3}{4}} f_{22}(\eta, T) + \ldots \tag{2.62}$$

where η is the similarity variable (2.19). The exponents are chosen in such a way to include the unsteady term $\dot{a}_1(T)$ in the solution; and $\gamma \neq 0$ is the eigenvalue to be found.

$f_{21}(x, Y, T)$ Solution

Substitution of (2.62) and viscous sublayer terms Ψ_0 (2.43) and Ψ_1 (2.57) into the Ψ_2 equation (2.60), then gathering terms of the same order of magnitude as $(-s) \to 0$,

gives the $f_{21}(\eta, T)$ equation:

$$f_{21}''' - \frac{1}{8}\lambda_0\eta^3 f_{21}'' + \frac{1}{2}\lambda_0\eta^2\left(\gamma + \frac{1}{4}\right) f_{21}' - \lambda_0\eta\gamma f_{21} = 0\,.$$

From (2.61), the appropriate no-slip conditions are

$$f_{21}(0,T) = f_{21}'(0,T) = 0\,, \qquad \forall\, T\,.$$

The general solution is:

$$f_{21} = \frac{1}{2}a_2(T)\eta^2\,, \qquad \forall\,\gamma \tag{2.63}$$

where $a_2(T)$ remains arbitrary until an initial profile condition is imposed.

$f_{22}(x, Y, T)$ Solution

To determine the eigenvalue γ, it is necessary to consider the $f_{22}(\eta, T)$ equation:

$$\begin{aligned}(-s)^\gamma &\left[f_{22}''' - \frac{1}{8}\lambda_0\eta^3 f_{22}'' + \frac{1}{2}(\gamma+1)\lambda_0\eta^2 f_{22}' - \left(\gamma + \frac{3}{4}\right)\lambda_0\eta f_{22}\right] \\ &= (-s)^{-\frac{3}{4}}\dot{a}_1\eta + (-s)^\gamma\left[\frac{3}{4}a_0\eta^2 f_{21}'' - a_0(\gamma+1)\eta f_{21}' - a_0\gamma f_{21}\right]\,.\end{aligned}$$

Setting the eigenvalue

$$\gamma = -\frac{3}{4} \tag{2.64}$$

ensures that the equation captures the unsteady effects of $\dot{a}_1(T)$ and hence:

$$f_{22}''' - \frac{1}{8}\lambda_0\eta^3 f_{22}'' + \frac{1}{8}\lambda_0\eta^2 f_{22}' = \dot{a}_1\eta + \frac{7}{8}a_0 a_2\eta^2\,. \tag{2.65}$$

The conditions are

$$f_{22}(0,T) = f_{22}'(0,T) = 0\,, \qquad \forall\, T \tag{2.66}$$

and that $f_{22}(\eta, T)$ does not grow exponentially as $\eta \to \infty$.

For a complimentary solution of (2.65), note that the equation is third order and

so three linearly independent Taylor series solutions can be constructed about the point $\eta = 0$ which begin with either 1, η or η^2. However, only the solution like η^2 is non-trivial after applying (2.66). Therefore, the complimentary solution is:

$$f_{22}^c = \frac{1}{2} b_2(T) \eta^2 \,, \tag{2.67}$$

where $b_2(T)$ remains arbitrary until an initial condition is imposed.

The particular solution of (2.65) is the linear combination of the particular solutions of the equations:

$$f_{22}''' - \frac{1}{8}\lambda_0 \eta^3 f_{22}'' + \frac{1}{8}\lambda_0 \eta^2 f_{22}' = \dot{a}_1 \eta \tag{2.68}$$

$$f_{22}''' - \frac{1}{8}\lambda_0 \eta^3 f_{22}'' + \frac{1}{8}\lambda_0 \eta^2 f_{22}' = \frac{7}{8} a_0 a_2 \eta^2 \,. \tag{2.69}$$

2.6.1 $\dot{a}_1(T)\eta$ Particular Solution by Frobenius Method

The behaviour of the particular solution $f_{22}^{p_1}(\eta, T)$ for (2.68) can be found from the balance of the orders of magnitude of the viscous and unsteady forces in the Ψ_2 equation (2.60), where

$$\frac{\partial^3 \Psi_2}{\partial Y^3} \sim (-s)^{-\frac{3}{4}} \dot{a}_1 \eta = (-s)^{-1} \dot{a}_1 Y \,.$$

Only a small vicinity of the point of zero skin friction is considered, hence:

$$\frac{\Delta \Psi_2}{\Delta Y^3} \sim (-s)^{-1} \dot{a}_1 Y$$

which implies

$$\Psi_2 \sim (-s)^{-1} \dot{a}_1 Y^4 = \dot{a}_1 \eta^4 \,.$$

In fact, if the $f'''_{22}(\eta, T)$ term of (2.68) is balanced with the term on the right hand side then the behaviour of the particular solution is also expected to be of the form:

$$f_{22}^{p_1} \sim \dot{a}_1 \eta^4 \,.$$

If instead, the $f'_{22}(\eta, T)$ term is balanced with the term on the right hand side then the particular solution has logarithmic behaviour and is expected to behave like:

$$f_{22}^{p_1} \sim \frac{8}{\lambda_0} \dot{a}_1 \ln \eta \,, \qquad \eta \to \infty \,.$$

When η is of order unity, $\eta = 0$ is a regular point and hence the particular solution can be obtained in the form of a Frobenius series:

$$f_{22}^{p_1} = \sum_{i=0}^{\infty} c_i(T) \eta^{i+\alpha} \,, \tag{2.70}$$

where α is an unknown exponent (which is not to be confused with the eigenvalue from Section 2.3). The functions of time $c_i(T)$ are analogous to $b_2(T)$ in (2.67) and by definition, $c_0(T) \neq 0$. Substituting (2.70) into (2.68) and making an index shift of i to $i-4$ in the second and third term on the left hand side, gives the equation:

$$\begin{aligned} &\sum_{i=0}^{\infty} c_i (i+\alpha)(i+\alpha-1)(i+\alpha-2) \eta^{i+\alpha-3} \\ &\qquad - \frac{1}{8} \lambda_0 \sum_{i=4}^{\infty} c_{i-4} (i+\alpha-4)(i+\alpha-6) \eta^{i+\alpha-3} \\ &\qquad = \dot{a}_1 \eta \,. \end{aligned}$$

For $i = 0$:

$$c_0 \alpha(\alpha-1)(\alpha-2) \eta^{\alpha-3} = \eta \dot{a}_1 \,.$$

To satisfy the definition $c_0(T) \neq 0$ then the exponent is

$$\alpha = 4$$

and

$$c_0 = \frac{1}{4!}\dot{a}_1 \,.$$

For $i = 1$:

$$c_1(\alpha+1)\alpha(\alpha-1)\eta^{\alpha-2} = \eta\dot{a}_1$$

and with $\alpha = 4$ then $c_1(T) = 0$. Analogously, $c_2(T) = c_3(T) = 0$. For $i = 4m$, $m = 1, 2, 3, \ldots$ and noting the change of subscript for all $c_i(T)$:

$$\left[c_m(i+4)(i+3)(i+2) - \frac{1}{8}\lambda_0 i(i-2)c_{m-1}\right]\eta^{i+1} = \eta\dot{a}_1 \,.$$

Upon rearrangement, there is a recurrence relation for $c_m(T)$:

$$c_m = \frac{\lambda_0}{32}\frac{m(m-\frac{1}{2})}{(m+1)(m+\frac{3}{4})(m+\frac{2}{4})}c_{m-1} \,, \qquad c_0 = \frac{1}{4!}\dot{a}_1 \,.$$

Hence, for all $m \geq 1$:

$$c_m = \left(\frac{\lambda_0}{32}\right)^m \frac{m(m-\frac{1}{2})}{(m+1)(m+\frac{3}{4})(m+\frac{2}{4})}\frac{(m-1)(m-\frac{3}{2})}{m(m-\frac{1}{4})(m-\frac{2}{4})}\cdots\frac{1\cdot\frac{1}{2}}{2\cdot\frac{7}{4}\cdot\frac{6}{4}}\frac{1}{4!}\dot{a}_1 \,,$$

and after cancelation of terms, $c_m(T)$ can be written:

$$c_m = \frac{1}{2\cdot 4!}\frac{(1)_m}{(\frac{7}{4})_m}\left(\frac{\lambda_0}{32}\right)^m \frac{1}{m!\cdot(m+1)(m+\frac{1}{2})}\dot{a}_1 \,,$$

with the Pochhammer symbol $(a)_m$ defined as (2.27).

Therefore, (2.70) is:

$$f_{22}^{p_1} = \frac{1}{2\cdot 4!}\dot{a}_1\eta^4\sum_{m=0}^{\infty}\frac{(1)_m}{(\frac{7}{4})_m}\frac{(\frac{\lambda_0}{32}\eta^4)^m}{m!}\frac{1}{(m+1)(m+\frac{1}{2})}$$

or in terms of confluent hypergeometric functions:

$$f_{22}^{p_1} = \frac{1}{3}\dot{a}_1\int_0^{\eta}\eta_2\int_0^{\eta_2}\eta_1\,{}_1F_1\left(1;\frac{7}{4};\frac{\lambda_0}{32}\eta_1^4\right)\,\mathrm{d}\eta_1\,\mathrm{d}\eta_2 \,.$$

The confluent hypergeometric function ${}_1F_1\left(1;\frac{7}{4};\frac{\lambda_0}{32}\eta_1^4\right)$ is defined as (2.26):

$$ {}_1F_1\left(1;\frac{7}{4};\frac{\lambda_0}{32}\eta_1^4\right)=\sum_{n=0}^{\infty}\frac{(1)_n}{(\frac{7}{4})_n}\frac{\left(\frac{\lambda_0}{32}\eta_1^4\right)^n}{n!}\,. $$

Therefore, the particular solution is:

$$ f_{22}^{p_1}=\frac{1}{3}\dot{a}_1\left[\frac{1}{8}\eta^4+\frac{1}{84}\left(\frac{\lambda_0}{32}\right)\eta^8+\ldots\right],\qquad \eta=O(1) \tag{2.71} $$

with the expected $O(\dot{a}_1\eta^4)$ behaviour. Additionally, (2.71) satisfies the no-slip conditions (2.66).

As $\eta\to\infty$, the confluent hypergeometric function behaves like

$$ \begin{aligned} {}_1F_1\left(1;\frac{7}{4};\frac{\lambda_0}{32}\eta^4\right)&=-\frac{\Gamma(\frac{7}{4})}{\Gamma(\frac{3}{4})}\left(\frac{32}{\lambda_0}\eta^{-4}\right)\\ &\quad\cdot\left[\sum_{m=0}^{R-1}(-1)^m\left(\frac{1}{4}\right)_m\left(\frac{\lambda_0}{32}\eta^4\right)^{-m}+O\left(\left|\frac{\lambda_0}{32}\eta^4\right|^{-R}\right)\right],\qquad \eta\to\infty \end{aligned} \tag{2.72} $$

and satisfies the condition of no exponential growth. Hence, the particular solution (2.71) also satisfies the condition. The expected logarithmic behaviour is seen in Section 2.7 with matching at the outer edge of the viscous sublayer with the inner edge of the main boundary layer.

2.6.2 $a_2(T)\eta^2$ Particular Solution

A particular solution $f_{22}^{p_2}(\eta,T)$ for (2.69) can be found from balancing the $f'_{22}(\eta,T)$ term and the right hand side term. A particular solution is:

$$ f_{22}^{p_2}=\frac{7}{\lambda_0}a_0a_2\eta\,. \tag{2.73} $$

Nevertheless, upon application of the no-slip conditions (2.66) then

$$ a_2(T)=0 \tag{2.74} $$

since $a_0 \neq 0$ to avoid a non-trivial steady solution Ψ_0.

If $a_2 \neq 0$ then another particular solution for (2.69) is found using the Frobenius method analogous to that described for finding (2.71). Beginning with the Frobenius series:

$$f_{22}^{p_2} = \sum_{j=0}^{\infty} d_j(T)\eta^{j+\beta}\,, \qquad d_0(T) \neq 0$$

(where the exponent β is not to be confused with the eigenvalue from Section 2.4) then

$$\beta = 5$$

so that

$$d_0 = \frac{7}{4 \cdot 5!} a_0 a_2\,.$$

For $n = 1, 2, \ldots$

$$d_n = \frac{7}{16 \cdot 4!} \frac{(\frac{3}{4})_n}{(\frac{7}{4})_n} \left(\frac{\lambda_0}{32}\right)^n \frac{1}{n! \cdot (n+1)(n+\frac{5}{4})} a_0 a_2\,, \qquad d_0 = \frac{7}{4 \cdot 5!} a_0 a_2\,.$$

Hence, the solution is:

$$f_{22}^{p_2} = \frac{7}{4!} a_0 a_2 \int_0^{\eta} \int_0^{\eta_2} \eta_1^3 \, {}_1F_1\left(\frac{3}{4}; \frac{7}{4}; \frac{\lambda_0}{32}\eta_1^4\right) \mathrm{d}\eta_1 \, \mathrm{d}\eta_2\,.$$

The confluent hypergeometric function:

$$\begin{aligned} {}_1F_1\left(\frac{3}{4}; \frac{7}{4}; \frac{\lambda_0}{32}\eta^4\right) &= -\frac{\Gamma(\frac{7}{4})}{\Gamma(\frac{3}{4})} e^{\frac{\lambda_0}{32}\eta^4} \left(\frac{32}{\lambda_0}\eta^{-4}\right) \\ &\quad \cdot \left[\sum_{n=0}^{S-1} \left(\frac{1}{4}\right)_n \left(\frac{\lambda_0}{32}\eta^4\right)^{-n} + O\left(\left|\frac{\lambda_0}{32}\eta^4\right|^{-S}\right)\right], \qquad \eta \to \infty \end{aligned}$$

grows exponentially without bound. To satisfy the condition of no exponential growth and thus, to ensure matching with the external region as $\eta \to \infty$ then the confluent hypergeometric function must be removed by making $a_2(T) = 0$.

2.7 The Viscous Sublayer

The general solution for the f_{22} equation (2.65), from combining the complimentary (2.67) and non-trivial particular (2.71) solutions, is

$$f_{22} = \frac{1}{2}b_2(T)\eta^2 + \frac{1}{3}\dot{a}_1\left[\frac{1}{8}\eta^4 + \frac{1}{84}\left(\frac{\lambda_0}{32}\right)\eta^8 + \ldots\right]. \tag{2.75}$$

The Ψ_2 stream function (2.62); from (2.63), (2.64), (2.74) and (2.75); is also:

$$\Psi_2 = \frac{1}{2}b_2(T)\eta^2 + \frac{1}{3}\dot{a}_1\left[\frac{1}{8}\eta^4 + \frac{1}{84}\left(\frac{\lambda_0}{32}\right)\eta^8 + \ldots\right] + \ldots \tag{2.76}$$

Hence, the stream function (2.16) for the viscous sublayer is

$$\begin{aligned}\Psi = &\left\{(-s)^{\frac{3}{4}}\frac{1}{6}\lambda_0\eta^3 + (-s)^{\frac{3}{2}}\frac{1}{2}a_0\eta^2 + (-s)^{\frac{7}{4}}\left[-\frac{1}{6}\lambda_1\eta^3 + \frac{2}{7!}\lambda_0\lambda_1\eta^7\right]\right.\\ &\left. + (-s)^{\frac{9}{4}}\left[\frac{1}{2}b_0\eta^2 - \frac{1}{5!}a_0^2\eta^5 + \frac{1}{8!}\lambda_0 a_0^2\eta^9\right] + \ldots\right\}\\ &+ \Delta k\left\{(-s)^{-\frac{1}{2}}\frac{1}{2}a_1\eta^2 + (-s)^{\frac{1}{4}}\frac{1}{2}b_1\eta^2 + \ldots\right\}\\ &+ \frac{\Delta k}{\sigma}\left\{\frac{1}{2}b_2(T)\eta^2 + \frac{1}{3}\dot{a}_1\left[\frac{1}{8}\eta^4 + \frac{1}{84}\left(\frac{\lambda_0}{32}\right)\eta^8 + \ldots\right]\right\}\\ &+ \ldots\end{aligned} \tag{2.77}$$

which is valid for $\eta = O(1)$ by (2.19), with $(-s)$ given by (2.12). When $\Delta k \neq 0$ and as $\sigma \to \infty$, there is a slow $O(\Delta k)$ perturbation to the steady stream function (2.43) as the angle of attack changes with $a_1(T) \sim \Delta k$. Perturbations of $O(\frac{\Delta k}{\sigma})$ are proportional to rate of change of angle of attack with respect to time as parameterised by $\dot{a}_1(T)$. The larger the angle of attack and the faster its increase then the greater the perturbations.

As the point of zero skin friction is approached and $(-s) \to 0$, there seems to be a singularity caused by the $O(\frac{\Delta k}{\sigma})$ perturbation. Further analysis of the flow structure must incorporate the interaction region in Chapter 3.

Matching at the Outer Viscous Sublayer

As $\eta \to \infty$, the main boundary layer is approached from the viscous sublayer below. Upon substitution of the confluent hypergeometric function (2.72) into the Ψ_2 solution (2.76), then

$$\begin{aligned}\Psi_2 = {} & \frac{1}{2}b_2\eta^2 - \frac{1}{3}\dot{a}_1\frac{\Gamma(\frac{7}{4})}{\Gamma(\frac{3}{4})}\left(\frac{32}{\lambda_0}\right)\left[\int_0^\eta \eta_2 \int_0^{\eta_2} \eta_1^{-3}\,\mathrm{d}\eta_1\,\mathrm{d}\eta_2\right] \\ & - \frac{1}{3}\dot{a}_1\frac{\Gamma(\frac{7}{4})}{\Gamma(\frac{3}{4})}\left(\frac{32}{\lambda_0}\right)\sum_{m=1}^{R-1}(-1)^m\left(\frac{1}{4}\right)_m\left(\frac{32}{\lambda_0}\right)^m \\ & \qquad \cdot \left[\int_0^\eta \eta_2 \int_0^{\eta_2} \eta_1^{-4m-3}\,\mathrm{d}\eta_1\,\mathrm{d}\eta_2\right] \\ & + \ldots \end{aligned} \tag{2.78}$$

The first integral:

$$\frac{1}{3}\dot{a}_1\frac{\Gamma(\frac{7}{4})}{\Gamma(\frac{3}{4})}\left(\frac{32}{\lambda_0}\right)\left[\int_0^\eta \eta_2 \int_0^{\eta_2} \eta_1^{-3}\,\mathrm{d}\eta_1\,\mathrm{d}\eta_2\right] = \frac{1}{3!}\frac{\Gamma(\frac{7}{4})}{\Gamma(\frac{3}{4})}\left(\frac{32}{\lambda_0}\right)\dot{a}_1\ln\eta\,,$$

and the second integral:

$$\begin{aligned}&\frac{1}{3}\dot{a}_1\frac{\Gamma(\frac{7}{4})}{\Gamma(\frac{3}{4})}\left(\frac{32}{\lambda_0}\right)\sum_{m=1}^{R-1}(-1)^m\left(\frac{1}{4}\right)_m\left(\frac{32}{\lambda_0}\right)^m\left[\int_0^\eta \eta_2 \int_0^{\eta_2} \eta_1^{-3}\,\mathrm{d}\eta_1\,\mathrm{d}\eta_2\right] \\ &\quad = \frac{1}{3}\dot{a}_1\frac{\Gamma(\frac{7}{4})}{\Gamma(\frac{3}{4})}\left(\frac{32}{\lambda_0}\right)\sum_{m=1}^{R-1}(-1)^m\left(\frac{1}{4}\right)_m\left(\frac{32}{\lambda_0}\right)^m\left[\frac{1}{(-4m+2)(-4m)}\eta^{-4m}\right].\end{aligned}$$

Therefore, the most significant terms of (2.78) are from the first integral which have the expected logarithmic behaviour. As $\eta \to \infty$:

$$\Psi_2 = \frac{1}{2}b_2\eta^2 + \frac{1}{3}\dot{a}_1\left[\frac{1}{2}\frac{\Gamma(\frac{7}{4})}{\Gamma(\frac{3}{4})}\frac{32}{\lambda_0}\ln\eta + \ldots\right] + \ldots \tag{2.79}$$

The stream function expansion for the viscous sublayer as $\eta \to \infty$, to match with the main boundary layer, is:

$$\begin{aligned}\Psi = &\left\{(-s)^{\frac{3}{4}}\frac{1}{6}\lambda_0\eta^3 + (-s)^{\frac{3}{2}}\frac{1}{2}a_0\eta^2 + \ldots \right.\\ &\qquad \left. + (-s)^{\frac{9}{4}}\left[\frac{1}{2}b_0\eta^2 - \frac{1}{5!}a_0^2\eta^5 + \frac{1}{8!}\lambda_0 a_0^2\eta^9\right] + \ldots \right\}\\ &+ \Delta k\left\{(-s)^{-\frac{1}{2}}\frac{1}{2}a_1\eta^2 + (-s)^{\frac{1}{4}}\frac{1}{2}b_1\eta^2 + \ldots\right\}\\ &+ \frac{\Delta k}{\sigma}\left\{\frac{1}{2}b_2\eta^2 + \frac{1}{3}\dot{a}_1\left[\frac{1}{2}\frac{\Gamma(\frac{7}{4})}{\Gamma(\frac{3}{4})}\frac{32}{\lambda_0}\ln\eta + \ldots\right] + \ldots\right\}\\ &+ \ldots \end{aligned} \tag{2.80}$$

2.8 The Main Boundary Layer

The main boundary layer (region 2) corresponds to the simple displacement of the boundary layer by the viscous sublayer (region 3), whilst the sublayer exists to ensure that the no-slip conditions are satisfied at the wall. It is of the same limit process as the viscous sublayer as given by (2.8), (2.12) and (2.13). A change of variables $\eta = (-s)^{-\frac{1}{4}}Y$ is made in (2.79) then terms of the same order of magnitude as $(-s) \to 0$ are gathered to obtain the Ψ_2 stream function perturbation for the main boundary layer:

$$\Psi_2 = \frac{1}{3!}\frac{\Gamma(\frac{7}{4})}{\Gamma(\frac{3}{4})}\frac{32}{\lambda_0}\dot{a}_1\ln Y - \frac{1}{4!}\frac{\Gamma(\frac{7}{4})}{\Gamma(\frac{3}{4})}\frac{32}{\lambda_0}\dot{a}_1\ln(-s) + (-s)^{-\frac{1}{2}}\frac{1}{2}b_2Y^2 + \ldots$$

From the principle of matched asymptotic expansions and (2.80), the main boundary layer stream function as $Y \to 0$ is like:

$$\begin{aligned}\Psi = & \frac{1}{6}\lambda_0 Y^3 \\ & + \left\{ (-s)\left[\frac{1}{2}a_0 Y^2 - \frac{1}{2\cdot 5!}a_0^2 Y^5 + \ldots\right] + (-s)^{\frac{7}{4}}\left[\frac{1}{2}b_0 Y^2 + \ldots\right] + \ldots \right\} \\ & + \Delta k\left\{ (-s)^{-1}\frac{1}{2}a_1 Y^2 + (-s)^{-\frac{1}{4}}\frac{1}{2}b_1 Y^2 + \ldots \right\} \\ & + \frac{\Delta k}{\sigma}\left\{ (-s)^{-\frac{2}{4}}\frac{1}{2}b_2 Y^2 + \frac{1}{3!}\frac{\Gamma(\frac{7}{4})}{\Gamma(\frac{3}{4})}\left(\frac{32}{\lambda_0}\right)\dot{a}_1\left[\ln Y - \frac{1}{4}\ln(-s)\right] + \ldots \right\} \\ & + \ldots \end{aligned} \tag{2.81}$$

Hence, the rate of change in angle of attack $\dot{a}_1(T)$ has a logarithmic perturbing effect on the main boundary layer close to the point of zero skin friction.

Chapter 3

The Interaction Region

Further analysis of the flow structure must incorporate another region about the point of zero skin friction with a new limit process. There is an interaction region (regions I, II, III in Figure 2.4) where the boundary layer analysis fails. The displacement of the streamlines from the boundary layer no longer have a negligible effect on the external inviscid flow and eigenfunctions (2.43), (2.57), (2.76) in the series expansion (2.77) for the viscous sublayer become the same order of magnitude. The same hierarchical process in Chapter 2 is used to determine stream function solutions there. The stream function solutions and triple-deck structure are consistent by the method of matched asymptotic expansions if a solvability condition is satisfied.

Furthermore, there are small perturbations due to a slow change in angle of attack of the airfoil on a large time scale T compared to the external region time scale t, such that (2.13):

$$T = \sigma^{-1} t = O(1)\,, \qquad \sigma \to \infty\,.$$

The change in angle of attack is characterised by an asymmetry parameter $k(T)$ (2.3) (See Figure 2.1.) At the critical value $k = k_0$ is the first appearance of a point of zero skin friction $x = x_s$. The small variable:

$$\Delta k = k(T) - k_0 \to 0$$

represents the small change in angle of attack.

The stream function of the form (2.16):

$$\Psi = \mathrm{Re}^{\frac{1}{2}}\psi = \Psi_0(x,Y) + \Delta k\Psi_1(x,Y,T) + \frac{\Delta k}{\sigma}\Psi_2(x,Y,T) + \dots$$

for the viscous sublayer (2.77) is :

$$\begin{aligned}\Psi = &\left\{(-s)^{\frac{3}{4}}\frac{1}{6}\lambda_0\eta^3 + (-s)^{\frac{3}{2}}\frac{1}{2}a_0\eta^2 + (-s)^{\frac{7}{4}}\left[-\frac{1}{6}\lambda_1\eta^3 + \frac{2}{7!}\lambda_0\lambda_1\eta^7\right]\right.\\ &\left. + (-s)^{\frac{9}{4}}\left[\frac{1}{2}b_0\eta^2 - \frac{1}{5!}a_0^2\eta^5 + \frac{1}{8!}\lambda_0 a_0^2\eta^9\right] + \dots\right\}\\ &+ \Delta k\left\{(-s)^{-\frac{1}{2}}\frac{1}{2}a_1\eta^2 + (-s)^{\frac{1}{4}}\frac{1}{2}b_1\eta^2 + \dots\right\}\\ &+ \frac{\Delta k}{\sigma}\left\{\frac{1}{2}b_2(T)\eta^2 + \frac{1}{3}\dot{a}_1\left[\frac{1}{8}\eta^4 + \frac{1}{84}\left(\frac{\lambda_0}{32}\right)\eta^8 + \dots\right]\right\}\\ &+ \dots\end{aligned}$$

The first eigenfunctions of the first, steady series Ψ_0 and the second, perturbation series $\Delta k\Psi_1$, which are the second term of Ψ_0: $(-s)^{\frac{3}{2}}\frac{1}{2}a_0\eta^2$ and the first term of $\Delta k\Psi_1$: $\Delta k(-s)^{-\frac{1}{2}}\frac{1}{2}a_1\eta^2$, become the same order of magnitude in a region where

$$(-s) = O\left(|\Delta k|^{\frac{1}{2}}\right) . \tag{3.1}$$

The second eigenfunction term of the perturbation series $\Delta k\Psi_1$: $\Delta k(-s)^{\frac{1}{4}}\frac{1}{2}b_1\eta^2$ and the first eigenfunction of the third, forcing series $(\frac{\Delta k}{\sigma})\Psi_2$: $(\frac{\Delta k}{\sigma})\frac{1}{2}b_2\eta^2$ become the same order of magnitude in a region where

$$(-s) = O\left(\sigma^{-4}\right) . \tag{3.2}$$

The boundary layer stream function collapses to an interaction region stream function

like:

$$\Psi^* = \Psi_{00}(x, Y) + \Delta k \Psi_{10}(x, Y, T) + \frac{\Delta k}{\sigma} \Psi_{20}(x, Y, T) + \dots$$

3.1 Induced Pressure Gradient

If there is an induced pressure gradient due to the displacement effect of the boundary layer then it is induced by the normal velocity driving the viscous sublayer. The normal velocity and the viscous forces are both of the same order of magnitude.

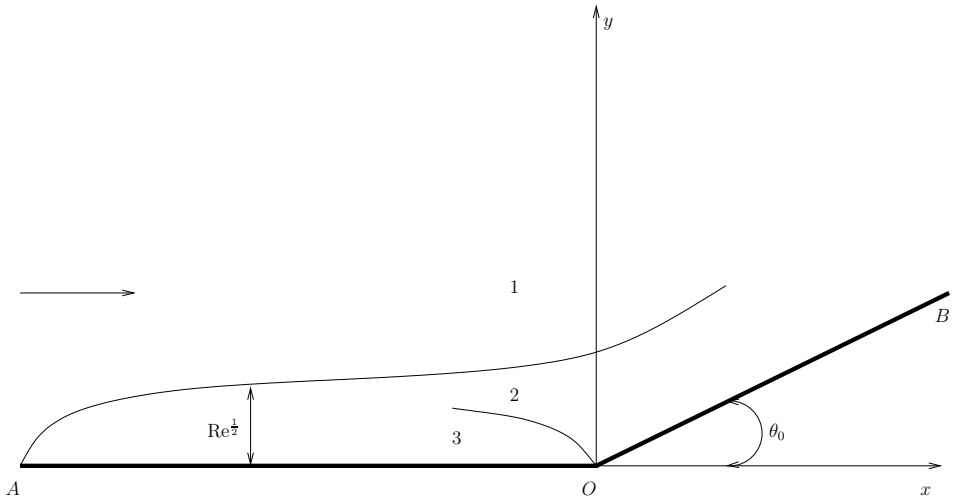

Figure 3.1: Asymptotic structure of characteristic flow regions: the external inviscid region 1; main boundary layer 2; viscous sublayer 3, near a stationary body contour AOB with small turning angle θ_0.

To determine the induced pressure gradient then consider the case of the onset of separation near a corner of a stationary body contour with small turning angle.[1] (See Figure 3.1.) Consider the region of external inviscid flow (region 1) where the asymptotic analysis of the Navier-Stokes equations is associated with the limit process $x = O(1)$, $y = O(1)$, as $\mathrm{Re} \to \infty$. The series expansions of the dependent flow variables tangential velocity u, normal velocity v and pressure p are of the form:

$$u = 1 + \epsilon u_1(x, y) + \dots \qquad v = \epsilon v_1(x, y) + \dots \qquad p = \epsilon p_1(x, y) + \dots$$

where ϵ is a small parameter inversely proportional to Re such that $\epsilon(\mathrm{Re}) \to 0$.

[1] Sychev, Ruban, Sychev & Korolev (1998d)

From the Navier-Stokes equations, the linearised Euler equations for u_1, v_1 and p_1 are obtained. It follows that the complex velocity

$$w_1(z) = u_1 - iv_1\,, \qquad z = x + iy$$

is an analytic function and the pressure perturbation satisfies the linearised Bernoulli equation

$$p_1 = -u_1\,.$$

The flow regime is such that separation is either absent or is localised within a small neighbourhood of the corner. The boundary condition at the surface of the solid body is the condition of no normal flow:

$$\begin{aligned} v_1(x,0) &= 0\,, & -1 < x < 0\,;\\ v_1(x,0) &= \theta_0\,, & 0 < x < l \end{aligned}$$

where l is the dimensionless length of the plate OB and θ_0 is the small turning angle of the contour. (See Figure (3.1).) The condition uniquely determines the leading series expansion term of the function w_1 in the vicinity of the corner:

$$w_1 = \frac{\theta_0}{\pi}\ln z + d - i\theta + o(1)\,, \qquad |z| \to 0\,.$$

The constant d can only be determined by solving the flow problem for the entire external inviscid flow taking into account all the boundary conditions.

The real part of the complex velocity w_1 is the tangential velocity u_1. By the linearised Bernoulli's equation $p_1 = -u_1$, the pressure at the outer edge of the boundary layer has a logarithmic singularity:

$$p_1 = -\frac{\theta_0}{\pi}\ln|x| - d + o(1)\,, \qquad |x| \to 0\,.$$

Hence, the pressure gradient behaves as

$$\frac{\mathrm{d}p_1}{\mathrm{d}x} = -\frac{\theta_0}{\pi}\frac{1}{x} + O(1)\,, \qquad |x| \to 0\,.$$

Using the body contour corner analogy, the pressure perturbation induced by the displacement effect of the boundary layer on the airfoil is

$$p_i \sim U_0^2 \cdot -\frac{\theta_0}{\pi} \ln|x - x_s| + O(1)\,, \qquad x \to x_s\,.$$

The pressure perturbation comes from the Bernoulli principle:

$$p_i \sim -U_0^2\,.$$

The tangential velocity U_0 is the value of the longitudinal velocity U_e at the outer edge of the boundary layer evaluated at the point of zero skin friction $x = x_s$ for $k = k_0$. When passing through the point of zero skin friction, the slope of the streamlines θ (by analogy to the angle of inclination (2.53)) changes by

$$\theta_0 = \mathrm{Re}^{-\frac{1}{2}} \cdot -\frac{2a_0}{\lambda_0}\,.$$

Therefore, the induced pressure is

$$p_i \sim \mathrm{Re}^{-\frac{1}{2}} \frac{2a_0 U_0^2}{\pi\lambda_0} \ln|x - x_s| + O(1)\,, \qquad x \to x_s$$

and the induced pressure gradient is

$$\frac{\mathrm{d}p_i}{\mathrm{d}x} \sim O\left(\frac{\mathrm{Re}^{-\frac{1}{2}}}{x - x_s}\right)\,, \qquad x \to x_s\,. \tag{3.3}$$

The pressure gradient is induced by the normal velocity of the same order of magnitude as the viscous forces. Hence, balancing the first eigenfunction from the

viscous sublayer stream function:

$$\frac{\partial^3 \Psi_0}{\partial Y^3} = (-s)^{\frac{3}{2}} \frac{1}{2} a_0^2 \eta^2 + \ldots \qquad s = x - x_s \,, \qquad \eta = O(1)$$

with the induced pressure gradient, then:

$$O\left((-s)^{\frac{3}{2}}\right) \sim O\left(\frac{\mathrm{Re}^{-\frac{1}{2}}}{s}\right) .$$

Therefore, an interaction region develops of the size:

$$(-s) = O\left(\mathrm{Re}^{-\frac{1}{5}}\right) \tag{3.4}$$

where the pressure perturbations induced by the displacement effect of the boundary layer influence flow in the boundary layer itself. By (3.1) and (3.4), the asymmetry parameter:

$$|\Delta k|^{\frac{1}{2}} = O\left(\mathrm{Re}^{-\frac{1}{5}}\right) . \tag{3.5}$$

Combining (3.4) and (3.2), the time parameter of a flow regime with an induced pressure gradient is:

$$\sigma = O\left(\mathrm{Re}^{\frac{1}{20}}\right) .$$

such that the time scale is:

$$T = \mathrm{Re}^{-\frac{1}{20}} t \,. \tag{3.6}$$

On this time scale, the induced pressure gradient exists.

Interaction Region Discussion

A restriction is placed on the asymmetry parameter Δk and time parameter σ such that the strength of the induced pressure gradient is negligible, in particular:

$$O\left(\sigma^{-4}\right) = O\left(|\Delta k|^{\frac{1}{2}}\right) > O\left(\mathrm{Re}^{-\frac{1}{5}}\right) . \tag{3.7}$$

This may be comparable to marginal separation theory, when an angle of attack is forced to approach a critical angle to reduce an adverse pressure gradient and Goldstein's singularity.

The quasi-steady interaction region considered here (as illustrated in Figure 3.2) is contained within the classical interaction region of length scale $\mathrm{Re}^{-\frac{1}{5}}$, so as to not destroy the triple-deck system. Consequently, as $\Delta k \to \mathrm{Re}^{-\frac{2}{5}}$ by (3.5), the induced pressure gradient comes into action and the classical interaction region results are recovered.[2]

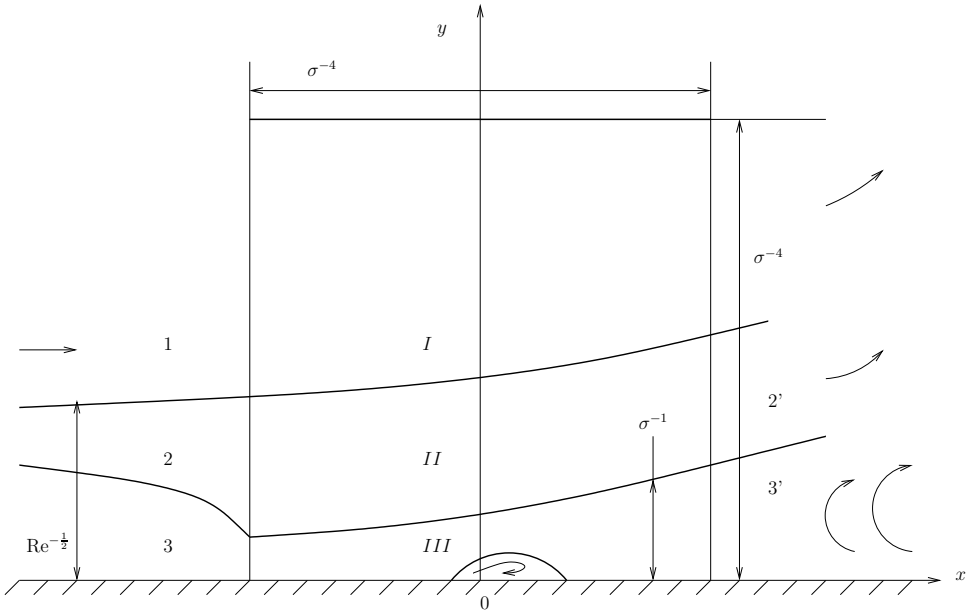

Figure 3.2: The triple-deck interaction region: I, II, III; viscous sublayer: 3, 3'; external inviscid region: 1; main boundary layer: 2, 2'.

From hereon in the analysis is of an interactive theory when (3.7) is true and the induced pressure gradient is negligible. The flow structure develops in an interaction region where

$$(-s) = O\left(\sigma^{-4}\right) , \qquad \Delta k = O\left(\sigma^{-8}\right) , \qquad O(\sigma) > O\left(\mathrm{Re}^{\frac{1}{20}}\right) . \tag{3.8}$$

The Reynolds number dependence has been removed from the analysis for now. The objective is to study the effects of the slow perturbations of the airfoil $a_1(T)$ in the

[2]Flow on the length scale (3.4) and time scale (3.6) follows marginal separation theory, as described by Sychev et al. (1998b), Smith (1982a) and Elliott & Smith (1987), for example.

large time scale T on the interaction region flow structure, and find a solvability condition using the hierarchical matching procedure (as illustrated in Figure 3.3.) A theory can be constructed on the basis of a the limit process:

$$k(T) = k_0 + \sigma^{-8} k_1(T)\,, \qquad k_1(T) = O(1)\,, \qquad \sigma \to \infty \tag{3.9}$$

which describes the appearance of the point of zero skin friction at the leading edge and allows the transition to the conventional boundary layer theory in the limit as $k_1(T) \to -\infty$. Indeed, with $\Delta k = O(\sigma^{-8}) > O(\mathrm{Re}^{-\frac{2}{5}})$, "this flow regime covers the whole range of angle of attack associated with the evolution of a short bubble from the moment of its generation until its destruction."[3]

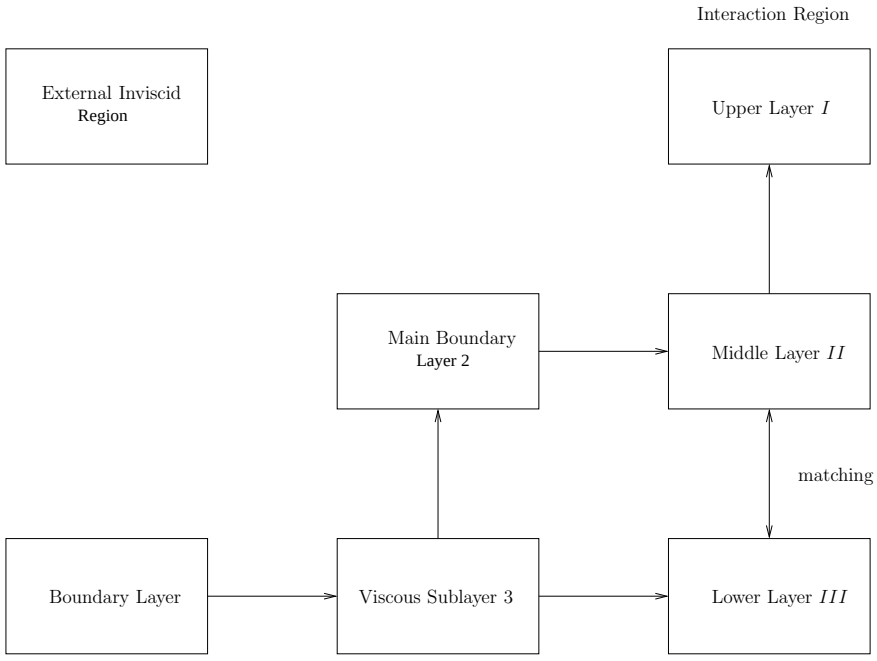

Figure 3.3: The hierarchical matching procedure to find stream functions series expansions for boundary layers and interaction regions.

[3]Sychev et al. (1998b).

3.2 The Middle Layer

The middle layer (region II in Figure 3.2) of the interaction region continues from the main boundary layer (region 2) and has a similar limit process:

$$s^* = x^* - x_s = \sigma^4 s = O(1)\,, \qquad Y = O(1)\,, \qquad \sigma \to \infty\,. \tag{3.10}$$

The main boundary layer stream function (2.81) in middle layer variables (3.9) and (3.10), is:

$$\Psi = \frac{1}{6}\lambda_0 Y^3 + \left\{ \sigma^{-4} s^* \left[\frac{1}{2} a_0 Y^2 - \frac{1}{2 \cdot 5!} a_0^2 Y^5 + \ldots \right] + \ldots \right\}$$
$$+ \sigma^{-8} k_1 \left\{ \sigma^4 s^{*-1} \frac{1}{2} a_1 Y^2 + \ldots \right\} + \ldots$$

that is

$$\Psi = \frac{1}{6}\lambda_0 Y^3 + \sigma^{-4} \left\{ s^* \left[\frac{1}{2} a_0 Y^2 - \frac{1}{2 \cdot 5!} a_0^2 Y^5 + \ldots \right] + k_1 s^{*-1} \frac{1}{2} a_1 Y^2 + \ldots \right\} + \ldots$$

Hence, the middle layer stream function is assumed to be of the form:

$$\Psi = \Psi_{00}(Y) + \sigma^{-4} \Psi_1^*(x^*, Y, T) + \ldots \qquad \Psi_{00}(Y) = \frac{1}{6}\lambda_0 Y^3 \tag{3.11}$$

and the condition of matching with the main boundary layer is

$$\Psi_1^*(x^*, Y, T) = s^* \left[\frac{1}{2} a_0 Y^2 - \frac{1}{2 \cdot 5!} a_0^2 Y^5 + \ldots \right] + k_1 s^{*-1} \frac{1}{2} a_1 Y^2 + \ldots \tag{3.12}$$
$$s^* \to -\infty\,.$$

The middle layer equation, from the boundary layer equation (2.14) with (3.10), is:

$$\frac{1}{\sigma} \frac{\partial^2 \Psi}{\partial T \partial Y} + \sigma^4 \frac{\partial \Psi}{\partial Y} \frac{\partial^2 \Psi}{\partial x^* \partial Y} - \sigma^4 \frac{\partial \Psi}{\partial x^*} \frac{\partial^2 \Psi}{\partial Y^2} = \frac{\partial^3 \Psi}{\partial Y^3} - \sigma^4 \frac{\partial p}{\partial x^*}\,.$$

The pressure gradient is the superposition of the original Taylor series expansion (2.15) and the induced pressure gradient: $\frac{\partial P^*}{\partial x^*}$, from (3.3):

$$\sigma^4 \frac{\partial p}{\partial x^*} = \lambda_0 + \sigma^{-4} s^* \lambda_1 + \ldots + \mathrm{Re}^{-\frac{1}{2}} \sigma^4 \frac{\partial P^*}{\partial x^*} + \ldots \tag{3.13}$$

Recall that the induced pressure gradient is negligible in this regime with scales (3.8).

Substituting (3.11) and (3.13) into the middle layer equation, and gathering the $O(1)$ terms, gives the $\Psi_1^*(x^*, Y, T)$ equation:

$$\frac{\partial \Psi_{00}}{\partial Y} \frac{\partial^2 \Psi_1^*}{\partial x^* \partial Y} - \frac{\partial^2 \Psi_{00}}{\partial Y^2} \frac{\partial \Psi_1^*}{\partial x^*} = \frac{\partial^3 \Psi_{00}}{\partial Y^3} - \lambda_0 \,.$$

Rearranging the $\Psi_1^*(x^*, Y, T)$ equation gives a solution for $\Psi_1^*(x^*, Y, T)$ in the form:

$$\Psi_1^* = \Psi_{00}' \left[\frac{A_1(x^*, T)}{\lambda_0} + s^* \int_0^Y \frac{\Psi_{00}''' - \lambda_0}{(\Psi_{00}')^2} \, \mathrm{d}Y \right] \tag{3.14}$$

where, by (3.11):

$$\Psi_{00}(Y) = \frac{1}{6} \lambda_0 Y^3 \,. \tag{3.15}$$

The $A_1(x^*, T)$ term is arbitrary except the condition of matching (3.12) to the main boundary layer requires that

$$A_1(x^*, T) = k_1 s^{*-1} a_1 + s^* \left[a_0 - \frac{1}{5!} a_0 Y^3 + \ldots \right] + \ldots \qquad s^* \to 0 \tag{3.16}$$

Moreover, substituting the middle layer stream function (3.11) and the pressure gradient (3.13) into the second, y-momentum equation (1.2) for the boundary layer then gathering $O(\mathrm{Re}^{\frac{1}{2}})$ terms, gives:

$$\frac{\partial p}{\partial Y} = 0 \,.$$

Differentiating with respect to x^* indicates that

$$\frac{\partial}{\partial Y}\left(\frac{\partial P^*}{\partial x^*}\right) = 0\,. \tag{3.17}$$

The induced pressure gradient, although negligible in this regime, would remain unchanged across the middle layer of the classical interaction region.

3.3 The Lower Layer

The lower layer (region III in Figure 3.2) of the interaction region continues from the viscous sublayer (region 3) and hence, has the limit process:

$$s^* = x^* - x_s = \sigma^4 s = O(1)\,,\; Y^* = \sigma Y = O(1)\,,\; \eta^* = \frac{Y^*}{(s^*)^{\frac{1}{4}}}\,,\; \sigma \to \infty\,. \tag{3.18}$$

The viscous sublayer stream function (2.77) in lower layer variables (3.9) and (3.18), is:

$$\begin{aligned}
\Psi = &\left\{ \sigma^{-3}\frac{1}{6}\lambda_0 Y^{*3} + \sigma^{-6}s^{*\frac{3}{2}}\frac{1}{2}a_0\eta^{*2} + \dots \right. \\
&\qquad \left. + \sigma^{-9}s^{*\frac{9}{4}}\left[\frac{1}{2}b_0\eta^{*2} - \frac{1}{5!}a_0^2\eta^{*5} + \frac{1}{8!}\lambda_0 a_0^2\eta^{*9}\right] + \dots \right\} \\
&+ \sigma^{-8}k_1\left\{ \sigma^2 s^{*-\frac{1}{2}}\frac{1}{2}a_1\eta^{*2} + \sigma^{-1}s^{*\frac{1}{4}}\frac{1}{2}b_1\eta^{*2} + \dots \right\} \\
&+ \sigma^{-9}k_1\left\{ \frac{1}{2}b_2\eta^{*2} + \dots \right\} \\
&+ \dots
\end{aligned}$$

that is

$$\Psi = \sigma^{-3}\frac{1}{6}\lambda_0 Y^{*3} + \sigma^{-6}\left\{ s^*\frac{1}{2}a_0 Y^{*2} + k_1 s^{*-1}\frac{1}{2}a_1 Y^{*2} + \dots \right\}$$
$$+ \sigma^{-9}\left\{ s^{*\frac{7}{4}}\frac{1}{2}b_0 Y^{*2} - s^*\frac{1}{5!}a_0^2 Y^{*5} + \frac{1}{8!}\lambda_0 a_0^2 Y^{*9} \right.$$
$$\left. + s^{*-\frac{1}{4}}k_1\frac{1}{2}b_1 Y^{*2} + s^{*-\frac{1}{2}}k_1\frac{1}{2}b_2 Y^{*2} + \dots \right\}$$
$$+ \dots \tag{3.19}$$

Hence, the lower layer stream function is assumed to be of the form:

$$\Psi = \sigma^{-3}\Psi^*_{00}(Y^*) + \sigma^{-6}\Psi^*_1(x^*, Y^*, T) + \sigma^{-9}\Psi^*_2(x^*, Y^*, T) + \dots \tag{3.20}$$
$$\Psi^*_{00} = \frac{1}{6}\lambda_0 Y^{*3}$$

The lower layer equation, from the boundary layer equation (2.14) with (3.18), is:

$$\frac{\partial^2\Psi}{\partial T\partial Y^*} + \sigma^6\frac{\partial\Psi}{\partial Y^*}\frac{\partial^2\Psi}{\partial x^*\partial Y^*} - \sigma^6\frac{\partial\Psi}{\partial x^*}\frac{\partial^2\Psi}{\partial Y^{*2}} = \sigma^3\frac{\partial^3\Psi}{\partial Y^{*3}} - \sigma^4\frac{\partial p}{\partial x^*}$$

3.3.1 $\Psi^*_1(x^*, Y^*, T)$ Solution

Substituting (3.20) and pressure gradient (3.13) into the lower layer equation, and gathering the $O(\sigma^{-3})$ terms, gives the Ψ^*_1 equation:

$$\frac{1}{2}\lambda_0 Y^{*2}\frac{\partial^2\Psi^*_1}{\partial x^*\partial Y^*} - \lambda_0 Y^{*2}\frac{\partial\Psi^*_1}{\partial x^*} = \frac{\partial^3\Psi^*_1}{\partial Y^{*3}}\,. \tag{3.21}$$

The boundary conditions are

$$\Psi^*_1 = \frac{\partial\Psi^*_1}{\partial Y^*} = 0\,, \qquad Y^* = 0\,. \tag{3.22}$$

The condition of matching with the middle layer (region II) and the viscous sublayer (region 3) is that

$$\Psi_1^* = \frac{1}{2}A_1(x^*,T)Y^{*2} + \dots \qquad Y^* \to \infty\,,\; x^* \to -\infty\,. \tag{3.23}$$

The solution of the boundary value problem (3.21), (3.22), (3.23) is:

$$\Psi_1^* = \frac{1}{2}A_1(x^*,T)Y^{*2}\,, \tag{3.24}$$

where the function $A_1(x^*,T)$ remains arbitrary in this layer.

3.3.2 $\Psi_2^*(x^*,Y^*,T)$ Solution & the $A_1(x^*,T)$ Function

To determine the function $A_1(x^*,T)$, the Ψ_2^* boundary value problem must also be considered. The Ψ_2^* equation is sought in a similar way to (3.21) but comes from collecting the $O(\sigma^{-6})$ terms instead. The Ψ_2^* equation is

$$\frac{\partial A_1}{\partial T}Y^* + \frac{1}{2}A_1\frac{\partial A_1}{\partial x^*}Y^{*2} + \frac{1}{2}\lambda_0 Y^{*2}\frac{\partial^2\Psi_2^*}{\partial x^*\partial Y^*} - \lambda_0 Y^*\frac{\partial\Psi_2^*}{\partial x^*} = \frac{\partial^3\Psi_2^*}{\partial Y^{*3}}\,. \tag{3.25}$$

The induced pressure gradient from (3.13): $\frac{\partial P^*}{\partial x^*}$, does not balance with the $O(\sigma^{-6})$ terms since $O(\sigma^{-6}) > O(\mathrm{Re}^{-\frac{1}{2}}\sigma^4)$, as discussed in Section 3.1. The boundary conditions are

$$\Psi_2^* = \frac{\partial\Psi_2^*}{\partial Y^*} = 0\,, \qquad Y^* = 0\,. \tag{3.26}$$

The condition of matching with the viscous sublayer (3.19) is

$$\Psi_2^* = \frac{1}{8!}\lambda_0 a_0^2 Y^{*9} + s^*\frac{1}{5!}a_0^2 Y^{*5} + \frac{1}{2}A_2(x^*,T)Y^{*2} + \dots \qquad x^* \to -\infty$$

where

$$A_2 = s^{*\frac{7}{4}}b_0 + s^{*-\frac{1}{4}}b_1 + s^{*-\frac{2}{4}}b_2 + \dots = O(s^{*\frac{7}{4}})\,, \qquad x^* \to -\infty\,. \tag{3.27}$$

The condition of matching with the middle layer (3.14) and (3.16), is constructed so that it is of the same order of magnitude as (3.27). By (3.16):

$$A_1^2 - x^{*2}a_0^2 - 2k_1a_0a_1 = x^{*-2}k_1^2a_1^2 + \ldots = O(s^{*-2})$$

and by the similarity variable (3.18): $Y^* = O(s^{*\frac{1}{4}})$. Hence, the condition of matching with the middle layer is

$$\Psi_2^* = \frac{1}{2\lambda_0}\left[A_1^2(x^*,T) - a_0^2x^{*2} - 2k_1a_0a_1\right]Y^* + \ldots = O(s^{*\frac{7}{4}})\,, \qquad Y^* \to \infty$$

The combined condition of matching to the viscous sublayer and middle layer is:

$$\begin{aligned}\Psi_2^* = {} & \frac{1}{8!}\lambda_0a_0^2Y^{*9} + s^*\frac{1}{5!}a_0^2Y^{*5} + \frac{1}{2}A_2(x^*,T)Y^{*2} \\ & + \frac{1}{2\lambda_0}\left[A_1^2(x^*,T) - a_0^2x^{*2} - 2k_1a_0a_1\right]Y^* + o(1)\,, \\ & Y^* \to \infty\,,\ x^* \to -\infty \end{aligned} \tag{3.28}$$

with $A_2(x^*,T)$ (3.27).[4] The $A_1(x^*,T)$ function is to be determined.

A Change Of Variable & Affine Transformation

Analogous to Ruban (1982b), a change of variable:

$$\Psi_2^* = \hat{\Psi}_2 + \frac{\lambda_0}{8!}a_0^2Y^{*9} + \frac{1}{5!}a_0^2x^*Y^{*5} + \frac{1}{2\lambda_0}\left[A_1^2 - a_0^2x^{*2} - 2k_1a_0a_1\right]Y^*$$

is made, to simplify the problem. The Ψ_2^* equation (3.25) becomes:

$$\frac{\partial A_1}{\partial T}Y^* + \frac{1}{2}\lambda_0Y^{*2}\frac{\partial^2\hat{\Psi}_2}{\partial x^*\partial Y^*} - \lambda_0Y^*\frac{\partial\hat{\Psi}_2}{\partial x^*} = \frac{\partial^3\hat{\Psi}_2}{\partial Y^{*3}}$$

[4] Ruban (1982a)

with the boundary conditions (3.26):

$$\hat{\Psi}_2 = 0\,, \qquad \frac{\partial \hat{\Psi}_2}{\partial Y^*} = \frac{1}{2\lambda_0}\left[A_1^2 - a_0^2 x^{*2} - 2k_1 a_0 a_1\right]\,, \qquad Y^* = 0$$

and condition of matching (3.28):

$$\hat{\Psi}_2 = \frac{1}{2} A_2(x^*, T) Y^{*2}\,, \qquad Y^* \to \infty\,,\, x^* \to -\infty\,.$$

Next, the affine transformations:

$$\begin{aligned}
&\hat{\Psi}_2 = a_0^{\frac{11}{10}} U_{00}^{\frac{9}{5}} \lambda_0^{-\frac{17}{10}} \bar{\Psi}_2\,, \quad x^* = a_0^{-\frac{2}{5}} U_{00}^{\frac{4}{5}} \lambda_0^{-\frac{1}{5}} \bar{x}\,, \quad T = a_0^{-\frac{9}{10}} U_{00}^{-\frac{1}{5}} \lambda_0^{\frac{3}{10}} \bar{T}\,,\\
&y^* = a_0^{-\frac{1}{10}} U_{00}^{\frac{1}{5}} \lambda_0^{-\frac{3}{10}} \bar{y}\,, \quad A_1 = a_0^{\frac{3}{5}} U_{00}^{\frac{4}{5}} \lambda_0^{-\frac{1}{5}} \bar{A}_1\,, \quad a = k_1(-a_1) a_0^{-\frac{1}{5}} U_{00}^{-\frac{8}{5}} \lambda_0^{\frac{2}{5}}
\end{aligned} \tag{3.29}$$

are applied, to reduce the number of parameters in the system. The equation becomes:

$$\frac{1}{2}\bar{Y}^2 \frac{\partial^2 \bar{\Psi}_2}{\partial \bar{x} \partial \bar{Y}} - \bar{Y} \frac{\partial \bar{\Psi}_2}{\partial \bar{x}} = \frac{\partial^3 \bar{\Psi}_2}{\partial \bar{Y}^3} - \frac{\partial \bar{A}_1}{\partial \bar{T}} \bar{Y} \tag{3.30}$$

with the boundary conditions:

$$\bar{\Psi}_2 = 0\,, \qquad \frac{\partial \bar{\Psi}_2}{\partial \bar{Y}} = g(\bar{x}, \bar{T}) = -\frac{1}{2}\left(\bar{A}_1^2 - \bar{x}^2 + 2a\right)\,, \qquad \bar{Y} = 0 \tag{3.31}$$

and the conditions of matching to the middle layer and viscous sublayer:

$$\bar{\Psi}_2 = O(\bar{Y}^2)\,,\, \bar{Y} \to \infty\,; \qquad \bar{\Psi}_2 = o(1)\,,\, \bar{x} \to -\infty\,. \tag{3.32}$$

3.3.3 The Fourier Transformation Boundary Value Problem

A Fourier transformation is applied to the boundary value problem (3.30), (3.31) and (3.32), where by definition:

$$\Phi(k, \bar{Y}, \bar{T}) = \frac{1}{\sqrt{2\pi}} \int_{-\infty}^{\infty} \bar{\Psi}_2(\bar{x}, \bar{Y}, \bar{T}) e^{-ik\bar{x}}\, \mathrm{d}\bar{x}\,.$$

Hence, the equation becomes

$$\frac{\mathrm{d}^3\Phi}{\mathrm{d}\bar{Y}^3} - \frac{1}{2}ik\bar{Y}^2\frac{\mathrm{d}\Phi}{\mathrm{d}\bar{Y}} + ik\bar{Y}\Phi = \bar{Y}R(k,\bar{T})\,, \tag{3.33}$$

where $R(k,\bar{T})$ is the Fourier transform of $\frac{\partial \bar{A}_1}{\partial T}$ such that

$$R(k,\bar{T}) = \frac{1}{\sqrt{2\pi}}\int_{-\infty}^{\infty}\frac{\partial \bar{A}_1}{\partial \bar{T}}(\bar{x},\bar{T})e^{ik\bar{x}}\,\mathrm{d}x\,.$$

The boundary conditions become

$$\Phi = 0\,;\ \frac{\mathrm{d}\Phi}{\mathrm{d}\bar{Y}} = G(k,\bar{T})\,, \qquad \bar{Y} = 0\,, \tag{3.34}$$

where $G(k,\bar{T})$ is the Fourier transform of $g(\bar{x},\bar{T})$ such that

$$G(k,\bar{T}) = \frac{1}{\sqrt{2\pi}}\int_{-\infty}^{\infty} g(\bar{x},\bar{T})e^{ik\bar{x}}\,\mathrm{d}\bar{x}\,.$$

The condition of matching is

$$\Phi = O(1)\,, \qquad \bar{Y}\to\infty\,. \tag{3.35}$$

The general solution of the problem (3.33), (3.34) and (3.35) is

$$\Phi = C_1\Phi_1 + C_2\Phi_2 + C_3\Phi_3 + R(k,\bar{T})\Phi^*\,,$$

where $\Phi_1(\bar{Y},\bar{T})$, $\Phi_2(\bar{Y},\bar{T})$, $\Phi_3(\bar{Y},\bar{T})$ are complimentary solutions of the homogeneous equation and $\Phi^*(\bar{Y},\bar{T})$ is the particular integral.

Complimentary Solutions

The complimentary solutions Φ_1, Φ_2 and Φ_3 are linearly independent solutions of the homogeneous form of (3.33). They can be chosen so that their Taylor series

expansions about the point $\bar{Y} = 0$ begin with 1, $\bar{Y}$ or $\bar{Y}^2$, respectively. The boundary conditions at $\bar{Y} = 0$:

$$\begin{aligned} &\Phi_1 = 1\,, \qquad \frac{\mathrm{d}\Phi_1}{\mathrm{d}\bar{Y}} = 0\,, \qquad \frac{\mathrm{d}^2\Phi_1}{\mathrm{d}\bar{Y}^2} = 0\,; \\ &\Phi_2 = 0\,, \qquad \frac{\mathrm{d}\Phi_2}{\mathrm{d}\bar{Y}} = 1\,, \qquad \frac{\mathrm{d}^2\Phi_2}{\mathrm{d}\bar{Y}^2} = 0\,; \\ &\Phi_3 = 0\,, \qquad \frac{\mathrm{d}\Phi_3}{\mathrm{d}\bar{Y}} = 0\,, \qquad \frac{\mathrm{d}^2\Phi_3}{\mathrm{d}\bar{Y}^2} = 1 \end{aligned} \tag{3.36}$$

require that

$$C_1 = 0\,, \qquad C_2 = G(k, \bar{T})\,, \qquad C_3 = C \tag{3.37}$$

where C is an arbitrary constant. Indeed, by observation:

$$\Phi_3 = \frac{1}{2}\bar{Y}^2\,.$$

The complimentary solution $\Phi_2(\bar{Y}, \bar{T})$ may be found using the Frobenius method:

$$\Phi_2 = \sum_{m=0}^{\infty} D_m(\bar{T})\bar{Y}^{4m+\beta}\,, \qquad D_0(\bar{T}) \neq 0$$

where $D_m(\bar{T})$ are functions of time to be found from initial conditions. For $m = 0$:

$$\frac{\mathrm{d}\Phi_2}{\mathrm{d}\bar{Y}} = D_0\beta\bar{Y}^{\beta-1} = 1 \Rightarrow D_0 = 1\,,\ \beta = 1$$

by the boundary conditions (3.36). Upon substitution into homogeneous form of (3.33), then:

$$\sum_{m=0}^{\infty} D_m(4m+1)(4m)(4m-1)Y^{4m-2} - \frac{1}{2}ik\sum_{m=1}^{\infty} D_{m-1}(4m-5)Y^{4m-2} = 0\,.$$

For $m = 0$, there is the trivially true: $D_0 \cdot 0 = 0$.

For all $m \geq 1$, there is the recurrence relation for $D_m(T)$:

$$D_m = \left(\frac{ik}{32}\right) \frac{(m-\frac{5}{4})}{(m+\frac{1}{4})(m)(m-\frac{1}{4})} D_{m-1}\,, \qquad D_0 = 1\,.$$

For example, for $m = 1$:

$$D_1 = \left(\frac{ik}{32}\right) \frac{-\frac{1}{4}}{\frac{5}{4}\cdot\frac{3}{4}}\,.$$

The functions for $m \geq 1$ can be written:

$$D_m = -\Gamma\left(\frac{5}{4}\right)\left(\frac{ik}{32}\right)^m \frac{1}{m!\cdot\Gamma(m+\frac{1}{4}+1)\cdot(4m-1)}\,.$$

Hence, the complimentary solution is:[5]

$$\Phi_2 = Y - \Gamma\left(\frac{5}{4}\right)\sum_{m=1}^{\infty}\left(\frac{ik}{32}\right)^m \frac{1}{m!\cdot\Gamma(m+\frac{1}{4}+1)\cdot(4m-1)}\bar{Y}^{4m+1}\,,$$

or, in terms of Bessel functions of the first kind:

$$\Phi_2 = -\frac{2\Gamma(\frac{5}{4})}{\Omega^{\frac{1}{4}}e^{\frac{i\pi}{4}}}\left\{ -\frac{1}{\Gamma(\frac{5}{4})}\left(\frac{\xi}{2}\right)^{\frac{1}{2}} + \frac{\xi}{8}\int_0^{\xi}\left(\frac{\xi_1}{2}\right)^{-\frac{3}{2}}\left[\left(\frac{\xi_1}{2}\right)^{-\frac{1}{4}} J_{\frac{1}{4}}(\xi_1) - \frac{1}{\Gamma(\frac{5}{4})}\right] \mathrm{d}\xi_1 \right\} \tag{3.38}$$

where

$$\Omega = \frac{ik}{2}\,, \qquad \xi = \frac{i\Omega^{\frac{1}{2}}\bar{Y}^2}{2}\,. \tag{3.39}$$

Bessel functions of the first kind are defined in Section 3.3.4.

Particular Solution

A particular solution of (3.33) which satisfies the condition of matching (3.35) can be determined from observation:

$$\Phi^* = \frac{1}{ik}\,,$$

[5]Ruban (1982a)

which is also the first term in an asymptotic series solution. Analogous to the Frobenius method for finding the complimentary solution (3.38), the particular solution, in terms of Bessel functions of the first kind, is:[6]

$$\Phi^* = \frac{\Gamma(\frac{3}{4})}{4\Omega}\left(\frac{\xi}{2}\right)\int_0^{\xi}\left(\frac{\xi_1}{2}\right)^{-\frac{7}{4}}\left[J_{-\frac{1}{4}}(\xi_1) - \frac{1}{\Gamma(\frac{3}{4})}\left(\frac{\xi_1}{2}\right)^{-\frac{1}{4}}\right]\mathrm{d}\xi_1 \tag{3.40}$$

with Ω and ξ as (3.39).

3.3.4 Bessel Functions of the First Kind

The Bessel function of the first kind is defined[7] for fixed real parameter ν (which is not to be confused with the kinematic viscosity in Chapter 1) and real $z \geq 0$, as:

$$J_\nu(z) = \sum_{m=0}^{\infty}\frac{(-1)^m}{m!\cdot\Gamma(m+\nu+1)}\left(\frac{1}{2}|z|^{2m+\nu}\right). \tag{3.41}$$

The behaviour of (3.41) for $\nu = \pm\frac{1}{4}$ ensures that the complimentary (3.38) and particular (3.40) solutions converge to finite values as $\xi \to 0$.

Furthermore, as $z \to \infty$, the Bessel function of the first kind behaves like:

$$J_\nu(z) = \sqrt{\frac{2}{(\pi z)}}\left\{\cos\left(z - \frac{1}{2}\nu\pi - \frac{1}{4}\pi\right) + e^{|\oint z|}O\left(|z|^{-1}\right)\right\}, \qquad |\arg z| < \pi\,. \tag{3.42}$$

[6] Ruban (1982a)

[7] See for example, Abramovich & Stegun (1972).

3.3.5 General Solution

To summarise, the general solution of the boundary value problem (3.33), (3.34) and (3.35) is

$$\begin{aligned}\Phi = &\frac{1}{2}C\bar{Y}^2 \\ &- G\cdot\frac{2\Gamma(\frac{5}{4})}{\Omega^{\frac{1}{4}}e^{\frac{i\pi}{4}}}\left\{-\frac{1}{\Gamma(\frac{5}{4})}\left(\frac{\xi}{2}\right)^{\frac{1}{2}}+\frac{\xi}{8}\int_0^{\xi}\left(\frac{\xi_1}{2}\right)^{-\frac{3}{2}}\left[\left(\frac{\xi_1}{2}\right)^{-\frac{1}{4}}J_{\frac{1}{4}}(\xi_1)-\frac{1}{\Gamma(\frac{5}{4})}\right]\,\mathrm{d}\xi_1\right\} \\ &+ R\cdot\frac{\Gamma(\frac{3}{4})}{4\Omega}\left(\frac{\xi}{2}\right)\int_0^{\xi}\left(\frac{\xi_1}{2}\right)^{-\frac{7}{4}}\left[J_{-\frac{1}{4}}(\xi_1)-\frac{1}{\Gamma(\frac{3}{4})}\left(\frac{\xi_1}{2}\right)^{-\frac{1}{4}}\right]\,\mathrm{d}\xi_1 \qquad (3.43)\end{aligned}$$

where (3.39):

$$\Omega = \frac{ik}{2}\,, \qquad \xi = \frac{i\Omega^{\frac{1}{2}}\bar{Y}^2}{2}\,.$$

Matching At The Outer Lower Layer

As the outer edge of the lower layer is approached and $\xi \to \infty$ then by (3.42), the complimentary solution (3.38) changes to

$$\Phi_2 = -\frac{\Gamma(\frac{5}{4})}{2\sqrt{\pi}\Omega^{\frac{1}{4}}e^{\frac{i\pi}{4}}}\left(\frac{\xi}{2}\right)^{-\frac{5}{4}}\sin\left(\xi-\frac{3}{8}\pi\right)+\ldots$$

and the particular solution (3.40) becomes

$$\Phi^* = \frac{\Gamma(\frac{3}{4})}{4\sqrt{\pi}\Omega}\left(\frac{\xi}{2}\right)^{-\frac{5}{4}}\sin\left(\xi-\frac{1}{8}\pi\right)+\ldots$$

Hence, as $\xi \to \infty$, the lower layer general solution (3.43) behaves like

$$\begin{aligned}\Phi = & \frac{1}{2}C\bar{Y}^2 \\ & - G \cdot \frac{\Gamma(\frac{5}{4})}{2\sqrt{\pi}\Omega^{\frac{1}{4}}} \left(\frac{\xi}{2}\right)^{-\frac{5}{4}} e^{-\frac{i\pi}{4}} \sin\left(\xi - \frac{3}{8}\pi\right) \\ & + R \cdot \frac{\Gamma(\frac{3}{4})}{4\sqrt{\pi}\Omega} \left(\frac{\xi}{2}\right)^{-\frac{5}{4}} \sin\left(\xi - \frac{1}{8}\pi\right) \\ & + \ldots\end{aligned}$$

The trigonometric terms $\sin\left(\xi - \frac{3}{8}\pi\right)$ and $\sin\left(\xi - \frac{1}{8}\pi\right)$ behave like complex hyperbolic functions since ξ (3.39) is complex. As $\xi \to \infty$, they grow unbounded. The condition of no exponential growth as $\xi \to \infty$ is satisfied when:[8]

$$R(k,\bar{T})(ik)^{-\frac{3}{4}} = G(k,\bar{T})\frac{\Gamma(\frac{5}{4})}{\Gamma(\frac{3}{4})}2^{\frac{1}{4}} \tag{3.44}$$

and the trigonometric terms are removed. The relation (3.44) completes the matching between the lower layer and the middle layer. When true, the interaction region flow structure, with a negligible induced pressure gradient, is consistent.

3.3.6 The $\bar{A}(\bar{x},\bar{T})$ Solvability Condition from Inverse Fourier Transformation

Recall from (3.33) and (3.34) that $R(k,\bar{T})$ and $G(k,\bar{T})$ are the Fourier transforms of $\frac{\partial \bar{A}_1}{\partial \bar{T}}(\bar{x},\bar{T})$ and $g(\bar{x},\bar{T}) = -\frac{1}{2}\left(\bar{A}_1^2 - \bar{x}^2 + 2a\right)$. Applying the inverse Fourier transformation to (3.44) results in:

$$\frac{1}{\sqrt{2\pi}}\int_{-\infty}^{\infty} R(k,\bar{T})(ik)^{-\frac{3}{4}}e^{i\bar{x}k}\,\mathrm{d}k = \left[\frac{\Gamma(\frac{5}{4})}{\Gamma(\frac{3}{4})}2^{\frac{1}{4}}\right]\frac{1}{\sqrt{2\pi}}\int_{-\infty}^{\infty} G(k,\bar{T})e^{i\bar{x}k}\,\mathrm{d}k \tag{3.45}$$

[8] A similar result for marginal separation with induced pressure gradient is found by Ruban (1982b). See also Samad (2004) and Stavrou (2004).

and hence:[9]

$$\left[\frac{\Gamma(\frac{5}{4})}{\Gamma(\frac{3}{4})}2^{\frac{1}{4}}\right] g(\bar{x},\bar{T}) = \frac{1}{2\pi}\int_{-\infty}^{\bar{x}} \mathrm{d}\xi \int_{-\infty}^{\infty} \frac{\partial \bar{A}_1}{\partial \bar{T}}(\xi,\bar{T})(ik)^{-\frac{3}{4}} e^{i(\bar{x}-\xi)k}\,\mathrm{d}k\,.$$

By rewriting $(\bar{x}-\xi)=p$, then:

$$\left[\frac{\Gamma(\frac{5}{4})}{\Gamma(\frac{3}{4})}2^{\frac{1}{4}}\right] g(\bar{x},\bar{T}) = \frac{1}{2\pi}\int_{-\infty}^{\bar{x}} \frac{\partial \bar{A}_1}{\partial \bar{T}}(\xi,\bar{T}) \left[\int_{-\infty}^{\infty} (ik)^{-\frac{3}{4}} e^{ipk}\,\mathrm{d}k\right] \mathrm{d}\xi\,.$$

Let the integral:[10]

$$I = \int_{-\infty}^{\infty} (ik)^{-\frac{3}{4}} e^{ipk}\,\mathrm{d}k\,.$$

In the k-plane, as illustrated in Figure 3.4:

$$e^{ipk} = e^{ip(k_r+ik_i)} = e^{-pk_i}e^{ipk_r}\,.$$

For all $p>0$, the contour of integration may be closed in the upper-half k-plane with a branch cut along the positive imaginary axis. Therefore,

$$I = \left(\oint_{C_1} - \int_{C_{11}} - \int_{C_{12}} + \oint_{C_2} - \int_{C_{21}} - \int_{C_{22}}\right) (ik)^{-\frac{3}{4}} e^{ipk}\,\mathrm{d}k\,.$$

Cauchy's residue theorem states:

$$\oint_C f(k)\,\mathrm{d}k = 2\pi i \sum_{j=1}^{n} \mathrm{Res}(f,a_j)$$

where

1. the contour C is a simple closed curve in the anti-clockwise direction;

2. the term $\mathrm{Res}(f,a_j)$ denotes the residue of f at the point $k=a_j$ for $j=$

[9] The integral term ξ is not the parameter ξ from the Fourier transform boundary value problem solution in Section 3.3.3 of the lower layer analysis.

[10] See also work by Samad (2004) and Stavrou (2004).

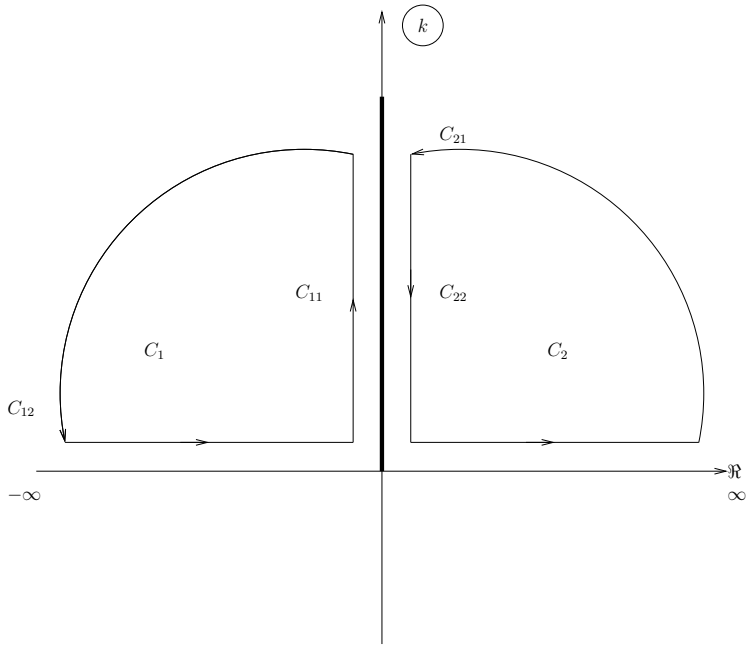

Figure 3.4: Contour integration on the k-plane.

1, 2, ..., n; and

3. the residue $\mathrm{Res}(f, a_j)$ is only non-zero at a singularity.

By Cauchy's residue theorem, the integrals:

$$\oint_{C_1} (ik)^{-\frac{3}{4}} e^{ipk}\,\mathrm{d}k = \oint_{C_2} (ik)^{-\frac{3}{4}} e^{ipk}\,\mathrm{d}k = 0$$

since the closed contours do not contain singularities. (See Figure 3.4.) Jordan's lemma states:

$$\left| \int_{C_R} f(k)\,\mathrm{d}k \right| \leq \frac{\pi}{p} \max_{\theta\in[0,\pi]} \left| g(Re^{i\theta}) \right|$$

where

1. the integrand $f(k)$ is a continuous function on the contour C_R in the form: $f(k) = e^{ipk} g(k)$;

2. the contour C_R is a continuous arc on a semi-circle (or in this case, a quarter-circle): $k = Re^{i\theta}$, centred at the origin and with radius R.

By Jordan's lemma, the upper bound of the integral on the quarter-circle arc C_{12}:

$$\left| \int_{C_{12}} (ik)^{-\frac{3}{4}} e^{ipk} \, \mathrm{d}k \right| \leq \frac{\pi}{2p} \max_{\theta \in \left[\frac{\pi}{2}, \pi\right]} \left| \left(iRe^{i\theta}\right)^{-\frac{3}{4}} \right| \to 0 \,, \qquad R \to \infty \,.$$

Analogously, the integral on the quarter-circle arc: $C_{21} = 0$.

For all $p < 0$ where the integration is performed in the lower-half k-plane, the integrand is analytic and the contribution to the integral is also zero.

The remaining non-zero integrals are therefore:

$$I = \left(- \int_{C_{11}} - \int_{C_{22}} \right) (ik)^{-\frac{3}{4}} e^{ipk} \, \mathrm{d}k \,,$$

of which

$$\int_0^\infty (ik)^{-\frac{3}{4}} e^{ipk} \, \mathrm{d}k = - \int_{C_{22}} (ik)^{-\frac{3}{4}} e^{ipk} \, \mathrm{d}k \,, \tag{3.46}$$

$$\int_{-\infty}^0 (ik)^{-\frac{3}{4}} e^{ipk} \, \mathrm{d}k = - \int_{C_{11}} (ik)^{-\frac{3}{4}} e^{ipk} \, \mathrm{d}k \,. \tag{3.47}$$

For (3.46), the contour can be parameterized by:

$$k = e^{i\frac{\pi}{2}} y = iy \,;$$

hence

$$\int_0^\infty (ik)^{-\frac{3}{4}} e^{ipk} \, \mathrm{d}k = e^{-i\frac{\pi}{4}} \int_0^\infty y^{-\frac{3}{4}} e^{-py} \, \mathrm{d}y \,,$$

and with a change of variable from y to t such that $y = \left(\frac{1}{p}\right) t$, then:

$$\int_0^\infty (ik)^{-\frac{3}{4}} e^{ipk} \, \mathrm{d}k = e^{-i\frac{\pi}{4}} p^{-\frac{1}{4}} \int_0^\infty t^{-\frac{3}{4}} e^{-t} \, \mathrm{d}t \,.$$

By definition of the Gamma function (2.29), then

$$\int_0^\infty (ik)^{-\frac{3}{4}} e^{ipk}\,\mathrm{d}k = e^{-i\frac{\pi}{4}} p^{-\frac{1}{4}} \Gamma\left(\frac{1}{4}\right) .$$

Analogously, for (3.47):

$$\int_{-\infty}^0 (ik)^{-\frac{3}{4}} e^{ipk}\,\mathrm{d}k = e^{-i\frac{3\pi}{4}} p^{-\frac{1}{4}} \Gamma\left(\frac{1}{4}\right) .$$

Therefore, the integral is

$$I = \frac{\sqrt{\pi}\Gamma\left(\frac{1}{4}\right)}{(\bar{x}-s)^{\frac{1}{4}}} .$$

Overall, (3.45) with integral I is

$$\bar{A}_1^2(\bar{x},\bar{T}) - \bar{x}^2 + 2a = -\frac{2^{\frac{3}{4}}}{\Gamma(\frac{5}{4})} \int_{-\infty}^{\bar{x}} \frac{\partial \bar{A}_1}{\partial \bar{T}}(\xi,\bar{T})\, \frac{\mathrm{d}\xi}{(\bar{x}-\xi)^{\frac{1}{4}}} . \tag{3.48}$$

The $\bar{A}_1(\bar{x},\bar{T})$ equation (3.48) is the necessary and sufficient *solvability condition* for the interaction region flow structure, with a negligible induced pressure gradient, to be consistent and hence, for solutions to exist. The solvability condition is a result of the condition of matching (3.28) between the middle layer and the lower layer of the interaction region; a change of variables and affine transformation (3.29); the subsequent Fourier transformation boundary value problem in Section 3.3.3; and the inverse Fourier transformation of the condition (3.45). It is a part of the hierarchical process for determining stream functions by region, as illustrated in Figure 3.3.

Abel Integral Transformation of the $\bar{A}(\bar{x},\bar{T})$ Solvability Condition

The Abel integral transform for a "sufficiently well behaved function u" is

$$f(x) = \frac{1}{\Gamma(\alpha)} \int_a^x (x-t)^{\alpha-1} u(t)\,\mathrm{d}t$$

for $a < x < b$, $-\infty \leq a < b \leq \infty$ and real $\alpha \in (0,1)$.[11] The inverse Abel integral transform for a sufficiently well behaved $f(x)$ is

$$u(x) = \frac{1}{\Gamma(1-\alpha)} \frac{\mathrm{d}}{\mathrm{d}x} \int_a^x (x-t)^{-\alpha} f(t)\, \mathrm{d}t\,.$$

Hence, the solvability condition (3.48) may be transformed to the conservative form:

$$\frac{\partial \bar{A}_1}{\partial \bar{T}}(\bar{x},\bar{T}) = -\frac{\Gamma(\frac{5}{4})}{2^{\frac{5}{4}}\pi} \frac{\partial}{\partial \bar{x}} \int_{-\infty}^{\bar{x}} \left[\bar{A}_1^2(s,\bar{T}) - s^2 + 2a(T)\right] \frac{\mathrm{d}s}{(\bar{x}-s)^{\frac{3}{4}}}\,, \tag{3.49}$$

with use of the Gamma multiplication theorem:

$$\Gamma(z)\Gamma\left(z+\frac{1}{2}\right) = 2^{1-2z}\sqrt{\pi}\Gamma(2z)\,,$$

and properties of the Gamma function (2.29).

Induced Pressure Gradient Discussion

Recall that if the induced pressure gradient is not negligible in this regime, then it remains unchanged across the middle layer, as discussed in Section 3.2.

Substituting the lower layer stream function (3.20) and the pressure gradient (3.13) into the second, y-momentum equation (1.2) for the boundary layer then gathering $O(\mathrm{Re}^{\frac{1}{2}}\sigma)$ terms, gives:

$$\frac{\partial p}{\partial Y^*} = 0\,.$$

Differentiating with respect to x^* indicates that

$$\frac{\partial}{\partial Y^*}\left(\frac{\partial P^*}{\partial x^*}\right) = 0\,.$$

The induced pressure gradient, although negligible in this regime, would remain unchanged across the lower layer as well as the middle layer.

[11] Gorenflo & Vessella (2008)

3.4 The Upper Layer

The interaction region problem is closed, with the derivation of the $A(x,T)$ solvability condition (3.48), because the induced pressure gradient is negligible. In other words, there is no need to consider an upper layer (region I in Figure 3.2) of the traditional triple deck theory for the interaction region.

In contrast, if the induced pressure gradient is not negligible, the $\frac{\partial P^*}{\partial x^*}$ term appears in the Ψ_2^* equation (3.25) of the lower layer analysis. The induced pressure gradient then remains undetermined in the lower layer analysis and to close the interaction region problem, it is necessary to consider the upper layer. The induced pressure gradient of the lower layer causes a displacement effect of the boundary layer in the upper layer.

A relationship between the pressure and displacement can be obtained by considering the classical triple deck interaction region flow regime. The induced pressure gradient is determined by the curvature of the streamlines in the lower layer adjacent to the wall and the integral of small perturbation theory (B.6).[12]

The curvature of the lower layer streamlines can be found from matching with the middle layer stream function solution (3.11) and (3.14). In the middle layer,

$$u = \Psi_{00}'(Y) + \dots$$

$$v = -\mathrm{Re}^{-\frac{1}{2}}\Psi_{00}'(Y)\left[\frac{A_1'(x^*)}{\lambda_0} + \int_0^Y \frac{\Psi_{00}''' - \lambda_0}{(\Psi_{00}')^2}\,\mathrm{d}Y\right] + \dots$$

Therefore, the angle of inclination of the velocity vector is

$$\theta = \frac{v}{u} = -\mathrm{Re}^{-\frac{1}{2}}\left[\frac{A_1'(x^*)}{\lambda_0} + \int_0^Y \frac{\Psi_{00}''' - \lambda_0}{(\Psi_{00}')^2}\,\mathrm{d}Y\right] + \dots$$

[12]The integral of small perturbation theory is derived in Appendix B.

and the curvature of the streamlines is

$$\frac{\partial\theta}{\partial x} = \mathrm{Re}^{-\frac{1}{2}}\sigma^{-4}\frac{A_1''(x^*)}{\lambda_0}\,.$$

As $\sigma \to \mathrm{Re}^{\frac{1}{20}}$ by (3.7), the induced pressure gradient becomes significant to the flow regime and the classical triple deck interaction region comes into action. When the curvature of the streamlines is substituted into the integral of small perturbation theory, then the *pressure-displacement relation* is obtained:

$$\frac{\partial P^*}{\partial x^*} = -\frac{U_0^2}{\pi\lambda_0}\int_{-\infty}^{\infty}\frac{A_1''(\xi)}{\xi - x^*}\,\mathrm{d}\xi\,. \tag{3.50}$$

The pressure-displacement relation closes the interaction region problem when an induced pressure gradient is present in the flow. It relates the displacement effect of the boundary layer to the induced pressure gradient.

Chapter 4

$A(x,T)$ Solvability Condition Analysis

The construction of the initial-boundary value problem for the solvability condition (3.48) for the interaction region:

$$A^2(x,T) - x^2 + 2a(T) = -\frac{2^{\frac{3}{4}}}{\Gamma(\frac{5}{4})} \int_{-\infty}^{x} \frac{\partial A}{\partial T}(\xi,T)\, \frac{\mathrm{d}\xi}{(x-\xi)^{\frac{1}{4}}} \tag{4.1}$$

and its numerical solution, based on the methods set out by Smith & Elliott (1985), follows. For simplicity, the bar and subscript notation is removed.

The $A(x,T)$ term originates from the perturbation solution (3.24):

$$\Psi_1^* = \frac{1}{2} A_1(x^*,T) Y^{*2}$$

of the lower layer (region III) stream function (3.20), where it has been manipulated by the affine transformation (3.29):

$$A_1 = a_0^{\frac{3}{5}} U_{00}^{\frac{4}{5}} \lambda_0^{-\frac{1}{5}} \bar{A}_1\,, \qquad \bar{A}_1 = A\,.$$

Hence, the $A(x,T)$ term is directly proportional to the skin friction, defined as

$$\tau = \left.\frac{\partial^2 \Psi}{\partial Y^2}\right|_{Y=0} = A(x,T) + \dots \tag{4.2}$$

If skin friction is positive then the fluid flow is attached and moving downstream. If skin friction is negative the flow is moving upstream against the current. Steady flow separation is deemed to have occurred when skin friction equals zero. Unsteady flow separation occurs at a point of zero skin friction and zero velocity.

The parameter $a(T)$ also comes from the affine transformation (3.29):

$$a = k_1(-a_1)a_0^{-\frac{1}{5}}U_{00}^{-\frac{8}{5}}\lambda_0^{\frac{2}{5}}\,.$$

The function $k_1(T)$ comes from the interaction region asymmetry function (3.9): $k(T) = k_0 + \sigma^{-8}k_1(T)$, as $\sigma \to \infty$. The parameter $a_1(T) \sim \Delta k$ is related to the change in angle of attack and comes from the first eigenvalue of the viscous sublayer stream function perturbation $\Psi_1(x,Y,T)$. Its rate of change: $\dot{a}_1(T)$, which is related to the rate of change of angle of attack, also appears in the forcing term $\Psi_2(x,Y,T)$.

In classic steady marginal separation theory, skin friction A solutions exist for large negative values of a up to a critical value $a_c = 1.33$. For larger values of a, no flow solutions can be obtained, or to be more precise, solutions becomes complex.[1]

For an airfoil with a slow change in angle of attack on the large time scale T then $a(T)$ can be set to sweep through a range of values over some time range $T \geq 0$. Moreover, for an airfoil close to stall then $a(T)$ can be set to start close to but below the critical value $a_c = 1.33$, which then gently approaches the point of no real solution at $a = a_c$. For example:

$$a(T) = 1.331 - (1.331 + 0.001)e^{-T}\,, \qquad T \geq 0\,, \tag{4.3}$$

[1] c.f. Stewartson et al. (1982) and the review by Sychev et al. (1998b) on marginal separation, in Section 1.4.

as illustrated in Figure 4.1.

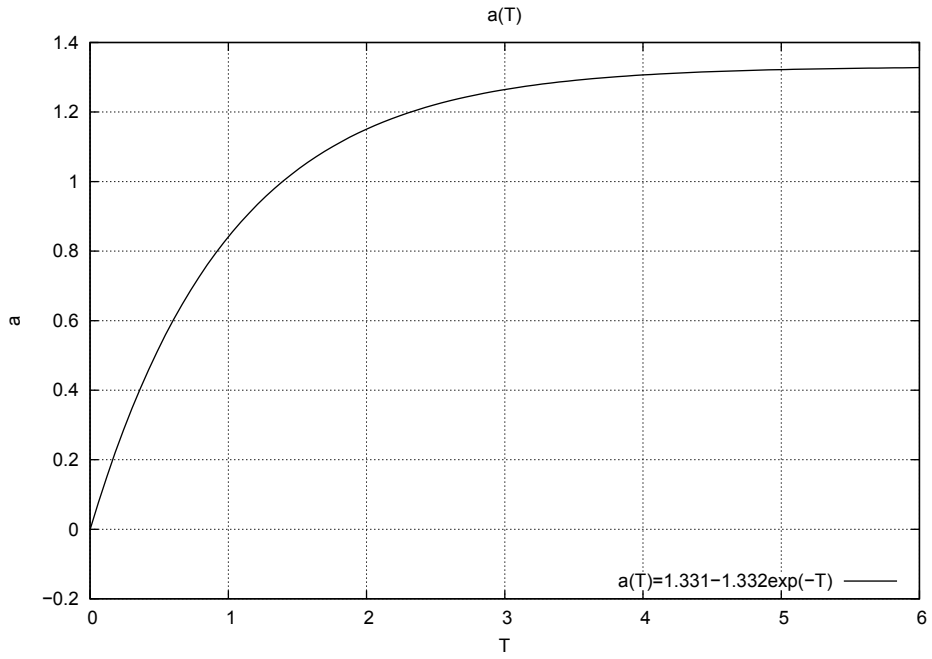

Figure 4.1: The airfoil angle of attack law (4.3): $a(T) = 1.331 - 1.332e^{-T}$, for $T = [0, 6]$.

The flow over the airfoil in the boundary layer and interaction region is steady on the external region time scale t and hence,

$$\frac{\partial A}{\partial T} \to 0\,, \qquad |x| \to \infty$$

which implies from (4.1) that

$$A(x,T) = |x| + \frac{a(T)}{|x|} + \ldots \qquad |x| \to \infty$$

such that

$$A^2(x,T) = |x|^2 + 2a(T) + \frac{a^2(T)}{|x|^2} + \ldots \qquad |x| \to \infty\,.$$

Far away from the local interaction:

$$A(x,T) = \left(|x|^2 + 2a(T)\right)^{\frac{1}{2}}\,, \qquad |x| \to \infty \tag{4.4}$$

with $a(T)$ by (4.3). The boundary condition (4.4) implies either:

1. the flow is attached to the surface; the skin friction is positive far away from the local interaction such that

$$A(x,T) = \left| \left(|x|^2 + 2a(T) \right)^{\frac{1}{2}} \right| , \qquad |x| \to \infty$$

(c.f. the boundary condition (1.7) from Ryzhov & Smith (1984) and Stewartson et al. (1982) on marginal separation), or

2. the flow direction is reversed far away from the interaction region and the negative root is taken such that

$$A(x,T) = - \left| \left(|x|^2 + 2a(T) \right)^{\frac{1}{2}} \right| , \qquad |x| \to \infty$$

(c.f. the boundary condition (1.8) from Ryzhov & Smith (1984) and Brown & Stewartson (1983)).

The thesis follows the theory of marginal separation from Stewartson et al. (1982). Hence, the class of far away attached flows is considered and the positive root of the boundary condition (4.4) is taken. Boundary conditions are important here because if they are not imposed, the solution is not unique. For example, if $a = 0$, the solvability condition (4.1) allows two solutions $A = x$ and $A = -x$ besides the solution(s) that meets the condition.

Initial conditions at $T = 0$: $A(x,0)$, are discussed in Section 4.4.1.

4.1 $A(x,T)$ Equation Numerical Treatment

Solutions for the $A(x,T)$ equation (4.1):

$$A^2(x,T) - x^2 + 2a(T) = -\frac{2^{\frac{3}{4}}}{\Gamma(\frac{5}{4})} \int_{-\infty}^{x} \frac{\partial A}{\partial T}(\xi,T) \, \frac{\mathrm{d}\xi}{(x-\xi)^{\frac{1}{4}}}$$

are found based on the following numerical treatment described by Smith & Elliott (1985). This numerical treatment is chosen because Smith & Elliott use the method to acquire solutions for a normalised quasi-steady version (4.5) of (4.1) where $2a(T)$ is a constant $\bar{\Gamma}$:

$$A^2(x,T) - x^2 + \bar{\Gamma} = \int_{-\infty}^{x} \frac{\partial A}{\partial T}(\xi,T)\, \frac{\mathrm{d}\xi}{(x-\xi)^{\frac{1}{4}}}\,. \tag{4.5}$$

The Smith & Elliott (1985) equation (4.5) is derived in a similar manner to (4.1).[2] The treatment is tested in the Sections 4.3 and 4.4.

Equation (4.1) is to be reformulated as a system of nonlinear equations on a uniform space x and time T grid. (See Figure 4.2.) Ultimately, the nonlinear system of equations will be solved numerically using Newton's method described in Section 4.2.

The computational spatial x-range is finite. It is discretised with a uniform step size $\mathrm{D}x$ into $m+1$ grid points, where x_1 is the large and negative (but not negative infinity) starting point of the computational domain; x_{m+1} is the large and positive end point; and the subscript i denotes evaluation at an internal grid point $x_i = x_1 + (i-1)\,\mathrm{D}x$ for $i = 1,\, 2,\, \ldots,\, m+1$. There are m steps from x_1 to x_{m+1}. The notation A_i denotes $A(x_i,T)$.

The forward time T-range is similarly discretised with a uniform step size $\mathrm{D}T$ into $n+1$ grid points where the time steps are $T_k = T_1 + (k-1)\,\mathrm{D}T$ for $k = 1,\, 2,\, \ldots,\, n+1$.[3] There are n steps from T_1 to T_{n+1}.

If $k = 1$ and $T = 0$, then the value $A_i^{(0)}$ at all x_i for $i = 1,\, 2,\, \ldots,\, m+1$ is known from an initial condition given in Section 4.4.1. The solutions A_1 and A_{m+1} for all time T are known from boundary conditions (4.4), now reformulated as

$$A(x,T) = \left(|x|^2 + 2a(T)\right)^{\frac{1}{2}}\,; \qquad x = x_1,\, x_{m+1}\,; \qquad \forall\, T\,. \tag{4.6}$$

Furthermore, the superscripts (0) and (1) are introduced to denote iteration levels

[2] See also Smith (1982a).

[3] The start point $T_1 = 0$ has subscript 1 and not 0 because it denotes the first entry into a vector in MATLAB.

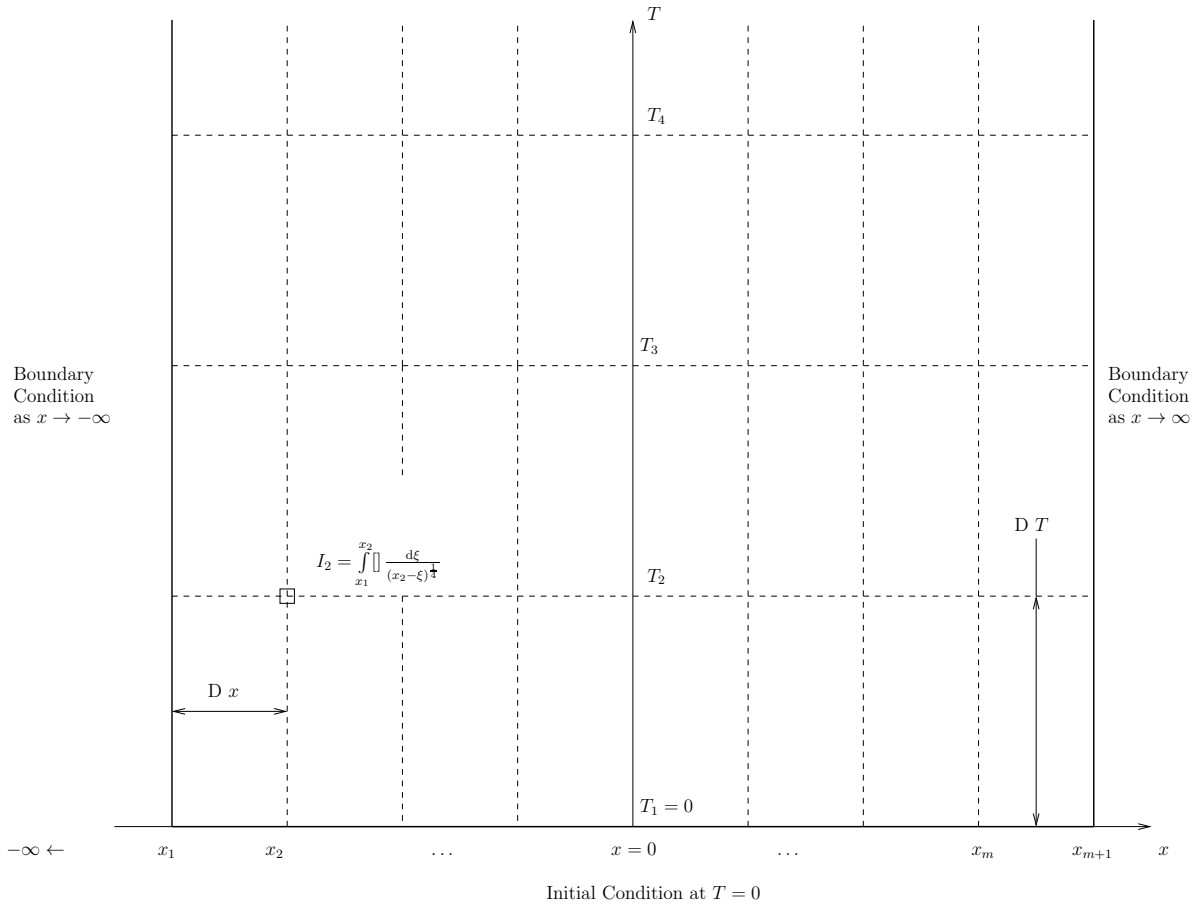

Figure 4.2: The uniform space x and time T grid, where the points x_1 and x_{m+1} are the start and end of the computational domain. An example integral with some integrand [] for $i = 1$: I_2, at $x = 2$ and time level T_2, is shown.

of Newton's method within each time level. A superscript (0) refers to values at the starting time level T_k for $k = 1, 2, \ldots, n+1$ and values at previous iterations. A superscript (1) refers to the updated value from an iteration. In the context of Newton's method, the value at (1) is continuously updated with each cycle of the method until an error E falls below a preset tolerance tol. (Error E and tolerance tol are defined in Section 4.2.) The value at (1) then becomes the solution at the next time level $T_{k+1} = T_k + \mathrm{D}T$. On each time level T_k, the $A(x,T)$ equation is solved using Newton's method to update all $A_i^{(1)}$. The process is repeated with the solution at T_{k+1} becoming the value $A^{(0)}$ at T_{k+2}, which is used to find the value at the next time level after that until the end is reached.

Centring

"[C]entring at $x = x_{i+\frac{1}{2}}$, $T = T + \frac{1}{2}\mathrm{D}T$ reflects the implicit elliptic nature of the problem."[4] The half-subscript $i + \frac{1}{2}$ for space means

$$x_{i+\frac{1}{2}} = \frac{1}{2}(x_i + x_{i+1})\,, \qquad i = 1,\, 2,\, \ldots,\, m\,.$$

Centring in time and space is demonstrated on the left hand side of the $(i+1)$-th equation for $i = 1,\, 2,\, \ldots,\, m$, which is discretised as

$$A^2(x,T) - x^2 + 2a(T) = \frac{1}{4}\left(A_i^{(1)\,2} + A_{i+1}^{(1)\,2} + A_i^{(0)\,2} + A_{i+1}^{(0)\,2}\right) - x_{i+\frac{1}{2}}^2 + \left(a^{(0)} + a^{(1)}\right) \tag{4.7}$$

The $\left(a^{(0)} + a^{(1)}\right)$ term replaces $2a(T)$ because of centring in time, where $a^{(0)}$ is the value of a at the current time level: $a(T)$, and $a^{(1)}$ is the value of a at the next time level: $a(T + \mathrm{D}T)$. Similarly, the first term on the right hand side is so because $A^2(x,T)$ is centred in both time and space. This left hand side (4.7) will match with the $(i+1)$-th integral on the right hand side (4.9) later.

Therefore, the $A(x,T)$ equation (4.1) is reformulated into a system of m nonlinear equations to solve for A_i and A_{i+1} on each time level. On the other hand, there are only $m-1$ unknowns from $m+1$ total A_i values minus two known boundary conditions. On each time level, there are m equations because the method involves centring. Although the equations are solved for one of the boundary conditions at each time level T_k, there is the clear condition which states that the solutions should match with the other boundary condition. The boundary conditions test appears in the Sections 4.3 and 4.4.

Each $(i+1)$-th equation uses information at the spatial point $x = x_{i+1}$ and at all the points leading up to it from the start of the domain $x = x_1$. Hence, the x term in the integrand and the upper limit of the $(i+1)$-th integral becomes $x = x_{i+1}$. The

[4]Smith & Elliott (1985)

information at $x = x_{i+1}$ is the value of A_{i+1}, known the initial distribution $A_{i+1}^{(0)}$.

The Integral

The integral on the right hand side of the $(i+1)$-th equation is written as

$$\int_{-\infty}^{x} \frac{\partial A}{\partial T}(\xi,T)\,\frac{\mathrm{d}\xi}{(x-\xi)^{\frac{1}{4}}} = \left\{ \int_{-\infty}^{x_1} + \int_{x_1}^{x_2} + \ldots + \int_{x_i}^{x_{i+1}} \right\} \frac{\partial A}{\partial T}(\xi,T)\,\frac{\mathrm{d}\xi}{(x_{i+1}-\xi)^{\frac{1}{4}}} \tag{4.8}$$

where it is noted that the upper limit of the integral and the x term in the integrand stop at the specific spatial point $x = x_{i+1}$. Also, x_1 is large and negative with $x_{i+1} > x_1$, as in Figure 4.2.

The contribution from the integral with limits from minus infinity to large and negative x_1, calculated at $x = x_{i+1}$:

$$\int_{-\infty}^{x_1} \frac{\partial A}{\partial T}(\xi,T)\,\frac{\mathrm{d}\xi}{(x_{i+1}-\xi)^{\frac{1}{4}}} \simeq 0\,,$$

which can be shown by using the boundary conditions (4.4) and introducing an anti-clockwise semi-circular contour in the complex plane, as illustrated in Figure 4.3, such that

$$\left\{ \int_{-\infty}^{x_1} = \oint_{C} - \int_{C_1} \right\} \frac{\partial A}{\partial T}(\xi,T)\,\frac{\mathrm{d}\xi}{(x_{i+1}-\xi)^{\frac{1}{4}}}\,.$$

By the boundary conditions (4.4), then

$$\frac{\partial A}{\partial T}(x,T) = \frac{\mathrm{d}a}{\mathrm{d}T}\left(|x|^2 + 2a(T)\right)^{-\frac{1}{2}}\,, \qquad |x| \to \infty$$

and from (4.3):

$$\frac{\mathrm{d}a}{\mathrm{d}T} = 1.332e^{-T}\,, \qquad T \geq 0\,.$$

Hence, the integral is

$$1.332e^{-T} \cdot \left\{ \int_{-\infty}^{x_1} = \oint_C - \int_{C_1} \right\} \frac{\mathrm{d}\xi}{(|\xi|^2 + 2a(T))^{\frac{1}{2}} (x_{i+1} - \xi)^{\frac{1}{4}}} .$$

By Cauchy's residue theorem, as defined in Section 3.3.5, the first integral:

$$\oint_C \frac{\mathrm{d}\xi}{(|\xi|^2 + 2a(T))^{\frac{1}{2}} (x_{i+1} - \xi)^{\frac{1}{4}}} = 0$$

since $a(T) > 0$ by (4.3) and there are no singularities of the integrand within the contour. Additionally, the estimation lemma states:

$$\left| \int_{C_R} f(k)\,\mathrm{d}k \right| \leq l(C_R) \max_{k \in C_R} |f(k)|$$

where

1. the integrand $f(k)$ is a continuous function on the contour C_R;
2. the contour C_R is a continuous arc;
3. the term $l(C_R)$ is the arc length of C_R.

Hence, the upper bound of the second integral:

$$\left| \int_{C_1} \frac{\mathrm{d}\xi}{(|\xi|^2 + 2a(T))^{\frac{1}{2}} (x_{i+1} - \xi)^{\frac{1}{4}}} \right| = \pi R \max_{\theta \in [0,\pi]} \left| \frac{1}{(|Re^{i\theta}|^2 + 2a(T))^{\frac{1}{2}} (x_{i+1} - Re^{i\theta})^{\frac{1}{4}}} \right| \to 0 ,$$

as $R \to \infty$. Therefore, the contribution:[5]

$$\int_{-\infty}^{x_1} \frac{\partial A}{\partial T}(\xi, T) \frac{\mathrm{d}\xi}{(x_{i+1} - \xi)^{\frac{1}{4}}} \simeq 0$$

[5]The contribution does not take into account the next order term of the integrand from the boundary condition (4.4). The contribution is mentioned again in Section 7.4 on further work.

and the $(i+1)$-th integral (4.8) is:

$$\int_{-\infty}^{x} \frac{\partial A}{\partial T}(\xi,T)\,\frac{\mathrm{d}\xi}{(x-\xi)^{\frac{1}{4}}} = \left\{ \int_{x_1}^{x_2} + \int_{x_2}^{x_3} + \ldots + \int_{x_i}^{x_{i+1}} \right\} \frac{\partial A}{\partial T}(\xi,T)\,\frac{\mathrm{d}\xi}{(x_{i+1}-\xi)^{\frac{1}{4}}}\,.$$

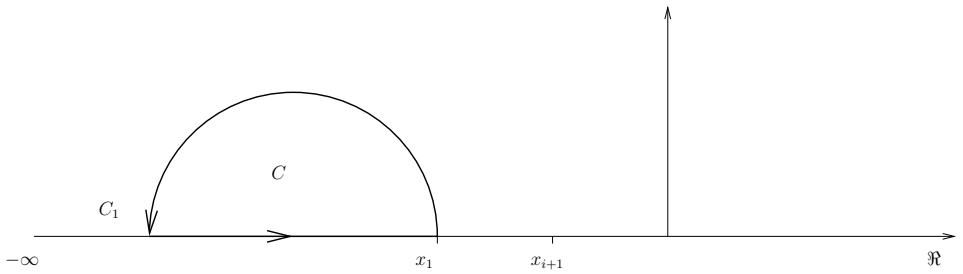

Figure 4.3: The contour in the complex plane for the integral $\int_{-\infty}^{x_1} \frac{\partial A}{\partial T}(\xi,T)\,\frac{\mathrm{d}\xi}{(x_{i+1}-\xi)^{\frac{1}{4}}}$.

The partial derivative of $A(x,T)$ with respect to time at each time level T_k and spatial point x_j is approximated by the midpoint rule with first order error:

$$\frac{\partial A}{\partial T}(x_j,T_{k+\frac{1}{2}}) = \frac{1}{\mathrm{D}T}\left(A_j^{(1)} - A_j^{(0)}\right)\,.$$

Therefore, the right hand side of the $(i+1)$-th equation (4.1) is:

$$\begin{aligned}
&-\frac{2^{\frac{3}{4}}}{\Gamma(\frac{5}{4})}\int_{-\infty}^{x} \frac{\partial A}{\partial T}(\xi,T)\,\frac{\mathrm{d}\xi}{(x-\xi)^{\frac{1}{4}}} \\
&\quad = -\frac{2^{\frac{3}{4}}}{\Gamma(\frac{5}{4})}\frac{1}{\mathrm{D}T}\left\{ \left(A_1^{(1)} - A_1^{(0)}\right)\int_{x_1}^{x_2} + \ldots + \left(A_i^{(1)} - A_i^{(0)}\right)\int_{x_i}^{x_{i+1}} \right\} \frac{\mathrm{d}\xi}{(x_{i+1}-\xi)^{\frac{1}{4}}} \\
&\quad = -\frac{2^{\frac{3}{4}}}{\Gamma(\frac{5}{4})}\frac{1}{\mathrm{D}T}\left\{ \sum_{j=1}^{i}\left(A_j^{(1)} - A_j^{(0)}\right)\int_{x_j}^{x_{j+1}} \right\} \frac{\mathrm{d}\xi}{(x_{i+1}-\xi)^{\frac{1}{4}}}
\end{aligned}$$

which can be solved to give

$$
\begin{aligned}
&-\frac{2^{\frac{3}{4}}}{\Gamma(\frac{5}{4})}\frac{1}{\mathrm{D}T}\left\{\sum_{j=1}^{i}\left(A_j^{(1)}-A_j^{(0)}\right)\int_{x_j}^{x_{j+1}}\right\}\frac{\mathrm{d}\xi}{(x_{i+1}-\xi)^{\frac{1}{4}}}\\
&\quad=-\frac{2^{\frac{3}{4}}}{\Gamma(\frac{5}{4})}\frac{1}{\mathrm{D}T}\left\{\sum_{j=1}^{i}\left(A_j^{(1)}-A_j^{(0)}\right)\cdot-\frac{4}{3}\left[(x_{i+1}-\xi)^{\frac{3}{4}}\right]_{x_j}^{x_{j+1}}\right\}\\
&\quad=-\frac{2^{\frac{3}{4}}}{\Gamma(\frac{5}{4})}\frac{3}{4\mathrm{D}T}\left\{\sum_{j=1}^{i}\left(A_j^{(1)}-A_j^{(0)}\right)\cdot\left[(x_{i+1}-x_j)^{\frac{3}{4}}-(x_{i+1}-x_{j+1})^{\frac{3}{4}}\right]\right\}\\
&\quad=-\frac{2^{\frac{3}{4}}}{\Gamma(\frac{5}{4})}\frac{3(\mathrm{D}x)^{\frac{3}{4}}}{4\mathrm{D}T}\left\{\sum_{j=1}^{i}\left(A_j^{(1)}-A_j^{(0)}\right)\cdot\left[(i+1-j)^{\frac{3}{4}}-(i-j)^{\frac{3}{4}}\right]\right\} \qquad (4.9)
\end{aligned}
$$

where $\mathrm{D}x$ and $\mathrm{D}T$ are the spatial and time grid steps. This right hand side integral (4.9) will match with the left hand side term (4.7).

Numerical Treatment

On each time level, the $A(x,T)$ equation (4.1) becomes a system of m nonlinear equations of second order accuracy:[6]

$$
\begin{aligned}
&\frac{1}{4}\left(A_i^{(1)\,2}+A_{i+1}^{(1)\,2}+A_i^{(0)\,2}+A_{i+1}^{(0)\,2}\right)-x_{i+\frac{1}{2}}^2+\left(a^{(0)}+a^{(1)}\right)\\
&\quad=-\frac{2^{\frac{3}{4}}}{\Gamma(\frac{5}{4})}\frac{3(\mathrm{D}x)^{\frac{3}{4}}}{4\mathrm{D}T}\left\{\sum_{j=1}^{i}\left(A_j^{(1)}-A_j^{(0)}\right)\cdot\left[(i+1-j)^{\frac{3}{4}}-(i-j)^{\frac{3}{4}}\right]\right\},\\
&i=1,\,2\,\ldots,\,m. \qquad (4.10)
\end{aligned}
$$

The system is regarded as a set of equations of quadratic form for $A_i^{(1)}$ which can be written $\mathbf{F}(\mathbf{A})=\mathbf{0}$ for vectors $\mathbf{A}=(A_1,A_2,\ldots,A_{m+1})$ and $\mathbf{0}=(0,0,\ldots,0)$ of $m+1$ components. A component $F_i(\mathbf{A})$ of the system $\mathbf{F}(\mathbf{A})$ is

$$F_i=\frac{1}{4}A_i^{(1)\,2}+bA_i^{(1)}+c=0 \qquad (4.11)$$

[6]Smith & Elliott (1985)

where

$$b = \frac{2^{\frac{3}{4}}}{\Gamma(\frac{5}{4})}\frac{4(\mathrm{D}x)^{\frac{3}{4}}}{3\mathrm{D}T} \tag{4.12}$$

and

$$\begin{aligned} c = {} & \frac{1}{4}\left(A_{i+1}^{(1)\,2} + A_i^{(0)\,2} + A_{i+1}^{(0)\,2}\right) - x_{i+\frac{1}{2}}^2 + \left(a^{(1)} + a^{(0)}\right) \\ & + \frac{2^{\frac{3}{4}}}{\Gamma(\frac{5}{4})}\frac{4(\mathrm{D}x)^{\frac{3}{4}}}{3\mathrm{D}T} \cdot \left\{\sum_{j=1}^{i-1}\left(A_j^{(1)} + A_j^{(0)}\right)\left[(i+1-j)^{\frac{3}{4}} - (i-j)^{\frac{3}{4}}\right]\right\} \\ & - \frac{2^{\frac{3}{4}}}{\Gamma(\frac{5}{4})}\frac{4(\mathrm{D}x)^{\frac{3}{4}}}{3\mathrm{D}T}A_i^{(0)}\,. \end{aligned} \tag{4.13}$$

The terms $bA_i^{(1)}$ and $\frac{4(\mathrm{D}x)^{\frac{3}{4}}}{3\mathrm{D}T}A_i^{(0)}$ in c come from the solved integral summation (4.9) when $j = i$. For $i = 1$:

$$\begin{aligned} F_1\left(\mathbf{A}^{(1)}\right) = {} & \frac{1}{4}A_1^{(1)\,2} + \frac{2^{\frac{3}{4}}}{\Gamma(\frac{5}{4})}\frac{4(\mathrm{D}x)^{\frac{3}{4}}}{3\mathrm{D}T}A_1^{(1)} \\ & + \left\{\frac{1}{4}\left(A_2^{(1)\,2} + A_1^{(0)\,2} + A_2^{(0)\,2}\right) - \left(\frac{x_1+x_2}{2}\right)^2 + \left(a^{(1)} + a^{(0)}\right)\right. \\ & \qquad \left. - \frac{2^{\frac{3}{4}}}{\Gamma(\frac{5}{4})}\frac{4(\mathrm{D}x)^{\frac{3}{4}}}{3\mathrm{D}T}A_1^{(0)}\right\} \\ = {} & 0\,; \end{aligned} \tag{4.14}$$

for $i = 2$:

$$\begin{aligned} F_2\left(\mathbf{A}^{(1)}\right) = {} & \frac{1}{4}A_2^{(1)\,2} + \frac{2^{\frac{3}{4}}}{\Gamma(\frac{5}{4})}\frac{4(\mathrm{D}x)^{\frac{3}{4}}}{3\mathrm{D}T}A_2^{(1)} \\ & + \left\{\frac{1}{4}\left(A_3^{(1)\,2} + A_2^{(0)\,2} + A_3^{(0)\,2}\right) - \left(\frac{x_2+x_3}{2}\right)^2 + \left(a^{(1)} + a^{(0)}\right)\right. \\ & \qquad + \frac{2^{\frac{3}{4}}}{\Gamma(\frac{5}{4})}\frac{4(\mathrm{D}x)^{\frac{3}{4}}}{3\mathrm{D}T}\left(A_1^{(1)} + A_1^{(0)}\right)\left[2^{\frac{3}{4}} - 1^{\frac{3}{4}}\right] \\ & \qquad \left. - \frac{2^{\frac{3}{4}}}{\Gamma(\frac{5}{4})}\frac{4(\mathrm{D}x)^{\frac{3}{4}}}{3\mathrm{D}T}A_2^{(0)}\right\} \\ = {} & 0 \end{aligned} \tag{4.15}$$

and so forth.

4.2 Newton's Method for a System of Nonlinear Equations

The system of m nonlinear equations in quadratic form $\mathbf{F}(\mathbf{A})$ (4.11) uses Newton's method (Newton-Raphson method) for systems of nonlinear equations so as to avoid making an awkward choice of sign in the square-root of the explicit solution to update $A_i^{(1)}$ at each iteration.

Newton's Method for $f(x) = 0$

A generalised Newton's method for a one variable function equation $f(x) = 0$ is demonstrated in Figure 4.4.[7] The function $f : \Re \to \Re$ is continuous and differentiable. The root x_α occurs when the graph intercepts the x-axis.

To start the process of iteration, an arbitrary initial estimate $x^{(0)}$ for the true root is made where $x^{(0)}$ should be reasonably close to x_α. To narrow the reasonably small interval about x_α, the intermediate value theorem can be used.[8] To improve on the estimate $x^{(0)}$, the function f is approximated by its tangent line. If $x^{(0)}$ is near x_α, the tangent line should be nearly coincident with the graph of $y = f(x)$ for points x about x_α and hence, the root of the tangent line should be nearly equal to x_α. The interception point of the tangent line with the x-axis is calculated and the root is denoted by $x^{(1)}$. The method is iterated.

To find a formula for $x^{(1)}$, consider the equation of the tangent line to the graph of $y = f(x)$ at $(x^{(0)}, f(x^{(0)}))$. The equation of the tangent line $y = t_1(x)$ is

$$t_1(x) = f(x^{(0)}) + f'(x^{(0)})(x - x^{(0)}) \,,$$

[7] A detailed description of Newton's method for rootfinding and solving nonlinear systems is given by Atkinson & Han (2003). A proof for Newton's method is given by Suli & Mayers (2003).

[8] The intermediate value theorem states that if f is a real-valued, continuous function on the interval $[a, b]$ and x_m is a number between $f(a)$ and $f(b)$ then there is a m such that $f(m) = x_m$.

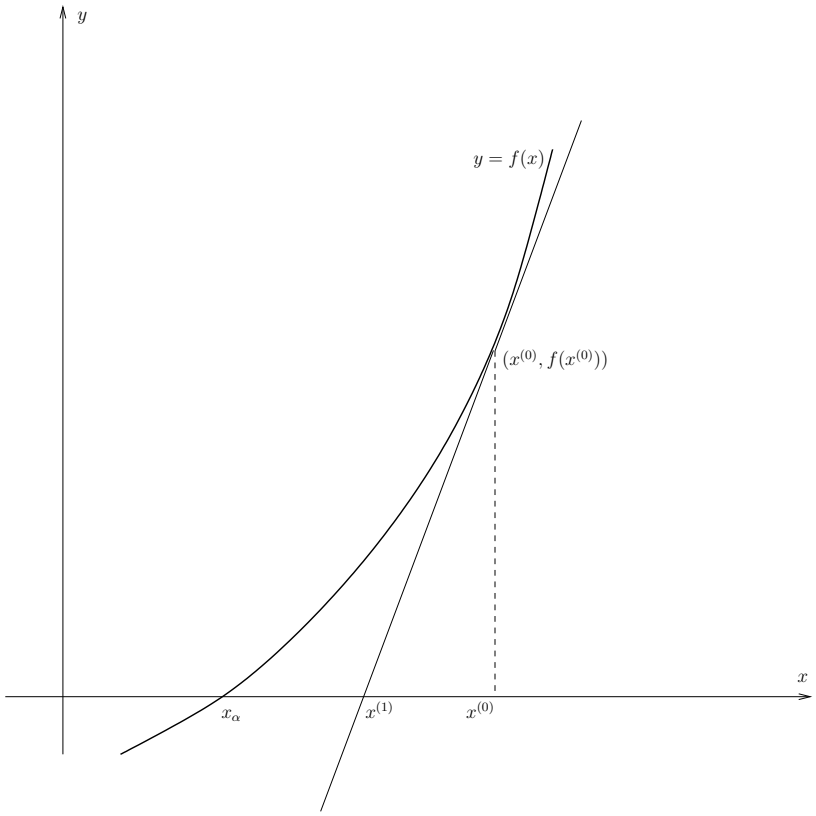

Figure 4.4: The schematic for Newton's method to solve $f(x) = 0$.

where the prime ($'$) notation denotes differentiation with respect to x. The root of $t_1(x)$ is obtained from solving

$$f(x^{(0)}) + f'(x^{(0)})(x^{(1)} - x^{(0)}) = 0$$

and hence,

$$x^{(1)} = x^{(0)} - \frac{f(x^{(0)})}{f'(x^{(0)})}\,.$$

The method is iterated since $x^{(1)}$ is expected to be closer to x_α than $x^{(0)}$ and the process generates the iterates $x^{(2)}$, $x^{(3)}$, ... which approach x_α. The iterates are defined recursively by the general *iteration formula*

$$x^{(n+1)} = x^{(n)} - \frac{f(x^{(n)})}{f'(x^{(n)})}$$

to solve $f(x) = 0$.

Newton's Method for a System of Nonlinear Equations

Newton's method for $f(x) = 0$ is extended accordingly to the system $\mathbf{F}(\mathbf{A}) = \mathbf{0}$.

The initial estimate for the true solution is $\mathbf{A}^{(0)} = (A_1^{(0)}, A_2^{(0)}, \ldots, A_{m+1}^{(0)})$. The formula for the iterate $\mathbf{A}^{(1)} = (A_1^{(1)}, A_2^{(1)}, \ldots, A_{m+1}^{(1)})$ is found analogously to that of the iterate $x^{(1)}$ in the one variable system. The tangent hyperplane for the multivariable system is also analogous to the tangent line for the one variable system. Therefore, at each time level T_k for $k = 2, 3, \ldots, n+1$:

$$\mathbf{A}^{(1)} = \mathbf{A}^{(0)} - \left[\mathbf{F}'\left(\mathbf{A}^{(0)}\right)\right]^{-1} \mathbf{F}\left(\mathbf{A}^{()}\right)$$

or

$$\mathbf{A}^{(1)} = \mathbf{A}^{(0)} - \mathbf{F}'\left(\mathbf{A}^{(0)}\right) \backslash \mathbf{F}\left(\mathbf{A}^{(0)}\right) . \tag{4.16}$$

1. The $m \times 1$ column vector $\mathbf{F}\left(\mathbf{A}^{(0)}\right)$ encapsulates system (4.11):

$$\mathbf{F}\left(\mathbf{A}^{(0)}\right) = \begin{pmatrix} \frac{1}{4}A_1^{(0)\,2} + bA_1^{(0)} + c \\ \frac{1}{4}A_2^{(0)\,2} + bA_2^{(0)} + c \\ \vdots \\ \frac{1}{4}A_m^{(0)\,2} + bA_m^{(0)} + c \end{pmatrix} ;$$

   with b and c by (4.12) and (4.13) respectively. The i-th component of the vector is the $(i+1)$-th equation (4.10). For example, the components for $i = 1$ and $i = 2$ are (4.14) and (4.15) respectively.

2. The function $\mathbf{F} : \Re^{m+1} \to \Re^{m+1}$ is differentiable. The *Frechet derivative* of $\mathbf{F}(\mathbf{A})$, written $\mathbf{F}'(\mathbf{A})$, is the $m \times (m+1)$ Jacobian matrix:

$$\mathbf{F}'\left(\mathbf{A}^{(0)}\right) = J_{\mathbf{F}}\left(A^{(0)}\right) = \begin{pmatrix} \frac{\partial F_1}{\partial A_1^{(0)}} & \frac{\partial F_1}{\partial A_2^{(0)}} & \cdots & \frac{\partial F_1}{\partial A_{m+1}^{(0)}} \\ \frac{\partial F_2}{\partial A_1^{(0)}} & \frac{\partial F_2}{\partial A_2^{(0)}} & \cdots & \frac{\partial F_2}{\partial A_{m+1}^{(0)}} \\ \vdots & \vdots & \ddots & \vdots \\ \frac{\partial F_m}{\partial A_1^{(0)}} & \frac{\partial F_m}{\partial A_2^{(0)}} & \cdots & \frac{\partial F_m}{\partial A_{m+1}^{(0)}} \end{pmatrix} ;$$

For the $i = 1$ component then by (4.14):

$$\begin{aligned}
\frac{\partial F_1}{\partial A_1^{(0)}} &= \frac{1}{2}A_1^{(0)} + \frac{2^{\frac{3}{4}}}{\Gamma(\frac{5}{4})}\frac{4(\mathrm{D}x)^{\frac{3}{4}}}{3\mathrm{D}T} \\
\frac{\partial F_1}{\partial A_2^{(0)}} &= \frac{1}{2}A_2^{(0)} \\
\frac{\partial F_1}{\partial A_3^{(0)}} &= \ldots = \frac{\partial F_1}{\partial A_{m+1}^{(0)}} = 0\,;
\end{aligned}$$

for the $i = 2$ component then by (4.15):

$$\begin{aligned}
\frac{\partial F_2}{\partial A_1^{(0)}} &= \frac{2^{\frac{3}{4}}}{\Gamma(\frac{5}{4})}\frac{4(\mathrm{D}x)^{\frac{3}{4}}}{3\mathrm{D}T}\left[2^{\frac{3}{4}} - 1^{\frac{3}{4}}\right] \\
\frac{\partial F_2}{\partial A_2^{(0)}} &= \frac{1}{2}A_2^{(0)} + \frac{2^{\frac{3}{4}}}{\Gamma(\frac{5}{4})}\frac{4(\mathrm{D}x)^{\frac{3}{4}}}{3\mathrm{D}T} \\
\frac{\partial F_2}{\partial A_3^{(0)}} &= \frac{1}{2}A_3^{(0)} \\
\frac{\partial F_2}{\partial A_4^{(0)}} &= \ldots = \frac{\partial F_2}{\partial A_{m+1}^{(0)}} = 0\,;
\end{aligned}$$

and so forth.

3. The backslash "\" indicates left matrix division as used in MATLAB.

MATLAB

The system of equations (4.16) to find iterates $\mathbf{A}^{(1)}$ of the Newton's method process are matrices in a MATLAB algorithm.

The boundary conditions (4.4) take into account parameter $a(T)$ (4.3) and are applied at the endpoints $x = x_1$ and $x = x_{m+1}$. The initial conditions are applied at the first time step $T_1 = 0$ to be used in the process to find a solution at T_2, the solution at T_2 is the 'initial condition' to find a solution at T_3, and so forth until T_{n+1}. There is the possibility of tens of thousands or more total time and spatial grid points and hence, only information for two iterates are stored in the computer memory at one instant. The iteration starts with $\mathbf{A}^{(0)}$ to find the update $\mathbf{A}^{(1)}$, which in turn replaces the original $\mathbf{A}^{(0)}$, to find a new update $\mathbf{A}^{(1)}$, and so on until the values of

$A_i^{(1)}$ from successive iterations differ by less than a small error E of tolerance *tol*. The solution at each spatial point for each time level is output into a data file. The method then moves up to the next time level.

The error is defined as the infinity norm of the difference between the values of two successive iterations:

$$\begin{aligned} E &= \left|\mathbf{A}^{(1)} - \mathbf{A}^{(0)}\right|_\infty \\ &= \max\left(\left|A_1^{(1)} - A_1^{(0)}\right|, \left|A_2^{(1)} - A_2^{(0)}\right|, \ldots, \left|A_{m+1}^{(1)} - A_{m+1}^{(0)}\right|\right) ; \end{aligned} \tag{4.17}$$

the tolerance *tol* is set as

$$tol = 1 \times 10^{-12} \tag{4.18}$$

and the maximum number of iterations is set as 50, at which point divergence is assumed. The tolerance and maximum number of iterations are both set arbitrarily.

4.3 Smith & Elliott (1985) Algorithm Test

The method used to solve the $A(x,T)$ equation (4.1) is tested using the normalised quasi-steady form (4.5) from Smith & Elliott (1985):

$$A^2(x,T) - x^2 - 1 = -\int_{-\infty}^{x} \frac{\partial A}{\partial T}(\xi,T)\,\frac{\mathrm{d}\xi}{(x-\xi)^{\frac{1}{4}}}$$

where $\bar{\Gamma} = -1$ (hence $a(T) = -0.5$) and the constant $\frac{2^{\frac{3}{4}}}{\Gamma(\frac{5}{4})}$ is replaced by 1. The numerical method described in Section 4.2 is adjusted accordingly. The boundary conditions (4.6) are

$$A(x,T) = (|x|^2 + 1)^{\frac{1}{2}}\,, \qquad x = x_1,\, x_{m+1}\,. \tag{4.19}$$

The initial conditions 0, 1, 2, 3 (abbreviated "IC0", "IC1", "IC2", "IC3") are,

respectively:

$$\text{IC0: } A(x,0) = \sqrt{(x^2+1)}\,, \tag{4.20}$$

$$\text{IC1: } A(x,0) = \begin{cases} \frac{\sqrt{(2.5^2+1)}}{\sqrt{(2.5^2+1+0.4)}}\sqrt{(x^2+1+0.4)}\,, & |x| \le 2.5 \\ \sqrt{(x^2+1)}\,, & |x| > 2.5\,; \end{cases} \tag{4.21}$$

$$\text{IC2: } A(x,0) = \begin{cases} 1.25|x|\,, & |x| \le 1.3 \\ \sqrt{(x^2+1)}\,, & |x| > 1.3\,; \end{cases} \tag{4.22}$$

$$\text{IC3: } A(x,0) = \begin{cases} -1.8\cos\left(\frac{\pi}{2}x\right), & |x| \le 1 \\ \frac{\sqrt{(x_{m+1}^2+1)}}{\sqrt{(x_{m+1}^2-1)}}\sqrt{(x^2-1)}\,, & |x| > 1 \end{cases} \tag{4.23}$$

where x_{m+1} is the positive end of the domain.[9]

"Typical computational solutions [are] with x-steps of 0.1 or 0.05, between $x = -15, 15$, and with a T-step of 0.01 or 0.005."[10] Hence, the MATLAB algorithm is tested from start time $T = 0$ to normalised end time $T = 1$; in either arbitrary domain $x \in [-20, 20]$ or $x \in [-40, 40]$; and on grids 1 and 2 as in Table 4.1. Grid 1 has step sizes $\mathrm{D}x = 0.1$, $\mathrm{D}T = 0.01$ and grid 2 has step sizes $\mathrm{D}x = 0.05$, $\mathrm{D}T = 0.005$, based on Smith & Elliott (1985). For the largest grid 2 in domain $x \in [-40, 40]$ then the number of T-levels are $(n+1) = 1001$ and x-steps are $(m+1) = 1601$. The smallest grid 0 in Table 4.1 with the largest step sizes is only used to confirm a pattern of convergence of results for IC2 and IC3 when comparing to those of Smith & Elliott (1985) later.

	$\mathrm{D}T$	$\mathrm{D}x$
grid 0	0.1	0.2
grid 1	0.01	0.1
grid 2	0.001	0.05

Table 4.1: Grids and step sizes for implementing the Smith & Elliott (1985) test in either domain $x \in [-20, 20]$ or $x \in [-40, 40]$.

[9]The initial conditions IC1, IC2 and IC3 from Smith & Elliott (1985) are not explicitly stated and only illustrated in Figures like 4.11 and 4.19, so an estimate by observation from the Figures has to be made. Initial conditions IC1 and IC2 are shown in Figure 4.11 whilst IC3 is in Figure 4.22. The authors Smith & Elliott were contacted for details on the numerical treatment of equation (4.5). However, "there is only the paper itself."

[10]Smith & Elliott (1985)

The MATLAB algorithm is deemed to have passed the test if all the following conditions are met.

1. The error E (4.17) reduces quadratically towards zero with each iteration when the iterate is sufficiently close to the solution, as is expected of Newton's method.

2. The boundary conditions (4.19) are satisfied at all time levels. Moreover, the boundary condition is treated as a function of x and the $A(x,T)$ solution must approach this function smoothly when $|x|$ is large such that it does not oscillate near the end points. The boundary condition test is also applied to solutions from IC2 and IC3 on grid 0.

3. The $A(x,T)$ solutions match with those of Smith & Elliott (1985).

Test Results for Error E

The error E (4.17) decreases quadratically to zero when sufficiently close to the solution for all combinations of initial condition, domain and grid. Sample errors taken from calculations starting from initial conditions IC0 (4.20), IC1 (4.21) and IC2 (4.22) in domain $x \in [-40, 40]$ on grid 2 from Table 4.1 are shown in Table 4.2. In particular, when the error is written in typical scientific notation then the exponents of base 10 double with each iteration until tolerance *tol* (4.18) is reached.

For initial condition IC3 (4.23), the error decreases quadratically to zero when sufficiently close to the solution, like in all the cases for IC0, IC1 and IC2, as shown in Table 4.3. However, it is also found that there is divergence of Newton's method, and there is no convergence within the maximum number of 50 iterations, after a critical point in time. The critical end time T_{end}, when breakdown is assumed to occur, recedes with increase in grid size. (See Table 4.4 and comparison of results with Smith & Elliott (1985) later.)

IC	iteration	error E
IC0	0	2.865067×10^{-6}
	1	$< 1 \times 10^{-12}$
IC1	0	$1.76728387 \times 10^{-4}$
	1	2×10^{-11}
	2	$< 1 \times 10^{-12}$
IC2	0	$1.407599599 \times 10^{-3}$
	1	3.555×10^{-9}
	2	$< 1 \times 10^{-12}$

Table 4.2: Errors E from IC0, IC1 and IC2; domain $x \in [-40, 40]$; grid 2; at $T_{1000} = 0.999$ to calculate $A(x,T)$ at $T_{1001} = 1.0$.

time T	iteration	error E
0.001	0	$4.323719199 \times 10^{-3}$
	1	1.4516×10^{-8}
	2	$< 1 \times 10^{-12}$
$\vdots$		
0.497	0	1109.437292575230
	1	1076.655195212564
	2	874.267009037706
	3	493.696351819074
	4	205.384173585640
	5	51.577313418186
	6	4.521632857525
	7	$3.8880380903 \times 10^{-2}$
	8	2.712953×10^{-6}
	9	1×10^{-12}

Table 4.3: Errors E from IC3; domain $x \in [-40, 40]$; grid 2; at $T_1 = 0$ to calculate $A(x,T)$ at $T_2 = 0.001$ and at $T_{495} = 0.496$ to calculate $A(x,T)$ at $T_{\text{end}} = 0.497$.

	domain	end time T_{end}
grid 0	$[-20, 20]$	convergence
	$[-40, 40]$	
grid 1	$[-20, 20]$	0.69
	$[-40, 40]$	0.68
grid 2	$[-20, 20]$	0.499
	$[-40, 40]$	0.497

Table 4.4: Initial condition IC3 end time points T_{end}, by domain and grid.

Test Results for Boundary Conditions

For all possible combinations of initial condition, domain and grid, the solutions matched the boundary conditions (4.19) for all time. The boundary condition function and the solutions are shown at sample time points as coinciding lines in the regions outside a small neighbourhood of the origin $x = 0$ in Figures 4.5 to 4.8.

Indeed for the steady state initial condition IC0 (4.20), which coincides with the boundary condition, there is no deviation from the start such that the solutions remain the same for all time. (See Figure 4.5.)

For initial condition IC3 (4.23), there is no convergence of Newton's method after the end time T_{end}. (See test results for error E and end times in Table 4.4.) However, the boundary conditions are still satisfied up to the end time.

Note that solutions near the origin in Figures 4.5 to 4.8, which can appear like oscillations, can be ignored here since the Figures intend to show that solutions satisfy the boundary conditions at the ends of the computational domain.

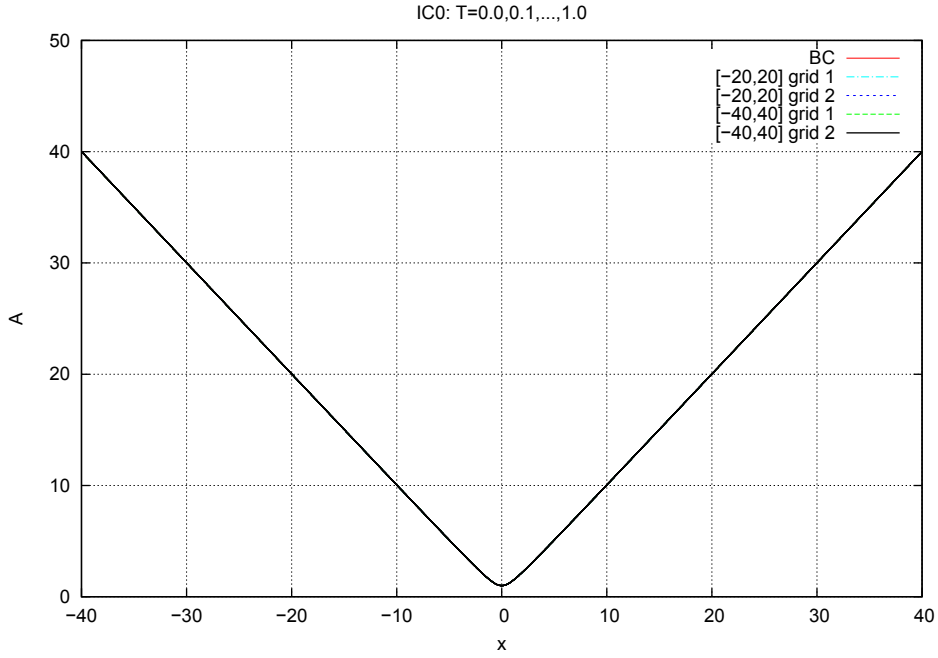

Figure 4.5: Boundary condition BC and $A(x,T)$ from IC0, at $T = 0.0, 0.1, \ldots, 1.0$, by domain and grid.

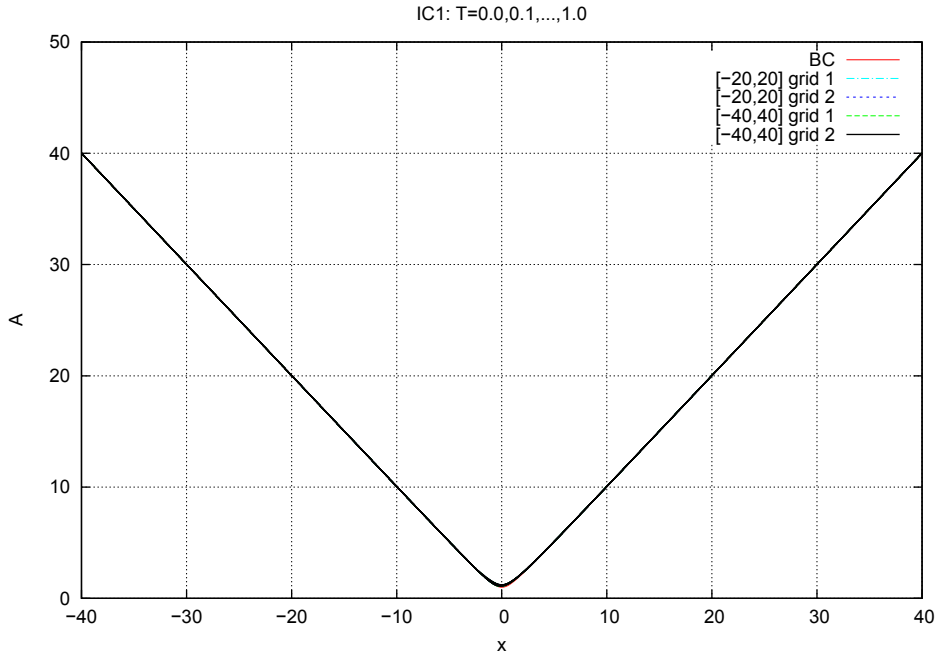

Figure 4.6: Boundary condition BC and $A(x,T)$ from IC1. See Figure 4.5.

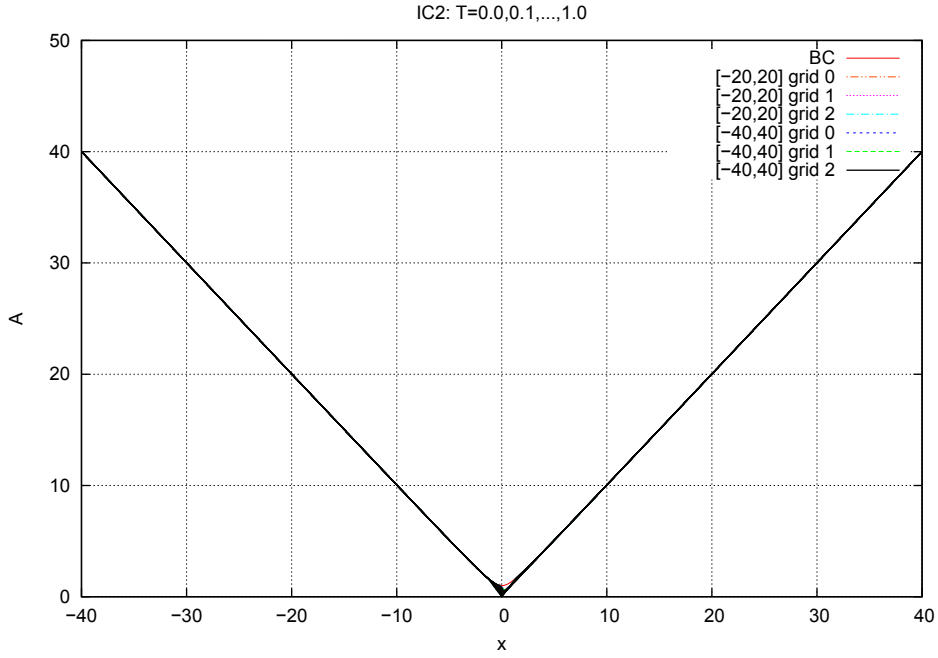

Figure 4.7: Boundary condition BC and $A(x,T)$ from IC2. See Figure 4.5.

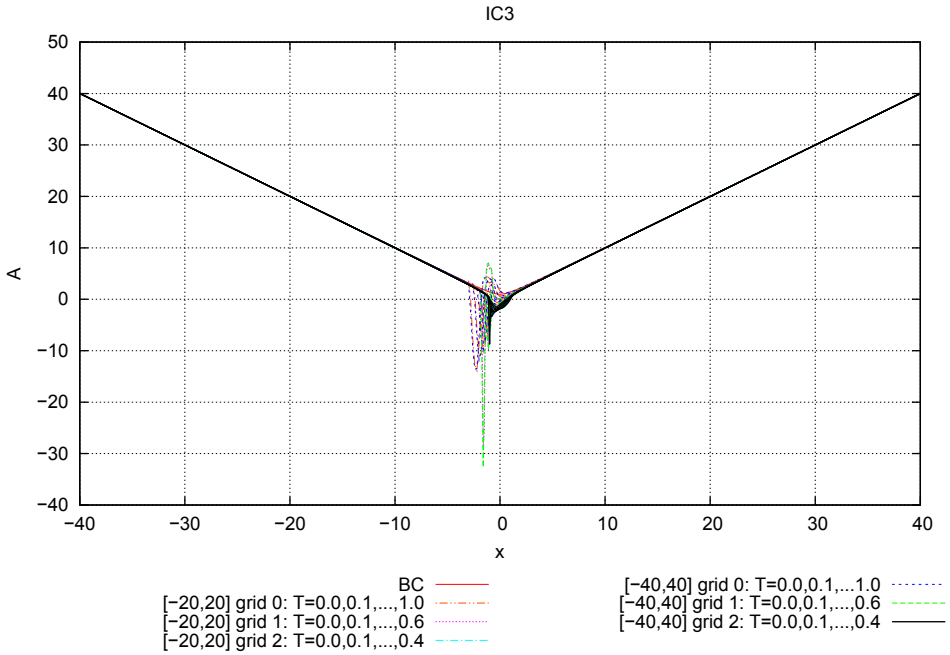

Figure 4.8: Boundary condition BC and $A(x,T)$ from IC3, at sample time levels at intervals of $\Delta T = 0.1$ until T_{end}, by domain and grid.

Comparison of Results with Smith & Elliott (1985)

All the solutions from each initial condition converge with increase in domain size and decrease in step sizes. They are also in good agreement with the corresponding solutions by Smith & Elliott (1985).

The solution from the steady state initial condition IC0 (4.20), as shown in Figure 4.9, is identical to the boundary condition and does not change for all time, which is correct and as expected.

The solution from IC1 (4.21) at $T = 0.6$, as shown in Figure 4.10, can be compared with the corresponding result from Smith & Elliott (1985) in Figure 4.11. The solutions, by domain and grid, appear identical.

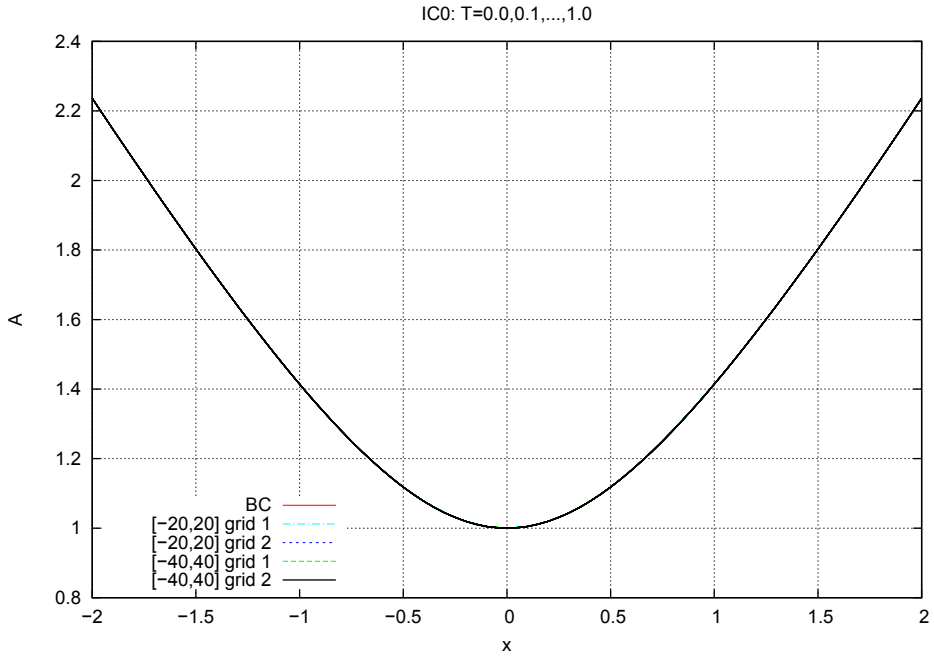

Figure 4.9: Boundary condition BC and $A(x,T)$ from IC0 at $T = 0.0, 0.1, \ldots, 1.0$, by domain and grid.

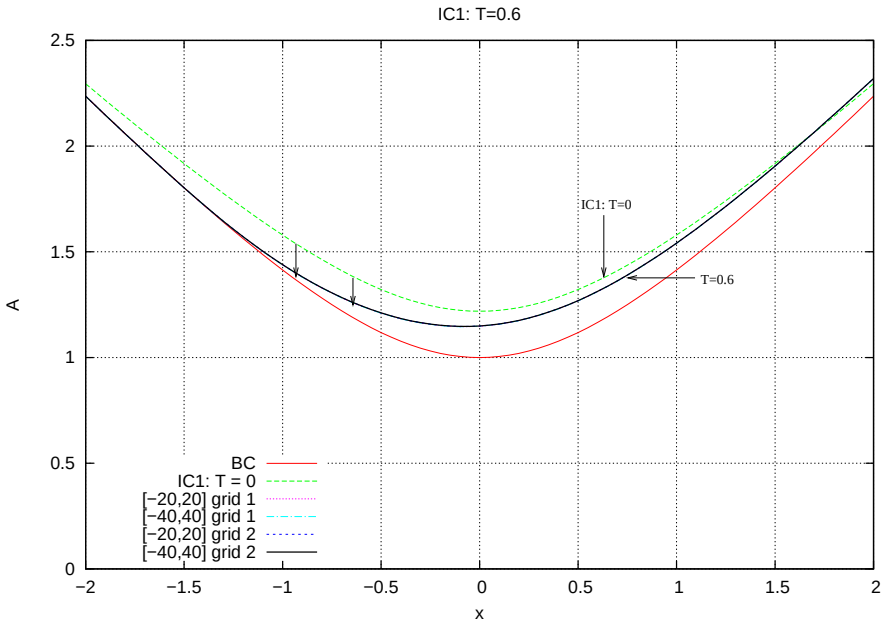

Figure 4.10: $A(x,T)$ from IC1 at $T = 0.6$, by domain and grid.

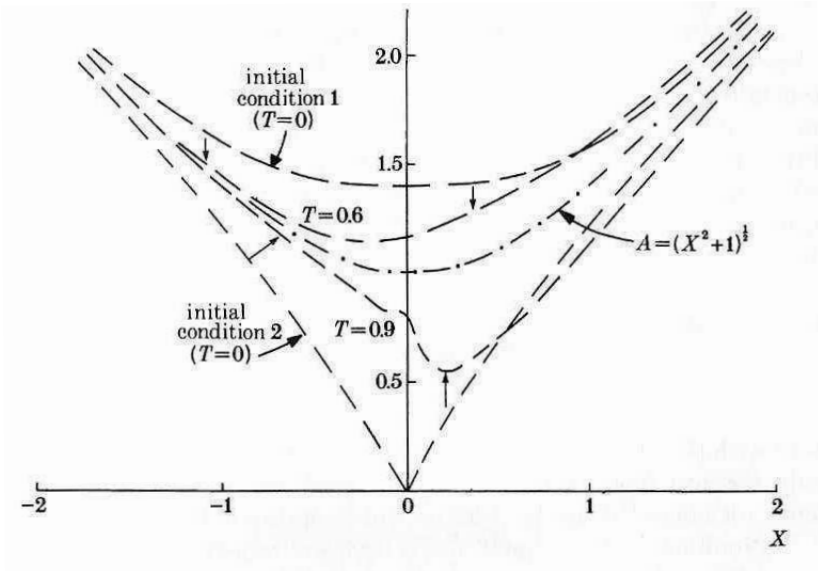

Figure 4.11: Smith & Elliott (1985) Figure 1(a), p. 8; $A(x,T)$ from initial condition 1 at $T = 0.6$; and from initial condition 2 at $T = 0.9$; also with boundary condition $A = (X^2 + 1)^{\frac{1}{2}}$, where X = x.

The solution from IC2 (4.22) at $T = 0.9$, arranged by grid in Figure 4.12, are identical such that, for example, the result for domain $x \in [-20, 20]$; grid 2 is the same as that for domain $x \in [-40, 40]$; grid 2. If the domain is sufficiently large then only step size, and thus grid size, affects the output. As the grids increase in size from 0, 1 to 2 in Table 4.1 and step sizes become smaller, the results converge to the solutions of Smith & Elliott (1985). The results from grid 1 and grid 2 are nearly identical. The solution for grid 2 at $T = 0.9$, as shown in Figure 4.13, can be compared with the corresponding result from Smith & Elliott (1985) in Figure 4.11.[11]

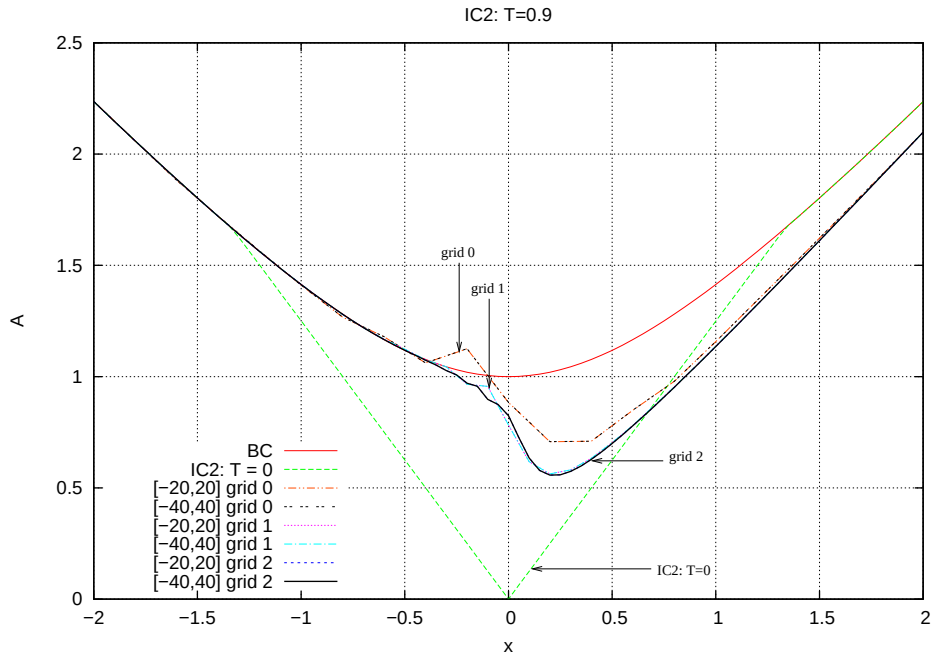

Figure 4.12: $A(x,T)$ from IC2 at $T = 0.9$, by domain and grid.

[11]The grid sizes and step sizes, for the results in Figure 4.13, are not explicitly stated by Smith & Elliott (1985).

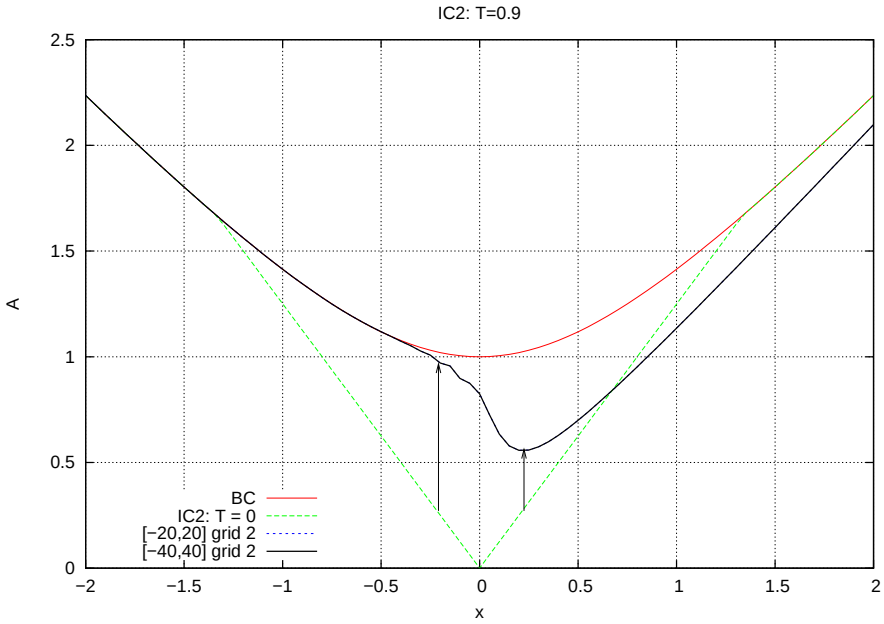

Figure 4.13: $A(x,T)$ from IC2, grid 2 at $T = 0.9$.

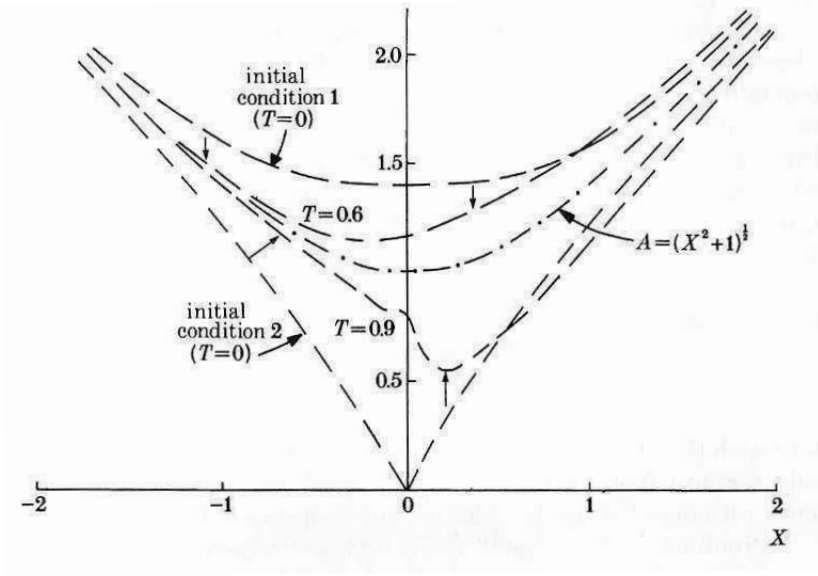

Figure 4.14: Smith & Elliott (1985); see Figure 4.11.

Similarly the solution from IC3 (4.23) at $T = 0.1, 0.2, 0.3$, arranged by grid in Figures 4.15, 4.16, 4.17, are identical on each time level and by domain such that only grid size affects the output, like in the case of IC2. The domain is sufficiently large as to not affect the output. As the grids increase in size from 0, 1 to 2, the results converge to the solutions of Smith & Elliott (1985). The results from grid 1 and grid 2 are nearly identical. The solution for grid 2 at $T = 0.1, 0.2, 0.3$, as shown in Figure 4.18, can be compared with the corresponding result from Smith & Elliott (1985) in Figure 4.19.[12] The results are not identical but are very alike. For example, the length of the parabola along the x-axis where $A(x,T)$ is negative is similar. Furthermore, the position and depth of the parabola apex are also similar. This is because the Smith & Elliott (1985) initial condition 3, of which IC3 is based, is not explicitly stated and an estimate by observation was made.

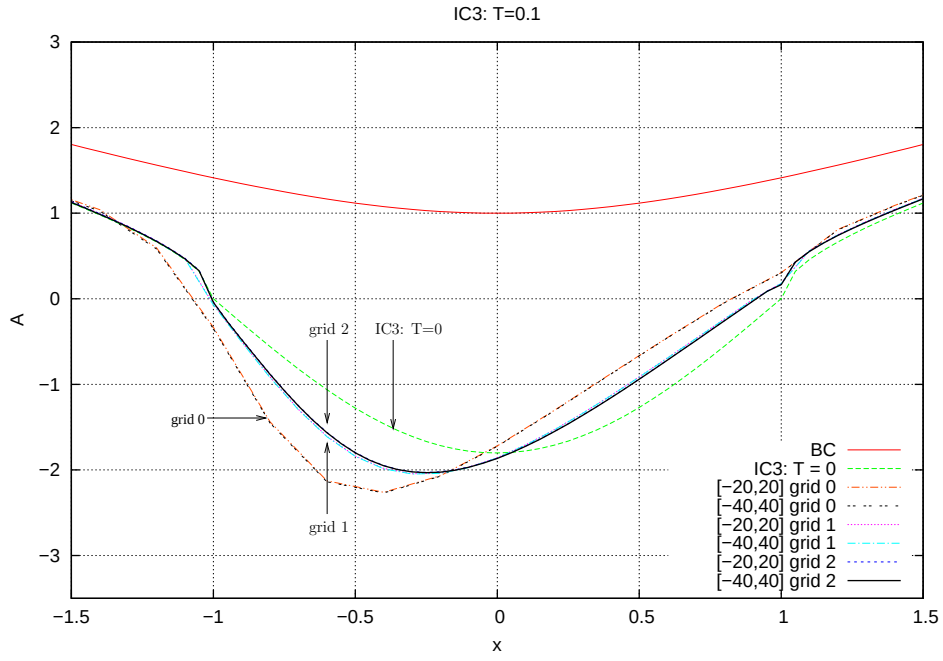

Figure 4.15: $A(x,T)$ from IC3 at $T = 0.1$, by domain and grid.

[12]The grid sizes and step sizes, for the results in Figure 4.19, are not explicitly stated by Smith & Elliott (1985).

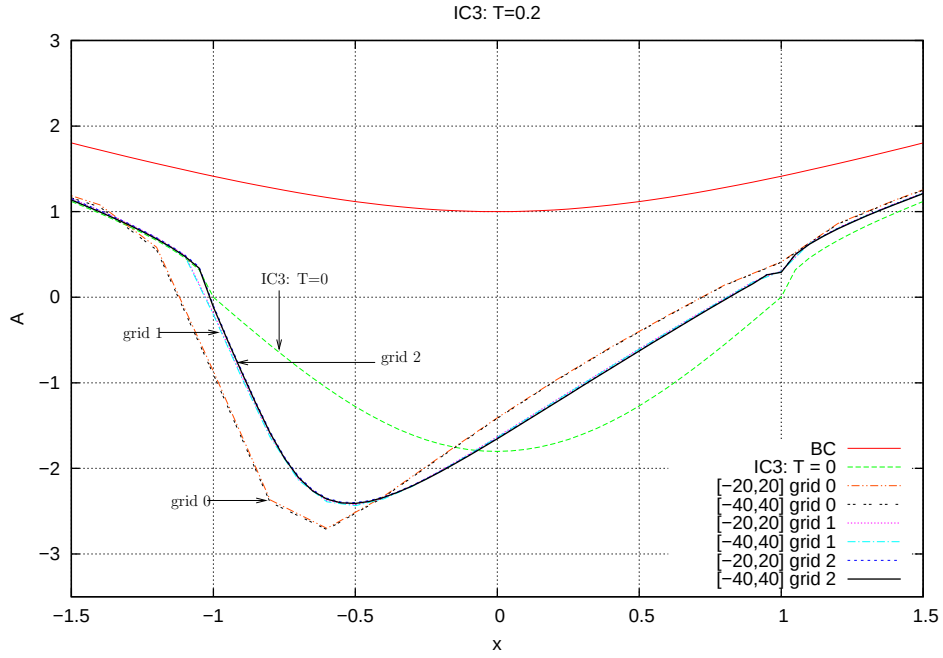

Figure 4.16: $A(x,T)$ from IC3 at $T = 0.2$, by domain and grid.

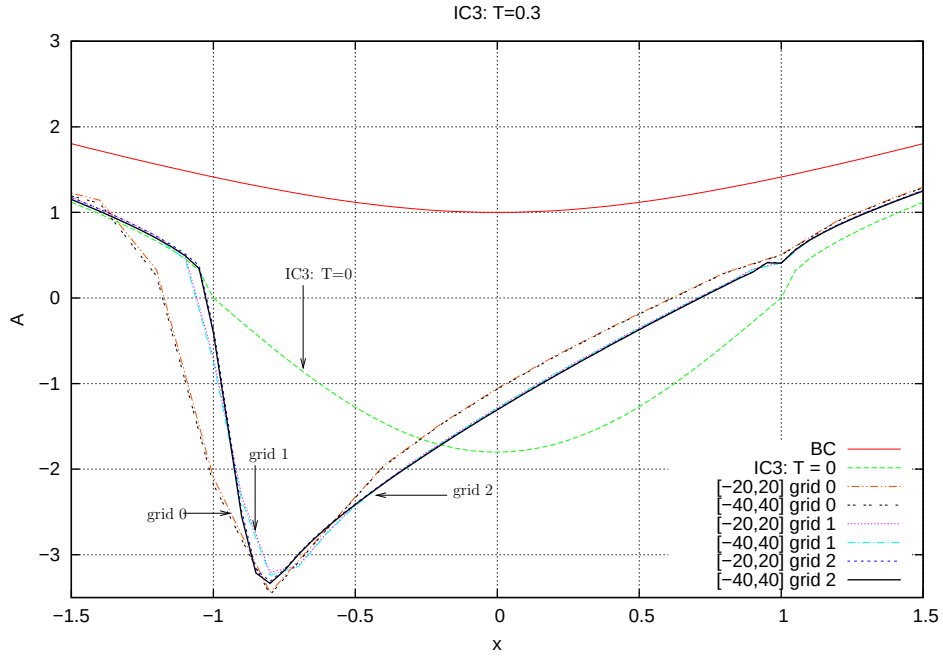

Figure 4.17: $A(x,T)$ from IC3 at $T = 0.3$, by domain and grid.

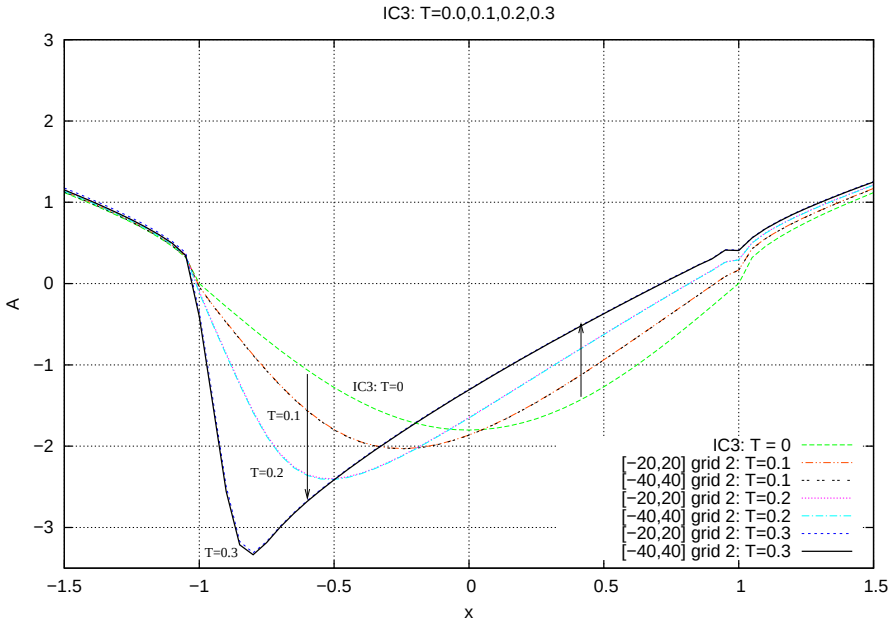

Figure 4.18: $A(x,T)$ from IC3, grid 2 at $T = 0.1,\ 0,2,\ 0.3$.

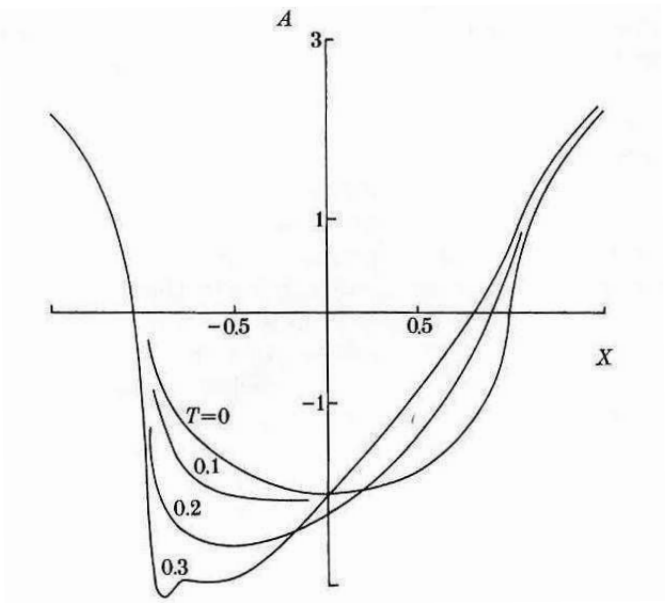

Figure 4.19: Smith & Elliott (1985) Figure 1(b), p. 8; $A(x,T)$ from initial condition 3 at $T = 0.0,\ 0.1,\ 0.2,\ 0.3$.

The small wrinkle in the solution at $x = \pm 1$, $A(x,T) \simeq 0$ in Figures 4.15, 4.16, 4.17 comes directly from a small jump in the crude statement of the initial condition

IC3 in MATLAB, also at approximately $x = \pm 1$. For example, IC3:

$$A(x,0) = \begin{cases} -1.8\cos\left(\frac{\pi}{2}x\right), & |x| \leq 1 \\ \frac{\sqrt{(x_{m+1}^2+1)}}{\sqrt{(x_{m+1}^2-1)}}\sqrt{(x^2-1)}, & |x| > 1 \end{cases}$$

is written in MATLAB for domain $x \in [-40, 40]$, grid 2, as

```
for j = 1:780
A(j,1) = (sqrt(c^2 - 2*O(1))/sqrt(c^2 - 1))*...
                 sqrt(x(j)^2 - 1);
end
for j = 822:1601
A(j,1) = (sqrt(c^2 - 2*O(1))/sqrt(c^2 - 1))*...
                 sqrt(x(j)^2 - 1);
end
for j = 781:821
A(j,1) = -1.8*cos((pi/2)*x(j));
end
```

where "c" is x_{m+1} and "O" is $a(T)$. However, the wrinkle disturbance is relatively small and localised, as shown in the sequence of Figures 4.15, 4.16, 4.17, and hence, does not have any major effect on the solution elsewhere, especially when compared to the occurrence of a breakdown.

Comparison of Initial Condition 3 Breakdown with Smith & Elliott (1985)

As the end time T_{end} as given in Table 4.4, and therefore a breakdown, is approached, the solutions from IC3 (4.23) differ for grids 1 and 2, as shown in Figure 4.20. They are nearly identical for time points $T = 0.1, 0.2, 0.3$ not close to the end time, as shown in Figures 4.15, 4.16 and 4.17. However, with mesh refinement and increase in time comes the characteristic steepening of the $A(x,T)$ singularity, which will cause difficulty for Newton's method in determining a solution.

The solution for grid 1, as shown in Figure 4.21, can be compared with the results from Smith & Elliott (1985) in Figure 4.22. The results share similar characteristics, such as the position and depth of the parabola apex; and also the length of the region where $A \leq 0$, between $x = -1$ and $x = 1$.

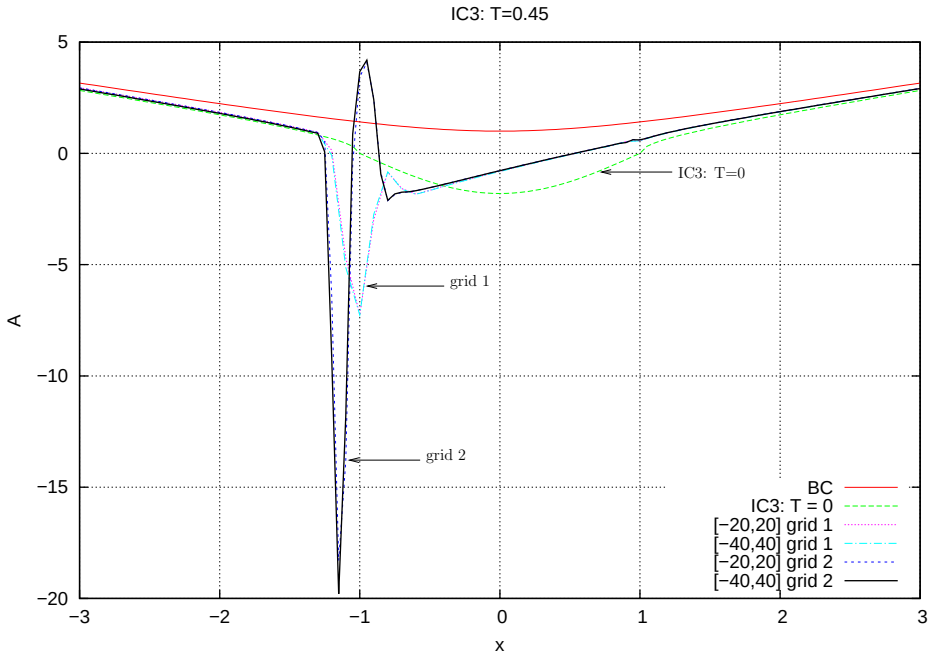

Figure 4.20: $A(x,T)$ from IC3 at $T = 0.45$, by domain and grid.

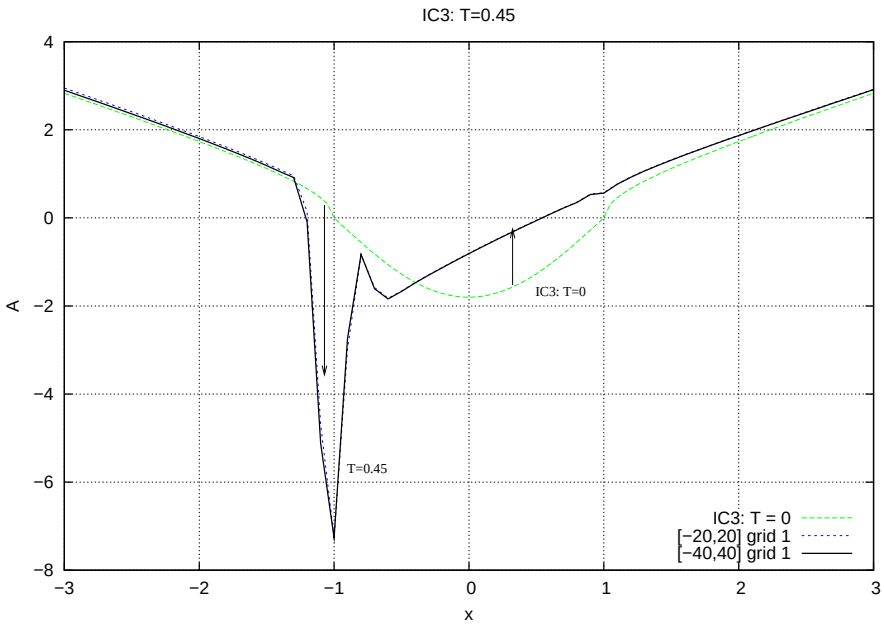

Figure 4.21: $A(x,T)$ from IC3, grid 1 at $T = 0.45$.

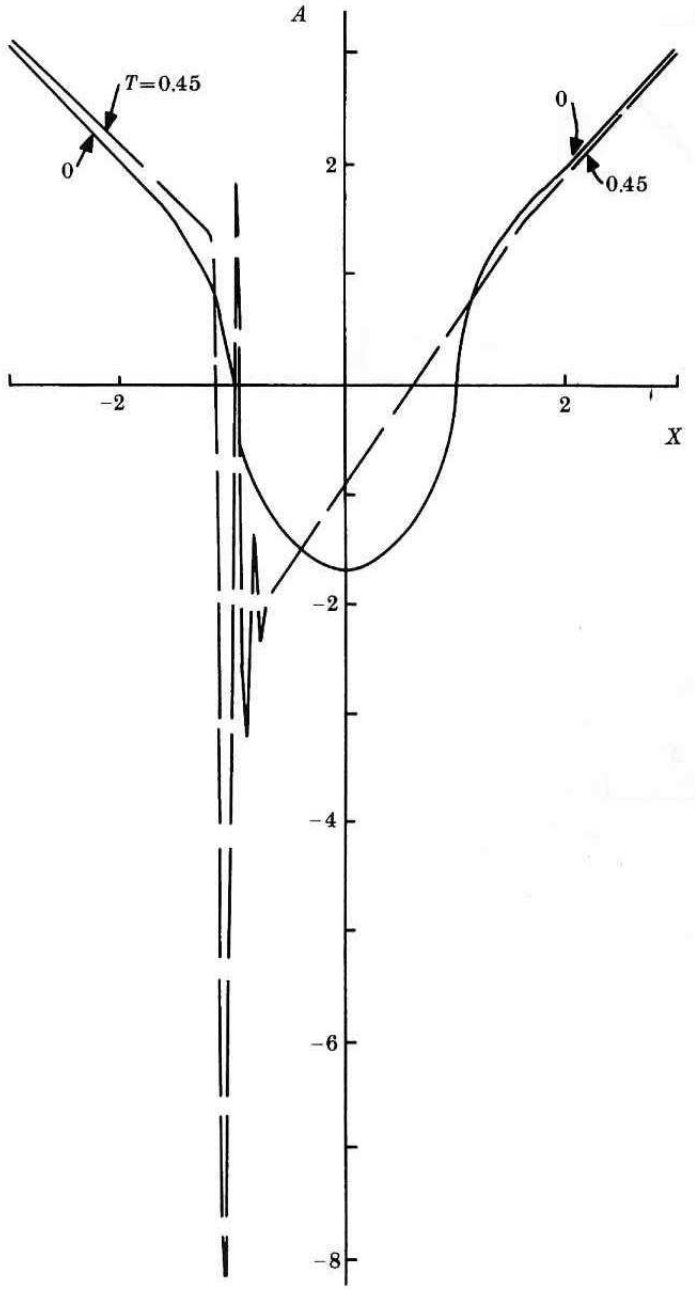

Figure 4.22: Smith & Elliott (1985) Figure 1(c), p. 9; $A(x,T)$ from initial conditions 3 at $T = 0.45$.

Smith & Elliott (1985) Test Summary

The MATLAB algorithm is working correctly.

1. The error decreases quadratically to zero with each iteration when the iterate is close to the true solution.

2. The $A(x,T)$ solutions satisfy the boundary conditions at $x = x_1,\ x_{m+1}$ and do not oscillate as the end points are approached.

3. The results from each of the initial conditions IC0, IC1, IC2, IC3 converge to their $A(x,T)$ solutions as the number of grid points are increased and step sizes are decreased. The domains $x \in [-20, 20]$ and $x \in [-40, 40]$ are sufficiently large such that the results are also domain independent and depend only on grid size. However, the results from initial condition IC3 for grid 1 and grid 2 are grid dependent as a breakdown at end time T_{end} is approached.[13]

4. The $A(x,T)$ solutions match those from Smith & Elliott (1985).

4.4 $A(x,T)$ Algorithm Test

The method used to solve the $A(x,T)$ equation (4.1) is tested using similar benchmarks from Section 4.3 such that the MATLAB algorithm for (4.1) is deemed to have passed the test if all the following conditions are met.

1. The error E (4.17) reduces quadratically towards zero with each iteration when the iterate is sufficiently close to the solution.

2. The boundary condition (4.6):

$$A(x,T) = \left(|x|^2 + 2a(T)\right)^{\frac{1}{2}}, \qquad x = x_1,\ x_{m+1}$$

[13]The breakdown is discussed in Section 4.5 and investigated further in Chapter 5.

with the angle of attack law (4.3):

$$a(T) = 1.331 - 1.332e^{-T}\,,$$

is satisfied at all time levels. Moreover, the boundary condition is treated as a function of x and T and the solution must approach this function smoothly such that it does not oscillate near the end points.

3. The results converge to true $A(x,T)$ solutions as the step sizes Dx and DT decrease towards zero. Following from Section 4.3, the test grids and the step sizes are those in Table 4.5. Furthermore, the test spatial domain is $x \in [-40, 40]$ since the size of the domain is sufficiently large such that only the grid affects the output.

	DT	Dx
grid 1	0.01	0.1
grid 2	0.001	0.05

Table 4.5: Grids and step sizes for implementing the $A(x,T)$ algorithm test in domain $x \in [-40, 40]$.

4.4.1 The Initial Conditions

Initial conditions applied at the start time $T = 0$ are based on but not identical to the initial conditions IC0 (4.20), IC1 (4.21), IC2 (4.22) and IC3 (4.23) from the Smith & Elliott (1985) test in Section 4.3. They take into account $a(T) \neq -0.5$ for all time T but $a(T)$ is a parameter for the angle of attack law (4.3) between $a(0) = -0.001$ and a value slightly above the critical value $a_c = 1.33$ as $T \to \infty$.

Initial conditions are directly related to skin friction by (4.2) and represent physical flow distributions. Thus:

1. Initial condition 0 (abbreviated "IC0") is

$$A(x,0) = \sqrt{(x^2 - 2a(0))}\,; \tag{4.24}$$

such that skin friction $A(x,T)$ is initially positive and continuous for all x and hence, the fluid flow is initially attached along the surface of the airfoil. It is similar to the boundary condition (4.6). The Smith & Elliott (1985) test analogy for $a(T) = -0.5$ in Section 4.3 leads to a steady state solution.

2. Initial condition 1 ("IC1") is a small deviation from IC0 (4.24):

$$A(x,0) = \begin{cases} \frac{\sqrt{(2.5^2-2a(0))}}{\sqrt{(2.5^2-2a(0)+0.4)}} \cdot \sqrt{(x^2-2a(0)+0.4)}\,, & |x| \le 2.5 \\ \sqrt{(x^2-2a(0))}\,, & |x| > 2.5\,; \end{cases} \tag{4.25}$$

and like IC0, the fluid flow is initially attached along the airfoil.

3. Initial condition 2 ("IC2") is

$$A(x,0) = \begin{cases} 1.25|x|\,, & |x| \le 0.1 \\ \sqrt{(x^2-2a(0))}\,, & |x| > 0.1\,; \end{cases} \tag{4.26}$$

such that there is point of zero skin friction on the surface. It is similar to the skin friction for the Ruban (1981) singular solution.

4. Initial condition 3 ("IC3") is

$$A(x,0) = \begin{cases} -1.8\cos\left(\frac{\pi}{2}x\right), & |x| \le 1 \\ \frac{\sqrt{(x_{m+1}^2-2a(0))}}{\sqrt{(x_{m+1}^2-1)}} \cdot \sqrt{(x^2-1)}\,, & |x| > 1\,; \end{cases} \tag{4.27}$$

where x_{m+1} is the positive end of the domain. A bubble of reversed flow is assumed to have formed on the surface where $A(x,0) \le 0$.

Test Results for Error E

The maximum time for calculations to take place is $T = 6$. In fact, a breakdown in the solution is approached as $a(T) \to 1.33+$ and there is no convergence of Newton's method within the maximum number of 50 iterations after a critical point in time T_{end}. (See Table 4.6.) Furthermore, the singularity affects Newton's method. As the

end time is approached, convergence occurs but quadratic convergence when close to the solution is not possible. The end time is defined as the final time point when convergence occurs even if it is not quadratic. End times for each initial condition, up to and including when convergence occurs, recedes with increase in grid size, as shown in Table 4.6 by grids from Table 4.5.

The error E (4.17) decreases quadratically to zero when sufficiently close to the solution for all combinations of initial condition and grid, as is expected of Newton's method, unless the time is close to the breakdown time T_{end}.

Sample errors taken from calculations starting from initial conditions IC0 (4.24), IC1 (4.25), IC2 (4.26), IC3 (4.27) are shown in Table 4.7. In particular, when the error is written in typical scientific notation then the exponents of base 10 double with each iteration until tolerance *tol* (4.18) is reached. This shows quadratic convergence when the iterate is sufficiently close to the true solution and when the time is not close to the end time.

Sample errors at time level $T_{\text{end}} - \mathrm{D}T$ to calculate $A(x,T)$ at T_{end} in Tables 4.8 and 4.9 show that convergence has occurred but the convergence is not always quadratic.

grid	IC	end time T_{end}
1	0	5.65
2		5.173
1	1	5.88
2		5.401
1	2	5.66
2		5.177
1	3	1.23
2		0.913

Table 4.6: Initial condition end times T_{end}, by grid.

IC	iteration	error E
IC0	0	6.766173×10^{-6}
	1	$< 1 \times 10^{-12}$
IC1	0	$2.51320030 \times 10^{-4}$
	1	4.2×10^{-11}
	2	$< 1 \times 10^{-12}$
IC2	0	2.0376042×10^{-7}
	1	$< 1 \times 10^{-12}$
IC3	0	$2.340954537 \times 10^{-3}$
	1	2.285×10^{-9}
	2	$< 1 \times 10^{-12}$

Table 4.7: Errors E from IC0, IC1, IC2 and IC3; grid 2; at $T_1 = 0$ to calculate $A(x,T)$ at $T_2 = 0.001$.

IC	time $T_{\text{end}} - \text{DT}$	iteration	error E
IC0	5.172	0	1717.592938318620
		1	1595.265344683801
		2	896.271970454078
		3	345.502932198180
		4	78.263549922884
		5	13.269820541586
		6	6.440831344971
		7	1.500206×10^{-6}
		8	1×10^{-12}
IC1	5.400	0	1797.811303470830
		1	1736.943973175772
		2	803.190652386907
		3	347.470163642688
		4	119.093827643628
		5	13.269820541586
		6	$1.68542552525 \times 10^{-1}$
		7	2.7045869×10^{-5}
		8	1×10^{-12}
		9	1×10^{-12}
		10	1×10^{-12}

Table 4.8: Errors E from IC0, IC1; grid 2; at $T_{\text{end}} - \text{D}T$ to calculate $A(x,T)$ at T_{end}.

IC	time $T_{\text{end}} - \text{DT}$	iteration	error E
IC2	5.172	0	2101.021631153894
		1	2221.167982868759
		2	963.744191383027
		3	744.053464031630
		4	334.137557127166
		5	95.012791953135
		6	8.6097901321272
		7	$7.0812114586 \times 10^{-2}$
		8	4.773039×10^{-6}
		9	$\sim 1 \times 10^{-12}$
		$\vdots$	$\vdots$
		25	$\sim 1 \times 10^{-12}$
IC3	0.913	0	2041.480693468861
		1	2027.071145151967
		2	1061.963965606352
		3	736.426077268789
		4	329.109635107306
		5	93.392652454807
		6	8.312139085395
		7	$6.5987627153 \times 10^{-2}$
		8	4.144692×10^{-6}
		9	$\sim 1 \times 10^{-12}$
		$\vdots$	$\vdots$
		15	$\sim 1 \times 10^{-12}$

Table 4.9: Errors E from IC2, IC3; grid 2; at $T_{\text{end}} - \text{D}T$ to calculate $A(x,T)$ at T_{end}.

Test Results for Boundary Conditions

The $A(x,T)$ solutions match the boundary conditions (4.6) at the far ends of the domain, as shown in Figures 4.23 to 4.26.

Note that solutions near the origin in Figures 4.23 to 4.26, which can appear like oscillations, can be ignored here since the Figures intend to show that solutions satisfy the boundary conditions at the ends of the computational domain.

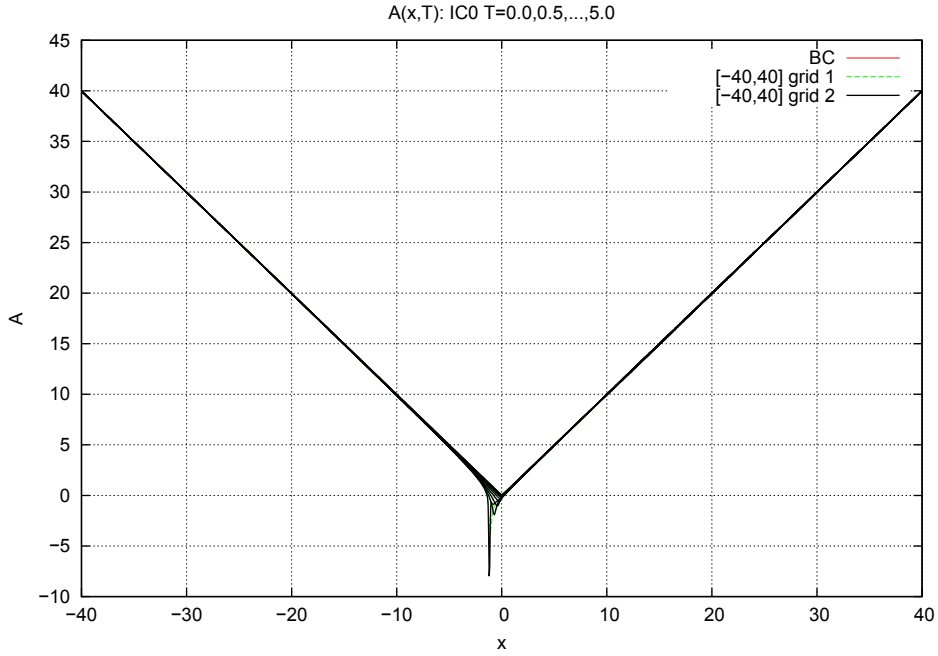

Figure 4.23: Boundary condition BC and $A(x,T)$ from IC0 at $T = 0.0, 0.5, \ldots, 5.0$, by grid, for domain $x \in [-40, 40]$.

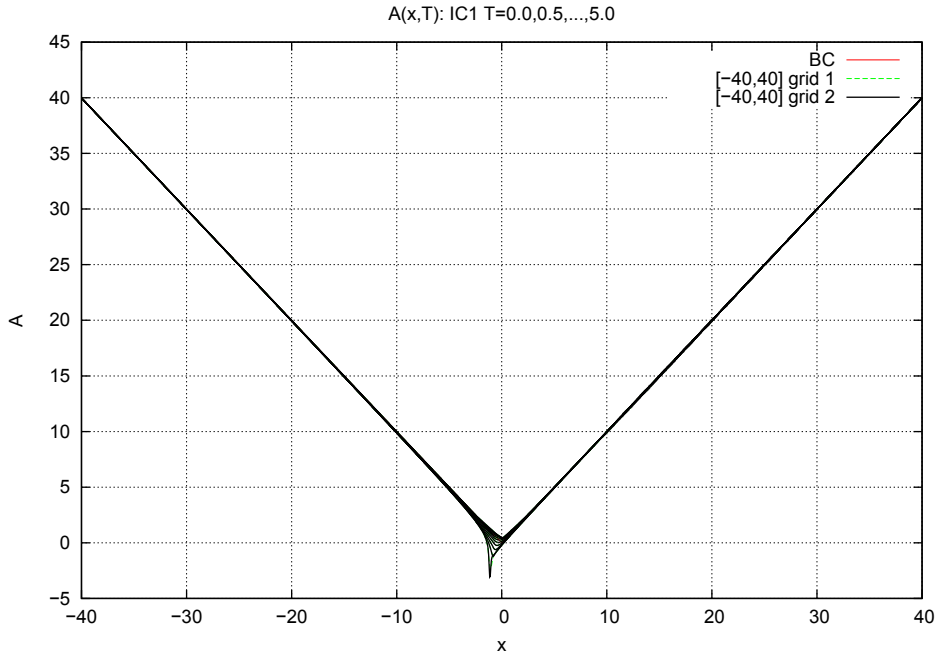

Figure 4.24: Boundary condition BC and $A(x,T)$ from IC1. See Figure 4.23.

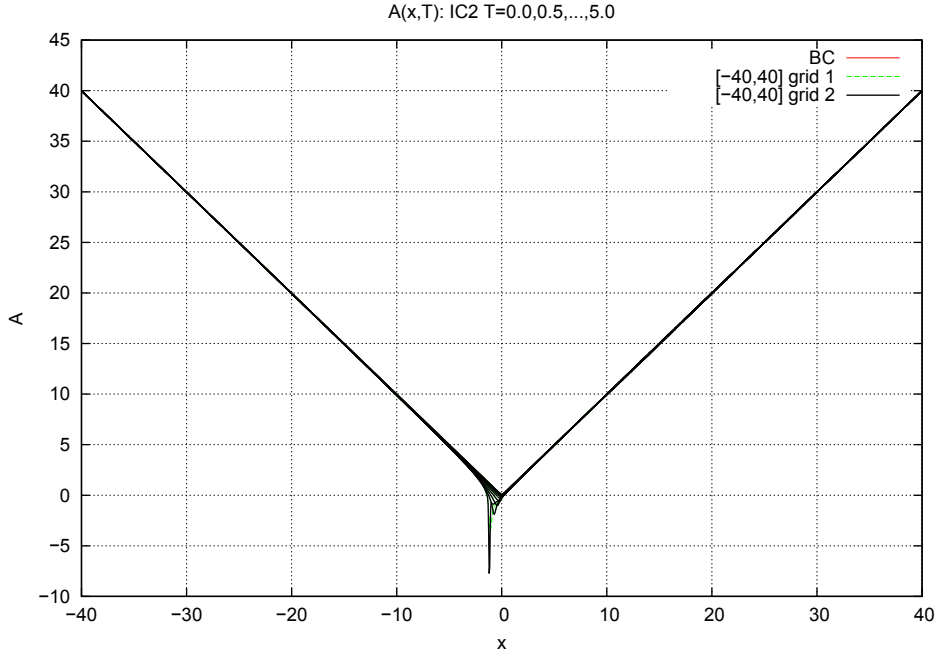

Figure 4.25: Boundary condition BC and $A(x,T)$ from IC2. See Figure 4.23.

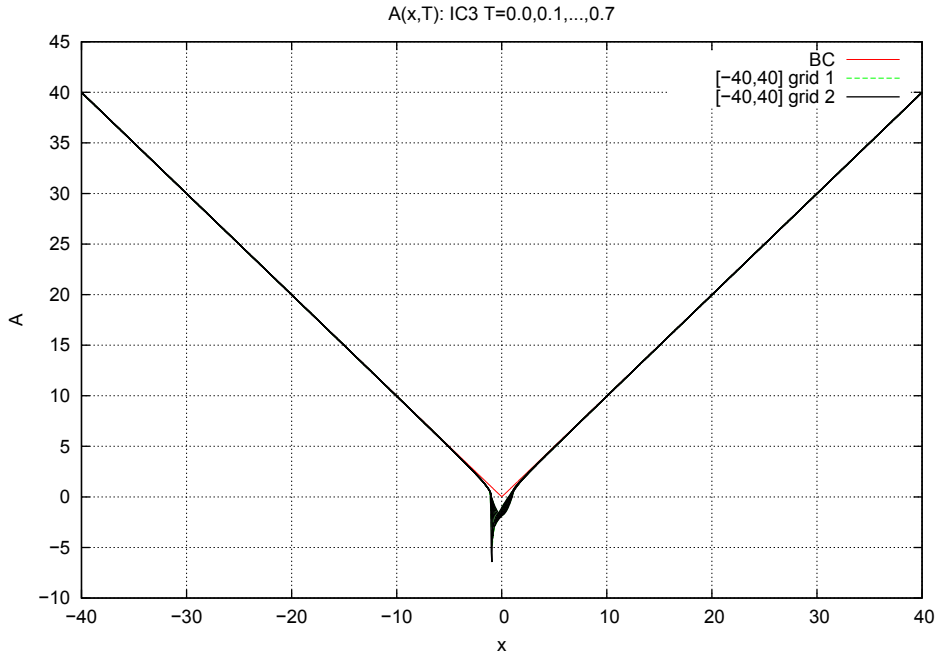

Figure 4.26: Boundary condition BC and $A(x,T)$ from IC3 at $T = 0.0,\ 0.1,\ \ldots,\ 0.7$, by grid, for domain $x \in [-40, 40]$.

Test Results for Grid Independence

The $A(x,T)$ solutions from initial conditions IC0 (4.24), IC1 (4.25), IC2 (4.26), IC3 (4.27) are grid independent up to times not close to breakdown at T_{end}, as shown in Figures 4.27 to 4.30.

Solutions from IC0, IC1 and IC2 break down at approximately $T = 5.5$ for grid 1 and at approximately $T = 5$ for grid 2. Results by grid begin to noticeably differ at approximately $T = 4$ and onwards, by observation. (See Figures 4.27 to 4.29.)

Solutions from IC3 break down at approximately $T = 1$ for grid 1 and approximately $T = 0.9$ for grid 2. Results become noticeably different from $T = 0.4$, again by observation. (See Figure 4.30.)

The difference in results by grid becomes more pronounced as the end time is approached. This is because Newton's method encounters difficulties as a singularity is approached, which is also seen in the tests for error E.

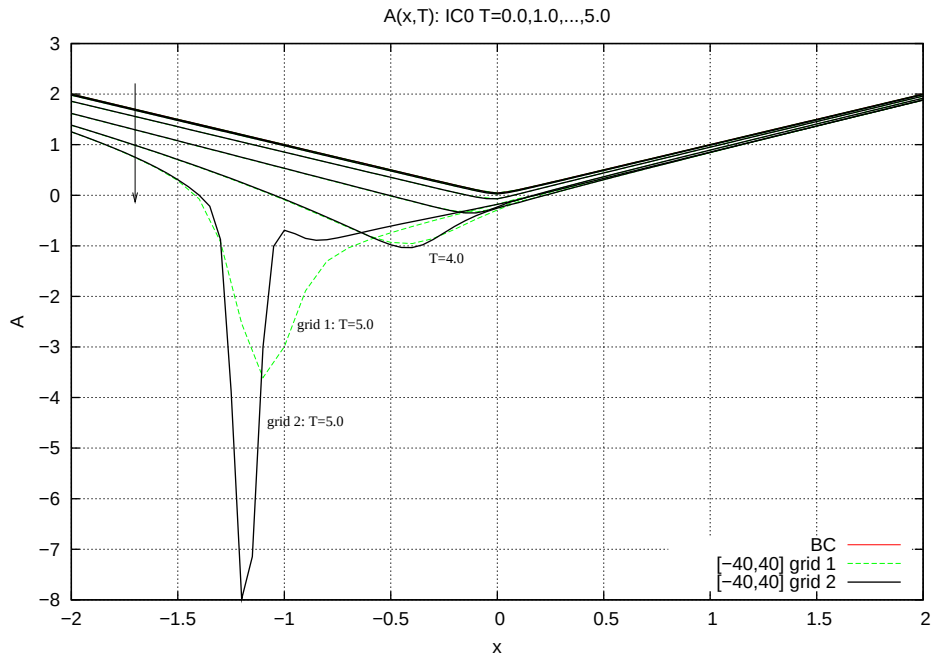

Figure 4.27: $A(x,T)$ from IC0 at $T = 0.0, 1.0, \ldots, 5.0$, by grid, for domain $x \in [-40, 40]$.

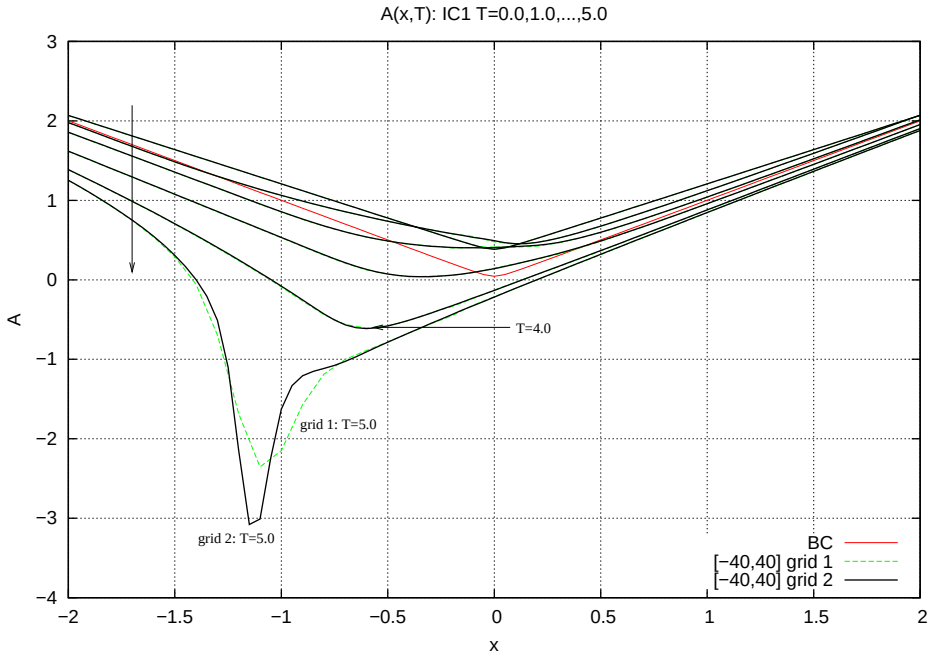

Figure 4.28: $A(x,T)$ from IC1 at $T = 0.0, 1.0, \ldots, 5.0$, by grid.

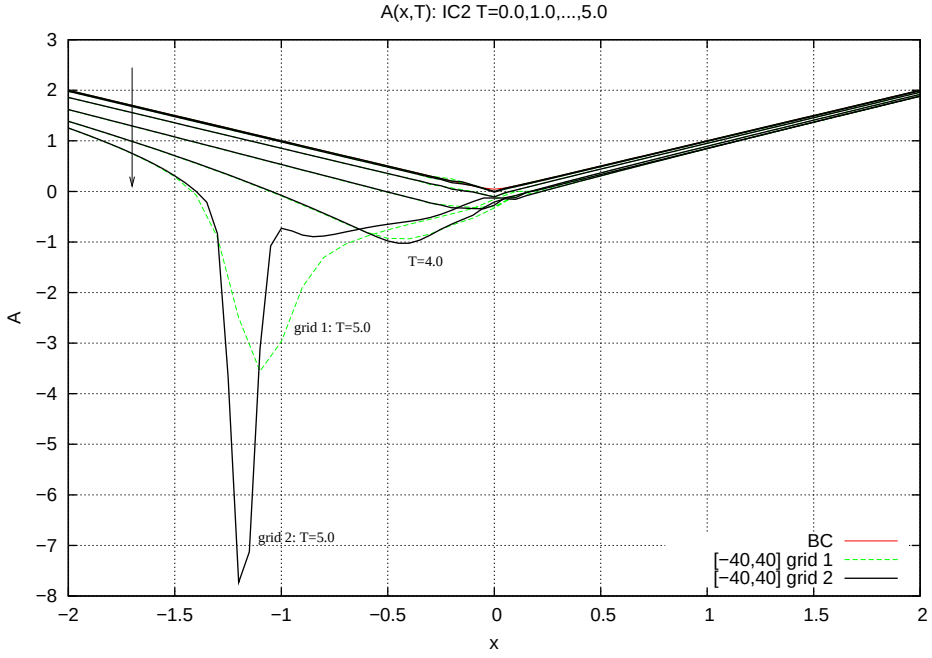

Figure 4.29: $A(x,T)$ from IC2 at $T = 0.0, 1.0, \ldots, 5.0$, by grid.

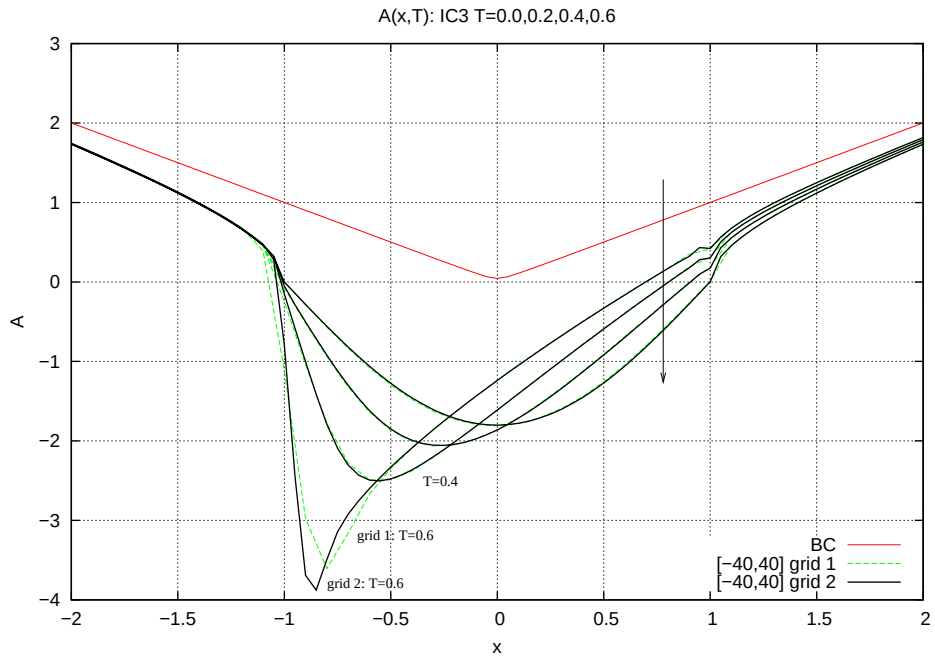

Figure 4.30: $A(x,T)$ from IC3 at $T = 0.0, 0.2, 0.4, 0.6$, by grid.

$A(x,T)$ Algorithm Test Summary

The $A(x,T)$ algorithm test results are similar to those for the Smith & Elliott (1985) test in Section 4.3. The MATLAB algorithm is working correctly.

1. The error decreases quadratically to zero with each iteration when the iterate is close to the true solution until a singularity at the end time T_{end} is approached. The steepening singularity causes difficulties for Newton's method.[14]

2. The $A(x,T)$ solutions satisfy the boundary conditions and they do no oscillate as the end points $x = x_1$ and $x = x_{m+1}$ are approached.

3. The results from each of the initial conditions IC0, IC1, IC2, IC3 converge to true solutions for $A(x,T)$ as the number of grid points are increased and step sizes are decreased. The domain $x \in [-40, 40]$ is sufficiently large such that the results are dependent only on grid size. In fact, the results for grid 1 and grid 2 are grid independent except until a breakdown at end time T_{end} is approached. This is also reflected in the test results for error E.

Similar to the jump in initial condition 3 (4.23) in Section 4.3 and thus the small wrinkles in solution from the Smith & Elliott (1985) test results, there are also small wrinkles in the solutions from IC2 (4.26) and from IC3 (4.27) as seen in the grid independence test Figures 4.29 and 4.30. For IC2, the small wrinkle at $x = -2.5$ comes directly from a small jump in the crude statement of the initial condition in MATLAB. For example, IC2:

$$A(x,0) = \begin{cases} 1.25|x|\,, & |x| \le 0.1 \\ \sqrt{(x^2 - 2a(0))}\,, & |x| > 0.1\,; \end{cases}$$

is written in MATLAB for domain $x \in [-40, 40]$, grid 2, as

```
for j = 2:797;
```

[14]The breakdown is discussed in Section 4.5 and investigated further in Chapter 5.

```
A(j,1) = sqrt(x(j)^2 - 2*O(1));
end
for j = 798:802;
A(j,1) = 1.25*abs(x(j));
end
for j = 803:1600;
A(j,1) = sqrt(x(j)^2 - 2*O(1));
end
```

where "O" is $a(T)$. For IC3, the small wrinkle at $x = \pm 1$ comes directly from a small jump in the crude statement of the initial condition in MATLAB. Again, for domain $x \in [-40, 40]$, grid 2, then IC3:

$$A(x,0) = \begin{cases} -1.8\cos\left(\frac{\pi}{2}x\right), & |x| \leq 1 \\ \frac{\sqrt{(x_{m+1}^2 - 2a(0))}}{\sqrt{(x_{m+1}^2 - 1)}} \cdot \sqrt{(x^2-1)}, & |x| > 1 \end{cases}$$

is written in MATLAB as

```
for j = 1:780
A(j,1) = (sqrt(c^2 - 2*O(1))/sqrt(c^2 - 1))*...
sqrt(x(j)^2 - 1);
end
for j = 822:1601
A(j,1) = (sqrt(c^2 - 2*O(1))/sqrt(c^2 - 1))*...
sqrt(x(j)^2 - 1);
end
for j = 781:821
A(j,1) = -1.8*cos((pi/2)*x(j));
end
```

where "c" is x_{m+1}. However, the wrinkle disturbances from the crude statements of IC2 and IC3 in MATLAB are small and localised, as shown in Figures 4.29 and 4.30.

Hence, they do not have any significant effect on the solution elsewhere, especially when compared to the major effects of approaching a breakdown.

4.5 Solutions Close To The Critical Angle

The $A(x,T)$ solutions for all initial conditions IC0 (4.24), IC1 (4.25) , IC2 (4.26) and IC3 (4.27) are shown within a region of interest $x \in [-2,2]$ in the Figures.

Solutions for Initial Conditions 0 **&** 1

From IC0, where the fluid flow is initially attached along the surface of the airfoil in a similar configuration to the boundary condition (4.6), $A(x,T)$ has a positive minimum that is decreasing with time, as shown at intervals of $\Delta T = 0.5$ in Figures 4.31 and 4.32. The $A(x,T)$ solution becomes very large and negative upstream of $x = -0.1$ and accelerates to a breakdown at the end time T_{end}. (See Table 4.10)

From IC1, where the fluid flow is initially attached along the surface but slightly perturbed from IC0, $A(x,T)$ has a positive minimum which increases as $T \to 1$ and shifts downstream from the origin to $x \simeq 0.1$, as shown at intervals of $\Delta T = 0.2$ in Figure 4.33. The flow structure is attempting to stabilise to a configuration with no separation. Figure 4.34 shows that between $T = 1.2$ and $T = 1.6$, the positive minimum levels out at $x \simeq 0.1$ where $A \simeq 0.45$. From $T = 1.6$, $A(x,T)$ decreases and shifts upstream until the minimum reaches zero at $x \simeq -0.1$, $T \simeq 3.0$, as shown at intervals of $\Delta T = 0.5$ in Figure 4.35. From thereon, $A(x,T)$ becomes negative and a closed bubble of reversed flow forms on the surface. The region of reversed flow becomes more accentuated upstream towards $x = -1$ with time T until there is breakdown at end time $T_{\text{end}} \simeq 5.5$.

grid	IC	end time T_{end}
1	0	5.65
2		5.173
1	1	5.88
2		5.401
1	2	5.66
2		5.177
1	3	1.23
2		0.913

Table 4.10: Initial condition end times T_{end}, by grids; repeated from Table 4.6.

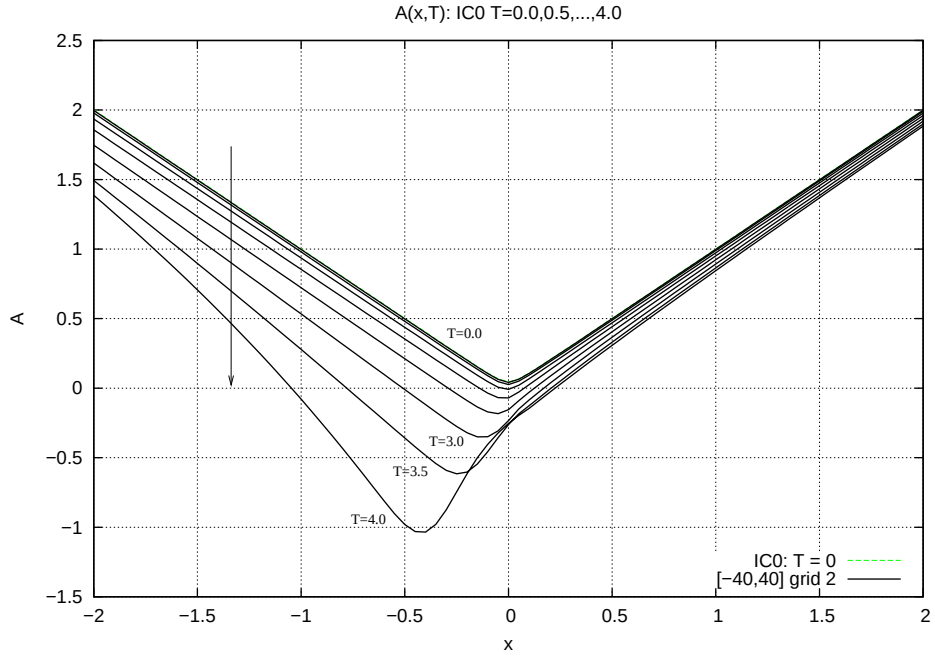

Figure 4.31: $A(x,T)$ from IC0 at $T = 0.0,\ 0.5,\ \ldots,\ 4.0$.

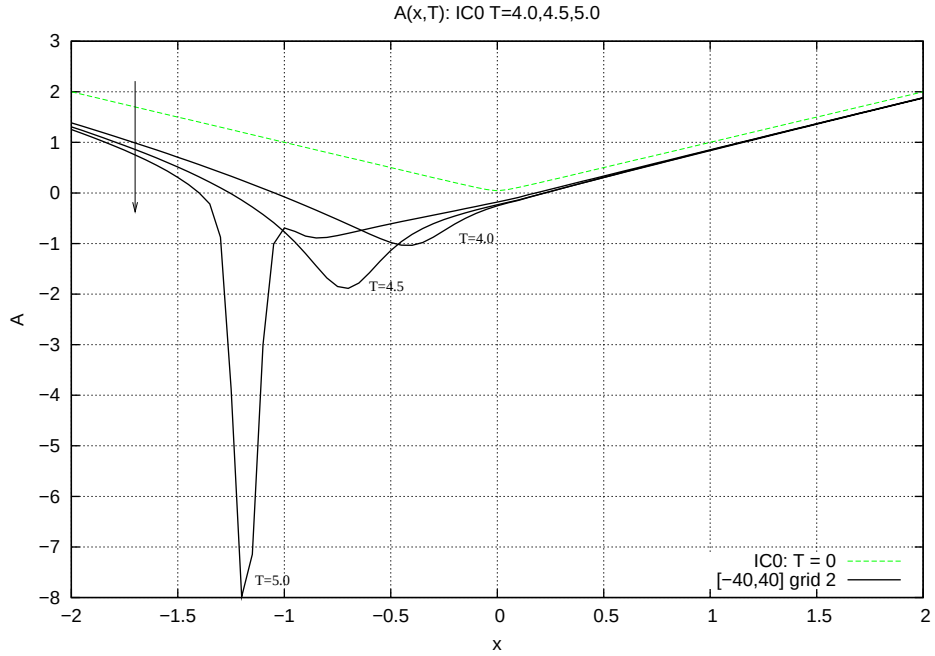

Figure 4.32: $A(x,T)$ from IC0 at $T = 4.0,\ 4.5,\ 5.0$.

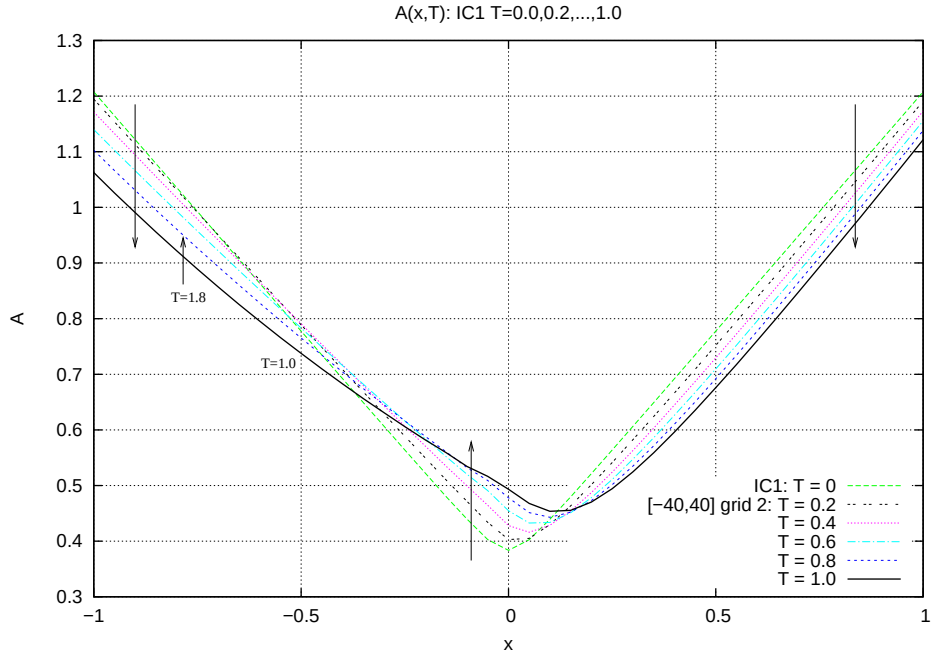

Figure 4.33: $A(x,T)$ from IC1 at $T = 0.0,\ 0.2,\ \ldots,\ 1.0$.

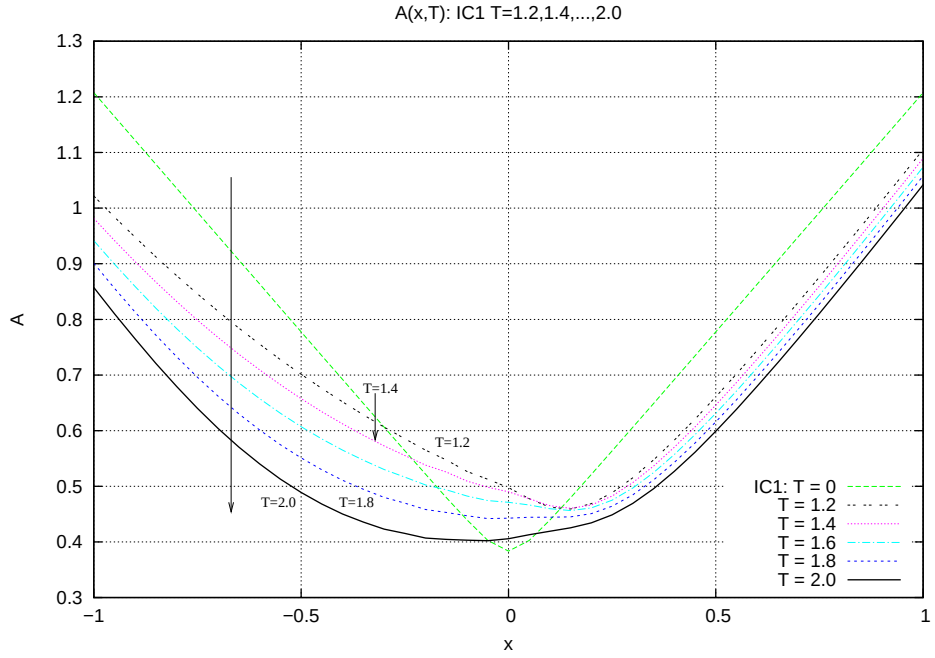

Figure 4.34: $A(x,T)$ from IC1 at $T = 1.2,\ 1.4,\ \ldots,\ 2.0$.

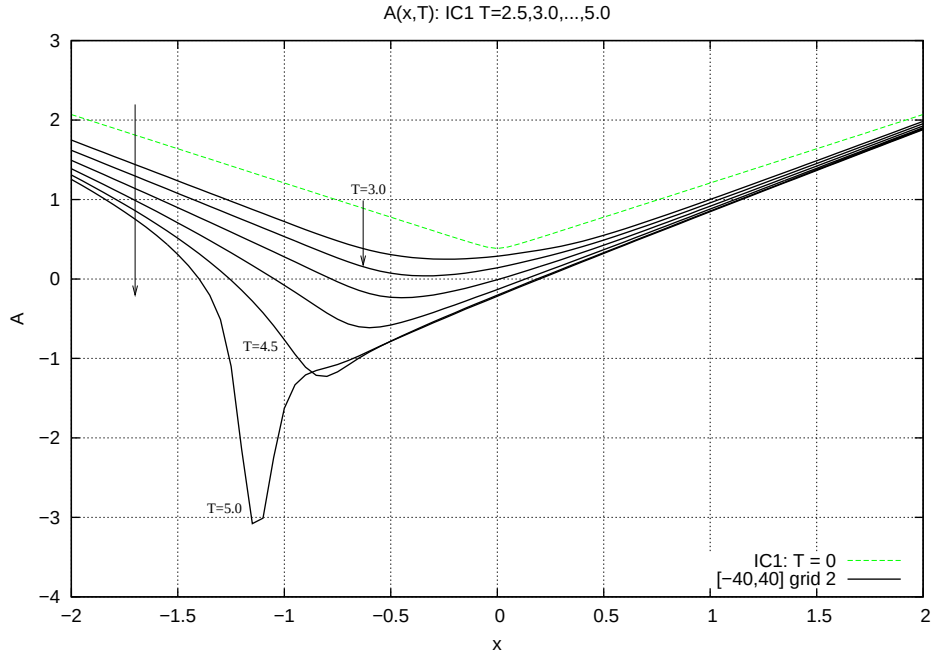

Figure 4.35: $A(x,T)$ from IC1 at $T = 2.5,\ 3.0,\ \ldots,5.0$.

Solutions for Initial Conditions 2 **&** 3

The $A(x,T)$ solutions from IC2 (4.26) as shown in Figures 4.36 and 4.37, are similar to the results from IC0 (4.24). There is a point of zero skin friction on the surface of the airfoil at the origin where $A(x,T)$ has a minimum. The minimum skin friction is decreasing with time and gradually shifts upstream. It becomes very large and negative and accelerates to a breakdown upstream of $x = -1$ at the end time T_{end}. (See Table 4.10.)

Where a closed region of reversed flow has formed on the surface, as from IC3 (4.27), $A(x,T)$ as shown in Figures 4.38 to 4.39, follows the same trends as the Smith & Elliott (1985) solutions from initial condition 3 (4.23) in Figures 4.18 and 4.19 of Section 4.3. The short bubble becomes increasingly accentuated upstream with time until breakdown occurs at the end time.

The small localised wrinkle in the solutions is explained in the $A(x,T)$ algorithm test summary in Section 4.4.

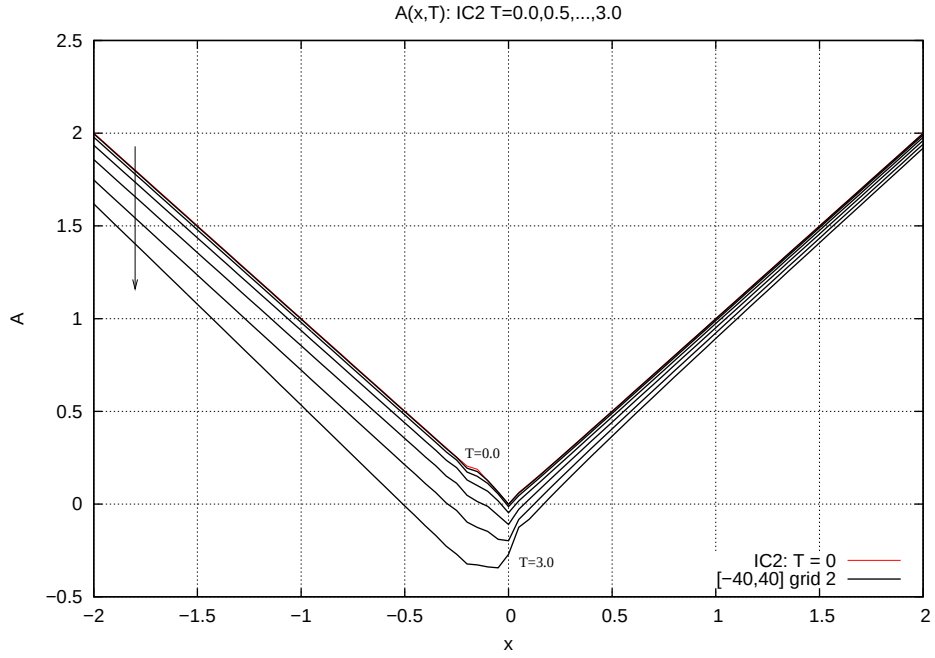

Figure 4.36: $A(x,T)$ from IC2 at $T = 0.0, 0.5, \ldots, 3.0$.

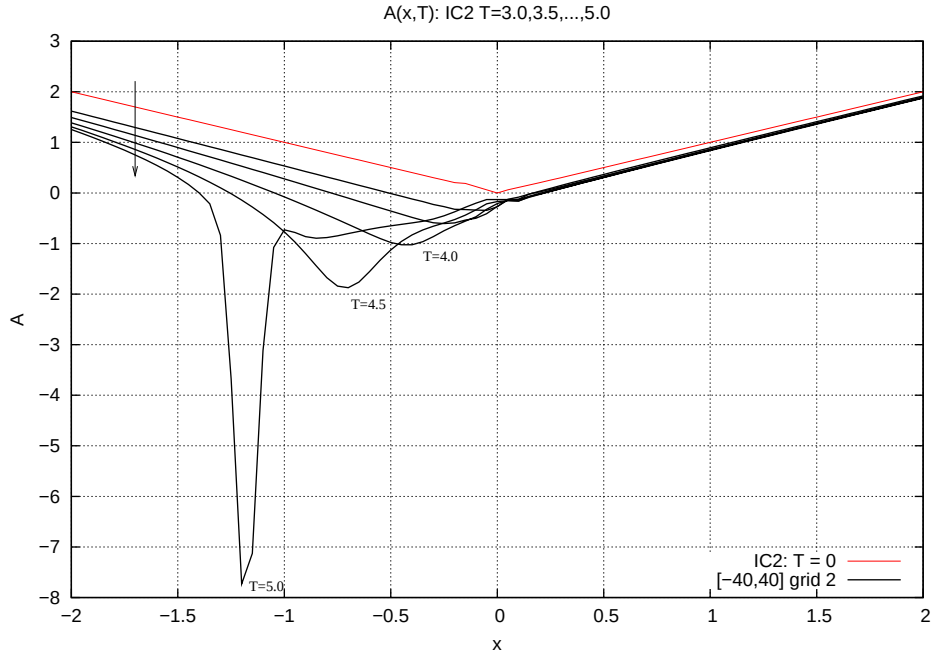

Figure 4.37: $A(x,T)$ from IC2 at $T = 3.0, 3.5, \ldots, 5.0$.

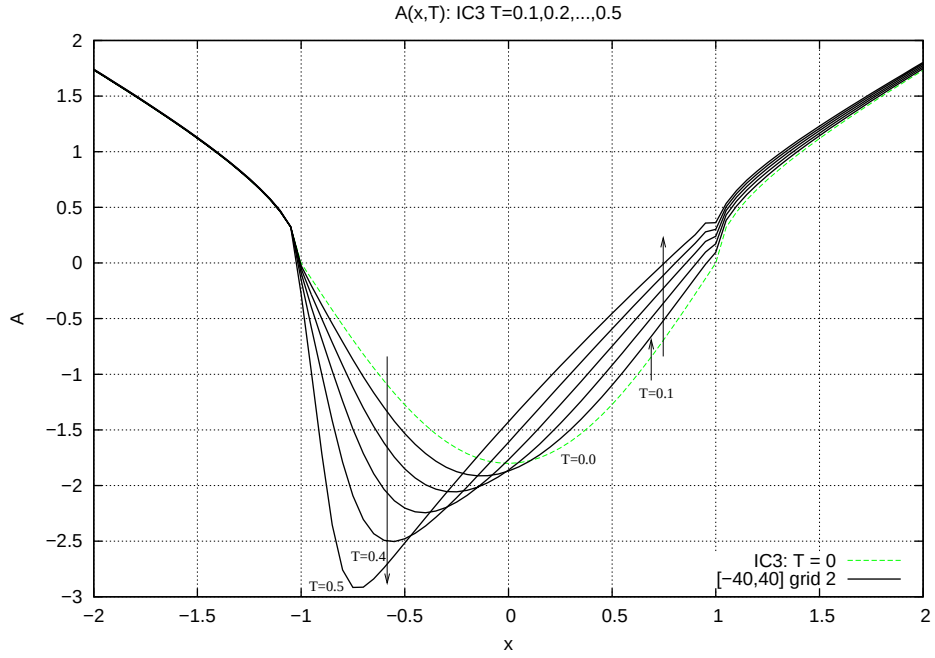

Figure 4.38: $A(x,T)$ from IC3 at $T = 0.0,\ 0.1,\ \ldots,\ 0.5$.

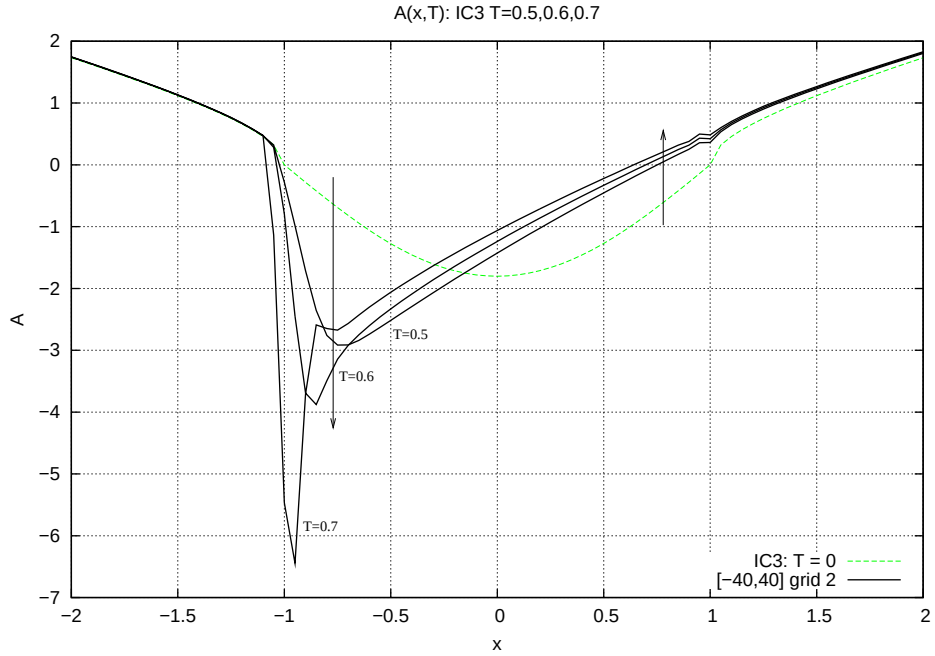

Figure 4.39: $A(x,T)$ from IC3 at $T = 0.5,\ 0.6,\ 0.7$.

4.5.1 Streamlines & Velocities

The $A(x,T)$ solution can be used to determine an approximation to the streamlines:

$$\Psi(x,Y,T) = \frac{1}{6}Y^3 + \frac{1}{2}A(x,T)Y^2 + \dots$$

and the tangential velocity:

$$u(x,Y,T) = \frac{\partial \Psi}{\partial Y} = \frac{1}{2}Y^2 + A(x,T)Y + \dots$$

The streamlines $\Psi(x,Y,T)$ and tangential velocities $u(x,Y,T)$ for initial condition IC1 at sample time levels $T = 0.0, 1.0, \dots, 5.0$; at intervals of $\Delta\Psi = 2.0$ and $\Delta u = 2.0$; starting from $\Psi = 2.0$ and $u = 2.0$, are shown in Figures 4.40 to 4.45. The streamlines and velocities for initial conditions IC0 and IC2 are similar to those of IC1 and the streamlines and velocities of IC3 are similar those at later times of IC1.

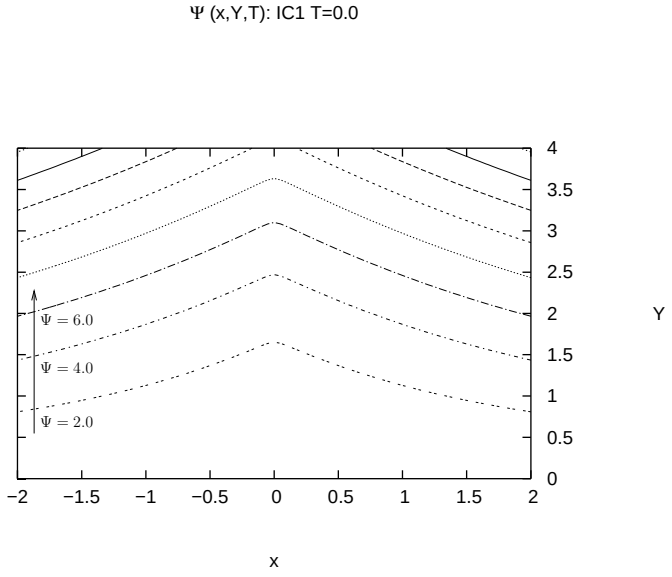

(a)

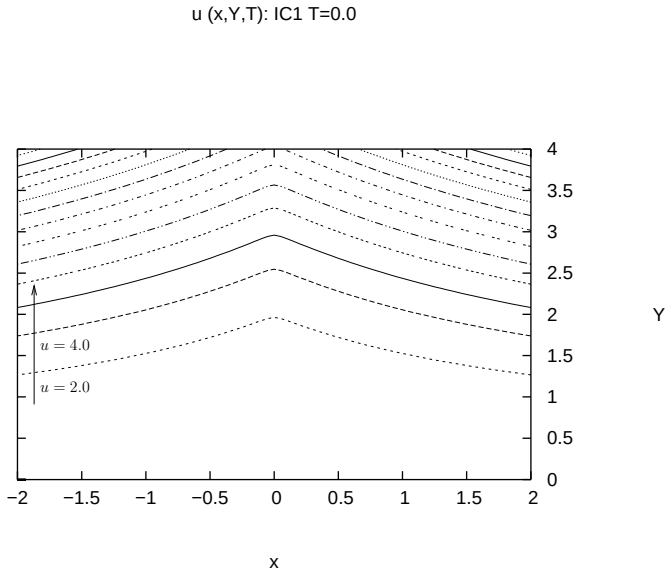

(b)

Figure 4.40: Streamlines $\Psi(x,Y,T)$ and tangential velocity $u(x,Y,T)$ from IC1 at $T = 0.0$; at increments of $\Delta\Psi = \Delta u = 2.0$; starting from $\Psi = u = 2.0$.

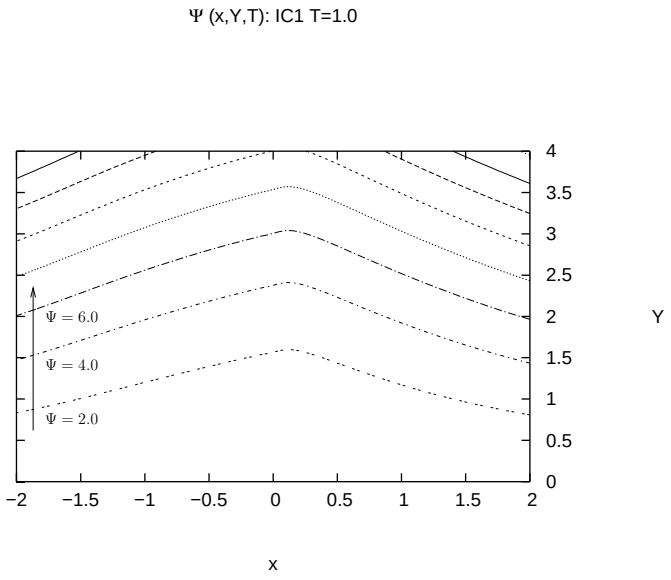

(a)

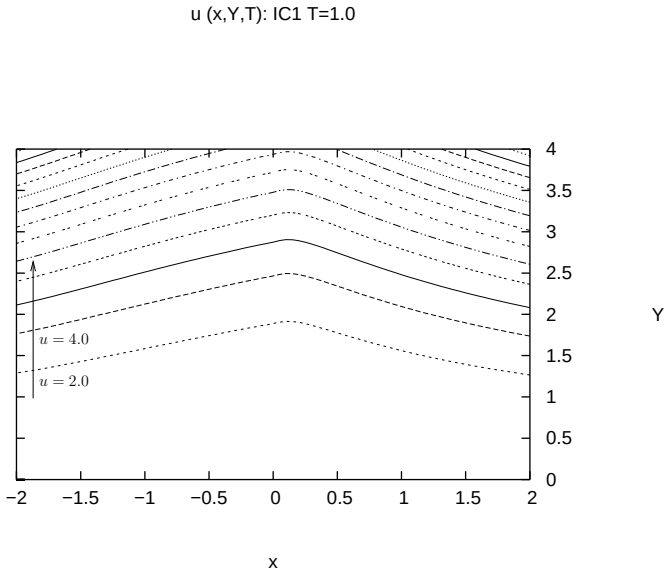

(b)

Figure 4.41: $\Psi(x,Y,T)$ and $u(x,Y,T)$ from IC1 at $T = 1.0$. See Figure 4.40.

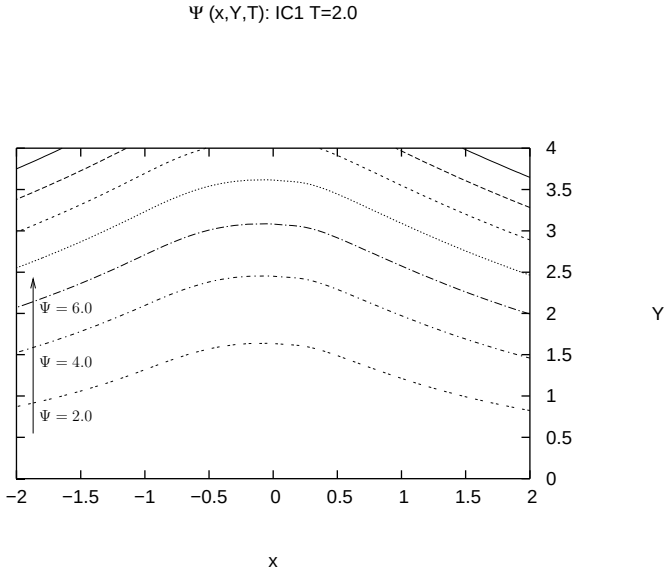

(a)

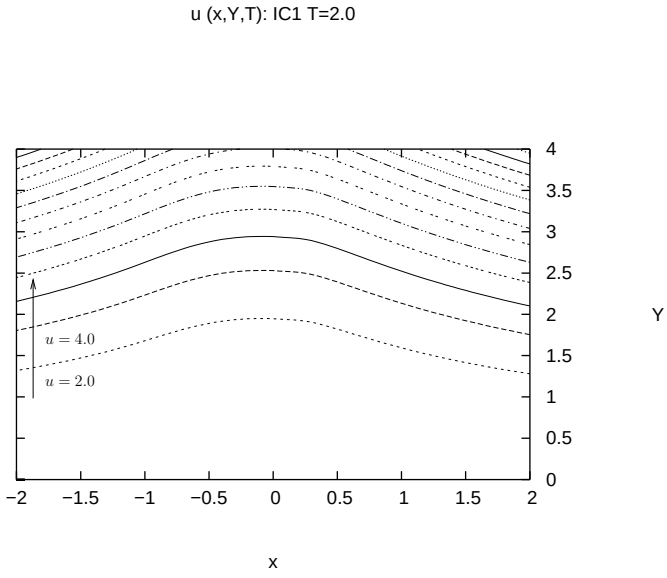

(b)

Figure 4.42: $\Psi(x,Y,T)$ and $u(x,Y,T)$ from IC1 at $T = 2.0$. See Figure 4.40.

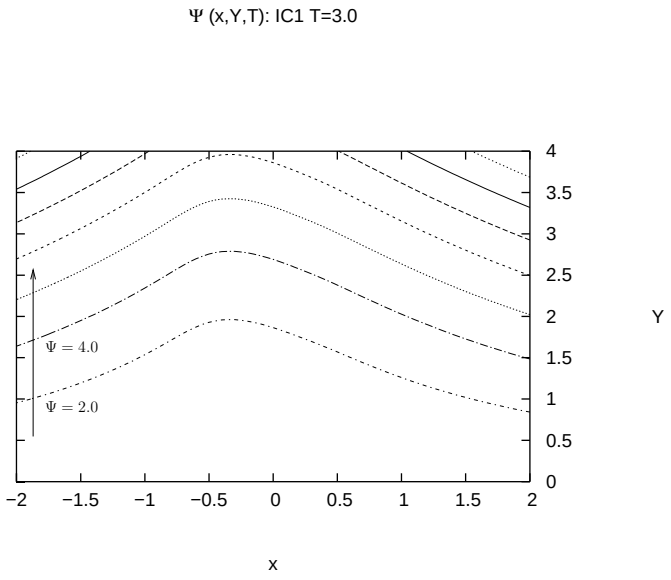

(a)

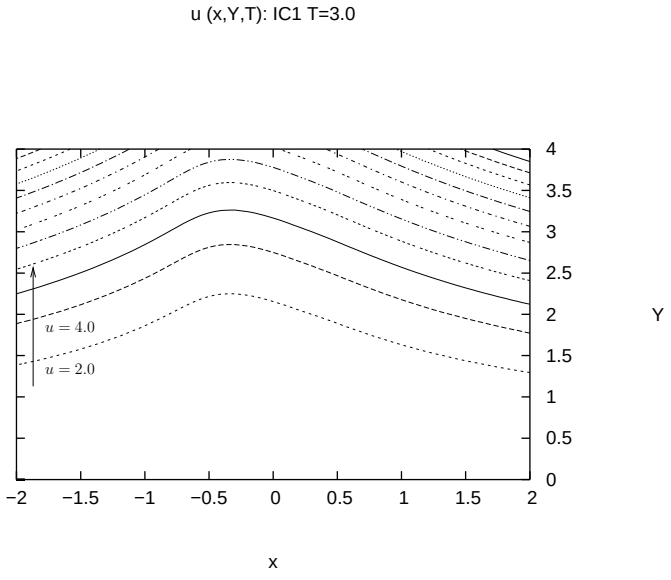

(b)

Figure 4.43: $\Psi(x,Y,T)$ and $u(x,Y,T)$ from IC1 at $T = 3.0$. See Figure 4.40.

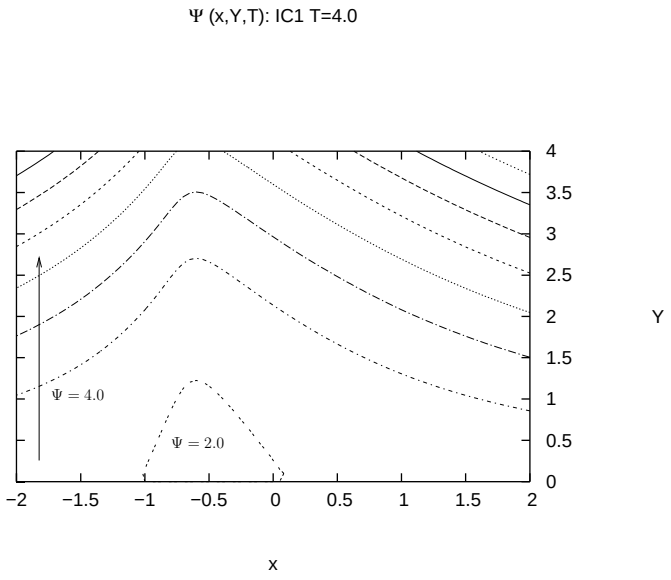

(a)

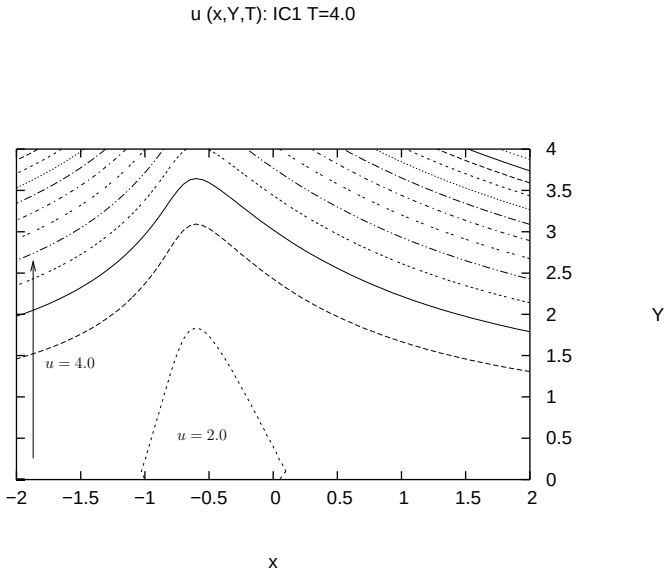

(b)

Figure 4.44: $\Psi(x,Y,T)$ and $u(x,Y,T)$ from IC1 at $T = 4.0$. See Figure 4.40.

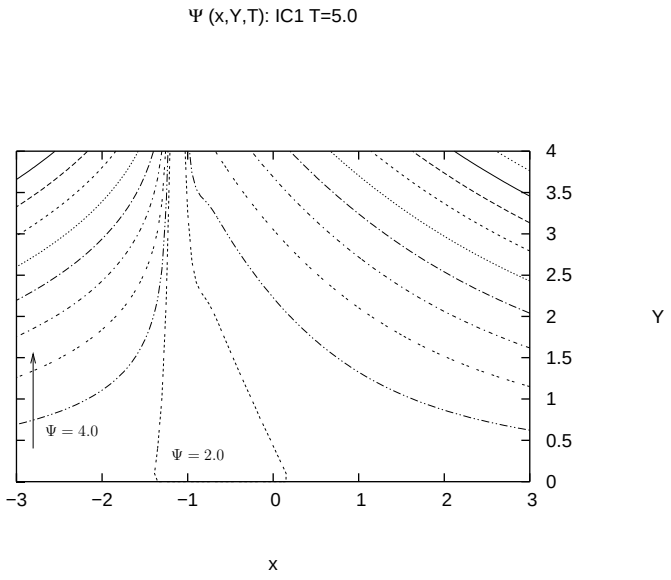

(a)

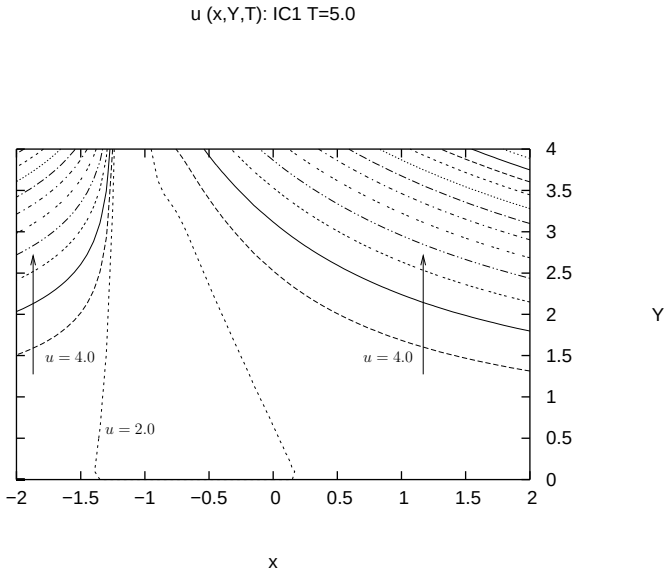

(b)

Figure 4.45: $\Psi(x,Y,T)$ and $u(x,Y,T)$ from IC1 at $T = 5.0$. See Figure 4.40.

4.5.2 Singularity & Skin Friction

The flow starting from any type of initial condition, whether the flow is initially attached along the entire surface of the airfoil, as in IC0 (4.24) and IC1 (4.25); the flow has a point of zero skin friction on the airfoil, as in IC2 (4.26); or there is a short bubble of reversed flow on the surface of the airfoil, as in IC3 (4.27); is unstable. The angle of attack of the airfoil is changing slowly on the large time scale T according to the law (4.3), as shown in Figure 4.1, so a steady state flow configuration is counter intuitive.

A singularity is approached as time increases. The singularity is a physical phenomenon as opposed to being a solely numerical method breakdown because it appears across all grids in Table 4.5, within a small neighbourhood about the point $x = -1$ and at approximately the same end time T_{end} in Table 4.10 for attached flow and point of zero skin friction initial conditions IC0, IC1 and IC2.

A short bubble of reversed flow will eventually form on the surface of the airfoil at approximately $T = 1.5$ from IC0, $T = 2.0$ from IC1 and almost immediately from IC2. Recall that when $A > 0$, the skin friction defined by (4.2) is positive and hence the fluid is travelling in the direction of the current along the surface of the airfoil. Analogously, when $A < 0$, the skin friction is negative and the fluid is travelling against the current. A point of zero skin friction, when $A = 0$, first occurs at the upstream end of the bubble and will recede upstream with time. The downstream end of the bubble, also where $A = 0$, is a closing point of the bubble of reversed flow. The bubble grows in length and volume until a singularity in reached at the end time T_{end}, when it bursts. When a bubble has already formed, as in initial condition IC3, the end time occurs sooner than those for IC0, IC1 and IC2 because the bubble is already accelerating in growth towards the breakdown.

From all initial conditions, the flow accelerates towards the breakdown despite the fact that change in angle of attack of the airfoil decelerates with time. This suggests the breakdown is a runaway process, occurring on even shorter time and length scales,

and the flow configurations are unstable.

Chapter 5

The Nonlinear Breakdown

The slow perturbations, from the small change in angle of attack, to the stream function solutions of the boundary layer occur on a larger time scale (2.13):

$$T = \sigma^{-1} t = O(1)\,, \qquad \sigma \to \infty$$

than the external inviscid flow time scale t. The small change in angle of attack is represented by asymmetry parameter:

$$\Delta k = k(T) - k_0 \to 0\,.$$

The boundary layer is of length scale (2.12):

$$s = x - x_s = O(1)\,.$$

On shorter length and time scales (3.8):

$$(-s) = O\left(\sigma^{-4}\right)\,, \quad \Delta k = O\left(\sigma^{-8}\right)\,, \quad O(\sigma) > O\left(\mathrm{Re}^{\frac{1}{20}}\right)\,; \quad \mathrm{Re}\,, \sigma \to \infty$$

is the interaction region where induced pressure gradient is negligible. Any viscous-inviscid interaction between the boundary layer and the external inviscid flow, and the

subsequent formation of the interaction region can be considered as a first interactive stage.

The flow structure of the interaction region holds for true skin friction $A(x,T)$ solutions of the solvability condition. As time increases, there is the formation a short bubble containing reversed recirculating flow, where skin friction $A(x,T) \leq 0$. The bubble growth accelerates with time, which is indicated by $A(x,T)$ also growing large and negative. The bubble erupts after a finite terminal time T_{end} and a singularity of $A(x,T)$ is reached.

Prior to the singularity, nonlinear breakdown occurs. Nonlinear breakdown can be considered as a *second interactive stage* on an even smaller and faster time scale than the first interactive stage. The second interactive stage is the developing eruption of the bubble of reversed flow, which causes the boundary layer to thicken.[1] Analysis of the second interactive stage shows that discontinuous skin friction solutions in the style of Heaviside function waves exist.

On even shorter time and length scales than the nonlinear breakdown, as $T \rightarrow T_{\text{end}}$, a fully unsteady third interactive stage comes into action. The third interactive stage is the creation and unsteady development of a vortex spanning the thickened boundary layer at the leading edge, that is eventually shed from the airfoil. Dynamic stall occurs as the vortex travels from leading edge of the airfoil to the trailing edge and is then ejected.[2] Thus, nonlinear breakdown initiates leading edge stall.

5.1 The Quasi-Steady Second Interactive Stage

The singularity is assumed to occur at the end time $T_{\text{end}} = T_s$ at the point $x = X_s$ (which is not to be confused with the point of zero skin friction $x = x_s$). Furthermore, there is a region X of the quasi-steady second interactive stage about the point of singularity. It is contained within the first interactive stage interaction region such

[1] A numerical solution of the second interactive stage for fully unsteady boundary layer separation in Lagrangian coordinates is found by Cassel et al. (1996).

[2] See for example, Cassel (2000); where also, the terminology originates for interactive stages. The third interactive stage is beyond the thesis.

that the coordinate x for the interaction region is written as[3]

$$x = X_s + (T_s - T)^\beta X\,, \qquad X = O(1)\,, \qquad T \to T_s\,, \qquad \beta > 0\,. \tag{5.1}$$

The second interactive region decays at a rate of order of magnitude $(T_s - T)^\beta$ as $T \to T_s$ and then, on an even shorter time scale before the singularity at T_s, the third interactive stage of vortex formation and shedding takes over. The second interactive region is described by the similarity variable

$$X = \frac{(x - X_s)}{(T_s - T)^\beta} = O(1)\,, \qquad T \to T_s\,, \qquad \beta > 0 \tag{5.2}$$

where the origin of the second interactive region $X = 0$ coincides with the point of singularity $x = X_s$. The eigenvalue β (which is not to be confused with the eigenvalue from Section 2.4 or the exponent from Section 2.6.2), is to be found in the analysis.

The point of zero skin friction $x = x_s$ is assumed to be travelling within the second interactive region towards the point of singularity, at a rate of order of magnitude $(T_s - T)^\alpha$, such that

$$X_s = x_s + C(T_s - T)^\alpha\,, \qquad T \to T_s\,, \qquad \alpha > 0\,. \tag{5.3}$$

The constant C is arbitrary but related to the speed of travel of the point of zero skin friction and the direction of travel, depending on its sign. The constant α (which is not to be confused with the eigenvalue from Section 2.3 or the exponent from Section 2.6.1) is also arbitrary except $0 < \alpha \leq \beta$ such that the point of zero skin friction is travelling towards the point of singularity at a slower rate than the second interactive region is decaying about it. The second interactive region is then an intact structure which does not destroy the interaction region from Chapters 3 and 4. (See Figure 5.1.)

Therefore, the first interactive stage interaction region with coordinate x (5.1)

[3]See also for example, Cassel et al. (1996).

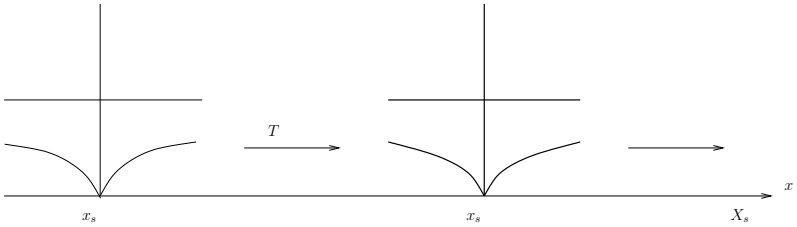

Figure 5.1: The point of zero skin friction $x = x_s$ and flow structure travelling towards the point of singularity $x = X_S$, when $\beta \geq \alpha > 0$.

contains a second interactive region with coordinate X and within, a point of zero skin friction $x = x_s$ travels towards the terminal point of singularity at $X = X_s$ (5.3) as $T \to T_s$:

$$x = x_s + C(T_s - T)^{\alpha} + (T_s - T)^{\beta} X \,, \tag{5.4}$$

$$X = O(1) \,, \qquad T \to T_s \,, \qquad \beta \geq \alpha > 0 \,.$$

The Secondary Interactive Stage Equation

The asymptotic form of the skin friction $A(x,T)$ can be found from balancing the non-linear and unsteady terms of the first interactive stage $A(x,T)$ solvability condition (4.1):

$$A^2(x,T) - x^2 + 2a(T) = -\frac{2^{\frac{3}{4}}}{\Gamma(\frac{5}{4})} \int_{-\infty}^{x} \frac{\partial A}{\partial T}(\xi,T) \, \frac{\mathrm{d}\xi}{(x-\xi)^{\frac{1}{4}}} \tag{5.5}$$

where $a(T) = 1.331 - 1332e^{-T}$ is the airfoil angle of attack law (4.3). The order of magnitude of $A(x,T)$ can be determined as

$$A^2 \sim \int_{-\infty}^{x} \frac{\partial A}{\partial T}(\xi,T) \, \frac{\mathrm{d}\xi}{(x-\xi)^{\frac{1}{4}}} \sim \frac{\partial A}{\partial T}(x - X_s)^{\frac{3}{4}} \sim \frac{A_s - A}{(T_s - T)}(x - X_s)^{\frac{3}{4}}$$

where A_s is the large and negative terminal value of A as $T \to T_s$. Hence,

$$A = O\left[(T_s - T)^{-1}(x - X_s)^{\frac{3}{4}}\right] .$$

Therefore, taking into account the x and T relation 5.4 where $x - X_s = (T_s - T)^\beta X$ and $X_s = x_s + C(T_s - T)^\alpha$, the skin friction $A(x,T)$ series expansion of the second interactive region arises in the form:

$$A(x,T) = (T_s - T)^{\frac{3}{4}n-1}\hat{A}(X) + \ldots \qquad \hat{A}(X) = O(1)\,. \tag{5.6}$$

The exponent and eigenvalue $n(\alpha,\beta)$ is a function of α and β with

$$0 < n < \frac{4}{3} \tag{5.7}$$

in order for $\frac{3}{4}n - 1 < 0$ and $|A(x,T)|$ to be large during the nonlinear breakdown process. The eigenvalue n is to be determined during the analysis.

Additionally, as $A(x,T)$ becomes large compared to x and $a(T)$ then by (5.5):

$$A^2 \sim \left(-x^2 + 2a(T)\right)^{-1}\,. \tag{5.8}$$

The Taylor series expansion of $-x^2 + 2a(T)$ about $x = X_s$ and $T = T_s$ is:

$$-x^2 + 2a(T) = -X_s^2 + 2a(T_s) + 2(T_s - T)\frac{\mathrm{d}a}{\mathrm{d}T}(T_s) + (T_s - T)^2\frac{\mathrm{d}^2a}{\mathrm{d}T^2}(T_s) + \ldots$$

then by the order of magnitude of $A(x,T)$ from (5.6):

$$-x^2 + 2a(T) = (T_s - T)^{2-\frac{3}{2}n}(-X_s^2 + 2a(T_s)) + \ldots$$

The $-x^2 + 2a(T)$ term cannot be balanced with A^2 in the second interactive region, that is the change in angle of attack $a(T)$ is no longer relevant once $A(x,T)$ is growing large and negative towards the nonlinear breakdown. This confirms the runaway process of nonlinear breakdown and leading edge stall, as first mentioned in Section 4.5.2

The analysis of the second interactive region proceeds. Substitution of the $A(x,T)$

series expansion (5.6) into the $A(x,T)$ equation (5.5) gives the terms:

$$A(x,T)^2 = (T_s - T)^{\frac{3}{2}n-2}\hat{A}^2(X)\,;$$

$$\begin{aligned}\frac{\partial A}{\partial T}(x,T) &= (T_s-T)^{\frac{3}{4}n-2}\left[-\left(\frac{3}{4}n-1\right)\right]\hat{A}(X) + (T_s-T)^{\frac{3}{4}n-1}\frac{\mathrm{d}\hat{A}}{\mathrm{d}X}(X)\frac{\partial X}{\partial T}\\ &= (T_s-T)^{\frac{3}{4}n-2}\left[-\left(\frac{3}{4}n-1\right)\right]\hat{A}(X) + (T_s-T)^{\frac{3}{4}n-2}\frac{\mathrm{d}\hat{A}}{\mathrm{d}X}(X)\beta X\\ &\quad + (T_s-T)^{\frac{3}{4}n+\alpha-\beta-2}\frac{\mathrm{d}\hat{A}}{\mathrm{d}X}(X)\alpha C\,.\end{aligned}$$

By (5.4):

$$X = (x - x_s - C(T_s-T)^{\alpha})\,(T_s-T)^{-\beta}$$

then

$$\begin{aligned}\frac{\partial X}{\partial T} &= \alpha C(T_s-T)^{\alpha-1}\cdot(T_s-T)^{-\beta}\\ &\qquad + (x-x_s-C(T_s-T)^{\alpha})\cdot -\beta(T_s-T)^{-\beta-1}\\ &= (T_s-T)^{\alpha-\beta-1}\alpha C\\ &\qquad - (x-x_s-C(T_s-T)^{\alpha})\,(T_s-T)^{-\beta}\cdot\beta(T_s-T)^{-1}\\ &= (T_s-T)^{-1}\beta X + (T_s-T)^{\alpha-\beta-1}\alpha C\,;\end{aligned}$$

and

$$\mathrm{d}x = (T_s-T)^{\beta}\mathrm{d}X \Rightarrow \mathrm{d}\xi = (T_s-T)^{\beta}\mathrm{d}X\,.$$

Hence, the integral:

$$\int_{-\infty}^{x}\cdot\frac{\mathrm{d}\xi}{(x-\xi)^{\frac{1}{4}}} \Rightarrow (T_s-T)^{\frac{3}{4}\beta}\int_{-\infty}^{X}\cdot\frac{\mathrm{d}\xi}{(X-\xi)^{\frac{1}{4}}}$$

Therefore, the second interactive region $\hat{A}(X)$ equation is

$$
\begin{aligned}
&(T_s - T)^{\frac{3}{4}n} \hat{A}^2(X) \\
&\quad = (T_s - T)^{\frac{3}{4}\beta} \cdot -\frac{2^{\frac{3}{4}}}{\Gamma(\frac{5}{4})} \int_{-\infty}^{X} \left[-\left(\frac{3}{4}n - 1\right) \hat{A}(\xi) + \beta\xi \frac{\mathrm{d}\hat{A}}{\mathrm{d}\xi}(\xi) \right] \frac{\mathrm{d}\xi}{(X-\xi)^{\frac{1}{4}}} \\
&\quad + (T_s - T)^{\alpha - \frac{1}{4}\beta} \cdot -\frac{2^{\frac{3}{4}}}{\Gamma(\frac{5}{4})} \int_{-\infty}^{X} \left[\alpha C \frac{\mathrm{d}\hat{A}}{\mathrm{d}\xi}(\xi) \right] \frac{\mathrm{d}\xi}{(X-\xi)^{\frac{1}{4}}} \,. \qquad (5.9)
\end{aligned}
$$

5.1.1 Second Interactive Flow Configuration

There are three physical flow cases, of which two cases (5.10) and (5.15) arise from the balance of terms in the second interactive region $\hat{A}(X)$ equation (5.9), that can be described by one nonlinear breakdown equation (5.16).

Firstly, if the order of magnitude of the nonlinear term of (5.9) is the same as that of both integrals on the right hand side, then

$$
\frac{3}{4}n = \alpha - \frac{1}{4}\beta = \frac{3}{4}\beta \iff n = \beta = \alpha \,. \qquad (5.10)
$$

The point of zero skin friction $x = x_s$ is travelling at the same rate at which the second interactive region is decaying, such that

$$
\begin{aligned}
&x = x_s + C(T_s - T)^{\beta} + (T_s - T)^{\beta} X = x_s + (T_s - T)^{\beta}[X + C] \,, \qquad (5.11) \\
&X = O(1)
\end{aligned}
$$

and the asymptotic structure of $A(x, T)$ is:

$$
A(x, T) = (T_s - T)^{\frac{3}{4}\beta - 1} \hat{A}(X) + \ldots \qquad (5.12)
$$

Hence, the second interactive region $\hat{A}(X)$ equation (5.9) becomes:

$$\hat{A}^2(X) = -\frac{2^{\frac{3}{4}}}{\Gamma(\frac{5}{4})} \int_{-\infty}^{X} \left[-\left(\frac{3}{4}\beta - 1\right) \hat{A}(\xi) + \beta(\xi + C)\frac{\mathrm{d}\hat{A}}{\mathrm{d}\xi}(\xi) \right] \frac{\mathrm{d}\xi}{(X-\xi)^{\frac{1}{4}}} \,.$$

With the Galilean transformation of the variables:

$$X \to X + C \,, \qquad \xi \to \xi + C \tag{5.13}$$

then

$$x = x_s + (T_s - T)^{\beta} X \,, \qquad X = O(1) \tag{5.14}$$

and the equation becomes

$$\hat{A}^2(X) = -\frac{2^{\frac{3}{4}}}{\Gamma(\frac{5}{4})} \int_{-\infty}^{X} \left[-\left(\frac{3}{4}\beta - 1\right) \hat{A}(\xi) + \beta\xi\frac{\mathrm{d}\hat{A}}{\mathrm{d}\xi}(\xi) \right] \frac{\mathrm{d}\xi}{(X-\xi)^{\frac{1}{4}}} \,.$$

The limits of the integral remain unchanged by the linear transformation since X is arbitrary and the positive end of the computational domain for the numerical method is expected to be a large and extended towards infinity.

On the other hand, setting $C = 0$ such that the point of skin friction is stationary within the observer's frame of reference also gives the same governing equation.

Secondly, if the order of magnitude of the nonlinear term is the same as that of the first integral on the right hand side of (5.9) whilst larger in order of magnitude than the second integral, then

$$\frac{3}{4}n = \frac{3}{4}\beta > \alpha - \frac{1}{4}\beta \iff n = \beta > \alpha \,. \tag{5.15}$$

The point of zero skin friction is travelling at a slower rate than the second interactive region is decaying, such that

$$x = x_s + C(T_s - T)^{\alpha} + (T_s - T)^{\beta} X \,, \qquad X = O(1) \,.$$

The interaction region flow structure is assumed to remain intact and moves with the point of zero skin friction, as shown in Figure 5.1. The structure of $A(x,T)$ is the same as that for the previous case when $n = \beta = \alpha$ such that

$$A(x,T) = (T_s - T)^{\frac{3}{4}\beta - 1}\hat{A}(X) + \dots$$

Indeed, by the similarity variable (5.2):

$$X = \frac{(x - X_s)}{(T_s - T)^{\beta}} = \frac{[x - x_s - C(T_s - T)^{\alpha}]}{(T_s - T)^{\beta}} = O(1)\,,$$

the denominator with eigenvalue β, that is the rate of decay of the region, is the dominant factor as opposed to the travelling speed of the point. The second interactive region $\hat{A}(X)$ equation (5.9) becomes

$$\begin{aligned}\hat{A}^2(X) = -\frac{2^{\frac{3}{4}}}{\Gamma(\frac{5}{4})}\int_{-\infty}^{X}\left[-\left(\frac{3}{4}\beta - 1\right)\hat{A}(\xi) + \beta\xi\frac{\mathrm{d}\hat{A}}{\mathrm{d}\xi}(\xi)\right]\frac{\mathrm{d}\xi}{(X-\xi)^{\frac{1}{4}}} \\ + (T_s - T)^{(\alpha-\beta)}\left\{-\frac{2^{\frac{3}{4}}}{\Gamma(\frac{5}{4})}\int_{-\infty}^{X}\left[\alpha C\frac{\mathrm{d}\hat{A}}{\mathrm{d}\xi}(\xi)\right]\frac{\mathrm{d}\xi}{(X-\xi)^{\frac{1}{4}}}\right\}\end{aligned}$$

As $T \to T_s$, the second integral cannot be balanced with the rest of equation since the exponent $\alpha - \beta > 0$. Hence, the equation is

$$\hat{A}^2(X) = -\frac{2^{\frac{3}{4}}}{\Gamma(\frac{5}{4})}\int_{-\infty}^{X}\left[-\left(\frac{3}{4}\beta - 1\right)\hat{A}(\xi) + \beta\xi\frac{\mathrm{d}\hat{A}}{\mathrm{d}\xi}(\xi)\right]\frac{\mathrm{d}\xi}{(X-\xi)^{\frac{1}{4}}}\,,$$

which is identical to the equation for the first case when $n = \beta = \alpha$ and the additional case of a fixed point of zero skin friction, when $C = 0$.

The flow involving a moving point of zero skin friction along a wall is closely related to steady flow when the point of zero skin friction is fixed. The velocity profiles are transformed to a wall-fixed frame by the Galilean transformation (5.13), that is by adding or subtracting the constant velocity C. If the point of zero skin

friction moves with variable speed $C(T-T_s)^{\alpha}$ but its acceleration is not large, that is $\alpha \leq \beta$, then this should not lead to qualitative changes in the flow structure when compared with that of a point of zero skin friction moving with constant speed C.[4] Therefore, the nonlinear breakdown equation for $n = \beta \geq \alpha > 0$ and/or $C = 0$ is

$$\hat{A}^2(X) = -\frac{2^{\frac{3}{4}}}{\Gamma(\frac{5}{4})} \int_{-\infty}^{X} \left[-\left(\frac{3}{4}\beta - 1\right) \hat{A}(\xi) + \beta\xi \frac{\mathrm{d}\hat{A}}{\mathrm{d}\xi}(\xi) \right] \frac{\mathrm{d}\xi}{(X-\xi)^{\frac{1}{4}}} \,. \tag{5.16}$$

The equation is subject to boundary conditions, derived in the next Section 5.1.2. The solutions describe the following three fluid flow configurations.

1. The point of zero skin friction is fixed within the observer's frame of reference such that $x = x_s + (T_s - T)^{\beta} X$.

2. The point of zero skin friction is travelling at a slower rate than the decay of the second interactive region.

3. The point of zero skin friction is travelling at the same rate as the decay of the second interactive region, in which case the $\hat{A}(X)$ solution is shifted to the origin by the constant C of the travelling speed of the point.

If the solutions from the flow regime with a moving point of zero skin friction also describe the flow regime of a fixed point of zero skin friction, the movement must not lead to qualitative changes in the flow structure. The flow structure is simply shifted, as illustrated in Figure 5.1. This occurs when $\beta \geq \alpha > 0$.

Note that the movement of the point of zero skin friction and the rate of decay of the second interactive region may or may not be related to each other.

Other Flow Configurations

There are two inconsistent flow configurations, which are as follows.

Firstly, if the order of magnitude of the nonlinear term is the same as that of the second integral on the right hand side whilst larger in order of magnitude than the

[4] This assertion is based on Moore (1958) for moving points of separation.

first integral, then

$$\frac{3}{4}n = \alpha - \frac{1}{4}\beta > \frac{3}{4}\beta \iff n = \frac{1}{3}(4\alpha - \beta)\,.$$

The structure of $A(x,T)$ is:

$$A(x,T) = (T_s - T)^{\alpha - \frac{1}{4}\beta - 1}\hat{A}(X) + \ldots$$

The equation (5.9) becomes:

$$\begin{aligned}\hat{A}^2(X) = &-\frac{2^{\frac{3}{4}}}{\Gamma(\frac{5}{4})}\int_{-\infty}^{X}\left[\alpha C\frac{\mathrm{d}\hat{A}}{\mathrm{d}\xi}(\xi)\right]\frac{\mathrm{d}\xi}{(X-\xi)^{\frac{1}{4}}} \\ &+ (T_s - T)^{(\beta-\alpha)} \\ &\cdot\left\{-\frac{2^{\frac{3}{4}}}{\Gamma(\frac{5}{4})}\int_{-\infty}^{X}\left[-\left(\frac{3}{4}n - 1\right)\hat{A}(\xi) + \beta\xi\frac{\mathrm{d}\hat{A}}{\mathrm{d}\xi}(\xi)\right]\frac{\mathrm{d}\xi}{(X-\xi)^{\frac{1}{4}}}\right\}.\end{aligned}$$

As $T \to T_s$, the second integral:

$$-\frac{2^{\frac{3}{4}}}{\Gamma(\frac{5}{4})}\int_{-\infty}^{X}\left[-\left(\frac{3}{4}n - 1\right)\hat{A}(\xi) + \beta\xi\frac{\mathrm{d}\hat{A}}{\mathrm{d}\xi}(\xi)\right]\frac{\mathrm{d}\xi}{(X-\xi)^{\frac{1}{4}}} \to \hat{A}^2(X = 0-)$$

grows large since $\beta - \alpha < 0$ and approaches the solution as described by the original equation (5.9) at $X = 0-$ as $x \to X_s-$. The balanced terms of equation excluding the second integral is

$$\hat{A}^2(X) = -\frac{2^{\frac{3}{4}}}{\Gamma(\frac{5}{4})}\int_{-\infty}^{X}\left[\alpha C\frac{\mathrm{d}\hat{A}}{\mathrm{d}\xi}(\xi)\right]\frac{\mathrm{d}\xi}{(X-\xi)^{\frac{1}{4}}}$$

of which an exact solution is the trivial:

$$\hat{A}(X) = 0\,, \qquad \forall\, X\,.$$

Secondly, if the nonlinear term is smaller than both integrals on the right hand side then

$$\frac{3}{4}n < \min\left(\frac{3}{4}\beta, \alpha - \frac{1}{4}\beta\right) ;$$

and equation (5.9) becomes:

$$\begin{aligned}\int_{-\infty}^{X} \left[-\left(\frac{3}{4}n - 1\right)\hat{A}(\xi) + \beta\xi\frac{\mathrm{d}\hat{A}}{\mathrm{d}\xi}(\xi)\right]\frac{\mathrm{d}\xi}{(X-\xi)^{\frac{1}{4}}} \\ + (T_s - T)^{\alpha-\beta}\int_{-\infty}^{X}\left[\alpha C\frac{\mathrm{d}\hat{A}}{\mathrm{d}\xi}(\xi)\right]\frac{\mathrm{d}\xi}{(X-\xi)^{\frac{1}{4}}} \\ = 0\,.\end{aligned}$$

Therefore, the nonlinear effects are excluded.

Nonetheless, the flow regimes are not consistent because the point of zero skin friction is travelling at a faster rate than the second interactive region is decaying about it. Hence, it destroys the structure of the interaction region. The flow structure, as shown in Figure 5.1, no longer exists. There must be new analysis starting from the boundary layer equations.

5.1.2 The Boundary Conditions for $\hat{A}(X)$

In order to find solutions to the second interactive region $\hat{A}(X)$ equation (5.16) then upstream and downstream boundary conditions for $X \to \pm\infty$ are required.

It is supposed that $A(x,T)$ remains regular in $(T_s - T)$ for $x \neq X_s$ with the Taylor series expansion

$$A(x,T) = A_0(x) + (T_s - T)A_1(x) + \ldots \qquad T \to T_s-$$

where

$$A_0(x) \sim \begin{cases} \lambda^-(X_s - x)^{\frac{3}{4}-\frac{1}{\beta}} + \ldots & x \to X_s- \\ \lambda^+(x - X_s)^{\frac{3}{4}-\frac{1}{\beta}} + \ldots & x \to X_s+ \end{cases}$$

for $0 < n = \beta < \frac{4}{3}$ and $\beta \geq \alpha > 0$. This first term of the Taylor series expansion, that is $A_0(x)$, can be justified as follows. The second interactive region similarity variable (5.2) and point of zero skin friction (5.3):

$$X = \frac{(x - X_s)}{(T_s - T)^\beta} = O(1)\,, \qquad X_s = x_s + C(T_s - T)^\alpha$$

implies

$$(T_s - T) = O\left[(x - X_s)^{\frac{1}{\beta}}\right]\,, \qquad (T_s - T)^{\frac{3}{4}\beta - 1} = O\left[(x - X_s)^{\frac{3}{4} - \frac{1}{\beta}}\right]\,.$$

Upon substitution of the $(T_s - T)$ term into the $A(x, T)$ series expansion (5.6) for $n = \beta$ then

$$A_0(x) = O\left[(x - X_s)^{\frac{3}{4} - \frac{1}{\beta}}\right]\,.$$

Therefore, the matching conditions from the second interactive region to the interaction region are

$$\hat{A}(X) \sim \begin{cases} \lambda^- |X|^{\frac{3}{4} - \frac{1}{\beta}}\,, & X \to -\infty \\ \lambda^+ X^{\frac{3}{4} - \frac{1}{\beta}}\,, & X \to \infty \end{cases} \tag{5.17}$$

since $x = X_s$ is an arbitrary position within the second interactive region. The boundary conditions remain unchanged with the Galilean transformations (5.13) which have been applied to the second interactive region $\hat{A}(X)$ equation (5.9).

5.1.3 $\hat{A}(X)$ Boundary Eigenvalue β Problem

The second interactive region eigenvalue β and $\hat{A}(X)$ boundary value problem consists of the nonlinear breakdown equation (5.16):

$$\hat{A}^2(X) = -\frac{2^{\frac{3}{4}}}{\Gamma(\frac{5}{4})} \int_{-\infty}^{X} \left[-\left(\frac{3}{4}\beta - 1\right) \hat{A}(\xi) + \beta\xi \frac{\mathrm{d}\hat{A}}{\mathrm{d}\xi}(\xi) \right] \frac{\mathrm{d}\xi}{(X - \xi)^{\frac{1}{4}}} \tag{5.18}$$

for $0 < n = \beta < \frac{4}{3}$ and $\beta \geq \alpha > 0$, with the boundary conditions (5.17):

$$\hat{A}(X) \sim \begin{cases} \lambda^{-}|X|^{\frac{3}{4}-\frac{1}{\beta}}, & X \to -\infty \\ \lambda^{+}X^{\frac{3}{4}-\frac{1}{\beta}}, & X \to \infty\,. \end{cases} \tag{5.19}$$

Transformation to the Smith & Elliott (1985) Nonlinear Breakdown Problem

The normalising transformations:

$$\hat{A}(X) \to \left(\frac{2^{\frac{3}{4}}}{\Gamma(\frac{5}{4})}\right)^{1-\frac{3}{4}\beta} \hat{A}(X)\,, \qquad X \to \left(\frac{2^{\frac{3}{4}}}{\Gamma(\frac{5}{4})}\right)^{-\beta} X \tag{5.20}$$

convert equation (5.18) to the nonlinear breakdown equation by Smith & Elliott (1985):

$$\hat{A}^2(X) = \int_{-\infty}^{X} \left[\left(\frac{3}{4}\beta - 1\right)\hat{A}(\xi) - \beta\xi\frac{\mathrm{d}\hat{A}}{\mathrm{d}\xi}(\xi)\right] \frac{\mathrm{d}\xi}{(X-\xi)^{\frac{1}{4}}}\,. \tag{5.21}$$

The boundary conditions remain unchanged by the normalising transformations.

The affine transformations:

$$\hat{A}(X) \to |\lambda^{-}|^{\frac{3}{4}\beta}\hat{A}(X)\,, \qquad X \to |\lambda^{-}|^{\beta}X \tag{5.22}$$

convert the boundary conditions (5.19) also to those by Smith & Elliott (1985). When the affine transformations are applied to the nonlinear breakdown equation, there is no change. The boundary equations become:

$$\hat{A}(X) \sim \begin{cases} \lambda_1|X|^{\frac{3}{4}-\frac{1}{\beta}}, & X \to -\infty \\ \lambda_2 X^{\frac{3}{4}-\frac{1}{\beta}}, & X \to \infty \end{cases}$$

where λ_2 is an arbitrary constant. The boundary value constant λ_1 is known to be either $\lambda_1 = +1$ for attached forward flow upstream or $\lambda_1 = -1$ for detached reverse flow upstream. From Smith & Elliott (1985), where $X = \hat{X}$, "it soon became fairly

clear that... $\lambda_1 = -1$ is necessary, since with $\lambda_1 = +1$ the solution for $\hat{A}$ always appeared to blow up eventually in $\hat{X} < 0$, in line numerically with the singularity

$$\hat{A} \propto -\hat{X}_1(\hat{X}_1 - \hat{X})^{\frac{1}{4}}, \qquad \text{as } \hat{X} \to \hat{X}_1-,$$

for $\hat{X}_1$ negative... This singularity is not removable..." Therefore, the boundary conditions to solve the nonlinear breakdown equation are:

$$\hat{A}(X) \sim \begin{cases} -|X|^{\frac{3}{4}-\frac{1}{\beta}}, & X \to -\infty \\ \lambda_2 X^{\frac{3}{4}-\frac{1}{\beta}}, & X \to \infty \end{cases} \tag{5.23}$$

where λ_2 is a boundary value constant to be found in the course of the solution.

A numerical solution to the boundary eigenvalue β problem for the $\hat{A}(X)$ equation (5.21) with boundary conditions (5.23) is given by Smith & Elliott (1985). Nevertheless, another numerical solution is found.

5.2 $\hat{A}(X)$ Equation Numerical Treatment

The boundary eigenvalue problem is solved using the numerical shooting method and Newton's method for a system of nonlinear equations with MATLAB. The discretisation of the $\hat{A}(X)$ equation (5.21) is analogous to the numerical treatment of the $A(x,T)$ equation in Section 4.1. From hereon, the notation X_i denotes the value $X(i)$ of a vector $\mathbf{X}$ and $\hat{A}_i$ denotes $\hat{A}(X(i))$ of a vector $\hat{\mathbf{A}}$.

The computational domain over which the problem is to be solved is discretised with a uniform grid size DX and $m+1$ spatial points starting at a large and negative X_1 and extending to a large and positive X_{m+1} such that $X_i = X_1 + (i-1)\mathrm{D}X$ for $i = 1, 2, \ldots, m+1$. The domain is arbitrarily chosen to be large; either $[-50, 50]$, $[-100, 100]$, $[-150, 150]$, $[-200, 200]$ or $[-250, 250]$; whilst the step size is one of $\mathrm{D}X = 0.4, 0.2, 0.1, 0.05$.

The eigenvalue β is an unknown constant except that it is in the range $0 < \beta < \frac{4}{3}$

and hence, it is reasonable that the problem is solved for each $\beta = 0.01,\ 0.02,\ \ldots, 1.33$, with the eigenvalue closest to the true value giving the $\hat{A}(X)$ solution which most satisfies the criteria for the true solution, as tested in Section 5.3.

A numerical shooting method is used first to determine if solutions exist by solving for each $\beta = 0.01,\ 0.02,\ \ldots, 1.33$. Secondly, Newton's method is used to solve the boundary value problem accurately using the information from the numerical shooting method as an initial distribution. Both methods are tested in Section 5.3.

Centring

In order to implement either method, the $\hat{A}(X)$ equation (5.21) is discretised into a system of m nonlinear equations for $m-1$ variables from the $m+1$ total values of $\hat{A}_i$ minus the two end point values $\hat{A}_1$ and $\hat{A}_{m+1}$ known from the boundary conditions.

There are m equations for $m-1$ variables because there is centring of the $\hat{A}(X)$ equation at $X = X_{i+\frac{1}{2}}$, where the half-subscript means

$$X_{i+\frac{1}{2}} = \frac{1}{2}(X_i + X_{i+1})\,.$$

The centring reflects the implicit nature of the problem. Each $(i+1)$-th equation for $i = 1,\ 2,\ \ldots,\ m$ solves for $\hat{A}_i$ and $\hat{A}_{i+1}$ and uses information at the spatial point $X = X_{i+1}$, that is the value of $\hat{A}_{i+1}$ known from an initial distribution, and at all the points leading up to it from the start of the domain X_1. Hence, the X term in the integrand becomes $X = X_{i+1}$.

The left hand side of the $(i+1)$-th equation is centred in space and is discretised as

$$\hat{A}^2(X) = \frac{1}{2}\left(\hat{A}_i^2 + \hat{A}_{i+1}^2\right)\,. \tag{5.24}$$

It is to match with the integral (5.27), with (5.28) and (5.29), on the right hand side later.

The Integral

The integral on the right hand side of the $(i+1)$-th equation is approximated as

$$\begin{aligned}
&\int_{-\infty}^{X} \left[\left(\frac{3}{4}\beta - 1 \right) \hat{A}(\xi) - \beta\xi \frac{\mathrm{d}\hat{A}}{\mathrm{d}\xi}(\xi) \right] \frac{\mathrm{d}\xi}{(X-\xi)^{\frac{1}{4}}} \\
&\qquad \simeq \left(\frac{3}{4}\beta - 1 \right) \left\{ \int_{-\infty}^{X_1} + \int_{X_1}^{X_2} + \ldots + \int_{X_i}^{X_{i+1}} \right\} \hat{A}(\xi) \frac{\mathrm{d}\xi}{(X-\xi)^{\frac{1}{4}}} \\
&\qquad - \beta \left\{ \int_{-\infty}^{X_1} + \int_{X_1}^{X_2} + \ldots + \int_{X_i}^{X_{i+1}} \right\} \xi \frac{\mathrm{d}\hat{A}}{\mathrm{d}\xi}(\xi) \frac{\mathrm{d}\xi}{(X-\xi)^{\frac{1}{4}}} \,. \qquad (5.25)
\end{aligned}$$

The upper limit of the integral and the X term in the integrand stop at the specific spatial point $X = X_{i+1}$. Also, X_1 is large and negative, and $X_{i+1} > X_1$.

The contribution from the integral between the limits $X = -\infty$ and the large and negative $X = X_1$, calculated at $X = X_{i+1}$, is:

$$\int_{-\infty}^{X_1} \left[\left(\frac{3}{4}\beta - 1 \right) \hat{A}(\xi) - \beta\xi \frac{\mathrm{d}\hat{A}}{\mathrm{d}\xi}(\xi) \right] \frac{\mathrm{d}\xi}{(X_{i+1}-\xi)^{\frac{1}{4}}} \simeq 0 \,. \qquad (5.26)$$

This is because the boundary condition (5.23):

$$\hat{A}(X) \sim -|X|^{\frac{3}{4}-\frac{1}{\beta}} \,, \qquad X \to -\infty \,;$$

$$\frac{\mathrm{d}\hat{A}}{\mathrm{d}X}(X) \sim -\left(\frac{3}{4} - \frac{1}{\beta} \right) |X|^{-\frac{1}{4}-\frac{1}{\beta}} \,, \qquad X \to -\infty$$

substituted into the integral (5.26) gives:[5]

$$\begin{aligned}
&\int_{-\infty}^{X_1} \left[\left(\frac{3}{4}\beta - 1 \right) \hat{A}(\xi) - \beta\xi \frac{\mathrm{d}\hat{A}}{\mathrm{d}\xi}(\xi) \right] \frac{\mathrm{d}\xi}{(X_{i+1} - \xi)^{\frac{1}{4}}} \\
&\quad \simeq \int_{-\infty}^{X_1} \left[\left(\frac{3}{4}\beta - 1 \right) \cdot - |\xi|^{\frac{3}{4} - \frac{1}{\beta}} - \beta\xi \cdot - \left(\frac{3}{4} - \frac{1}{\beta} \right) |\xi|^{-\frac{1}{4} - \frac{1}{\beta}} \right] \frac{\mathrm{d}\xi}{(X_{i+1} - \xi)^{\frac{1}{4}}} \\
&\quad \simeq 0 \,.
\end{aligned}$$

Hence, the $(i+1)$-th integral (5.25) is

$$\begin{aligned}
&\int_{-\infty}^{X} \left[\left(\frac{3}{4}\beta - 1 \right) \hat{A}(\xi) - \beta\xi \frac{\mathrm{d}\hat{A}}{\mathrm{d}\xi}(\xi) \right] \frac{\mathrm{d}\xi}{(X - \xi)^{\frac{1}{4}}} \\
&\quad \simeq \left(\frac{3}{4}\beta - 1 \right) \left\{ \int_{X_1}^{X_2} + \int_{X_2}^{X_3} + \ldots + \int_{X_i}^{X_{i+1}} \right\} \hat{A}(\xi) \frac{\mathrm{d}\xi}{(X - \xi)^{\frac{1}{4}}} \\
&\quad - \beta \left\{ \int_{X_1}^{X_2} + \int_{X_2}^{X_3} + \ldots + \int_{X_i}^{X_{i+1}} \right\} \xi \frac{\mathrm{d}\hat{A}}{\mathrm{d}\xi}(\xi) \frac{\mathrm{d}\xi}{(X - \xi)^{\frac{1}{4}}} \,.
\end{aligned}$$

The $\hat{A}(X)$ term in the first set of integrals is centred in space, similar to the left hand side of the $(i+1)$-th equation (5.24), such that

$$\hat{A}(X_{j+\frac{1}{2}}) = \frac{1}{2} \left(\hat{A}_j + \hat{A}_{j+1} \right) .$$

The derivative of $\hat{A}(X)$ with respect to X in the second set of integrals is approximated using the midpoint rule with first order error:

$$\frac{\mathrm{d}\hat{A}}{\mathrm{d}X}(X_{j+\frac{1}{2}}) = \frac{1}{\mathrm{D}X} \left(\hat{A}_{j+1} - \hat{A}_j \right) .$$

Therefore, the complete integral (5.25) on the right hand side of the $(i+1)$-th equation

[5]The solution of the integral is a constant which can theoretically be taken to be zero since the integral is between two values. The next order terms of the integrand from the boundary condition (5.23) series must be considered because they contribute also. However, the terms are not found here. The contribution is discussed in Section 7.4 on further work.

is:

$$\begin{aligned}
&\int_{-\infty}^{X} \left[\left(\frac{3}{4}\beta - 1 \right) \hat{A}(\xi) - \beta\xi \frac{\mathrm{d}\hat{A}}{\mathrm{d}\xi}(\xi) \right] \frac{\mathrm{d}\xi}{(X-\xi)^{\frac{1}{4}}} \\
&\quad \simeq \left(\frac{3}{4}\beta - 1 \right) \frac{1}{2} \left\{ (\hat{A}_1 + \hat{A}_2) \int_{X_1}^{X_2} + \ldots + (\hat{A}_i + \hat{A}_{i+1}) \int_{X_i}^{X_{i+1}} \right\} \frac{\mathrm{d}\xi}{(X_{i+1}-\xi)^{\frac{1}{4}}} \\
&\qquad - \beta \frac{1}{\mathrm{D}X} \left\{ (\hat{A}_2 - \hat{A}_1) \int_{X_1}^{X_2} + \ldots + (\hat{A}_{i+1} - \hat{A}_i) \int_{X_i}^{X_{i+1}} \right\} \xi \frac{\mathrm{d}\xi}{(X_{i+1}-\xi)^{\frac{1}{4}}} \\
&\quad = \left(\frac{3}{4}\beta - 1 \right) \frac{1}{2} \left\{ \sum_{j=1}^{i} \left(\hat{A}_j + \hat{A}_{j+1} \right) \int_{X_j}^{X_{j+1}} \right\} \frac{\mathrm{d}\xi}{(X_{i+1}-\xi)^{\frac{1}{4}}} \\
&\qquad - \beta \frac{1}{\mathrm{D}X} \left\{ \sum_{j=1}^{i} \left(\hat{A}_{j+1} - \hat{A}_j \right) \int_{X_j}^{X_{j+1}} \right\} \xi \, \frac{\mathrm{d}\xi}{(X_{i+1}-\xi)^{\frac{1}{4}}} \, .
\end{aligned} \tag{5.27}$$

The integrals can be solved to respectively give

$$\begin{aligned}
&\frac{1}{2} \left\{ \sum_{j=1}^{i} \left(\hat{A}_j + \hat{A}_{j+1} \right) \int_{X_j}^{X_{j+1}} \right\} \frac{\mathrm{d}\xi}{(X_{i+1}-\xi)^{\frac{1}{4}}} \\
&\quad = \frac{1}{2} \left\{ \sum_{j=1}^{i} \left(\hat{A}_j + \hat{A}_{j+1} \right) \cdot -\frac{4}{3} \left[(X_{i+1}-\xi)^{\frac{3}{4}} \right]_{X_j}^{\hat{x}_{j+1}} \right\} \\
&\quad = \frac{1}{2} \cdot \frac{4}{3} \left\{ \sum_{j=1}^{i} \left(\hat{A}_j + \hat{A}_{j+1} \right) \cdot \left[(X_{i+1}-X_j)^{\frac{3}{4}} - (X_{i+1}-X_{j+1})^{\frac{3}{4}} \right] \right\} \\
&\quad = \frac{2(\mathrm{D}X)^{\frac{3}{4}}}{3} \left\{ \sum_{j=1}^{i} \left(\hat{A}_j + \hat{A}_{j+1} \right) \cdot \left[(i+1-j)^{\frac{3}{4}} - (i-j)^{\frac{3}{4}} \right] \right\}
\end{aligned} \tag{5.28}$$

and

$$\begin{aligned}
&\frac{1}{\mathrm{D}X}\left\{\sum_{j=1}^{i}\left(\hat{A}_{j+1}-\hat{A}_j\right)\int_{X_j}^{X_{j+1}}\right\}\xi\,\frac{\mathrm{d}\xi}{(X_{i+1}-\xi)^{\frac{1}{4}}}\\
&\quad=\frac{1}{\mathrm{D}X}\sum_{j=1}^{i}\left\{\left(\hat{A}_{j+1}-\hat{A}_j\right)\cdot\left[-\frac{4}{3}\left[\xi(X_{i+1}-\xi)^{\frac{3}{4}}\right]_{X_j}^{X_{j+1}}+\frac{4}{3}\int_{X_j}^{X_{j+1}}(X_{i+1}-\xi)^{\frac{3}{4}}\,\mathrm{d}\xi\right]\right\}\\
&\quad=\frac{4}{3\mathrm{D}X}\sum_{j=1}^{i}\left\{\left(\hat{A}_{j+1}-\hat{A}_j\right)\cdot\left\{\left[X_j(X_{i+1}-X_j)^{\frac{3}{4}}-X_{j+1}(X_{i+1}-X_{j+1})^{\frac{3}{4}}\right]\right.\right.\\
&\qquad\left.\left.+\frac{4}{7}\left[(X_{i+1}-X_j)^{\frac{7}{4}}-(X_{i+1}-X_{j+1})^{\frac{7}{4}}\right]\right\}\right\}\\
&\quad=\frac{4}{3\mathrm{D}X}\sum_{j=1}^{i}\left\{\left(\hat{A}_{j+1}-\hat{A}_j\right)\cdot\left\{(\mathrm{D}X)^{\frac{3}{4}}\left[X_j(i+1-j)^{\frac{3}{4}}-X_{j+1}(i-j)^{\frac{3}{4}}\right]\right.\right.\\
&\qquad\left.\left.+\frac{4(\mathrm{D}X)^{\frac{7}{4}}}{7}\left[(i+1-j)^{\frac{7}{4}}-(i-j)^{\frac{7}{4}}\right]\right\}\right\} \qquad (5.29)
\end{aligned}$$

where $\mathrm{D}X$ and $\mathrm{D}T$ are the spatial and time grid steps. The right hand side integral (5.27) will match with the left hand side term (5.24).

Numerical Method

The second interactive region $\hat{A}(X)$ equation (5.21) becomes a system of m nonlinear equations for $i = 1, 2 \ldots, m$:

$$\begin{aligned}
\frac{1}{2}(\hat{A}_i^2+\hat{A}_{i+1}^2)&=\left(\frac{3}{4}\beta-1\right)\frac{2(\mathrm{D}X)^{\frac{3}{4}}}{3}\left\{\sum_{j=1}^{i}\left(\hat{A}_j+\hat{A}_{j+1}\right)\cdot\left[(i+1-j)^{\frac{3}{4}}-(i-j)^{\frac{3}{4}}\right]\right\}\\
&\quad-\beta\frac{4}{3\mathrm{D}X}\sum_{j=1}^{i}\left\{\left(\hat{A}_{j+1}-\hat{A}_j\right)\cdot\left\{(\mathrm{D}X)^{\frac{3}{4}}\left[X_j(i+1-j)^{\frac{3}{4}}-X_{j+1}(i-j)^{\frac{3}{4}}\right]\right.\right.\\
&\qquad\left.\left.+\frac{4(\mathrm{D}X)^{\frac{7}{4}}}{7}\left[(i+1-j)^{\frac{7}{4}}-(i-j)^{\frac{7}{4}}\right]\right\}\right\}. \qquad (5.30)
\end{aligned}$$

The system of equations is rearranged to a set of quadratic equations for $\hat{A}_{i+1}$ which will be called $\hat{\mathbf{F}}(\hat{\mathbf{A}})$ for the vector $\hat{\mathbf{A}} = (\hat{A}_1, \hat{A}_2, \ldots, \hat{A}_{m+1})$. A component $\hat{F}_i(\hat{\mathbf{A}})$ of

the system $\hat{\mathbf{F}}(\hat{\mathbf{A}})$ is

$$\hat{F}_i = \frac{1}{2}\hat{A}_{i+1}^2 + b\hat{A}_{i+1} + c = 0\,, \tag{5.31}$$

where

$$b = \left[-\left(\frac{3}{4}\beta - 1\right)\right]\frac{1}{2}\frac{4(\mathrm{D}X)^{\frac{3}{4}}}{3} + \beta\frac{4}{3(\mathrm{D}X)^{\frac{1}{4}}}\left[X_i + \frac{4\mathrm{D}X}{7}\right], \tag{5.32}$$

and

$$\begin{aligned} c = {} & \frac{1}{2}\hat{A}_i^2 + \left[-\left(\frac{3}{4}\beta - 1\right)\right]\frac{1}{2}\frac{4(\mathrm{D}X)^{\frac{3}{4}}}{3}\hat{A}_i - \beta\frac{4}{3(\mathrm{D}X)^{\frac{1}{4}}}\left[X_i + \frac{4\mathrm{D}X}{7}\right]\hat{A}_i \\ & + \left[-\left(\frac{3}{4}\beta - 1\right)\right]\frac{1}{2}\frac{4(\mathrm{D}X)^{\frac{3}{4}}}{3}\sum_{j=1}^{i-1}(\hat{A}_j + \hat{A}_{j+1})\left[(i+1-j)^{\frac{3}{4}} - (i-j)^{\frac{3}{4}}\right] \\ & + \beta\frac{4}{3(\mathrm{D}X)^{\frac{1}{4}}}\sum_{j=1}^{i-1}(\hat{A}_{j+1} - \hat{A}_j)\Bigg\{\left[X_j(i+1-j)^{\frac{3}{4}} - X_{j+1}(i-j)^{\frac{3}{4}}\right] \\ & \quad + \frac{4\mathrm{D}X}{7}\left[(i+j-1)^{\frac{7}{4}} - (i-j)^{\frac{7}{4}}\right]\Bigg\}. \end{aligned} \tag{5.33}$$

For $i = 1$:

$$\begin{aligned} \hat{F}_1\left(\hat{\mathbf{A}}\right) = {} & \frac{1}{2}\hat{A}_2^2 + \left[\left[-\left(\frac{3}{4}\beta - 1\right)\right]\frac{1}{2}\frac{4(\mathrm{D}X)^{\frac{3}{4}}}{3} + \beta\frac{4}{3(\mathrm{D}X)^{\frac{1}{4}}}\left[X_1 + \frac{4\mathrm{D}X}{7}\right]\right]\hat{A}_2 \\ & + \left\{\frac{1}{2}\hat{A}_1^2 + \left[\left[-\left(\frac{3}{4}\beta - 1\right)\right]\frac{1}{2}\frac{4(\mathrm{D}X)^{\frac{3}{4}}}{3} + \beta\frac{4}{3(\mathrm{D}X)^{\frac{1}{4}}}\left[X_1 + \frac{4\mathrm{D}X}{7}\right]\right]\hat{A}_1\right\} \\ = {} & 0\,; \end{aligned} \tag{5.34}$$

for $i = 2$:

$$\begin{aligned} \hat{F}_2\left(\hat{\mathbf{A}}\right) = {} & \frac{1}{2}\hat{A}_3^2 + \left[\left[-\left(\frac{3}{4}\beta - 1\right)\right]\frac{1}{2}\frac{4(\mathrm{D}X)^{\frac{3}{4}}}{3} + \beta\frac{4}{3(\mathrm{D}X)^{\frac{1}{4}}}\left[X_2 + \frac{4\mathrm{D}X}{7}\right]\right]\hat{A}_3 \\ & + \left\{\frac{1}{2}\hat{A}_2^2 + \left[\left[-\left(\frac{3}{4}\beta - 1\right)\right]\frac{1}{2}\frac{4(\mathrm{D}X)^{\frac{3}{4}}}{3} + \beta\frac{4}{3(\mathrm{D}X)^{\frac{1}{4}}}\left[X_2 + \frac{4\mathrm{D}X}{7}\right]\right]\hat{A}_2\right. \\ & \quad \left. + \beta\frac{4}{3(\mathrm{D}X)^{\frac{1}{4}}}(\hat{A}_2 - \hat{A}_1)\left[\left[X_1(2)^{\frac{3}{4}} - \hat{x}_2(1)^{\frac{3}{4}}\right] + \frac{4\mathrm{D}X}{7}\left[(2)^{\frac{7}{4}} - (1)^{\frac{7}{4}}\right]\right]\right\} \\ = {} & 0 \end{aligned} \tag{5.35}$$

and so forth.

5.2.1 The Minimising Function Φ , Eigenvalue β & Boundary Value Constant λ_2

The boundary condition (5.23) at the start of the computational domain $X = X_1$ is $\hat{A}_1 = -|X_1|^{\frac{3}{4}-\frac{1}{\beta}}$. However, the value of $\hat{A}_{m+1}$ at the end of the domain:

$$\hat{A}_{m+1} = \lambda_2 X_{m+1}^{\frac{3}{4}-\frac{1}{\beta}} \tag{5.36}$$

remains unknown since λ_2 is an arbitrary constant. The boundary condition at $X = X_{m+1}$ can be satisfactorily achieved, with the constant λ_2 found, by implementation of a *minimising function*. The $\hat{A}(X)$ solution must satisfy the minimising function to be a true solution.

Treating the boundary condition (5.36) as a function of X and differentiating, then:

$$\left.\frac{\mathrm{d}\hat{A}}{\mathrm{d}X}\right|_{X=X_m} = \hat{A}'_m = \lambda_2 \left(\frac{3}{4} - \frac{1}{\beta}\right) X_m^{\frac{3}{4}-\frac{1}{\beta}-1} .$$

A minimising function Φ (which is not to be confused with the Fourier transformation in Section 3.3.3) can then be defined from the boundary condition derivative $\hat{A}'_m$:

$$\Phi(\beta; X_m; \hat{A}_m, \hat{A}_{m+1}) = \frac{\hat{A}'_m}{\frac{1}{2}(\hat{A}_m + \hat{A}_{m+1})} - \left(\frac{3}{4} - \frac{1}{\beta}\right)\frac{1}{X_m} = 0 .$$

The minimising function is also centred in space at $X_{m+\frac{1}{2}}$. A first order approximation of the $\hat{A}'(X)$ term is

$$\left.\frac{\mathrm{d}\hat{A}}{\mathrm{d}X}\right|_{X=X_m} = \frac{\hat{A}_{m+1} - \hat{A}_m}{\mathrm{D}X} .$$

A second order approximation to $\hat{A}'(X)$ is not appropriate since there is a discontinuity along the X-axis according to the analysis in Section 5.2.3. Therefore, the

minimising function Φ is

$$\Phi(\beta; X_m; \hat{A}_m, \hat{A}_{m+1}) = \frac{\hat{A}_{m+1} - \hat{A}_m}{\mathrm{D}X \cdot \frac{1}{2}(\hat{A}_m + \hat{A}_{m+1})} - \left(\frac{3}{4} - \frac{1}{\beta}\right)\frac{1}{X_m} = 0 \tag{5.37}$$

and the value of the true eigenvalue β is found from rearranging (5.37):

$$\beta = \left| X_m \cdot \left(\frac{\hat{A}_{m+1} - \hat{A}_m}{\mathrm{D}X \cdot \frac{1}{2}(\hat{A}_m + \hat{A}_{m+1})} \right) - \frac{3}{4} \right|^{-1} . \tag{5.38}$$

The minimising function Φ is so-called because it is used to force the iterate solution towards the boundary condition at $X = X_{m+1}$, and thus the true $\hat{A}(X)$ solution, with each iteration of Newton's method. The minimising function is also used to help determine the true $\hat{A}(X)$ solution and a narrow neighbourhood of the true eigenvalue β when using the shooting method.

Furthermore, the value of constant λ_2 is found from rearranging the boundary condition (5.36) at $X = X_{m+1}$:

$$\lambda_2 = \frac{\hat{A}_{m+1}}{X_{m+1}^{\frac{3}{4}-\frac{1}{\beta}}} \tag{5.39}$$

using the values for (5.37).

The use of (5.37), (5.38) and (5.39) *in situ* is shown in Sections 5.2.2 and 5.2.4.

5.2.2 Numerical Shooting Method

The eigenvalue β is known to be in the range $0 < \beta < \frac{4}{3}$ in order for first interactive stage $A(x,T)$ to be large at breakdown and second interactive stage $\hat{A}(X)$ to be of order unity. The range of eigenvalue is discretised by uniform increments of $\Delta\beta = 0.01$, starting at $\beta_1 = 0.01$ and ending at $\beta_{133} = 1.33$, such that $\beta_k = \beta_1 + (k-1)\Delta\beta$ for $k = 1, 2, \ldots, 1.33$.

A crude technique is to start at $\beta_1 = 0.01$ and shoot from the known boundary condition $\hat{A}_1$ (5.23) to solve each $\hat{A}_{i+1}$ of the component equation (5.31) in turn for $i = 1, 2, \ldots, m$. Next, march forward in β by the increment of $\Delta\beta = 0.01$ to

$\beta_2 = 0.02$ and repeat the shooting, until $\beta = 1.33$ is reached.

The $\hat{A}_{i+1}$ solution to each component equation:

$$\hat{F}_i = \frac{1}{2}\hat{A}_{i+1}^2 + b\hat{A}_{i+1} + c = 0$$

is given by the quadratic formula:

$$\hat{A}_{i+1} = \frac{-b \pm \sqrt{b^2 - 4ac}}{2a}$$

where from the numerical treatment in Section 5.2: $a = \frac{1}{2}$ and b, c are given by (5.32), (5.33) respectively. A choice of sign must be made for the solution $\hat{A}_{i+1}$ of the quadratic formula. The solution is expected to be discontinuous at $X = 0$, negative for $X < 0$ and positive for $X > 0$ from the work by Smith & Elliott (1985) and the discontinuous functions analysis in Section 5.2.3. Hence, the corresponding root is chosen. For $i = 1$, the $\hat{A}_2$ solution to the $\hat{F}_1(\hat{\mathbf{A}})$ equation (5.34) is:

$$\begin{aligned}\hat{A}_2 = &- \left[\left[-\left(\frac{3}{4}\beta - 1\right)\right]\frac{1}{2}\frac{4(\mathrm{D}X)^{\frac{3}{4}}}{3} + \beta\frac{4}{3(\mathrm{D}X)^{\frac{1}{4}}}\left[X_1 + \frac{4\mathrm{D}X}{7}\right]\right] \\ &- \left\{\left[\left[-\left(\frac{3}{4}\beta - 1\right)\right]\frac{1}{2}\frac{4(\mathrm{D}X)^{\frac{3}{4}}}{3} + \beta\frac{4}{3(\mathrm{D}X)^{\frac{1}{4}}}\left[X_1 + \frac{4\mathrm{D}X}{7}\right]\right]^2\right. \\ &\left. - 2\left\{\frac{1}{2}\hat{A}_1^2 + \left[\left[-\left(\frac{3}{4}\beta - 1\right)\right]\frac{1}{2}\frac{4(\mathrm{D}X)^{\frac{3}{4}}}{3} + \beta\frac{4}{3(\mathrm{D}X)^{\frac{1}{4}}}\left[X_1 + \frac{4\mathrm{D}X}{7}\right]\right]\hat{A}_1\right\}\right\}\end{aligned}$$

with the negative root chosen because $X_2 < 0$.

Better approximations to the solution and hence the eigenvalue are made by repeating the same crude technique for a narrower range of β. If at some β_k: $\Phi < 0$ and at the adjacent increment $\beta_k + \Delta\beta$: $\Phi > 0$ (or vice versa, β_k: $\Phi > 0$ and $\beta_k + \Delta\beta$: $\Phi < 0$) then by the intermediate value theorem, $\Phi = 0$ at some value of β in the range $(\beta_k, \beta_k + \Delta\beta)$. The process of discretisation and shooting is repeated for the range until the true eigenvalue is found to, for example, 3 significant figures.

The true $\hat{A}(X)$ solution, corresponding with the true eigenvalue β, occurs when

the minimising function Φ (5.37) is satisfied. When the true solution is found then the constant λ_2 is given by (5.39).

The shooting method is tested in Section 5.3.1.

5.2.3 Discontinuous $A(x,T)$ & $\hat{A}(X)$ Analysis

The $A(x,T)$ solvability condition (4.1):

$$A^2(x,T) - x^2 + 2a(T) = -\frac{2^{\frac{3}{4}}}{\Gamma(\frac{5}{4})} \int_{-\infty}^{x} \frac{\partial A}{\partial T}(\xi,T) \, \frac{\mathrm{d}\xi}{(x-\xi)^{\frac{1}{4}}} \,,$$

of which the second interactive stage $\hat{A}(X)$ equation (5.21):

$$\hat{A}^2(X) = -\frac{2^{\frac{3}{4}}}{\Gamma(\frac{5}{4})} \int_{-\infty}^{X} \left[-\left(\frac{3}{4}\beta - 1\right) \hat{A}(\xi) + \beta\xi \frac{\mathrm{d}\hat{A}}{\mathrm{d}\xi}(\xi) \right] \frac{\mathrm{d}\xi}{(X-\xi)^{\frac{1}{4}}}$$

originates, can be shown to admit discontinuous forms of $A(x,T)$ like travelling Heaviside function waves (although they are not solved with boundary conditions). If discontinuous forms of $A(x,T)$ can exist for the solvability condition then by the series expansion (5.6):

$$A(x,T) = (T_s - T)^{\frac{3}{4}n-1} \hat{A}(X) + \ldots \qquad \hat{A}(X) = O(1) \,,$$

discontinuous forms of $\hat{A}(X)$ can also exist in the second interactive region.

When $A(x,T)$ becomes large and negative, and the term $-x + 2a(T)$ becomes insignificant, then the Abel inverse transform version of the $A(x,T)$ equation, that is (3.49) without bar or subscript notation, becomes:

$$\frac{\partial A}{\partial T}(x,T) = -\frac{\Gamma(\frac{5}{4})}{2^{\frac{5}{4}}\pi} \frac{\partial}{\partial x} \int_{-\infty}^{x} A^2(\xi,T) \, \frac{\mathrm{d}\xi}{(x-\xi)^{\frac{3}{4}}} \,. \tag{5.40}$$

A discontinuous form of $A(x,T)$ is

$$A(x,T) = \bar{C}T^{\alpha}H\left[x - vT^{\beta}\right] , \tag{5.41}$$

where α, β are arbitrary constants (not to be confused with eigenvalues α, β in the Chapter 5 or exponents elsewhere in the thesis); $\bar{C} \geq 0$ is a constant and amplitude parameter; v is the velocity; and $H\left[x - vT^{\beta}\right]$ denotes the Heaviside step function:

$$H\left[x - vT^{\beta}\right] = \begin{cases} 0\,, & x < vT^{\beta} \\ 1\,, & x \geq vT^{\beta}\,. \end{cases} \tag{5.42}$$

The discontinuous wave (5.41) takes into account forms of $A \geq 0$ with $\bar{C} \geq 0$ but does not describe any $A < 0$.

Differentiating (5.41) with respect to T gives the left hand side of the $A(x,T)$ equation (5.40):

$$\frac{\partial A}{\partial T}(x,T) = \bar{C}\alpha T^{\alpha-1}H\left[x - vT^{\beta}\right] - \bar{C}\beta v T^{\alpha+\beta-1}\delta\left[x - vT^{\beta}\right] \tag{5.43}$$

where, by the properties of the Heaviside function:

$$\frac{\partial H}{\partial T}\left[x - vT^{\beta}\right] = -\beta v T^{\beta-1}\delta\left[x - vT^{\beta}\right] .$$

Similarly:

$$\frac{\partial H}{\partial x}\left[x - vT^{\beta}\right] = \delta\left[x - vT^{\beta}\right])$$

with the Dirac delta function defined by

$$\delta\left[x - vT^{\beta}\right] = \begin{cases} 0\,, & x \neq vT^{\beta} \\ \infty\,, & x = vT^{\beta}\,. \end{cases} \tag{5.44}$$

Substituting (5.41) and (5.43) into the $A(x,T)$ equation, then

$$\begin{aligned}&\bar{C}\alpha T^{\alpha-1}H\left[x-vT^{\beta}\right]-\bar{C}\beta vT^{\alpha+\beta-1}\delta\left[x-vT^{\beta}\right]\\&\quad=-\frac{\Gamma(\frac{5}{4})}{2^{\frac{5}{4}}\pi}\bar{C}^2T^{2\alpha}\frac{\partial}{\partial x}\int\limits_{-\infty}^{x}H^2\left[\xi-vT^{\beta}\right]\frac{\mathrm{d}\xi}{(x-\xi)^{\frac{3}{4}}}\,.\end{aligned}\tag{5.45}$$

By the definition of the Heaviside step function (5.42):

$$H\left[x-vT^{\beta}\right]=\left(H\left[x-vT^{\beta}\right]\right)^2=\left(H\left[x-vT^{\beta}\right]\right)^{\frac{1}{2}}\,.$$

Hence, the integral on the right hand side of (5.45) becomes

$$\begin{aligned}\int\limits_{-\infty}^{x}H^2\left[\xi-vT^{\beta}\right]\frac{\mathrm{d}\xi}{(x-\xi)^{\frac{3}{4}}}&=\int\limits_{-\infty}^{x}H\left[\xi-vT^{\beta}\right]\frac{\mathrm{d}\xi}{(x-\xi)^{\frac{3}{4}}}\\&=4\left(x-vT^{\beta}\right)^{\frac{1}{4}}H\left[x-vT^{\beta}\right]-4\int\limits_{-\infty}^{x}\left(\xi-vT^{\beta}\right)^{\frac{1}{4}}\delta\left[\xi-vT^{\beta}\right]\\&=4\left(x-vT^{\beta}\right)^{\frac{1}{4}}H\left[x-vT^{\beta}\right]\end{aligned}\tag{5.46}$$

from integration by parts. This is because, by the Dirac delta function (5.44):

$$4\int\limits_{-\infty}^{x}\left(\xi-vT^{\beta}\right)^{\frac{1}{4}}\delta\left[\xi-vT^{\beta}\right]=0\,,\qquad x\neq vT^{\beta}\,.$$

Differentiating (5.46) with respect to x, then the right hand side of (5.45) becomes

$$\begin{aligned}4\frac{\partial}{\partial x}\left(\left(x-vT^{\beta}\right)^{\frac{1}{4}}H\left[x-vT^{\beta}\right]\right)&=\left(x-vT^{\beta}\right)^{-\frac{3}{4}}H\left[x-vT^{\beta}\right]\\&\quad+4\left(x-vT^{\beta}\right)^{\frac{1}{4}}\delta\left[x-vT^{\beta}\right]\,.\end{aligned}\tag{5.47}$$

By combining (5.45), (5.46) and (5.47), the $A(x,T)$ equation (5.40) becomes

$$\begin{aligned}\bar{C}\alpha T^{\alpha-1}H\left[x-vT^{\beta}\right]-\bar{C}\beta vT^{\alpha+\beta-1}\delta\left[x-vT^{\beta}\right]\\ =-\frac{\Gamma(\frac{5}{4})}{2^{\frac{5}{4}}\pi}\bar{C}^2T^{2\alpha}\Bigg\{\left(x-vT^{\beta}\right)^{-\frac{3}{4}}H\left[x-vT^{\beta}\right]\\ +4\left(x-vT^{\beta}\right)^{\frac{1}{4}}\delta\left[x-vT^{\beta}\right]\Bigg\}. \qquad (5.48)\end{aligned}$$

In the region upstream from the shock, where $x < vT^{\beta}$, (5.48) is a trivial equality: $0 = 0$, by definitions of the Heaviside and Dirac delta functions (5.42) and (5.44).

Where $x > vT^{\beta}$, in the region downstream of the shock, then the Heaviside function coefficients of (5.48) form the relation:

$$\bar{C}\alpha T^{\alpha-1}=-\frac{\Gamma(\frac{5}{4})}{2^{\frac{5}{4}}\pi}\bar{C}^2T^{2\alpha}\left(x-vT^{\beta}\right)^{-\frac{3}{4}}\,.$$

Exponentiating by $-\frac{4}{3}$:

$$\bar{C}^{-\frac{4}{3}}\alpha^{-\frac{4}{3}}T^{-\frac{4}{3}(\alpha-1)}=\left(-\frac{\Gamma(\frac{5}{4})}{2^{\frac{5}{4}}\pi}\right)^{-\frac{4}{3}}\bar{C}^{-\frac{8}{3}}T^{-\frac{8}{3}\alpha}\left(x-vT^{\beta}\right)\,;$$

multiplying by $\bar{C}^{\frac{8}{3}}\alpha^{\frac{4}{3}}\left(-\frac{\Gamma(\frac{5}{4})}{2^{\frac{5}{4}}\pi}\right)^{\frac{4}{3}}T^{\frac{8}{3}\alpha}$:

$$\bar{C}^{\frac{4}{3}}\left(-\frac{\Gamma(\frac{5}{4})}{2^{\frac{5}{4}}\pi}\right)^{\frac{4}{3}}T^{\frac{4}{3}(\alpha+1)}=\alpha^{\frac{4}{3}}\left(x-vT^{\beta}\right)\,;$$

and then rearranging, the relation becomes

$$\alpha^{\frac{4}{3}}x-\alpha^{\frac{4}{3}}vT^{\beta}-\bar{C}^{\frac{4}{3}}\left(\frac{\Gamma(\frac{5}{4})}{2^{\frac{5}{4}}\pi}\right)^{\frac{4}{3}}T^{\frac{4}{3}(\alpha+1)}=0\,. \qquad (5.49)$$

The branch

$$(-1)^{\frac{4}{3}}=\left((-1)^4\right)^{\frac{1}{3}}=1$$

is taken.

Similarly, the coefficients of the Dirac delta function terms in (5.48) form the relation:

$$-\bar{C}\beta v T^{\alpha+\beta-1} = -\frac{\Gamma(\frac{5}{4})}{2^{\frac{5}{4}}\pi}\bar{C}^2 T^{2\alpha} 4 (x - vT^{\beta})^{\frac{1}{4}} .$$

Exponentiating by 4:

$$\bar{C}^4\beta^4 v^4 T^{4(\alpha+\beta-1)} = \left(\frac{\Gamma(\frac{5}{4})}{2^{\frac{5}{4}}\pi}\right)^4 \bar{C}^8 T^{8\alpha} 4^4 \left(x - vT^{\beta}\right) ;$$

multiplying by $\bar{C}^{-4}T^{-8\alpha}$:

$$\beta^4 v^4 T^{4(\beta-\alpha-1)} = \left(\frac{\Gamma(\frac{5}{4})}{2^{\frac{5}{4}}\pi}\right)^4 \bar{C}^4 4^4 \left(x - vT^{\beta}\right) ;$$

and then rearranging, the relation becomes

$$\left(\frac{\Gamma(\frac{5}{4})}{2^{\frac{5}{4}}\pi}\right)^4 \bar{C}^4 4^4 x - \left(\frac{\Gamma(\frac{5}{4})}{2^{\frac{5}{4}}\pi}\right)^4 \bar{C}^4 4^4 v T^{\beta} - \beta^4 v^4 T^{4(\beta-\alpha-1)} = 0 . \tag{5.50}$$

Comparing the coefficients of either x or T^{β} in (5.49) and (5.50), then

$$\alpha = \left(\frac{\Gamma(\frac{5}{4})}{2^{\frac{5}{4}}\pi}\right)^3 4^3 \bar{C}^3 . \tag{5.51}$$

Comparing the remaining terms from (5.49) and (5.50), then

$$-\bar{C}^{\frac{4}{3}} \left(\frac{\Gamma(\frac{5}{4})}{2^{\frac{5}{4}}\pi}\right)^{\frac{4}{3}} T^{\frac{4}{3}(\alpha+1)} = -\beta^4 v^4 T^{4(\beta-\alpha-1)}$$

where equating the indices gives

$$\beta = \frac{4}{3}(\alpha + 1) \tag{5.52}$$

and equating the coefficients of the T terms gives

$$v = \frac{\left(\frac{\Gamma(\frac{5}{4})}{2^{\frac{5}{4}}\pi}\right)^{\frac{1}{3}} \bar{C}^{\frac{1}{3}}}{\beta} . \tag{5.53}$$

For the four unknown values α, β, v and $\bar{C}$ in the discontinuous form of $A(x,T)$ (5.41), there are three equations for α: (5.51); β: (5.52); v: (5.53). This implies there are a family of shock wave solutions with infinite members which differ in amplitude parameter $\bar{C}$.

A discontinuous form of $A(x,T)$ can be found by somewhat normalising the amplitude parameter of the wave by setting

$$\bar{C} = 1$$

and it follows from (5.51), (5.52), (5.53) that

$$\alpha = \left(\frac{\Gamma(\frac{5}{4})}{2^{\frac{5}{4}}\pi}\right)^3 4^3; \tag{5.54}$$

$$\beta = \frac{4}{3}\left(\left(\frac{\Gamma(\frac{5}{4})}{2^{\frac{5}{4}}\pi}\right)^3 4^3 + 1\right); \tag{5.55}$$

$$v = \frac{\left(\frac{\Gamma(\frac{5}{4})}{2^{\frac{5}{4}}\pi}\right)^{\frac{1}{3}}}{\frac{4}{3}\left(\left(\frac{\Gamma(\frac{5}{4})}{2^{\frac{5}{4}}\pi}\right)^3 4^3 + 1\right)}. \tag{5.56}$$

Therefore, a wave form of $A(x,T)$ is:

$$A(x,T) = T^{\alpha} H\left[x - vT^{\beta}\right] \tag{5.57}$$

with $\bar{C} = 1$; α: (5.54); β: (5.55); v: (5.56), as shown in Figures 5.2 and 5.3. The $A(x,T)$ wave advances downstream with time, whilst growing in amplitude. Initially, the wave growth is fast (as shown at intervals of $\Delta T = 0.2$ in Figure 5.2) but the speed is slow. As time increases, the growth slows and the speed of the wave increases (as shown at intervals of $\Delta T = 1.0$ in Figure 5.3). Discontinuous forms of $A(x,T)$ and thus $\hat{A}(X)$ in the second interactive stage are justified.

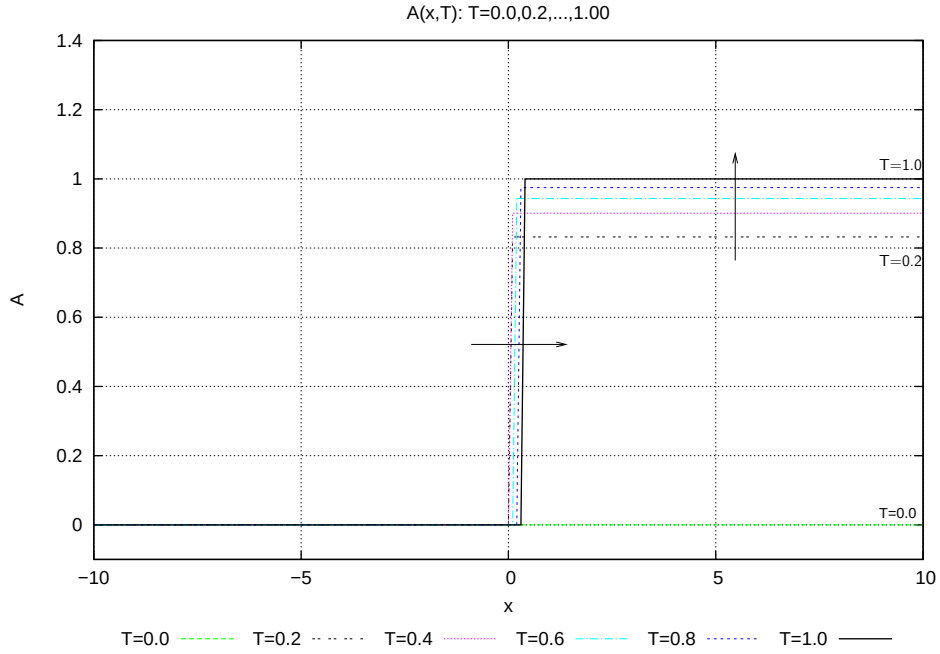

Figure 5.2: A discontinuous $A(x,T)$ wave for amplitude parameter $\bar{C} = 1$ at $T = 0.0, 0.2, \ldots, 1.0$.

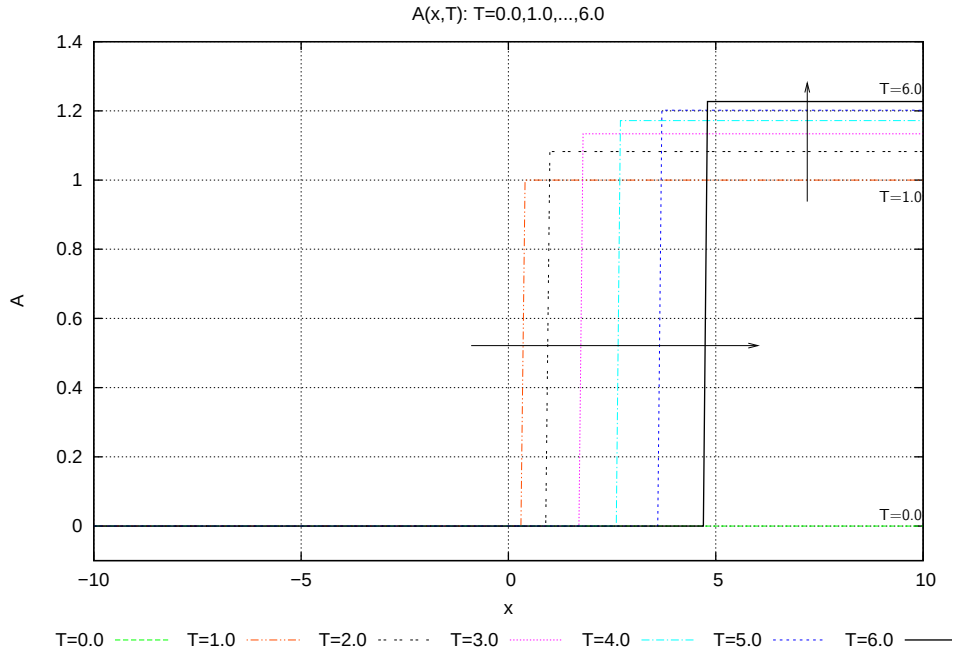

Figure 5.3: A discontinuous $A(x,T)$ wave for $\bar{C} = 1$ at $T = 0.0$ then $T = 1.0, 2.0, \ldots, 6.0$.

5.2.4 Newton's Method with Minimising Function Φ

Newton's method for a system of nonlinear equations is an iterative method already discussed in Section 4.2.

The superscripts (0) and (1) denote iteration levels. A superscript (0) refers to start values. A superscript (1) refers to the updated value from an iteration of Newton's method. The iteration starts with an initial eigenvalue $\beta^{(0)}$ and distribution $\hat{\mathbf{A}}^{(0)}$, for example, a solution from the numerical shooting method, to find a new iterates $\beta^{(1)}$ and $\hat{\mathbf{A}}^{(1)}$. At each iteration, the eigenvalue $\beta^{(1)}$ is found from (5.38), using the information at $\hat{A}_m^{(1)}$ and $\hat{A}_{m+1}^{(1)}$:

$$\beta^{(1)} = \left| \frac{3}{4} - X_m \cdot \left(\frac{\hat{A}_{m+1}^{(1)} - \hat{A}_m^{(1)}}{\mathrm{D}X \cdot \frac{1}{2}(\hat{A}_m^{(1)} - \hat{A}_{m+1}^{(1)})} \right) \right|^{-1} . \tag{5.58}$$

The β function (5.58) incorporates the minimising function Φ (5.37) to drive the iterate solution towards the true solution. In turn $\beta^{(1)}$ and $\hat{\mathbf{A}}^{(1)}$ replace the original values $\beta^{(0)}$ and $\hat{\mathbf{A}}^{(0)}$ in order to find further new updates $\hat{\mathbf{A}}^{(1)}$ and $\beta^{(1)}$, and so on until the error E falls less than the tolerance tol. There is the possibility of thousands or more total spatial grid points and so only information for two iterates are stored in the computer memory at one time.

The error E is defined as the infinity norm of the difference between the values of two successive iterations:

$$\begin{aligned} E &= \left| \hat{\mathbf{A}}^{(1)} - \hat{\mathbf{A}}^{(0)} \right|_\infty \\ &= \max \left(\left| \hat{A}_1^{(1)} - \hat{A}_1^{(0)} \right|, \left| \hat{A}_2^{(1)} - \hat{A}_2^{(0)} \right|, \ldots, \left| \hat{A}_{m+1}^{(1)} - \hat{A}_{m+1}^{(0)} \right| \right) ; \end{aligned} \tag{5.59}$$

the tolerance tol is set as:

$$tol = 1 \times 10^{-12} \tag{5.60}$$

and the maximum number of iterations is set as 50, at which point divergence is assumed. The tolerance and maximum number of iterations are both set arbitrarily.

The true $\hat{A}(X)$ solution at every $X = X_i$, corresponding eigenvalue β and boundary value constant λ_2 found from (5.39):

$$\lambda_2 = \frac{\hat{A}_{m+1}}{X_{m+1}^{\frac{3}{4}-\frac{1}{\beta}}}\,, \tag{5.61}$$

are output into a data file. The minimising function Φ and β function (5.58) ensure that the boundary condition (5.36) at $X = X_{m+1}$:

$$\hat{A}_{m+1} = X_{m+1}^{\frac{3}{4}-\frac{1}{\beta}}$$

is met by the true solution. There is also the stipulation that the boundary condition at $X = X_1$:

$$\hat{A}_1 = -|X_1|^{\frac{3}{4}-\frac{1}{\beta}}$$

is also satisfied.

The formula for the iterate $\hat{\mathbf{A}}^{(1)} = (\hat{A}_1^{(1)}, \hat{A}_2^{(1)}, \ldots, \hat{A}_{m+1}^{(1)})$ is

$$\hat{\mathbf{A}}^{(1)} = \hat{\mathbf{A}}^{(0)} - \left[\hat{\mathbf{F}}'\left(\hat{\mathbf{A}}^{(0)}\right)\right]^{-1} \hat{\mathbf{F}}\left(\hat{\mathbf{A}}^{(0)}\right)$$

or

$$\hat{\mathbf{A}}^{(1)} = \hat{\mathbf{A}}^{(0)} - \hat{\mathbf{F}}'\left(\hat{\mathbf{A}}^{(0)}\right) \backslash \hat{\mathbf{F}}\left(\hat{\mathbf{A}}^{(0)}\right)\,. \tag{5.62}$$

1. The $m \times 1$ column vector $\hat{\mathbf{F}}(\hat{\mathbf{A}}^{(0)})$ encapsulates the components of the system (5.31):

$$\hat{\mathbf{F}}\left(\hat{\mathbf{A}}^{(0)}\right) = \begin{pmatrix} \frac{1}{2}\hat{A}_2^{(0)\,2} + b\hat{A}_2^{(0)} + c \\ \frac{1}{2}\hat{A}_3^{(0)\,2} + b\hat{A}_3^{(0)} + c \\ \vdots \\ \frac{1}{2}\hat{A}_{m+1}^{(0)\,2} + b\hat{A}_{m+1}^{(0)} + c \end{pmatrix};$$

with b and c from (5.32) and (5.33). For example, the components for $i = 1$ and $i = 2$ are (5.34) and (5.35) respectively.

2. The function $\hat{\mathbf{F}} : \Re^{m+1} \rightarrow \Re^{m+1}$ is differentiable. The *Frechet derivative* of $\hat{\mathbf{F}}(\hat{\mathbf{A}})$, written $\hat{\mathbf{F}}'(\hat{\mathbf{A}})$, is the $m \times (m+1)$ Jacobian matrix:

$$\hat{\mathbf{F}}'\left(\hat{\mathbf{A}}^{(0)}\right) = J_{\hat{\mathbf{F}}}\left(\hat{A}^{(0)}\right) = \begin{pmatrix} \frac{\partial \hat{F}_1}{\partial \hat{A}_1^{(0)}} & \frac{\partial \hat{F}_1}{\partial \hat{A}_2^{(0)}} & \cdots & \frac{\partial \hat{F}_1}{\partial \hat{A}_{m+1}^{(0)}} \\ \frac{\partial \hat{F}_2}{\partial \hat{A}_1^{(0)}} & \frac{\partial \hat{F}_2}{\partial \hat{A}_2^{(0)}} & \cdots & \frac{\partial \hat{F}_2}{\partial \hat{A}_{m+1}^{(0)}} \\ \vdots & \vdots & \ddots & \vdots \\ \frac{\partial \hat{F}_m}{\partial \hat{A}_1^{(0)}} & \frac{\partial \hat{F}_m}{\partial \hat{A}_2^{(0)}} & \cdots & \frac{\partial \hat{F}_m}{\partial \hat{A}_{m+1}^{(0)}} \end{pmatrix};$$

For the $i = 1$ component then by (5.34):

$$\begin{aligned} \frac{\partial \hat{F}_1}{\partial \hat{A}_1^{(0)}} &= \hat{A}_1^{(0)} + \left[\left[-\left(\frac{3}{4}\beta - 1\right)\right]\frac{1}{2}\frac{4(\mathrm{D}X)^{\frac{3}{4}}}{3} + \beta\frac{4}{3(\mathrm{D}X)^{\frac{1}{4}}}\left[X_1 + \frac{4\mathrm{D}X}{7}\right]\right] \\ \frac{\partial \hat{F}_1}{\partial \hat{A}_2^{(0)}} &= \hat{A}_2^{(0)} + \left[\left[-\left(\frac{3}{4}\beta - 1\right)\right]\frac{1}{2}\frac{4(\mathrm{D}X)^{\frac{3}{4}}}{3} + \beta\frac{4}{3(\mathrm{D}X)^{\frac{1}{4}}}\left[X_1 + \frac{4\mathrm{D}X}{7}\right]\right] \\ \frac{\partial \hat{F}_1}{\partial \hat{A}_3^{(0)}} &= \ldots = \frac{\partial \hat{F}_1}{\partial \hat{A}_{m+1}^{(0)}} = 0\,; \end{aligned}$$

for the $i = 2$ component then by (5.35):

$$\begin{aligned} \frac{\partial \hat{F}_2}{\partial \hat{A}_1^{(0)}} &= -\beta\frac{4}{3(\mathrm{D}X)^{\frac{1}{4}}}\left[\left[X_1(2)^{\frac{3}{4}} - X_2(1)^{\frac{3}{4}}\right] + \frac{4\mathrm{D}X}{7}\left[(2)^{\frac{7}{4}} - (1)^{\frac{7}{4}}\right]\right] \\ \frac{\partial \hat{F}_2}{\partial \hat{A}_2^{(0)}} &= \hat{A}_2^{(0)} + \left[\left[-\left(\frac{3}{4}\beta - 1\right)\right]\frac{1}{2}\frac{4(\mathrm{D}X)^{\frac{3}{4}}}{3} + \beta\frac{4}{3(\mathrm{D}X)^{\frac{1}{4}}}\left[X_1 + \frac{4\mathrm{D}X}{7}\right]\right] \\ &\quad + \beta\frac{4}{3(\mathrm{D}X)^{\frac{1}{4}}}\left[\left[X_1(2)^{\frac{3}{4}} - X_2(1)^{\frac{3}{4}}\right] + \frac{4\mathrm{D}X}{7}\left[(2)^{\frac{7}{4}} - (1)^{\frac{7}{4}}\right]\right] \\ \frac{\partial \hat{F}_2}{\partial A_3^{(0)}} &= \hat{A}_3^{(0)} + \left[\left[-\left(\frac{3}{4}\beta - 1\right)\right]\frac{1}{2}\frac{4(\mathrm{D}X)^{\frac{3}{4}}}{3} + \beta\frac{4}{3(\mathrm{D}X)^{\frac{1}{4}}}\left[X_1 + \frac{4\mathrm{D}X}{7}\right]\right] \\ \frac{\partial \hat{F}_2}{\partial \hat{A}_4^{(0)}} &= \ldots = \frac{\partial \hat{F}_2}{\partial \hat{F}_{m+1}^{(0)}} = 0\,; \end{aligned}$$

and so forth.

3. the backslash "\" indicates left matrix division as used in MATLAB.

Newton's method is tested with various initial distributions in Section 5.3.2.

5.3 $\hat{A}(X)$ Algorithm Test

There are many tests to ensure that the numerical shooting and Newton's method give the true $\hat{A}(X)$ solution with corresponding eigenvalue β and boundary value constant λ_2. The methods are tested across domains $[-50, 50]$, $[-100, 100]$, $[-150, 150]$, $[-100, 100]$ and $[-250, 250]$ with each of the grid step sizes $\Delta X = 0.05$, 0.1, 0.2, 0.4, as shown in Table 5.1.

DX	domain
0.4	$[-50, 50]$
	$[-100, 100]$
	$[-150, 150]$
	$[-200, 200]$
	$[-250, 250]$
0.2	$[-50, 50]$
	$[-100, 100]$
	$[-150, 150]$
	$[-200, 200]$
	$[-250, 250]$
0.1	$[-50, 50]$
	$[-100, 100]$
	$[-150, 150]$
	$[-200, 200]$
	$[-250, 250]$
0.05	$[-50, 50]$
	$[-100, 100]$
	$[-150, 150]$
	$[-200, 200]$
	$[-250, 250]$

Table 5.1: The second interactive stage test domains in X and grid step sizes DX.

5.3.1 Numerical Shooting Method Test

The numerical shooting method is working correctly if the $\hat{A}(X)$ solutions for domains and step sizes DX from Table 5.1, corresponding eigenvalue β and boundary condition constant λ_2, converge to their true values as the size of the domain increases and the step size decreases.

Test Results for Eigenvalue β & Boundary Value Constant λ_2

The true eigenvalue $\beta \in \left(0, \frac{4}{3}\right)$ is given when the minimising function $\Phi = 0$, as defined by (5.37). The adopted "true" eigenvalue β and boundary condition constant λ_2 are those when Φ is closest to zero. The results for eigenvalue β and boundary condition constant λ_2 are displayed in Table 5.2. There appears to be no discernible pattern for Φ when compared to increase in size of domain and/or decrease in step size except that it is always small with orders of magnitude between 10^{-7} and 10^{-9}.

By inspection, the eigenvalue when Φ is closest to zero is independent of domain, particularly when the step size D$X \leq 0.2$. (See Figure 5.4.) The eigenvalue is dependent on step size, but converges to a constant value $\beta = 1.23$ (rounded up to 3 significant figures, because of Figure 5.5) as step size decreases.

DX	domain	Φ	β	λ_2
0.4	$[-50, 50]$	7.21919×10^{-7}	1.208	1.130
	$[-100, 100]$	5.924×10^{-9}	1.207	1.147
	$[-150, 150]$	3.8635×10^{-8}	1.207	1.154
	$[-200, 200]$	3.8110×10^{-8}	1.207	1.158
	$[-250, 250]$	2.7785×10^{-8}	1.206	1.160
0.2	$[-50, 50]$	2.55879×10^{-7}		1.017
	$[-100, 100]$	1.07077×10^{-7}		1.035
	$[-150, 150]$	5.8933×10^{-8}	1.217	1.043
	$[-200, 200]$	3.8080×10^{-8}		1.047
	$[-250, 250]$	2.7031×10^{-8}		1.050
0.1	$[-50, 50]$	2.8261×10^{-8}		0.960
	$[-100, 100]$	1.4050×10^{-8}		0.979
	$[-150, 150]$	7.654×10^{-9}	1.223	0.987
	$[-200, 200]$	4.619×10^{-9}		0.992
	$[-250, 250]$	2.996×10^{-9}		0.995
0.05	$[-50, 50]$	158852×10^{-7}		0.932
	$[-100, 100]$	4.1618×10^{-8}		0.952
	$[-150, 150]$	1.9411×10^{-8}	1.227	0.960
	$[-200, 200]$	1.1456×10^{-8}		0.964
	$[-250, 250]$	7.670×10^{-9}		0.967

Table 5.2: Numerical shooting method: Minimising function Φ; eigenvalue β and boundary condition constant λ_2 (both written to 4 significant figures), by step size DX and domain.

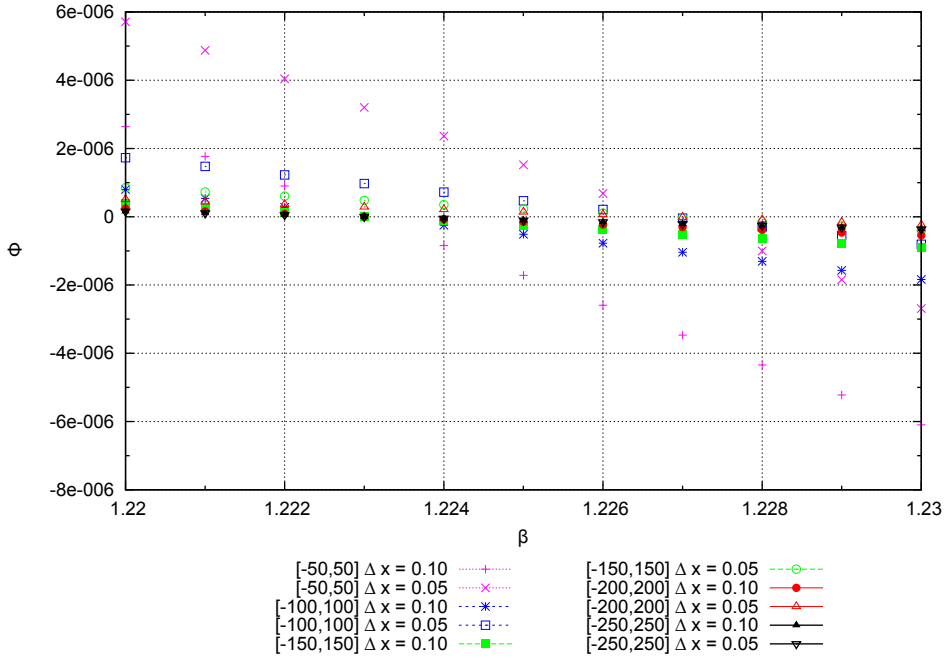

Figure 5.4: Numerical shooting method: Eigenvalue β versus minimising function Φ for step sizes D$X = 0.05$, 0.1, by domain.

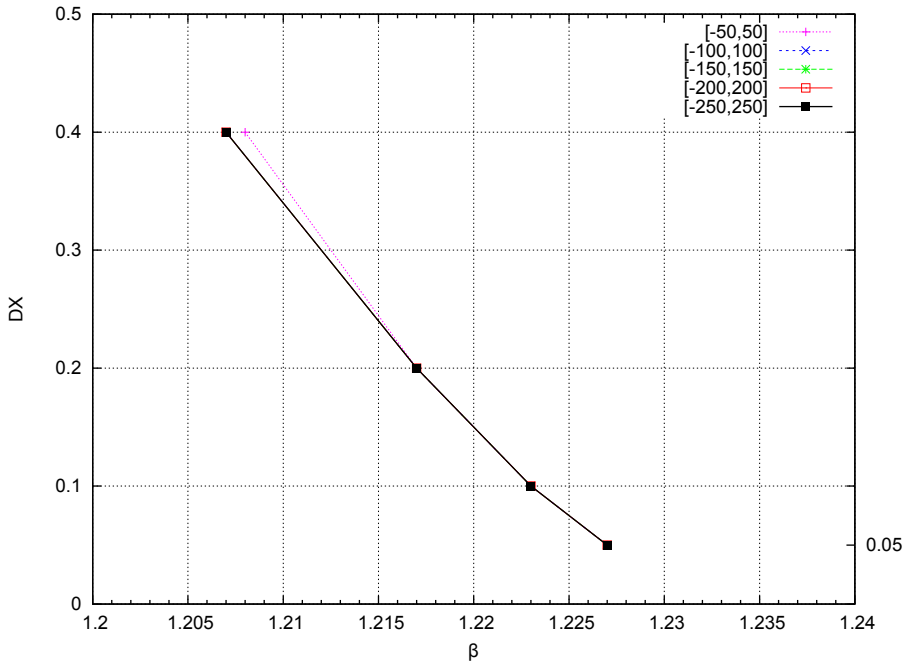

Figure 5.5: Numerical shooting method: Eigenvalue β versus step size DX, by domain.

Similarly, the constant λ_2 of the boundary condition, whose requirement to formulate a boundary value problem was removed by the minimising function Φ, converges to a value of $\lambda_2 = 0.96$ (rounded up to 3 significant figures, because of Figure 5.6) with increase in size of domain and decrease in step size. (See Table 5.2.)

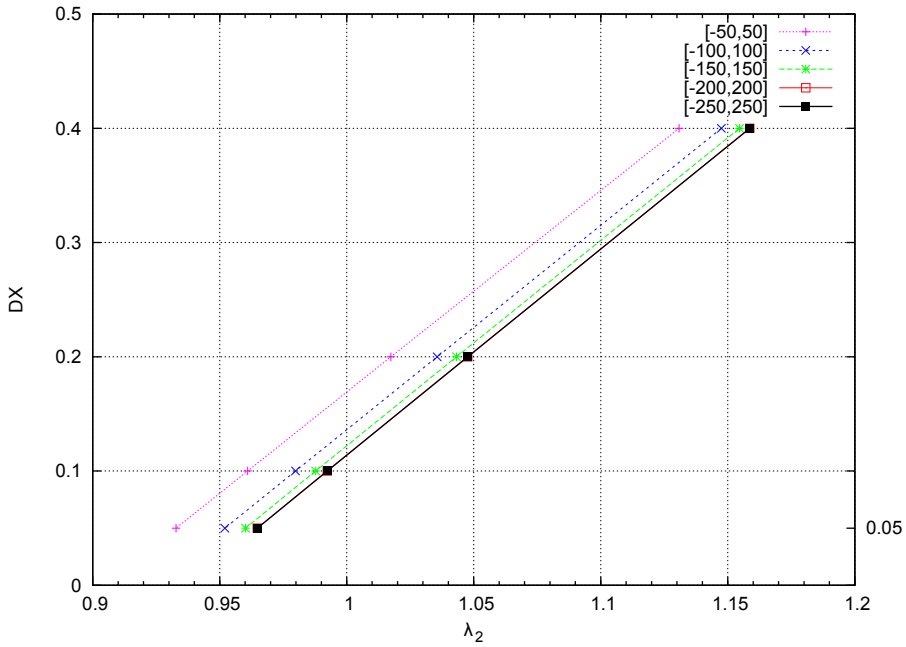

Figure 5.6: Numerical shooting method: Boundary condition constant λ_2 versus step size DX, by domain.

Test Results for Grid Independence & Boundary Condition

The $\hat{A}(X)$ solutions are grid dependent but converge towards the true solution as step size decreases, regardless of the size of domain. (See Figures 5.7 to 5.11.) For the smallest computational step size D$X = 0.05$, the $\hat{A}(X)$ solutions are nearly identical, as shown in Figure 5.12. Furthermore, those solutions converge to the boundary condition (5.23) for $\beta = 1.23$ and $\lambda_2 = 0.96$ (from the previous test results):

$$\hat{A}(X) \sim \begin{cases} -|X|^{\frac{3}{4}-\frac{1}{1.23}}, & X \to -\infty \\ 0.96\, X^{\frac{3}{4}-\frac{1}{1.23}}, & X \to \infty\,. \end{cases} \tag{5.63}$$

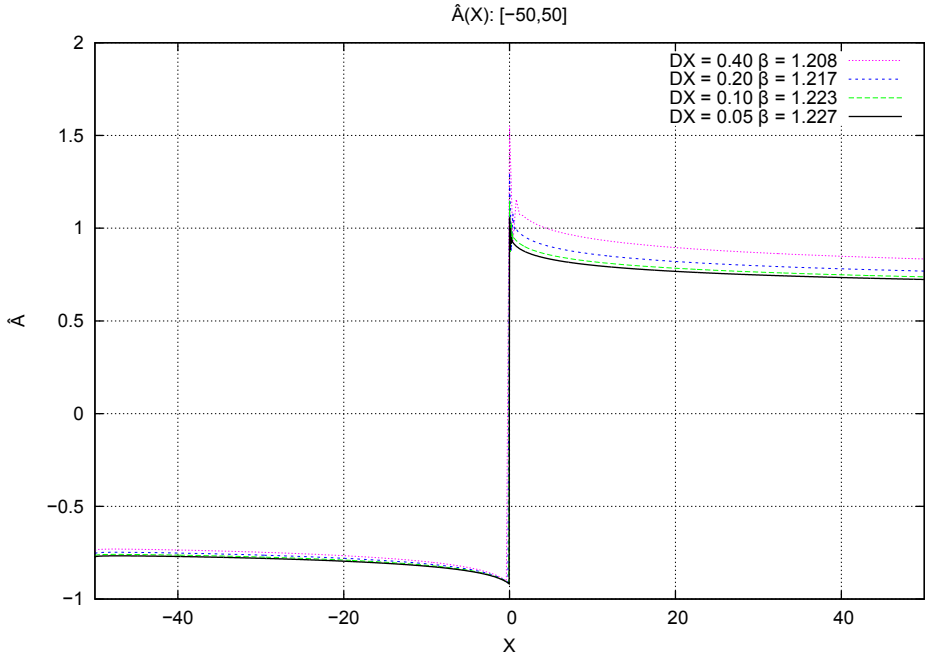

Figure 5.7: Numerical shooting method: $\hat{A}(X)$ for domain $X \in [-50, 50]$, by step size DX.

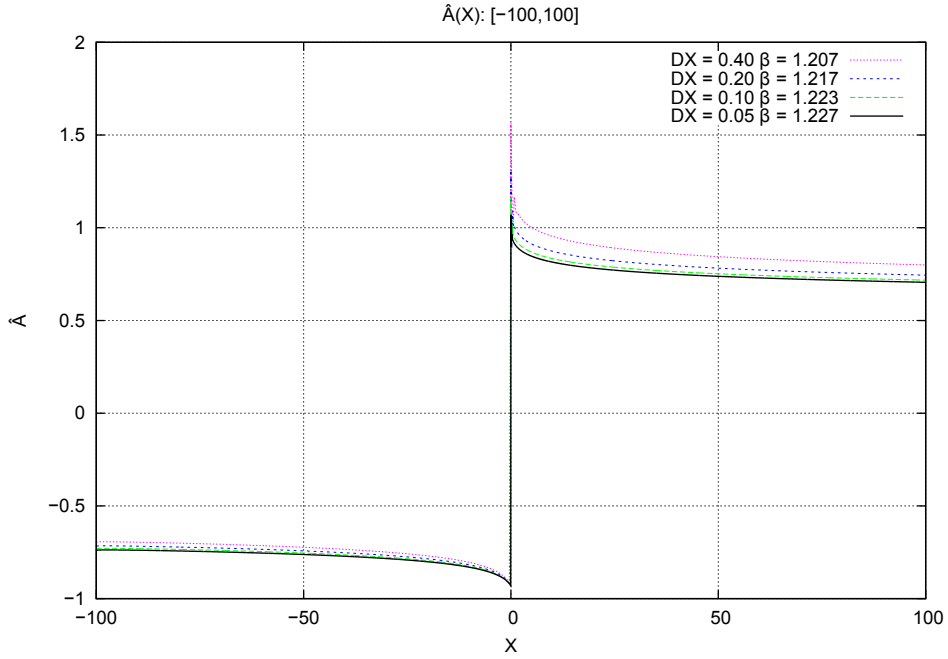

Figure 5.8: Numerical shooting method: $\hat{A}(X)$ for $X \in [-100, 100]$, by step size DX.

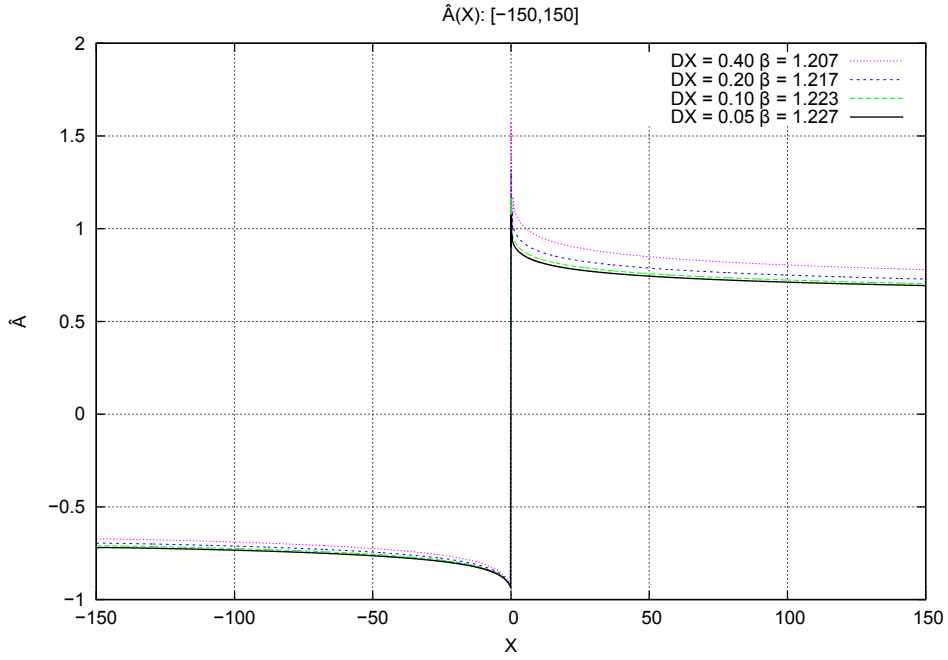

Figure 5.9: Numerical shooting method: $\hat{A}(X)$ for $X \in [-150, 150]$, by step size DX.

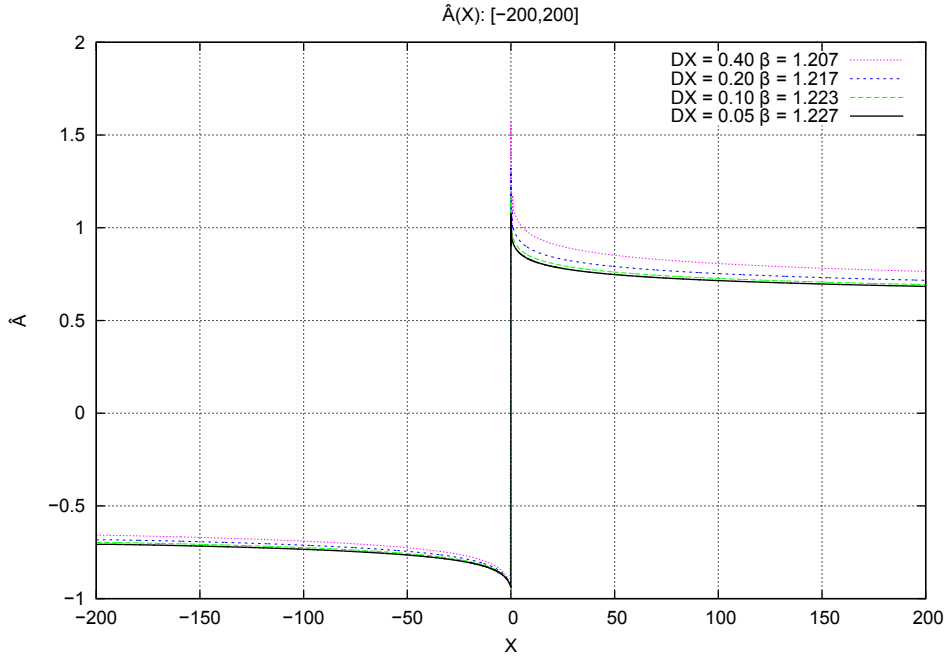

Figure 5.10: Numerical shooting method: $\hat{A}(X)$ for $X \in [-200, 200]$, by step size DX.

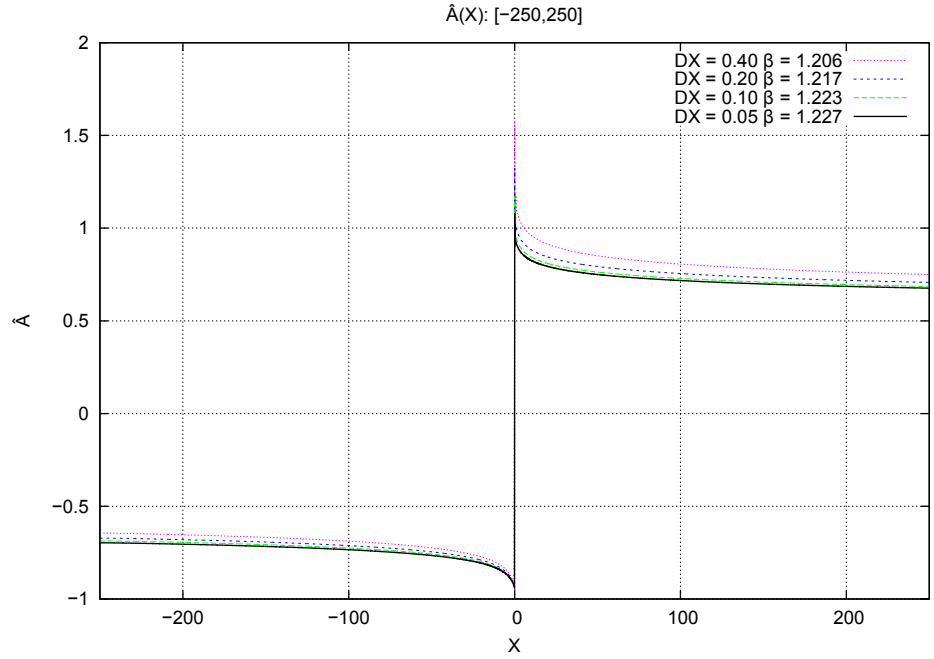

Figure 5.11: Numerical shooting method: $\hat{A}(X)$ for $X \in [-250, 250]$, by step size DX.

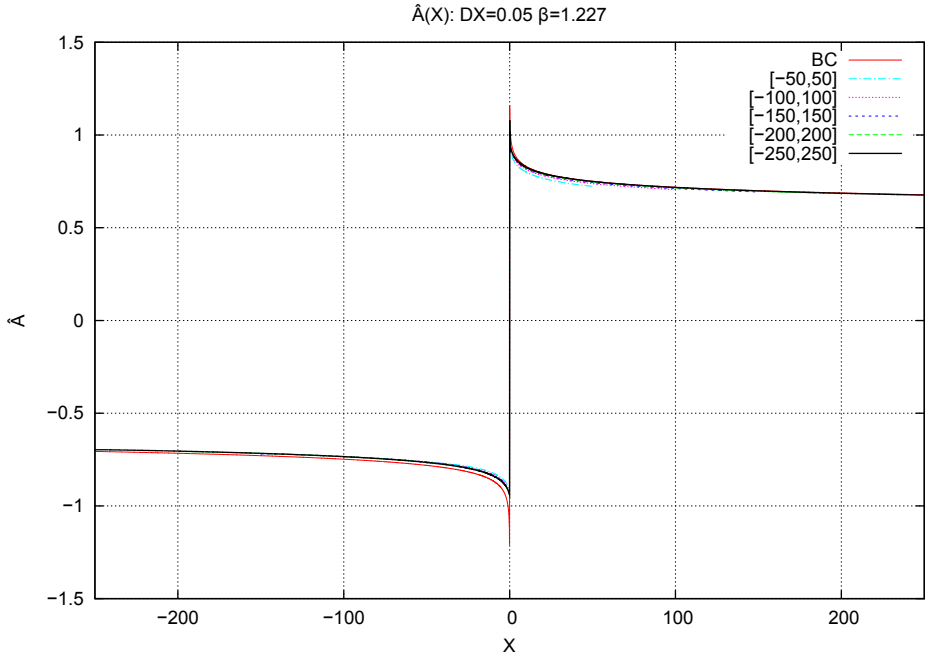

Figure 5.12: Numerical shooting method: $\hat{A}(X)$ and boundary condition BC (5.63) for step size DX = 0.05, boundary condition constant $\lambda_2 = 0.96$ and eigenvalue $\beta = 1.227$, by domain.

Numerical Shooting Method Test Summary

The test concludes that as the size of the domain increases towards infinity and the step size decreases towards zero then the $\hat{A}(X)$ solutions by the numerical shooting method, with the minimising function Φ (5.37), converge to the true solution as shown in Figure 5.12. The eigenvalue is $\beta = 1.23$ and the boundary value constant is $\lambda_2 = 0.96$ (both rounded up to 3 significant figures) such that the boundary condition (5.63) is:

$$\hat{A}(X) \sim \begin{cases} -|X|^{\frac{3}{4}-\frac{1}{1.23}}, & X \to -\infty \\ 0.96\, X^{\frac{3}{4}-\frac{1}{1.23}}, & X \to \infty\,. \end{cases}$$

However, the shooting method may only be accurate enough to give an initial distribution for Newton's method and not for the true solution. The Newton's method test follows in Section 5.3.2 and then a comparison of results from both methods is given in Section 5.3.4.

5.3.2 Newton's Method Test

Newton's method with the minimising function Φ (5.37) is tested based on the Newton's method test in Section 4.4 and is deemed to be working correctly if all the following conditions are met.

1. The error E (5.59) reduces quadratically towards zero with each iteration when the iterate is sufficiently close to the true solution but only if there is no interference from the minimising function driving the iterate solution towards the boundary condition at $X = X_{m+1}$ with each iteration. The initial value of $\beta^{(0)} = \beta^{(1)}$ is static with each iteration.

2. The boundary conditions (5.23):

$$\hat{A}(X) \sim \begin{cases} -|X|^{\frac{3}{4}-\frac{1}{\beta}}, & X = X_1 \\ \lambda_2 X^{\frac{3}{4}-\frac{1}{\beta}}, & X = X_{m+1} \end{cases}$$

   are satisfied. The constant λ_2 is to be found. Moreover, the solution must approach the boundary condition smoothly as $|X|$ becomes large such that the solution does not oscillate near the end points.

3. The $\hat{A}(X)$ solution converges to the true solution whilst the eigenvalue β and boundary value constant λ_2 converge to their respective true values as the size of domain increases towards infinity and the step size DX decreases towards zero. The test domains and step sizes are in Table 5.1.

4. The true $\hat{A}(X)$ solution, eigenvalue β and boundary value constant λ_2 are similar to their respective values from the numerical shooting method. A comparison of results is given in Section 5.3.4.

5.3.3 The Initial Conditions

There are three types of initial distribution $\hat{\mathbf{A}}^{(0)}$ and initial eigenvalue $\beta^{(0)}$ for testing Newton's method with the minimising function.

1. The first type of initial condition, which is named "IC00", is the corresponding $\hat{A}(X)$ solution and eigenvalue β of domain and step size given by the numerical shooting method, as described in Sections 5.2.2 and 5.3.1.

   For example, if using Newton's method in the domain $X \in [-50, 50]$ with step size $\mathrm{D}X = 0.4$ then the initial distribution $\hat{\mathbf{A}}^{(0)}$ is the $\hat{A}(X)$ solution by the shooting method also in the domain $X \in [-50, 50]$ with step size $\mathrm{D}X = 0.4$. The initial eigenvalue $\beta^{(0)} = 1.20$ is 3 significant figures of the corresponding result in Table 5.2.

2. The second type of initial distribution, which is named "IC01", is the corresponding $\hat{A}(X)$ distribution of step size and eigenvalue β by Smith & Elliott (1985), as given in Table 5.3.[6] The $\hat{A}(X)$ distribution is calculated by the numerical shooting method. However, the distribution may not satisfy the boundary condition as $X \to X_{m+1}$.

$\mathrm{D}X$	β
0.4	0.454
0.2	0.517
0.1	0.551
$\Delta X \to 0$	0.58

Table 5.3: Smith & Elliott (1985) step size $\mathrm{D}X$ and eigenvalue β results, for initial distribution IC01.

   For example, if using Newton's method in the domain $X \in [-50, 50]$ with step size $\mathrm{D}X = 0.4$ then the initial distribution $\hat{\mathbf{A}}^{(0)}$ is the $\hat{A}(X)$ solution by the shooting method also in the domain $X \in [-50, 50]$ with step size $\mathrm{D}X = 0.4$. The initial eigenvalue is $\beta^{(0)} = 0.454$, from Table 5.3.

3. The third type of initial distribution, which is named "IC1" (and is not to be confused with the test condition (4.21) in Section 4.3 or the initial conditon (4.25) for the $A(x, T)$ problem in Section 4.5), is like the Heaviside function. The boundary condition constant is normalised as $\lambda_2 = 1$. The initial distribution

[6] There is no description of computational domain by Smith & Elliott (1985) so the assumption is that the domain is large, like in Table 5.1.

is:

$$\hat{A}(X) \sim \begin{cases} -|X|^{\frac{3}{4}-\frac{1}{\beta}}, & X < 0\,, \\ 0\,, & X = 0\,, \\ X^{\frac{3}{4}-\frac{1}{\beta}}, & X > 0\,. \end{cases}$$

The initial eigenvalue $\beta^{(0)}$ is the corresponding value from initial condition IC00.

The following test results for error E, minimising function Φ, eigenvalue β, boundary condition constant λ_2, grid independence and boundary condition are for initial distribution IC00. The test results for initial distributions IC01 and IC1 are under "Newton's Method Test with Other Initial Distributions".

Test Results for Error E

The minimising function Φ is not utilised for the Newton's method error test and hence, whether the boundary condition at $X = X_{m+1}$ is satisfied or not is of less concern since the iterate solution is not driven towards it by Φ.

The error E (5.59) converges quadratically to zero for all domains and steps sizes. Therefore, Newton's method is working correctly. For example, in the smallest computational domain $X \in [-50, 50]$ with the largest step size $\mathrm{D}X = 0.4$, and thus $\beta^{(0)} = \beta^{(1)} = 1.20$ since the numerical shooting method gives $\beta = 1.208$ in Table 5.2, the error E does indeed converge quadratically to zero, as shown in Table 5.4. The exponents double with each iteration. By the third iteration, convergence is deemed to have occurred when tolerance (5.60) is reached.

iteration	error E
0	$1.2767404722 \times 10^{-2}$
1	1.8297082×10^{-5}
2	8.6×10^{-11}
3	$< 1 \times 10^{-12}$

Table 5.4: Newton's method without Φ: Errors E from IC00; $\beta^{(0)} = \beta^{(1)} = 1.20$; domain $X \in [-50, 50]$; and step size $\mathrm{D}X = 0.4$.

The Φ Effect on Error E

When the minimising function Φ (5.37) is utilised at each iteration of Newton's method to drive the iterate solution towards the boundary condition at $X = X_{m+1}$ then only slow, linear convergence is possible. Nevertheless, there is convergence for all domains and step sizes, even if there are hundreds of iterations, with the number of iterations to convergence increasing with the number of grid points.

Continuing with the example in domain $X \in [-50, 50]$ with step size $\mathrm{D}X = 0.4$ (such that there are 401 grid points), there are 255 iterations to convergence when starting from eigenvalue $\beta^{(0)} = 1.20$. (See Table 5.5.) In the domain $X \in [-250, 250]$ with step size $\mathrm{D}X = 0.05$ (such that there are 10001 grid points), there are 978 iterations to convergence when starting from $\beta^{(0)} = 1.22$. (See Table 5.6.)

iteration	error E
0	$1.2767403107 \times 10^{-2}$
1	$9.52675141 \times 10^{-4}$
2	$8.78172024 \times 10^{-4}$
$\vdots$	
254	1×10^{-12}
255	1×10^{-12}

Table 5.5: Newton's method with Φ: Errors E from IC00; $\beta^{(0)} = 1.20$; domain $X \in [-50, 50]$; step size $\mathrm{D}X = 0.4$.

iteration	error E
0	$1.5866593310 \times 10^{-2}$
1	$2.82110816 \times 10^{-4}$
2	$2.85409628 \times 10^{-4}$
$\vdots$	
977	1×10^{-12}
978	$< 1 \times 10^{-12}$

Table 5.6: Newton's method with Φ: Errors E from IC00; $\beta^{(0)} = 1.22$; domain $X \in [-250, 250]$; step size $\mathrm{D}X = 0.05$.

Test Results for Eigenvalue β & Boundary Condition Constant λ_2

With each iteration k of Newton's method with minimising function Φ (5.37), the eigenvalue and boundary value constant iterates, $\beta^{(k)}$ and $\lambda_2^{(k)}$, advance to constant values.

For example, in domain $X \in [-50, 50]$ with step size $\mathrm{D}X = 0.4$, the eigenvalue $\beta^{(k)} \to 1.20$ and the boundary value constant $\lambda_2^{(k)} \to 1.31$ (both written to 3 significant figures). (See Table 5.7 and also Table 5.8.)

Nevertheless, as the domain is extended towards infinity and step size $\mathrm{D}X$ decreases towards zero, the eigenvalue $\beta \to 1.23$ and the boundary value constant $\lambda_2 \to 0.96$ (rounded up to 3 significant figures, because of Figures 5.13, 5.14). (See Table 5.8.)

iteration k	$\beta^{(k)}$	$\lambda_2^{(k)}$
0	1.20	1.137820459891
1	1.200604177534	1.137273048410
2	1.201154885959	1.136788161797
⋮		
254	1.207695325765	1.131091713121
255	1.207695325765	1.131091713121

Table 5.7: Newton's method with Φ: Eigenvalue $\beta^{(k)}$ and boundary value constant $\lambda_2^{(k)}$ at iterations k from IC00; domain $X \in [-50, 50]$; step size $\mathrm{D}X = 0.4$.

DX	domain	β	λ_2
0.4	$[-50, 50]$	1.207	1.131
	$[-100, 100]$	1.207	1.147
	$[-150, 150]$	1.206	1.154
	$[-200, 200]$	1.206	1.159
	$[-250, 250]$	1.206	1.160
0.2	$[-50, 50]$	1.216	1.017
	$[-100, 100]$		1.035
	$[-150, 150]$		1.043
	$[-200, 200]$		1.047
	$[-250, 250]$		1.050
0.1	$[-50, 50]$	1.223	0.960
	$[-100, 100]$		0.979
	$[-150, 150]$		0.987
	$[-200, 200]$		0.992
	$[-250, 250]$		0.995
0.05	$[-50, 50]$	1.226	0.932
	$[-100, 100]$		0.952
	$[-150, 150]$		0.960
	$[-200, 200]$		0.964
	$[-250, 250]$		0.967

Table 5.8: Newton's method with Φ: Eigenvalue β and boundary value constant λ_2 (written to 4 significant figures) from IC00, by domain and step size DX.

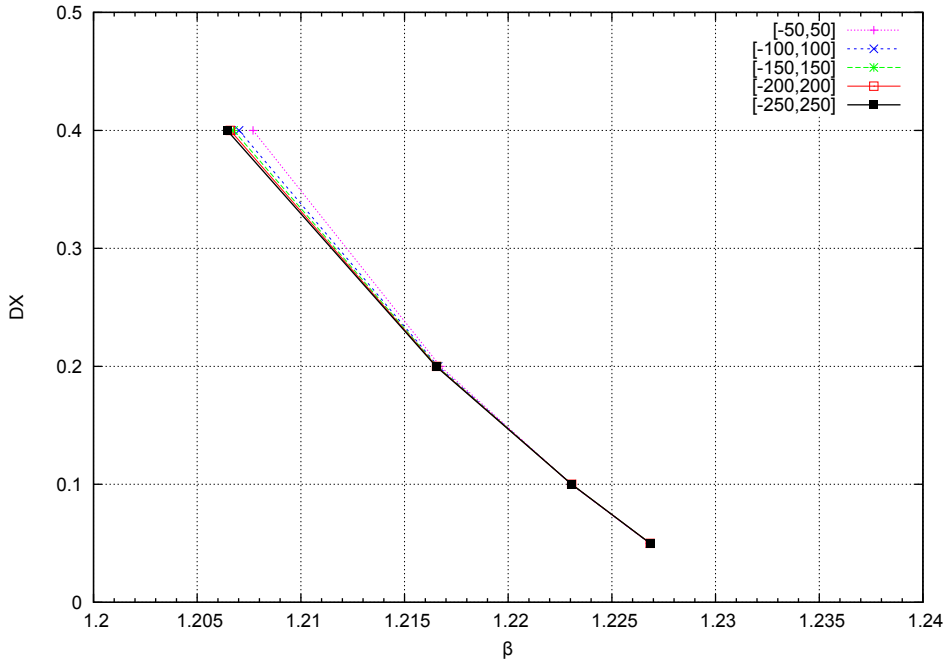

Figure 5.13: Newton's method with Φ: Eigenvalue β versus step size DX from IC00, by domain.

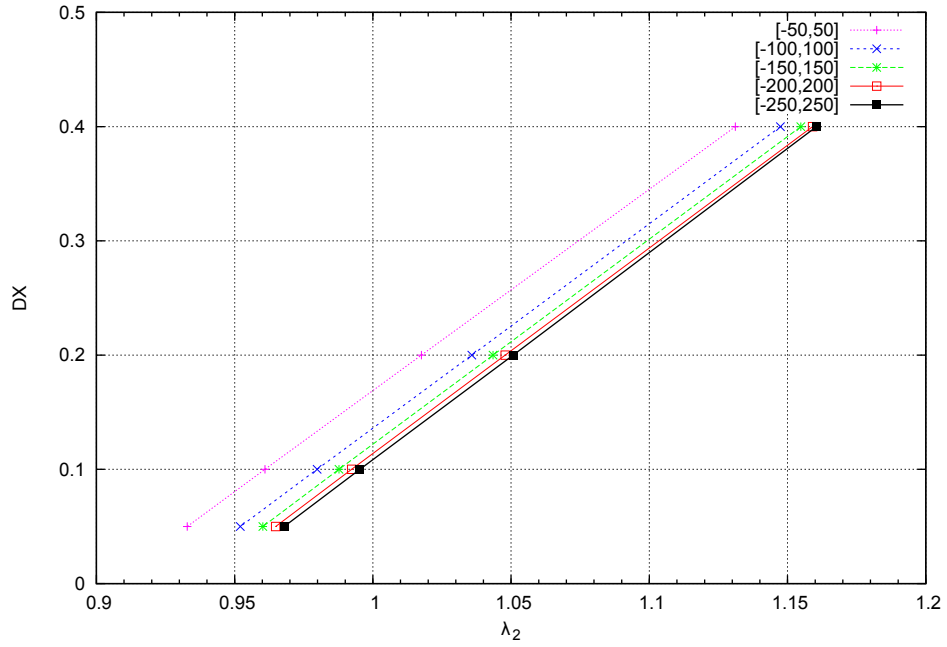

Figure 5.14: Newton's method with Φ: Boundary value constant λ_2 versus step size DX from IC00, by domain.

Test Results for Grid Independence

The $\hat{A}(X)$ solutions are grid dependent but converge to the true solution as the domain is extended towards infinity and as step size DX decreases towards zero, especially when $\beta \to 1.23$ with $\lambda_2 \to 0.96$. (See Figures 5.15 to 5.20.)

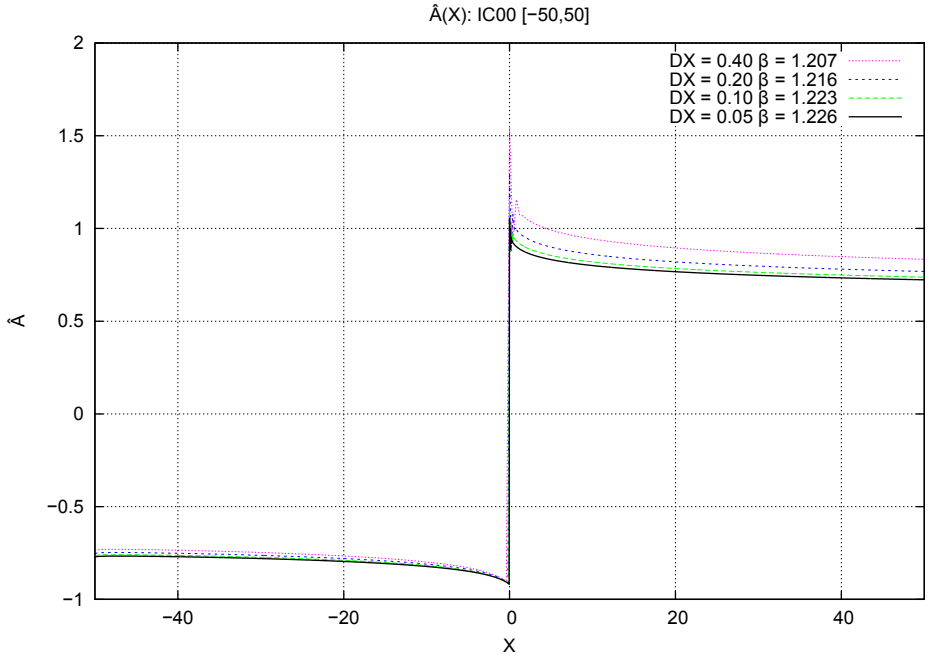

Figure 5.15: Newton's method with Φ: $\hat{A}(X)$ for IC00; domain $X \in [-50, 50]$; step sizes DX = 0.40, 0.20, 0.10, 0.05 and respective eigenvalues β = 1.207, 1.216, 1.223, 1.226.

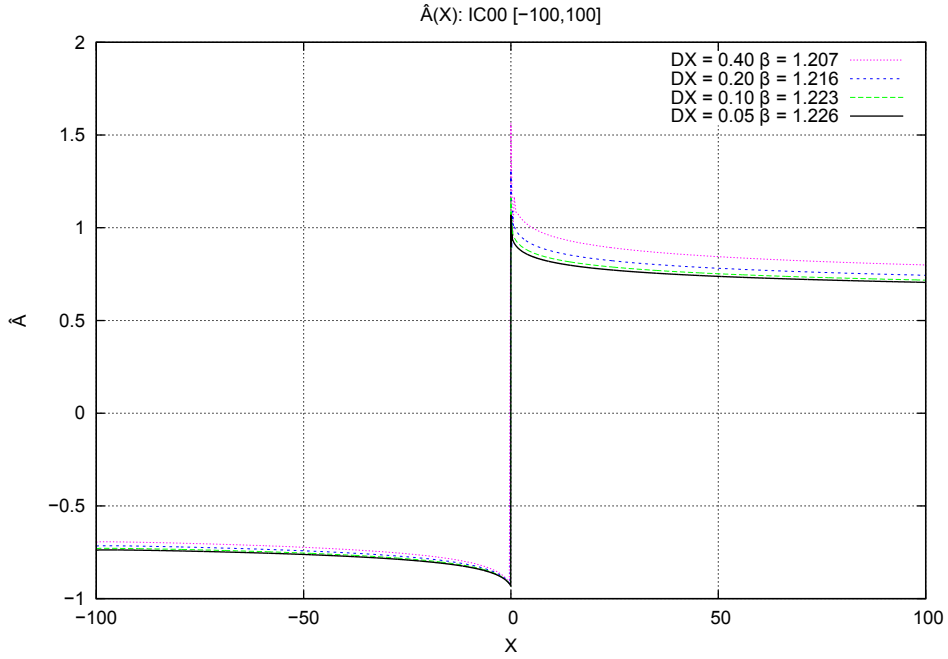

Figure 5.16: Newton's method with Φ: $\hat{A}(X)$ for IC00; $X \in [-100, 100]$; DX = 0.40, 0.20, 0.10, 0.05 and respective $\beta = 1.207, 1.216, 1.223, 1.226$.

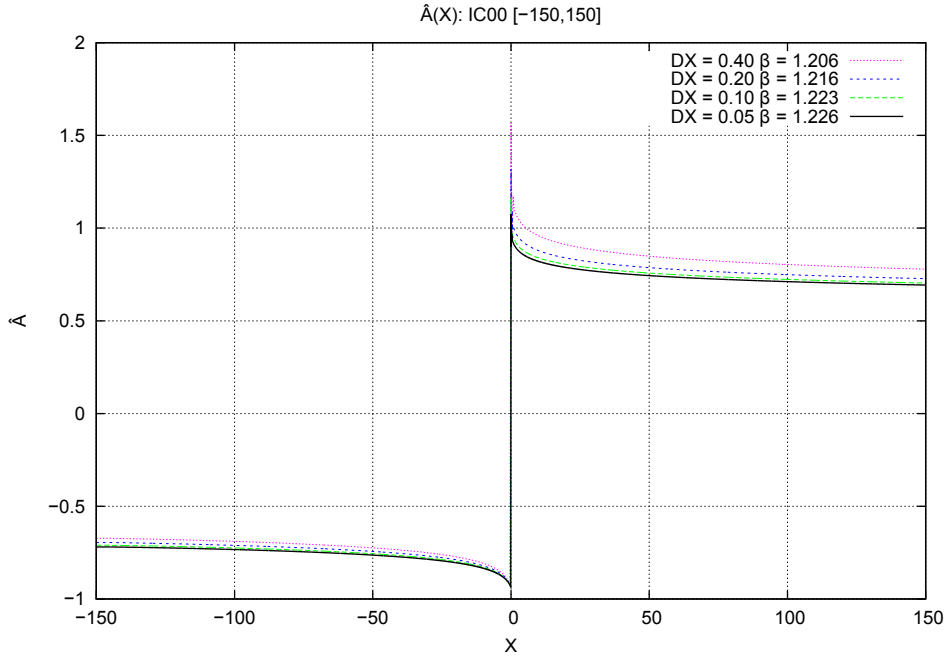

Figure 5.17: Newton's method with Φ: $\hat{A}(X)$ for IC00; $X \in [-150, 150]$; DX = 0.40, 0.20, 0.10, 0.05 and respective $\beta = 1.206, 1.216, 1.223, 1.226$.

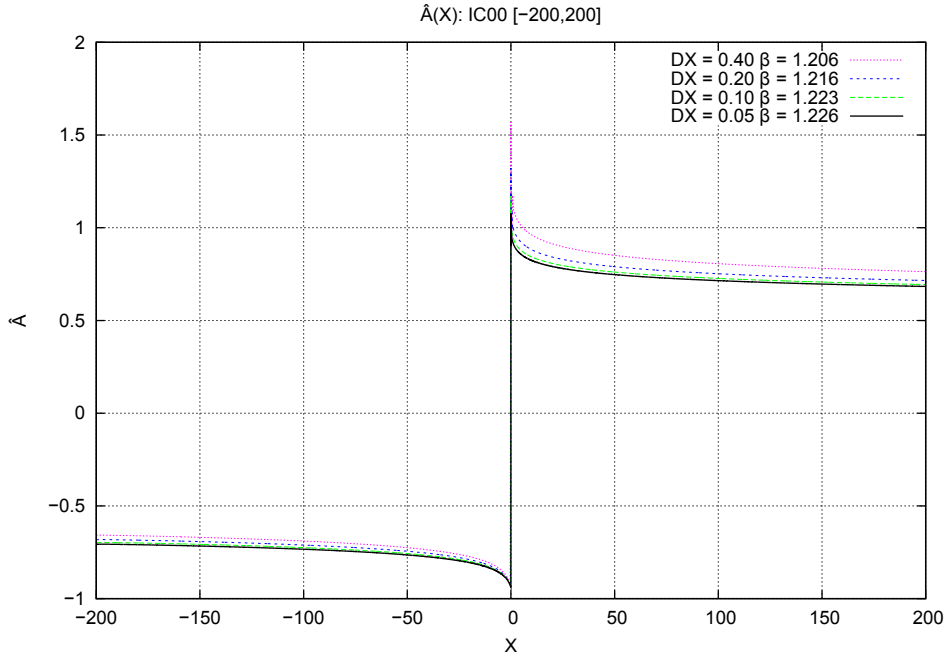

Figure 5.18: Newton's method with Φ: $\hat{A}(X)$ for IC00; $X \in [-200, 200]$; DX = 0.40, 0.20, 0.10, 0.05 and respective $\beta = 1.206, 1.216, 1.223, 1.226$.

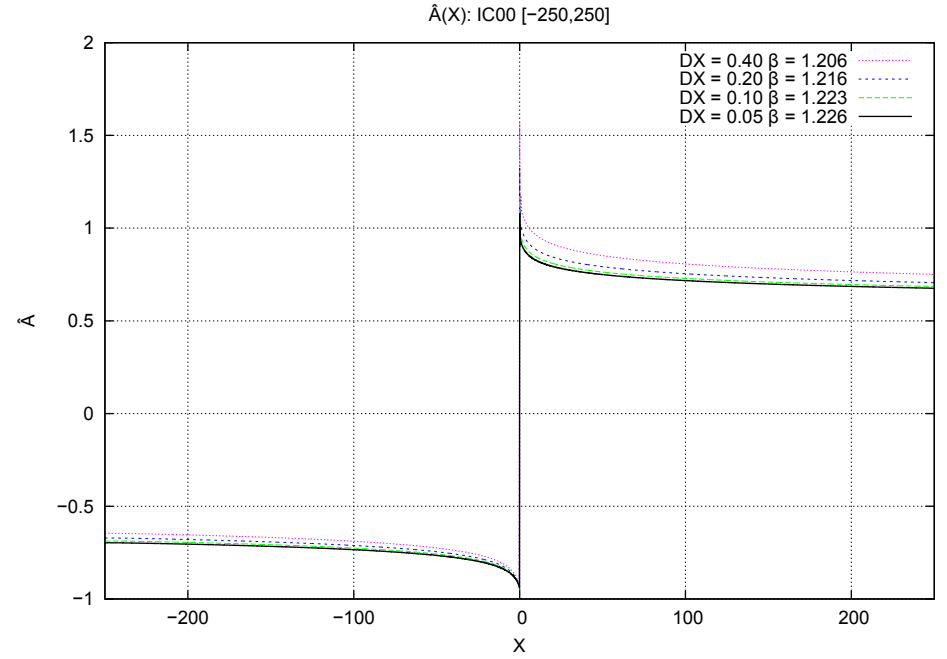

Figure 5.19: Newton's method with Φ: $\hat{A}(X)$ for IC00; $X \in [-250, 250]$; DX = 0.40, 0.20, 0.10, 0.05 and respective $\beta = 1.206, 1.216, 1.223, 1.226$.

Test Results for Boundary Conditions

The $\hat{A}(X)$ solutions for all domains and step size D$X = 0.05$ satisfy the boundary conditions (5.63) for $\beta = 1.23$ and $\lambda_2 = 0.96$ (from the previous tests):

$$\hat{A}(X) \sim \begin{cases} -|X|^{\frac{3}{4}-\frac{1}{1.23}}, & X \to -\infty \\ 0.96\, X^{\frac{3}{4}-\frac{1}{1.23}}, & X \to \infty \end{cases}$$

as shown in Figure 5.20. The minimising function Φ (5.37) converges to zero which indicates that the boundary condition at $X = X_{m+1}$ is satisfied. This is shown for example, for domain $X \in [-50, 50]$, step size D$X = 0.05$ and eigenvalue $\beta = 1.226$, in Table 5.9.

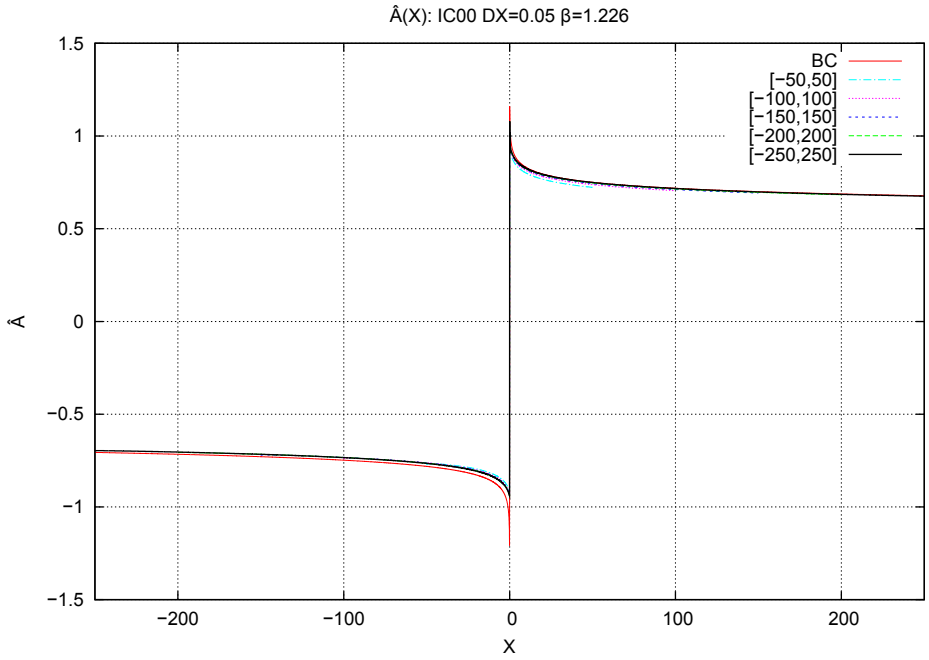

Figure 5.20: Newton's method with Φ $\hat{A}(X)$ and boundary condition BC (5.63) from IC00; step size D$X = 0.05$; and eigenvalue $\beta = 1.226$, by domain.

Newton's Method Test with Other Initial Distributions

When using the second type of initial distribution IC01 with initial eigenvalues $\beta^{(0)} =$ 1.20, 1.21, 1.22, 1.22 for respective step sizes D$X = 0.4$, 0.2, 0.1, 0.05 from Table 5.8, the $\hat{A}(X)$ functions do not converge to a solution with increase in the size of domain

iteration	Φ
0	5.822488×10^{-6}
1	5.378955×10^{-6}
2	5.041613×10^{-6}
⋮	
312	$< 1 \times 10^{-12}$
313	$< 1 \times 10^{-12}$

Table 5.9: Newton's method with Φ: Minimising function Φ from IC00; domain $X \in [-50, 50]$; step size D$X = 0.05$.

or decrease in step size, as shown for example domain $X \in [-50, 50]$ in Figure 5.21. The initial distribution IC01 is based on the work by Smith & Elliott (1985) which implies that the eigenvalue $\beta \to 0.58$ as step size D$X \to 0$, as shown in Table 5.3. However, the $\hat{A}(X)$ functions do not converge to a solution with reduction in step size, as shown for example domain $X \in [-50, 50]$ in Figure 5.22. Hence, the true $\hat{A}(X)$ solution cannot be found with the second type of distribution IC01.

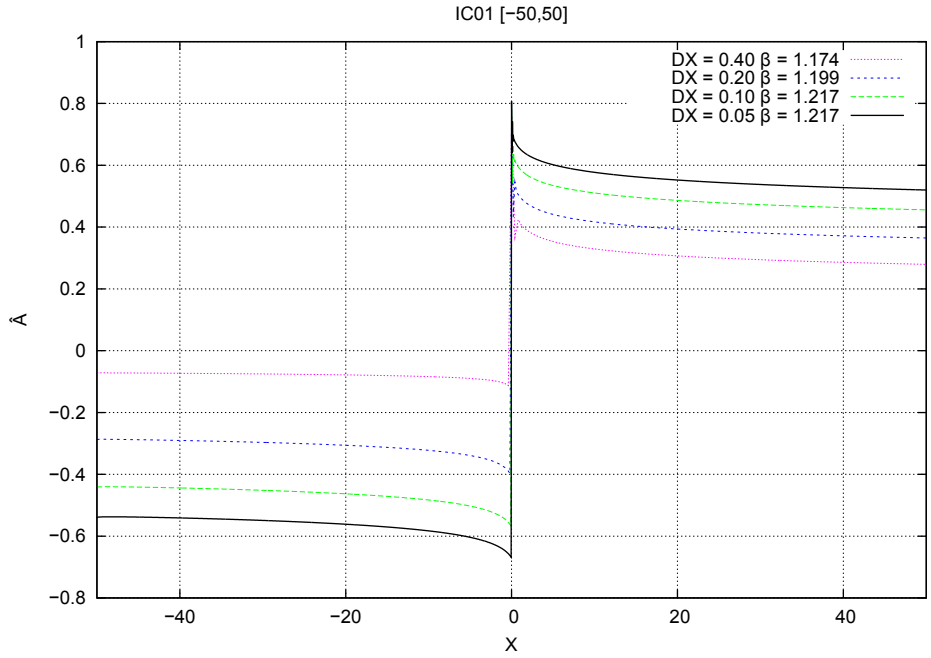

Figure 5.21: Newton's method with Φ: Functions $\hat{A}(X)$ for IC01; $X \in [-50, 50]$; D$X = 0.4$, 0.2, 0.1, 0.05 and respective $\beta^{(0)} = 1.20$, 1.21, 1.22, 1, 22.

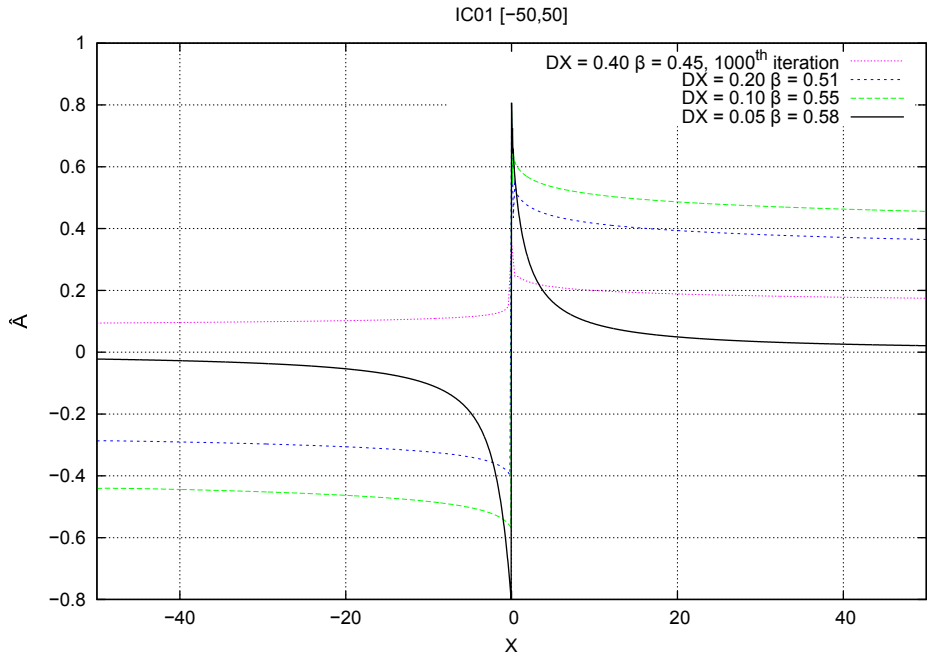

Figure 5.22: Newton's method with Φ: Functions $\hat{A}(X)$ for IC01; $X \in [-50, 50]$; D$X = 0.4$, 0.2, 0.1, 0.05 and respective $\beta^{(0)} = 0.45$, 0.51, 0.55, 0.58.

If using the third type of initial distribution IC1 then continuing with the example case for the domain $X \in [-50, 50]$, there is no convergence after 1000 iterations. Convergence seems unlikely given that the $\hat{A}^{(1000)}$ function has no resemblance to a discontinuous function that is expected. (See Figure 5.23.) Hence, the true $\hat{A}(X)$ solution cannot be found with the third type of distribution IC1.

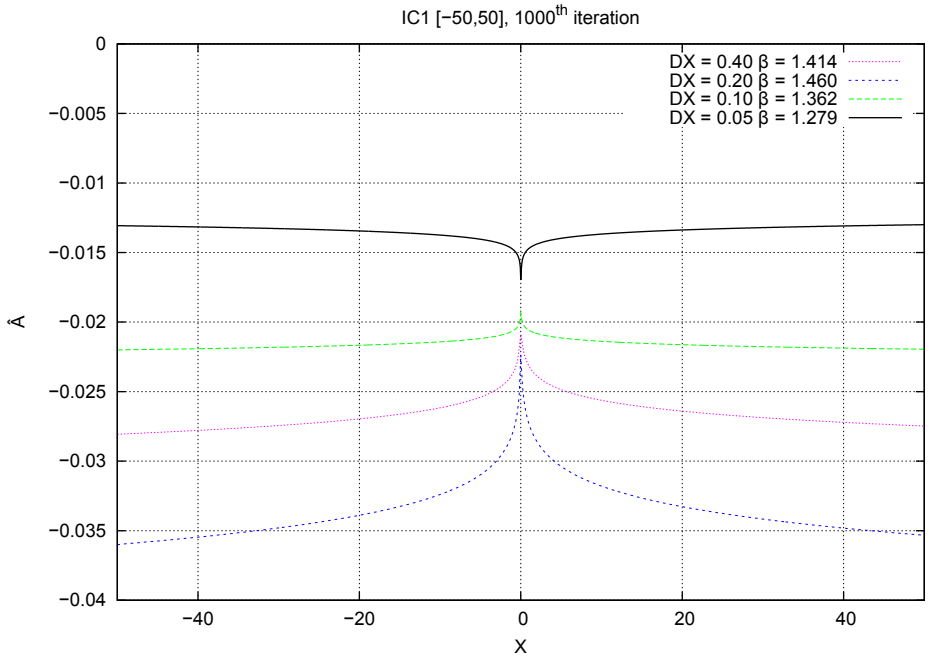

Figure 5.23: Newton's method with Φ: Functions $\hat{A}(X)^{(1000)}$ for IC1; $X \in [-50, 50]$; D$X = 0.4$, 0.2, 0.1, 0.05 and respective $\beta^{(0)} = 1.20$, 1.21, 1.22, $1, 22$.

Therefore, only the first type of initial distribution IC00 gives the true $\hat{A}(X)$ solution; eigenvalue β and boundary value constant λ_2.

5.3.4 Comparison of the Shooting Method & Newton's Method with Φ

The results from the numerical shooting method (denoted "S") in Section 5.3.1 and those from Newton's method with minimising function Φ (denoted "N") in Section 5.3.2, for the $\hat{A}(X)$ solution, eigenvalue β and boundary value constant λ_2 agree. The methods give the true eigenvalue $\beta \to 1.23$ and the boundary condition constant $\lambda_2 \to 0.96$ (both rounded up to 3 significant figures) as the domain increases towards infinity and step size DX decreases towards zero. (See Table 5.10 and Figures 5.24, 5.25.)

		Shooting (S)		Newton's (N)	
DX	domain	β	λ_2	β	λ_2
0.4	$[-50, 50]$	1.208	1.130	1.207	1.131
	$[-100, 100]$	1.207	1.147	1.207	1.147
	$[-150, 150]$	1.207	1.154	1.206	1.154
	$[-200, 200]$	1.207	1.158	1.206	1.159
	$[-250, 250]$	1.206	1.160	1.206	1.160
0.2	$[-50, 50]$		1.017		1.017
	$[-100, 100]$		1.035		1.035
	$[-150, 150]$	1.217	1.043	1.216	1.043
	$[-200, 200]$		1.047		1.047
	$[-250, 250]$		1.050		1.050
0.1	$[-50, 50]$		0.960		0.960
	$[-100, 100]$		0.979		0.979
	$[-150, 150]$	1.223	0.987	1.223	0.987
	$[-200, 200]$		0.992		0.992
	$[-250, 250]$		0.995		0.995
0.05	$[-50, 50]$		0.932		0.932
	$[-100, 100]$		0.952		0.952
	$[-150, 150]$	1.227	0.960	1.226	0.960
	$[-200, 200]$		0.964		0.964
	$[-250, 250]$		0.967		0.967

Table 5.10: Shooting method (S) and Newton's method with Φ (N): Eigenvalue β and boundary value constant λ_2 (written to 4 significant figures), by step size DX and domain.

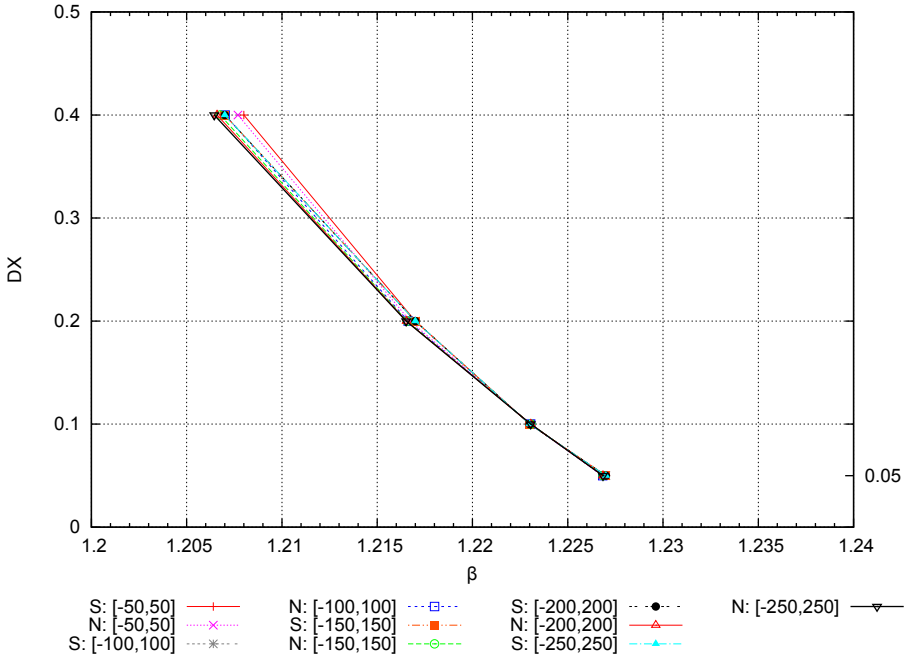

Figure 5.24: Eigenvalue β versus step size DX by shooting method (S) and Newton's method with Φ (N) from IC00, by domain.

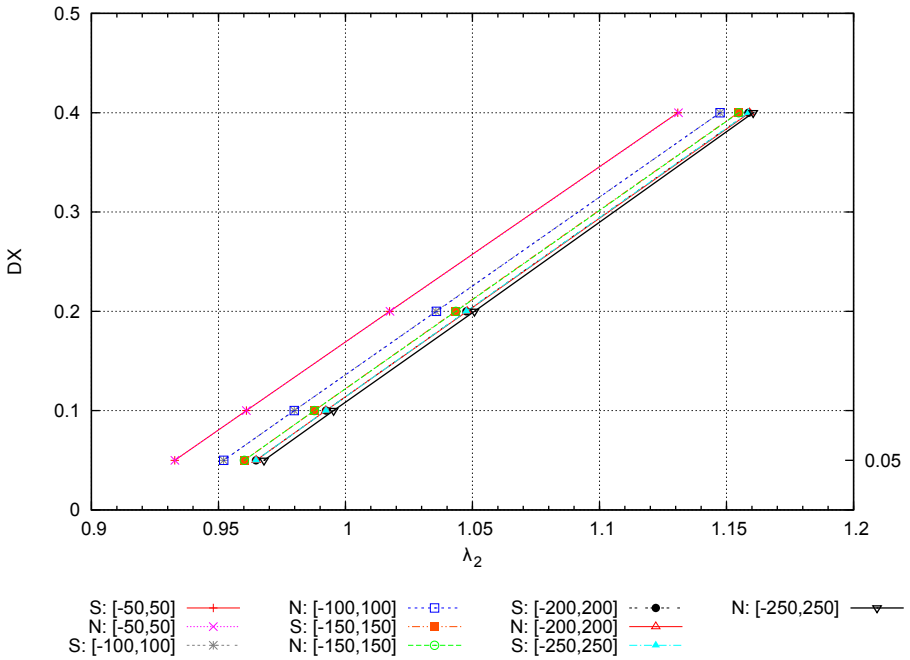

Figure 5.25: Boundary value constant λ_2 versus eigenvalue β by shooting method (S) and Newton's method with Φ (N) from IC00, by domain.

Additionally, the methods give consistent results for the $\hat{A}(X)$ solution as the domain increases towards infinity and step size DX decreases towards zero. (See Figures 5.26 to 5.30.)

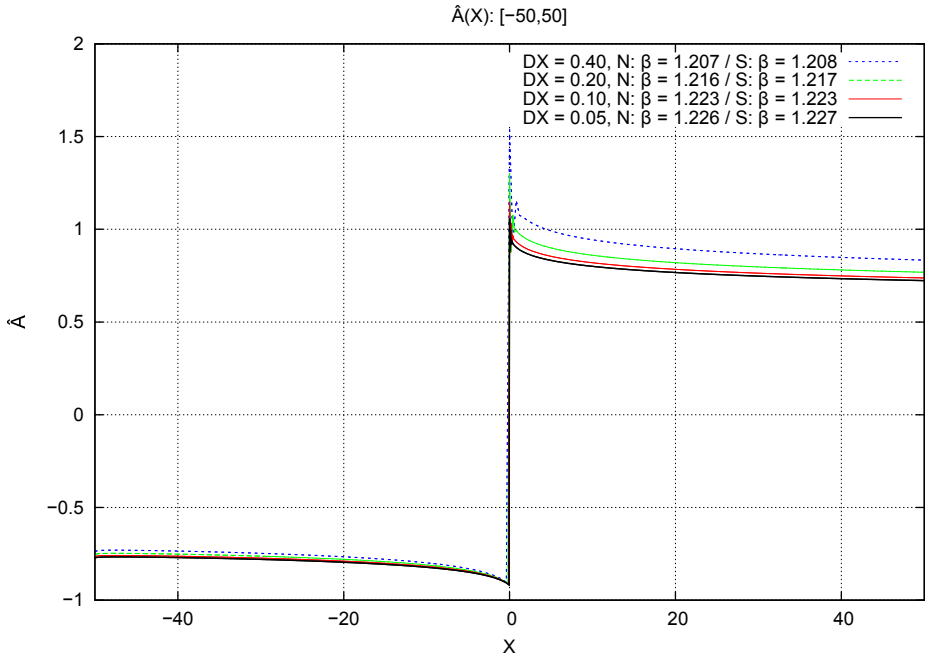

Figure 5.26: $\hat{A}(X)$ by shooting method (S) and Newton's method with Φ (N) from IC00; $X \in [-50, 50]$, by step size DX and eigenvalue β.

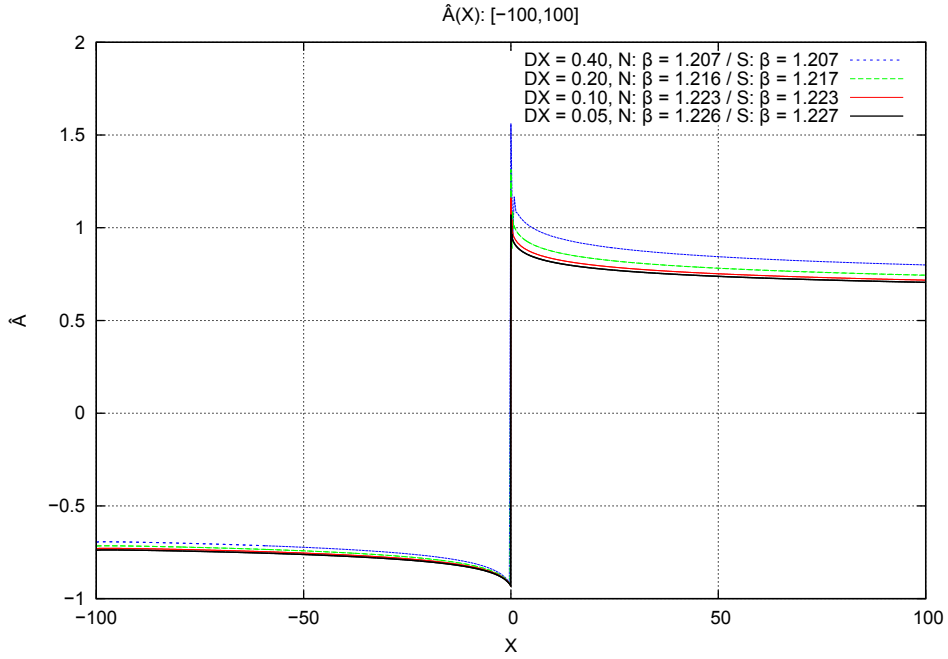

Figure 5.27: $\hat{A}(X)$ by shooting method (S) and Newton's method with Φ (N) from IC00; $X \in [-100, 100]$, by step size DX and eigenvalue β.

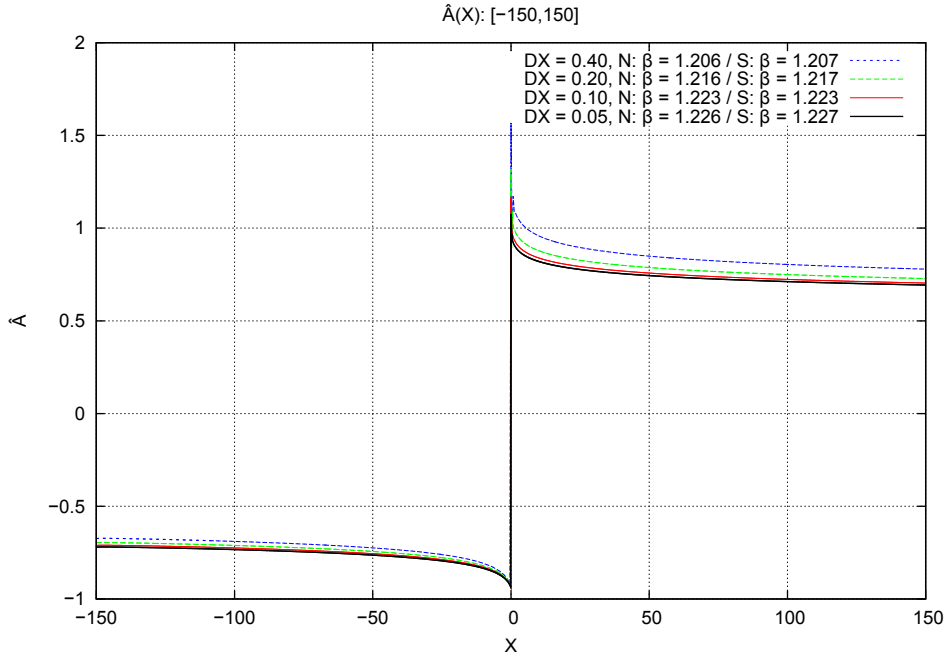

Figure 5.28: $\hat{A}(X)$ by shooting method (S) and Newton's method with Φ (N) from IC00; $X \in [-150, 150]$, by step size DX and eigenvalue β.

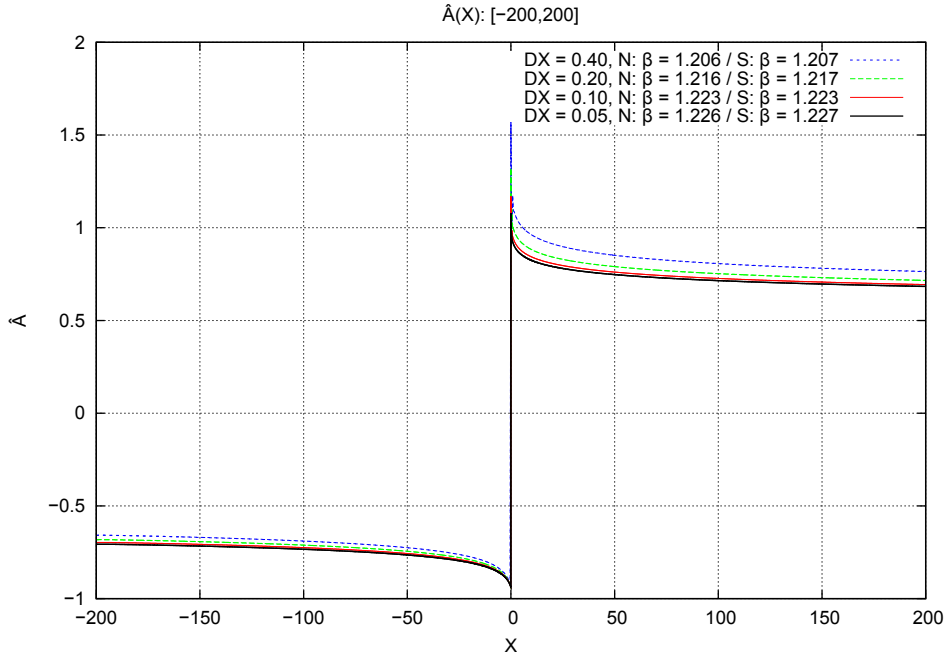

Figure 5.29: $\hat{A}(X)$ by shooting method (S) and Newton's method (N) from IC00; $X \in [-200, 200]$, by step size DX and eigenvalue β.

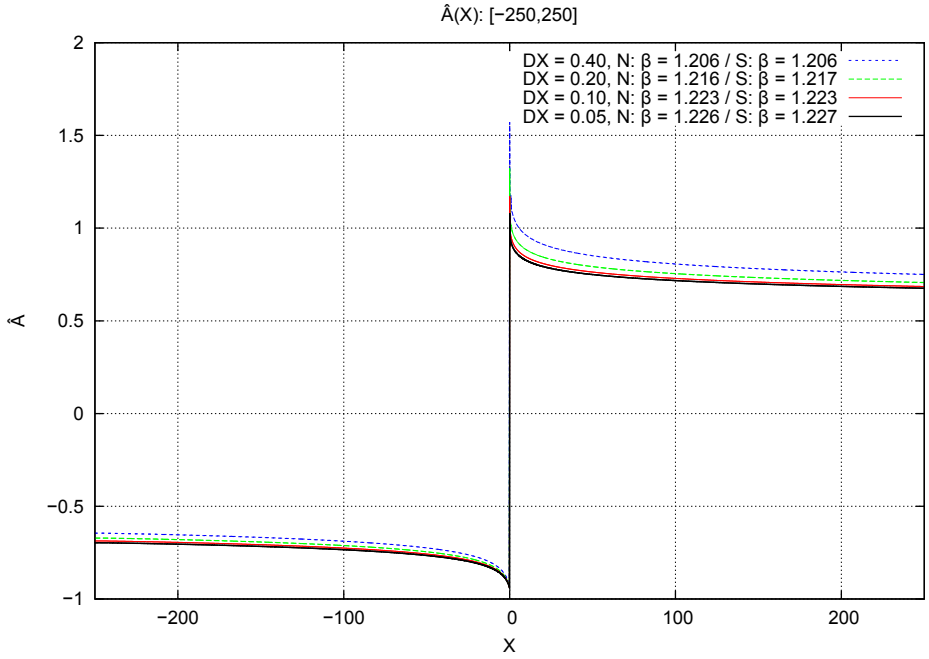

Figure 5.30: $\hat{A}(X)$ by shooting method (S) and Newton's method with Φ (N) from IC00; $X \in [-250, 250]$, by step size DX and eigenvalue β.

On the other hand, the methods do not reproduce results from Smith & Elliott (1985) even when using parameters from Table 5.3, as shown when comparing any solution with the Figure 5.31 from Smith & Elliott (1985). One reason is that the shooting method and Newton's method with minimising function Φ happen to find another true $\hat{A}(X)$ solution as eigenvalue $\beta \to 1.23$ and $\lambda_2 \to 0.96$.

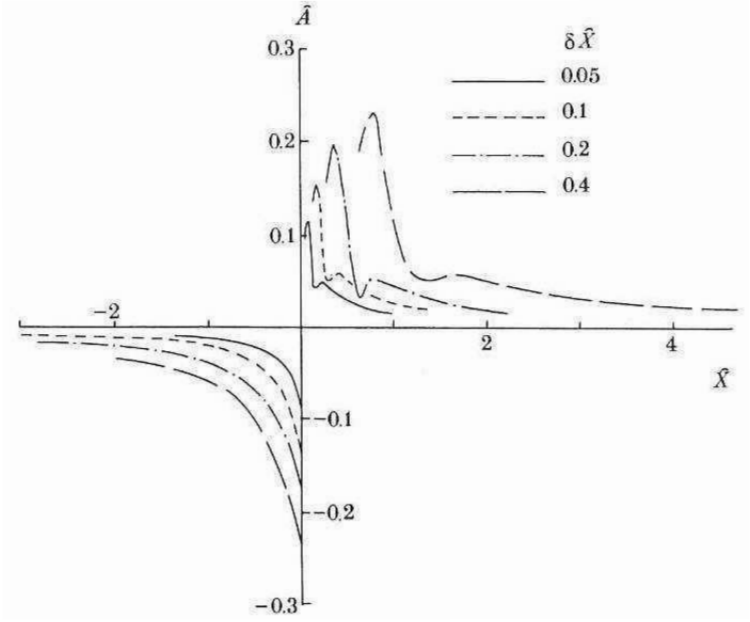

Figure 5.31: Smith & Elliott (1985), Figure 3, p. 18: "Numerical solutions... showing the shock-like (abrupt reattachment) trend near the origin."

5.4 Second Interactive Stage Solutions

The true eigenvalue $\beta \to 1.23$ and the boundary value constant $\lambda_2 \to 0.96$. Hence, the point of zero skin friction $x = x_s$ and the second interactive region X, behave like

$$x = X_s + (T_s - T)^{1.23} X\,, \quad X_s = x_s + C(T_s - T)^{\alpha}\,, \quad 0 < \alpha \leq 1.23\,; \tag{5.64}$$

whilst the first interactive stage skin friction $A(x,T)$ (5.6) and the second interactive stage $\hat{A}(X)$ analogy, behave like

$$A(x,T) = (T_s - T)^{-0.0775} \hat{A}(X) + \ldots \qquad \hat{A}(X) = O(1)\,, \tag{5.65}$$

as the singularity at $X = X_s$, $T = T_s$ is approached during nonlinear breakdown. The boundary condition (5.23) of the second interactive region, to match with the first interactive stage interaction region, is

$$\hat{A}(X) \sim \begin{cases} -|X|^{-0.063}, & X \to -\infty \\ 0.96X^{-0.063}, & X \to \infty\,. \end{cases}$$

The $\hat{A}(X)$ solution to the second interactive stage equation (5.21):

$$\hat{A}^2(X) = -\int_{-\infty}^{X} \left[0.0775\hat{A}(\xi) + 1.23\xi\frac{\mathrm{d}\hat{A}}{\mathrm{d}\xi}(\xi)\right] \frac{\mathrm{d}\xi}{(X-\xi)^{\frac{1}{4}}}$$

exhibits a shock or discontinuity. There is an abrupt jump from a negative value $\hat{A}(X \simeq -1)$ to its modulus $\hat{A}(X \simeq +1)$ within a small number of grid points.[7] Elsewhere, the numerical results show the existence of a smooth form of $\hat{A}(X)$ whenever $X \neq 0$. (See Figures 5.33a to 5.33c.)

Recall that the $\hat{A}(X)$ solution describes the three fluid flow configurations when the point of zero skin friction is either fixed; is travelling at a slower rate than the decay of the second interactive region; or is travelling at the same rate as the decay of the second interactive region. Furthermore, the flow structure is simply shifted with the point of zero skin friction, as illustrated in Figure 5.32.

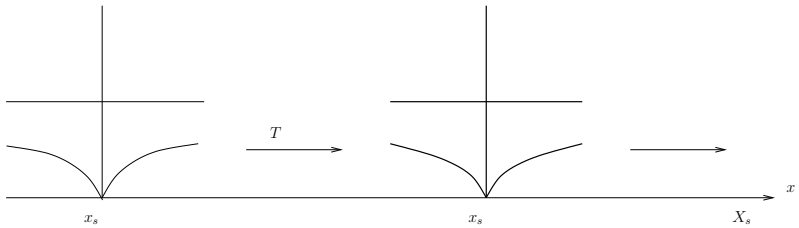

Figure 5.32: The point of zero skin friction $x = x_s$ and flow structure travelling towards the point of singularity $x = X_S$, when $0 < \alpha \leq 1.23$.

Therefore, the shock at the point of zero skin friction shows a point of detachment or abrupt reattachment of a bubble or reversed flow to the airfoil.[8] The skin friction,

[7] Further analytic support for the existence of a shock is given by Smith & Elliott (1985).
[8] Smith & Elliott (1985)

being negative for $X < 0$, shows forward attached flow; and being positive for $X > 0$, shows reversed flow in the closed bubble. The shock can either be stationary or travelling along the airfoil towards a point of singularity. Coinciding with the decay of the second interactive region is the increasing accentuation of the bubble which thickens the boundary layer. Eventually, the flow scale returns to that of the boundary layer as the bubble spans the entire layer. This is analysed in Chapter 6

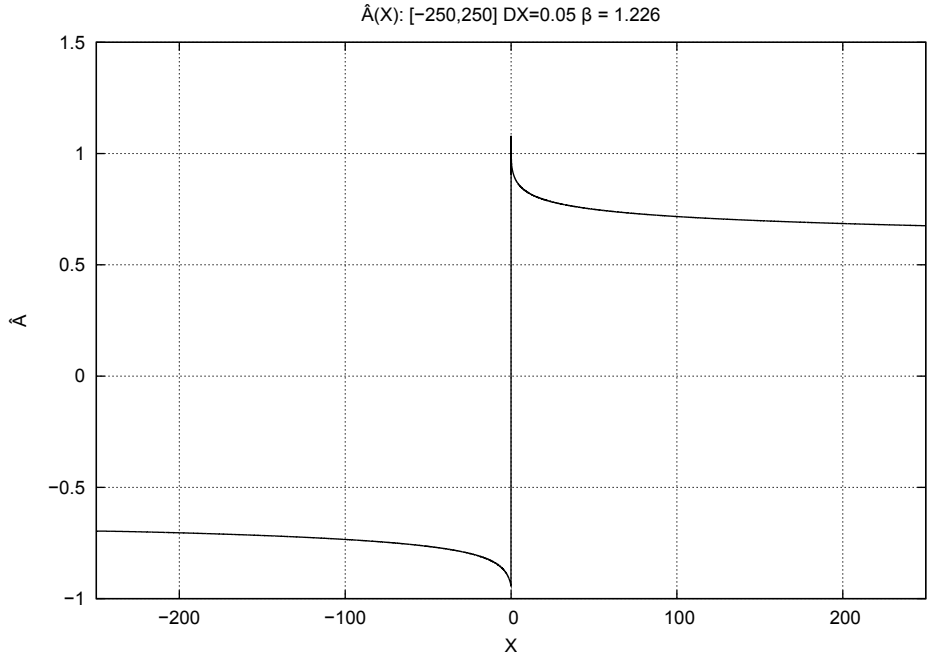

(a)

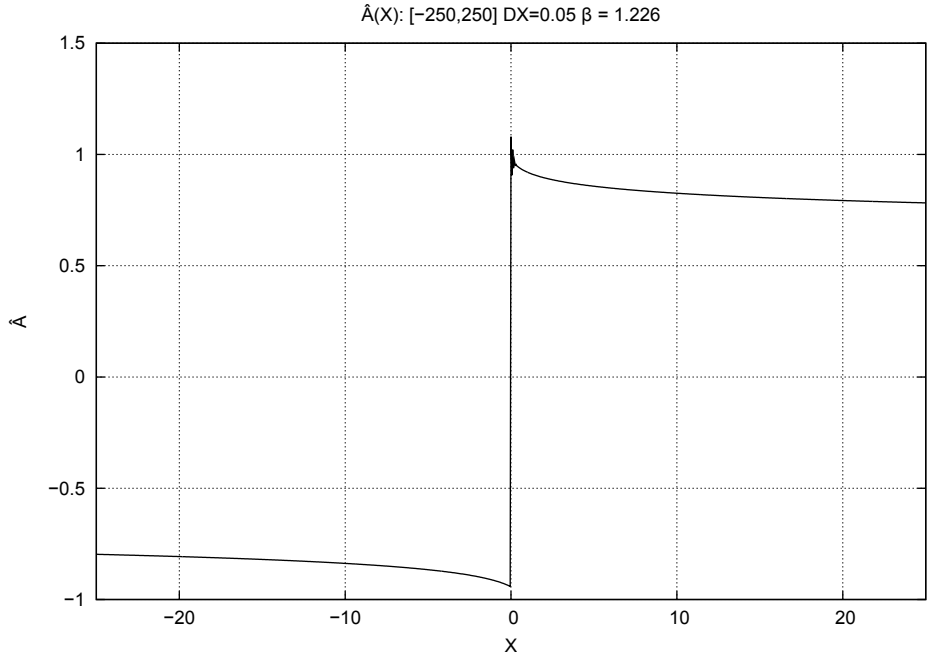

(b)

Figure 5.33: $\hat{A}(X)$ for domain $X \in [-250, 250]$, step size D$X = 0.05$; eigenvalue $\beta = 1.226$; boundary value constant $\lambda_2 = 0.96$, as shown in regions $X \in [-250, 250]$ and $X \in [-25, 25]$.

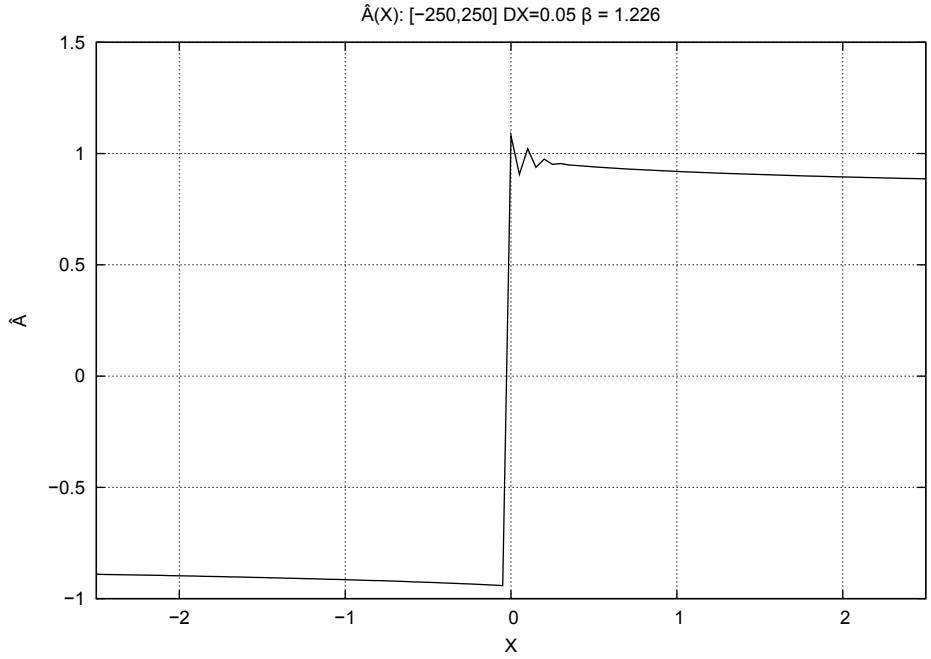

(c)

Figure 5.33: $\hat{A}(X)$, as shown in region $X \in [-2.5, 2.5]$. See Figures 7.7a and 7.7b.

The waning oscillations close to the discontinuity at $X = 0$, as shown closely in Figure 7.7c and seen in Smith & Elliott (1985) Figure 7.8, appear in all $\hat{A}(X)$ solutions from Newton's method with Φ, regardless of size of domain or grid. The oscillations are assumed to appear in Newton's method solutions because there is discontinuity at $X = 0$ and the second interactive stage equation being solved is nonlinear. On the other hand, the oscillations are dampened with increase in size of domain and decrease in step size, as shown for example in the sequence of Figures 5.26 to 5.30 in Section 5.3.4.

Chapter 6

Leading Edge Stall

The process of leading edge stall continues from the second interactive stage nonlinear breakdown (Chapter 5), where there is runaway growth of a bubble of reversed flow and discontinuous skin friction advancing towards a singularity. The induced pressure gradient (Section 3.1), that was made negligible in the interaction region by the slow perturbations to the airfoil on a large time scale T, exists in the unsteady interactive structure, regardless of the time scale on which the structure exists. Ultimately, the flow regime is that where time and length scales shorten to the scale of boundary layer thickness. The flow reaches a nonlinear Euler stage where the growth of the bubble spans the boundary layer. Evidence for the terminal flow is from analysis of the leading edge, starting with the boundary layer and its governing equations. The analysis follows from that of dynamic stall due to unsteady marginal separation by Elliott & Smith (1987), which has been adapted here.

6.1 The Unsteady Boundary Layer

The boundary layer has the normal coordinate (2.8):

$$Y = \mathrm{Re}^{\frac{1}{2}} y = O(1)\,, \tag{6.1}$$

stream function (2.10):

$$\Psi = \mathrm{Re}^{\frac{1}{2}}\psi = O(1)\,. \tag{6.2}$$

and similarity variable (2.19):

$$\eta = \frac{Y}{(-s)^{\frac{1}{4}}} = O(1) \Rightarrow Y = \left[(-s)^{\frac{1}{4}}\right] \tag{6.3}$$

where

$$s = x - x_s = O(1) \tag{6.4}$$

and $x = x_s$ is the point of zero skin friction. (Section 2.2)

The boundary layer is governed by the classical equations (1.4), (2.14) for traditional velocities u, v:

$$u = \frac{\partial \Psi}{\partial Y}\,, \qquad v = -\mathrm{Re}^{-\frac{1}{2}}\frac{\partial \Psi}{\partial x}\,; \tag{6.5}$$

$$\frac{1}{\sigma}\frac{\partial^2 \Psi}{\partial T \partial Y} + \frac{\partial \Psi}{\partial Y}\frac{\partial^2 \Psi}{\partial x \partial Y} - \frac{\partial \Psi}{\partial x}\frac{\partial^2 \Psi}{\partial Y^2} = \frac{\partial^3 \Psi}{\partial Y^3} - \frac{\partial p}{\partial x}\,.$$

The boundary layer equation (2.14), in terms of velocity u and external inviscid flow velocity $U_e(x,t)$, is

$$\frac{1}{\sigma}\frac{\partial u}{\partial T} + u\frac{\partial u}{\partial x} - \frac{\partial \Psi}{\partial x}\frac{\partial u}{\partial Y} = \frac{\partial^2 u}{\partial Y^2} + \frac{1}{\sigma}\frac{\partial U_e}{\partial T} + U_e\frac{\partial U_e}{\partial x}\,. \tag{6.6}$$

The unsteady Bernoulli's principle at the outer edge of the boundary layer requires that the pressure gradient and external inviscid flow velocity are related by

$$\frac{\partial p}{\partial x} = -\frac{1}{\sigma}\frac{\partial U_e}{\partial T} - U_e\frac{\partial U_e}{\partial x}\,.$$

The governing equations (6.5) and (6.6) are subject to the no-slip conditions:

$$u = \Psi = 0\,, \qquad Y = 0 \tag{6.7}$$

and the condition of matching with the external inviscid region:

$$\Psi \sim U_e(x,t)[Y-\delta^*]\,, \qquad u=\frac{\partial \Psi}{\partial Y} \to U_e(x,t)\,, \qquad Y\to\infty \tag{6.8}$$

where

$$\delta^* = \mathrm{Re}^{-\frac{1}{2}}\delta(x,t) \tag{6.9}$$

is the boundary layer displacement. Given a suitable initial condition, the problem (6.6), (6.7), (6.8) can be solved.

Length Scales

A nonlinear-unsteady-viscous balance of forces in the boundary layer equation (6.6) gives

$$u\frac{\partial u}{\partial x} \sim \frac{\partial p}{\partial x} \Rightarrow p = O(u^2)\,, \tag{6.10}$$

$$u\frac{\partial u}{\partial x} \sim \frac{\partial^2 u}{\partial Y^2} \Rightarrow u = O\left[\frac{(-s)}{Y^2}\right]\,, \tag{6.11}$$

$$\frac{1}{\sigma}\frac{\partial u}{\partial T} \sim \frac{\partial^2 u}{\partial Y^2} \Rightarrow Y = O\left[(\sigma T)^{\frac{1}{2}}\right]\,. \tag{6.12}$$

The boundary layer solution of (6.6) has a well-known tangential velocity profile at separation with the behaviour (2.43):

$$u = u_0(Y) \sim \frac{1}{2}\lambda_0 Y^2 = O(Y^2)\,, \qquad Y\to 0\,, \tag{6.13}$$

$$u_0(Y) \to U_e(x_s)\,, \qquad Y\to\infty\,.$$

The boundary layer profile is assumed to be simply displaced which then rides over the viscous sublayer. This is because any induced pressure gradient, from the displacement of the boundary layer, is simply transmitted across the middle layer of the interaction region, according to (3.17). The boundary layer displacement in Y is

a small change to the separation profile $u = u_0(Y)$, like

$$\Delta u = O\left[(-s)^{\frac{1}{4}}\right] \tag{6.14}$$

due to a small change in similarity variable (6.3): $\Delta Y = O[(-s)^{\frac{1}{4}}]$. Similarly, the boundary layer displacement gives rise to a normal velocity v at the outer edge of the boundary layer ($Y \to \infty$), which behaves like:[1]

$$v = O\left[\mathrm{Re}^{-\frac{1}{2}}(-s)^{-\frac{3}{4}}\right] . \tag{6.15}$$

Therefore, by combining (6.13) and (6.3):

$$u = O\left[(-s)^{\frac{1}{2}}\right] ; \tag{6.16}$$

by combining (6.10) and (6.3):

$$p = O\left[(-s)\right] ; \tag{6.17}$$

and by combining (6.12) and (6.16):

$$T = O\left[\frac{(-s)}{\sigma}\right] , \tag{6.18}$$

for length scale s (6.4) and time parameter $\sigma \to \infty$.

6.2 The Interaction Region

As the point of zero skin friction $x = x_s$ is approached and $(-s) \to 0$, the boundary layer theory breaks down and there is an interaction region where displacement of the boundary layer becomes the same order of magnitude as the boundary layer itself.

[1] See also Elliott & Smith (1987).

The interaction region has time and length scales:

$$t - \sigma T = O(1)\,, \quad (-s) = O\left(\sigma^{-4}\right)\,, \quad O(\sigma) > O\left(\mathrm{Re}^{\frac{1}{20}}\right)\,; \quad \mathrm{Re}\,, \sigma \to \infty \qquad (6.19)$$

such that induced pressure gradient from the displacement of the boundary layer is negligible. (Chapter 3) In particular, the length scale (3.10) or (3.18) is

$$s^* = x^* - x_s = \sigma^4 s = O(1)\,. \qquad (6.20)$$

If $O(\sigma) \to O\left(\mathrm{Re}^{\frac{1}{20}}\right)$, the induced pressure gradient returns to the flow.

Recall that the flow structure of the interaction region is consistent if the solvability condition (4.1) for skin friction $A(x,T)$:

$$A^2(x,T) - x^2 + 2a(T) = -\frac{2^{\frac{3}{4}}}{\Gamma(\frac{5}{4})} \int_{-\infty}^{x} \frac{\partial A}{\partial T}(\xi,T)\, \frac{\mathrm{d}\xi}{(x-\xi)^{\frac{1}{4}}}$$

is satisfied. (Chapter 4) Furthermore, a second interactive stage nonlinear breakdown occurs on a faster time scale and shorter length scale like (5.64) and (5.65) as a singularity in $A(x,T)$ is approached. (Chapter 5)

There is an unsteady interactive region coinciding with the nonlinear breakdown and the runaway growth of bubble of reversed flow from the solutions of the $A(x,T)$ equation.

6.3 An Unsteady Interactive Structure

An interactive structure may be constructed, to smooth the singular behaviour in normal velocity (6.15). The pressure induced by the normal velocity must be comparable to the pressure needed to drive the viscous sublayer. Any induced pressure gradient which perturbs the separation profile and the normal velocity must be of

the same order. Hence, from (6.17) and (6.15):

$$(-s) = O\left(\mathrm{Re}^{-\frac{2}{7}}\right) . \tag{6.21}$$

Therefore, there is an interactive structure of length scale (6.21):

$$x - x_s - \sigma^{-4}x^* = \mathrm{Re}^{-\frac{2}{7}}\bar{X} , \tag{6.22}$$

spanning the boundary layer (6.4) and interaction region (6.20) length scales. The normal coordinate (6.1), similarity variable (6.3) and length scale (6.21) imply $y = \mathrm{Re}^{-\frac{1}{2}-\frac{1}{4}\cdot\frac{2}{7}}\bar{Y}$. Hence, the normal coordinate of the new region is

$$y = \mathrm{Re}^{-\frac{4}{7}}\bar{Y} , \qquad Y = \mathrm{Re}^{-\frac{1}{14}}\bar{Y} . \tag{6.23}$$

By combining (6.18), (6.19) and (6.21), the time scale in which the new region exists is

$$t = \sigma T , \qquad T = \mathrm{Re}^{-\frac{1}{7}} \cdot \sigma^{-1}\bar{T} \tag{6.24}$$

such that

$$t - \sigma T = \mathrm{Re}^{-\frac{1}{7}}\bar{T} . \tag{6.25}$$

The profile at separation (6.13) implies $\Psi = O(Y^3)$ then combining with (6.3) and (6.21) gives $\Psi = \mathrm{Re}^{\frac{3}{4}\cdot-\frac{2}{7}}\bar{\Psi}$. Hence,

$$\psi = \mathrm{Re}^{-\frac{1}{2}}\Psi \qquad \Psi = \mathrm{Re}^{-\frac{3}{14}}\bar{\Psi} . \tag{6.26}$$

Similarly, (6.16) and (6.21) combine to give

$$u = \mathrm{Re}^{-\frac{1}{7}}\bar{U} . \tag{6.27}$$

Finally, (6.17) and (6.21) combine to give

$$p = \mathrm{Re}^{-\frac{2}{7}} \bar{P} \,. \tag{6.28}$$

The boundary layer displacement (6.9) is assumed to have an asymptotic series expansion of the form:[2]

$$\delta^*(x,t) = \mathrm{Re}^{-\frac{1}{2}} \delta_0 - \mathrm{Re}^{-\frac{4}{7}} \bar{A}(\bar{X},\bar{T}) + \ldots$$

and hence,

$$\delta^*(x,t) = \mathrm{Re}^{-\frac{1}{2}} [\delta_0 - \mathrm{Re}^{-\frac{1}{14}} \bar{A}(\bar{X},\bar{T}) + \ldots] \,. \tag{6.29}$$

The $\bar{A}(\bar{X},\bar{T})$ term is the displacement correlation in $\bar{Y}$ of the same order of magnitude as the perturbation to the boundary layer $\Delta\bar{Y}$ (6.23). It is analogous to the skin friction which determines the size of the bubble of reversed flow on the airfoil.

Thus, there is an unsteady interactive structure with the variables $\bar{X}$ (6.22) and $\bar{T}$ (6.25):

$$x - x_s - \mathrm{Re}^{-\frac{1}{5}} x^* = \mathrm{Re}^{-\frac{2}{7}} \bar{X} \,, \qquad t - \sigma T = \mathrm{Re}^{-\frac{1}{7}} \bar{T} \,. \tag{6.30}$$

The boundary layer equation (6.6) becomes:

$$\frac{\partial \bar{U}}{\partial \bar{T}} + \bar{U} \frac{\partial \bar{U}}{\partial \bar{X}} - \frac{\partial \bar{\Psi}}{\partial \bar{X}} \frac{\partial \bar{U}}{\partial \bar{Y}} = \frac{\partial^2 \bar{U}}{\partial \bar{Y}^2} - \frac{\partial \bar{P}}{\partial \bar{X}} \,. \tag{6.31}$$

It is subject to the no-slip conditions:

$$\bar{U} = \bar{\Psi} = 0 \,, \qquad \bar{Y} = 0 \,;$$

the condition of matching of the viscous flow to the displaced flow:[3]

$$\bar{\Psi} \sim \frac{1}{6} \lambda_0 \left[\bar{Y} + \bar{A}(\bar{X},\bar{T}) \right]^3 + \ldots \qquad \bar{Y} \to \infty \,, \tag{6.32}$$

[2]See also Elliott & Smith (1987).
[3]See also Elliott & Smith (1987).

and the condition of matching to the attached boundary layer upstream and downstream:

$$\bar{U} \to \frac{1}{2}\lambda_0 \bar{Y}^2 \,, \qquad \frac{\partial \bar{P}}{\partial \bar{X}} \to \lambda_0 \,, \qquad |\bar{X}| \to \infty \,. \tag{6.33}$$

The condition of matching (6.32) is obtained from the profile at separation (6.13) in the variables (6.30), assuming there is simple displacement $\bar{A}(\bar{X}, \bar{T})$ in $\bar{Y}$ of the unsteady region. The condition (6.33) matches the pressure gradient to the classical boundary layer pressure gradient λ_0 (2.15).

Finally, there is also the subsonic pressure-displacement relation:[4]

$$\frac{\partial \bar{P}}{\partial \bar{X}}(\bar{X}, \bar{T}) = \frac{1}{\pi} \int\!\!\!\!\!\!- \, _{-\infty}^{\infty} \frac{\partial^2 \bar{A}}{\partial \xi^2}(\xi, \bar{T}) \, \frac{\mathrm{d}\xi}{(\bar{X} - \xi)} \,. \tag{6.34}$$

Without it, the problem is not closed since the pressure term on the right hand side of (6.31) remains unknown. The subsonic pressure-displacement relation is due to the interaction between the boundary layer and external inviscid potential flow. Importantly, it signifies the existence of an induced pressure gradient on the length and time scales (6.30) which was otherwise removed from the interaction region by a slow change in angle of attack on a large time scale (6.19). The interaction region without an induced pressure gradient does not have an upper layer, as discussed in Section 3.4. Therefore, with the existence of the induced pressure gradient is the return to classical triple deck theory.

6.4 The Finite-Time Breakdown Problem

Ultimately, the bubble of reversed flow spans the boundary layer such that the time and length scales shorten to the scale of boundary layer thickness. The flow reaches a nonlinear Euler stage.

Assuming that the displacement $\bar{A}(\bar{X}, \bar{T})$ of the boundary layer becomes large,

[4] A subsonic pressure-displacement relation (3.50) obtained in Section 3.4 is derived from the integral of small perturbation theory (B.6) in Appendix B.

then balancing terms from the condition of matching (6.32) of the viscous flow to the displaced flow, the variables are of order:

$$\bar{Y} = O(\bar{A})\,, \qquad \bar{\Psi} = O(\bar{A}^3)\,, \qquad \bar{U} = O(\bar{A}^2)\,, \qquad \bar{Y} \to \infty\,. \tag{6.35}$$

The balance of unsteady-inertial-pressure forces in the governing equation (6.31) reveals:

$$\frac{\partial \bar{U}}{\partial \bar{T}} \sim \bar{U}\frac{\partial \bar{U}}{\partial \bar{X}} \Rightarrow \bar{T} \sim \bar{X} \cdot \bar{A}^{-2} \tag{6.36}$$

$$\frac{\partial \bar{U}}{\partial \bar{T}} \sim \frac{\partial \bar{\Psi}}{\partial \bar{X}}\frac{\partial \bar{U}}{\partial \bar{Y}} \Rightarrow \bar{T} \sim \bar{X} \cdot \bar{A}^{-2} \tag{6.37}$$

$$\frac{\partial \bar{U}}{\partial \bar{T}} \sim \frac{\partial \bar{P}}{\partial \bar{X}} \Rightarrow \bar{T} \sim \bar{X} \cdot \bar{P}^{-1} \cdot \bar{A}^{-2}\,. \tag{6.38}$$

In order for (6.36), (6.37) and (6.38) to be consistent, then

$$\bar{P} = O(\bar{A}^4)\,. \tag{6.39}$$

Furthermore, if $|\bar{X}|$ and $|\bar{T}|$ are chosen to be[5]

$$\bar{X} = O(\bar{A}^{-3})\,, \qquad \bar{T} = O(\bar{A}^{-5}) \tag{6.40}$$

such that (6.36), (6.37) and (6.38) remain true and that there is a runaway effect on the time and length scales as displacement parameter $\bar{A}$ grows large, then the $O(1)$ viscous term: $\frac{\partial^2 \bar{U}}{\partial \bar{Y}^2}$ cannot be balanced.

Therefore, to leading order, there is an inviscid structure with a fast time scale and length scale:

$$\bar{X} = O(\bar{T}^{-\frac{3}{5}})\,, \qquad \bar{Y} = O(\bar{T}^{-\frac{1}{5}})\,. \tag{6.41}$$

Furthermore, there is a bursting effect of the viscous sublayer as $\bar{T} \to 0$. The governing equations are

$$\bar{U} = \frac{\partial \bar{\Psi}}{\partial \bar{Y}}\,; \tag{6.42}$$

[5]See also Elliott & Smith (1987).

$$\frac{\partial \bar{U}}{\partial \bar{T}} + \bar{U}\frac{\partial \bar{U}}{\partial \bar{X}} - \frac{\partial \bar{\Psi}}{\partial \bar{X}}\frac{\partial \bar{U}}{\partial \bar{Y}} = -\frac{\partial \bar{P}}{\partial \bar{X}}\,, \tag{6.43}$$

subject to the inviscid constraint of tangential flow:

$$\bar{\Psi} = O(\bar{Y})\,, \qquad \bar{Y} \to 0\,;$$

the condition of matching to the external inviscid flow:

$$\bar{\Psi} \sim \frac{1}{6}\lambda_0 \left[\bar{Y} + \bar{A}(\bar{X}, \bar{T})\right]^3 + \ldots \qquad \bar{Y} \to \infty\,;$$

and the pressure displacement law: (6.34). The finite-time breakdown problem, consisting of equations (6.42), (6.43) and their conditions, holds as long as a viscous sublayer exists which brings the fluid flow velocity to rest at the surface. The problem continues from the analogous problem by Smith (1982a) such that there is a continuing increase of reversed flow associated with increase in $\bar{A}$.

According to the analysis, there is a short-scale breakdown with $|\bar{X} - \bar{X}_0| \sim |\bar{T} - \bar{T}_0|^{\frac{3}{5}}$, and with the viscous flow splitting into two.[6] There is an external inviscid part which erupts like $\bar{Y} \sim |\bar{T} - \bar{T}_0|^{-\frac{1}{5}}$ and a diminishing inner viscous region with $\bar{Y} \sim |\bar{T} - \bar{T}_0|^{-\frac{1}{2}}$ (derived from the nonlinear-unsteady-viscous balance in the unsteady boundary layer equation (6.31); similar to (6.12)). Eventually the external region will be indistinguishable from the majority of the boundary layer of thickness $O(\mathrm{Re}^{-\frac{1}{2}})$. This occurs when the Eulerian scalings:

$$\begin{aligned} t - \sigma T - \mathrm{Re}^{-\frac{1}{7}}\bar{T}_0 &= O\left(\mathrm{Re}^{-\frac{1}{2}}\right) \\ x - x_s - \mathrm{Re}^{\frac{1}{5}}x^* - \mathrm{Re}^{-\frac{2}{7}}\bar{X}_0 &= O\left(\mathrm{Re}^{-\frac{1}{2}}\right) \end{aligned} \tag{6.44}$$

are true. The velocity and pressure disturbances become increased to order unity and so the Euler equations come into operation across the entire boundary layer. A vortex starts to span the boundary layer and its evolution becomes a vortex sheet

[6] See also Elliott & Smith (1987).

problem.

The effects described in this Chapter mark the end of the second interactive stage of the thickening of the boundary layer and the start of a third interactive stage where there is unsteady vortex development and ejection. The third interactive stage is the process of leading edge stall.

Chapter 7

Summary & Conclusions

The thesis aimed to bridge the work on marginal separation with that on steady flow over a downstream-moving surface, unsteady marginal separation and dynamic stall. In particular, the focus was on the quasi-steady flow structure which develops over a very large time scale when there are very slow perturbations to the otherwise steady stream functions. The slow perturbations are from a slow change in angle of attack over a small range as it gradually approaches the critical angle where stream function solutions become complex and nonlinear breakdown occurs. (See Figure 7.1.)

The original work comprises of manipulating marginal separation theory, where the angle of attack is altered to reduce the strength of an adverse pressure gradient and Goldstein's singularity, to include the effects of slow perturbations and change in angle of attack on a large time scale as to render induced pressure gradient negligible in the interaction region. In short, the fundamental equation of unsteady marginal separation (1.11) for skin friction loses the term representing the pressure-displacement relation from the induced pressure gradient and notably, gains an unsteady term representing the slow change in angle of attack. The unsteady term ultimately comes from making the first constant in the largest perturbation of the steady stream function solution, a function of the large time scale and assigning the change in angle of attack to it. Solutions to the equation are found. The subsequent finite-time, nonlinear breakdown equation is shown to allow another discontinuous

skin friction solution different to that of Smith & Elliott (1985). Furthermore, the discontinuous solution can travel towards the singularity but the movement is only observable on the large time scale. This draws upon the connections in steady flow over a downstream-moving surface to steady flow over a fixed surface.

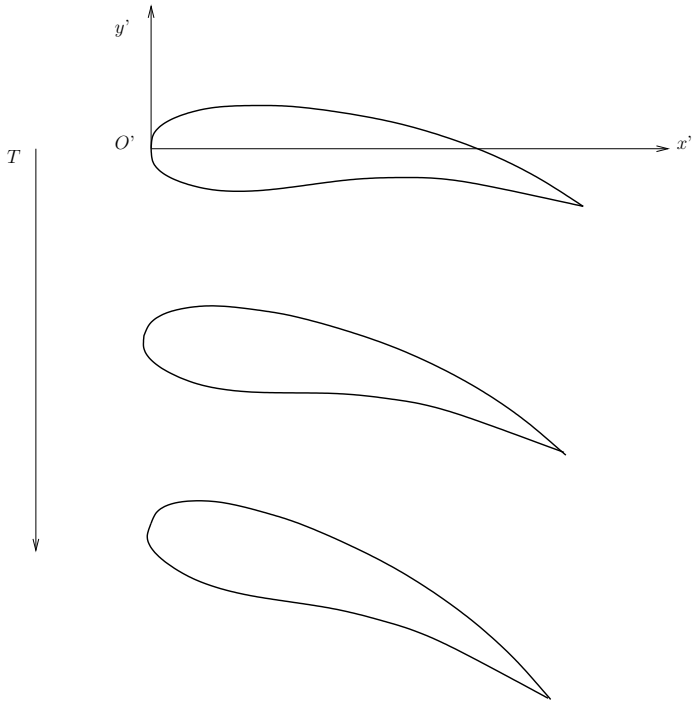

Figure 7.1: The airfoil with a very slow change of angle of attack causing a downstream movement of the surface on a very large time scale. The range of angle of attack is small but exaggerated here.

7.1 Boundary Layer Analysis & the Interaction Region

The airfoil is subject to a very slow perturbation only observable on a very large time scale T compared to the external region time scale t, such that

$$T = \sigma^{-1} t = O(1)\,, \qquad \sigma \to \infty\,. \tag{7.1}$$

The time scale is sufficiently large such that the induced pressure gradient by the displaced boundary layer is of relatively small order of magnitude compared to the

unsteady or viscous forces acting on the boundary layer.

The change in angle of attack is characterised by k (2.3), which is a function of time T. At the critical value $k = k_0$ is the first appearance of a point of zero skin friction $x = x_s$. The small variable:

$$\Delta k = k(T) - k_0 \to 0$$

is introduced to represent the small change in angle of attack. On the external region time scale t is steady flow over a fixed surface such that the no-slip conditions apply. Meanwhile, on the boundary layer time scale T, there are slow and small $O(\Delta k)$ perturbations to the steady flow caused by the slow and small change in angle of attack. (See Section 2.2.)

Only a local region of the point of zero skin friction $x = x_s$ is considered and so the variable (2.12):

$$s = x - x_s = O(1)$$

is introduced. Also, a similarity variable of the viscous sublayer (region 3 in Figure 7.2) can be defined as (2.19):

$$\eta = \frac{Y}{(-s)^{\frac{1}{4}}} = O(1)\,.$$

The asymptotic series expansion of the boundary layer stream function $\Psi(x, Y, T)$ is defined as (2.16):

$$\Psi = \mathrm{Re}^{\frac{1}{2}}\psi = \Psi_0(x, Y) + \Delta k \Psi_1(x, Y, T) + \frac{\Delta k}{\sigma}\Psi_2(x, Y, T) + \ldots \tag{7.2}$$

The steady flow is represented by the term: $\Psi_0(x, Y)$. The flow perturbations are represented by the terms $\Delta k \Psi_1(x, Y, T)$ and $\frac{\Delta k}{\sigma}\Psi_2(x, Y, T)$.

The steady flow $\Psi_0(x, Y)$ solution (2.43) is from Ruban (1982a) and given in Section 2.3. The flow perturbations $\Psi_1(x, Y, T)$ and $\Psi_2(x, Y, T)$ are found for the

boundary layer (regions 2 and 3 in Figure 7.2) by the hierarchical principle and the method of matched asymptotic expansions in Sections 2.4 and 2.6.

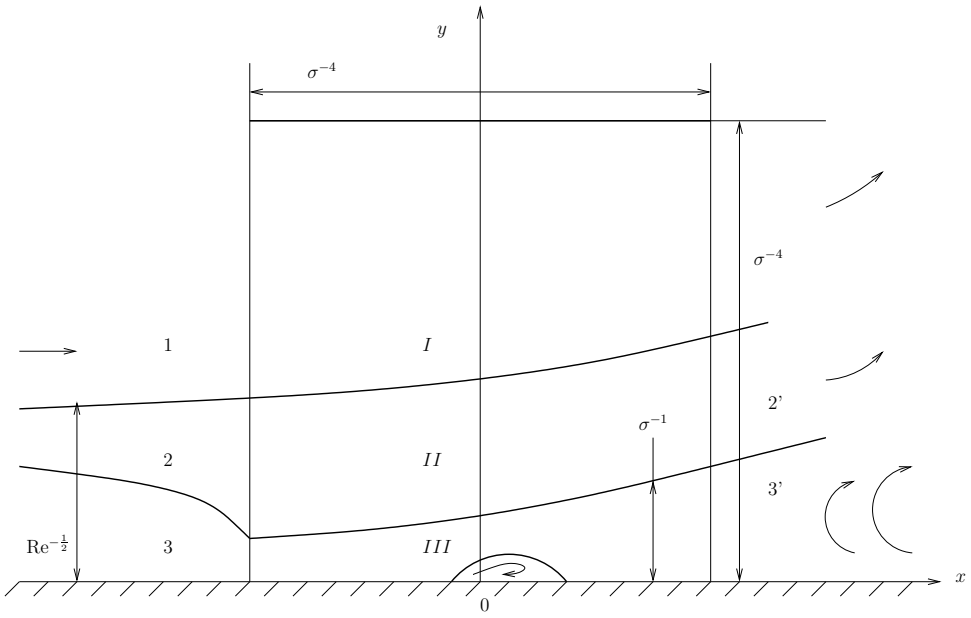

Figure 7.2: The triple-deck interaction region: I, II, III; viscous sublayer: 3, 3'; external inviscid region: 1; main boundary layer: 2, 2'.

To adapt the viscous sublayer (region 3) stream function so it allows slow perturbations of the airfoil on the large time scale T, any constants a_n and b_n for $n \geq 1$ of the perturbation components Ψ_1 and Ψ_2, are functions of time $a_n(T)$ and $b_n(T)$. The angle of attack α and asymmetry parameter k are also time-dependent such that (for example) $a_1(T)$ is related to k (2.3) and is of a small order of magnitude Δk.

For the viscous sublayer, the Ψ_1 component (2.57) is:

$$\Psi_1 = (-s)^{-\frac{1}{2}}\frac{1}{2}a_1\eta^2 + (-s)^{\frac{1}{4}}\frac{1}{2}b_1\eta^2 + \ldots \tag{7.3}$$

and the Ψ_2 component (2.76):

$$\Psi_2 = \frac{1}{2}b_2(T)\eta^2 + \frac{1}{3}\dot{a}_1\left[\frac{1}{8}\eta^4 + \frac{1}{84}\left(\frac{\lambda_0}{32}\right)\eta^8 + \ldots\right] + \ldots \tag{7.4}$$

When $\Delta k \neq 0$ and as $\sigma \to \infty$, there is a slow $O(\Delta k)$ perturbation (7.3) to the steady stream function (2.43) as the angle of attack changes with $a_1(T)$. Perturbations of

$O(\frac{\Delta k}{\sigma})$ (7.4) are proportional to rate of change of angle of attack with respect to time as parameterised by $\dot{a}_1(T) = \frac{\mathrm{d}a}{\mathrm{d}T}$. The larger the angle of attack and the faster its increase then the greater the perturbations. (See Section 2.7.)

For the main boundary layer (region 2 in Figure 7.2), the Ψ_1 component (2.58) with (2.48), is

$$\Psi_1 = (-s)^{-1}\frac{a_1}{\lambda_0}a_1\frac{\mathrm{d}\Psi_{00}}{\mathrm{d}Y} + O\left[(-s)^{-\frac{1}{4}}\right], \qquad s \to -0\,, \tag{7.5}$$
$$\Psi_{00} = \frac{1}{6}\lambda_0 Y^3 + \frac{2}{7!}\lambda_0\lambda_1 Y^7 + \frac{1}{8!}\lambda_0 a_0^2 Y^9 + \ldots \qquad Y \to 0\,;$$

and the Ψ_2 component (2.81) is

$$\Psi_2 = \frac{1}{3!}\frac{\Gamma(\frac{7}{4})}{\Gamma(\frac{3}{4})}\frac{32}{\lambda_0}\dot{a}_1 \ln Y - \frac{1}{4!}\frac{\Gamma(\frac{7}{4})}{\Gamma(\frac{3}{4})}\frac{32}{\lambda_0}\dot{a}_1 \ln(-s) + (-s)^{-\frac{1}{2}}\frac{1}{2}b_2 Y^2 + \ldots \tag{7.6}$$

Hence, the rate of change in angle of attack $\dot{a}_1(T)$ has a logarithmic perturbing effect on the main boundary layer close to the point of zero skin friction. (See Section 2.8.)

As the point of zero skin friction is approached and $(-s) \to 0$, there seems to be a singularity caused by the $O(\frac{\Delta k}{\sigma})$ perturbation. Further analysis of the flow structure must incorporate the interaction region (regions I, II, III in Figure 7.2), in Chapter 3, where the displacement of the streamlines from the boundary layer no longer have a negligible effect on the external inviscid flow and eigenfunctions in the series expansions (2.43), (7.3), (7.4) for the viscous sublayer become the same order of magnitude.

A restriction is placed on the asymmetry parameter Δk and time parameter σ such that the strength of the induced pressure gradient is negligible, in particular (3.7):

$$O\left(\sigma^{-4}\right) = O\left(|\Delta k|^{\frac{1}{2}}\right) > O\left(\mathrm{Re}^{-\frac{1}{5}}\right).$$

This may be comparable to marginal separation theory, when an angle of attack is forced to approach a critical angle to reduce an adverse pressure gradient and Goldstein's singularity. The flow structure develops in an interaction region where

(3.8):

$$(-s) = O\left(\sigma^{-4}\right) , \qquad \Delta k = O\left(\sigma^{-8}\right) , \qquad O(\sigma) > O\left(\mathrm{Re}^{\frac{1}{20}}\right) . \tag{7.7}$$

A theory can be constructed on the basis of a the limit process (3.9):

$$k(T) = k_0 + \sigma^{-8} k_1(T) , \qquad k_1(T) = O(1) , \qquad \sigma \to \infty$$

which describes the appearance of the point of zero skin friction at the leading edge and allows the transition to the conventional boundary layer theory in the limit as $k_1(T) \to -\infty$.[1]

The interaction region considered is contained within the classical interaction region of length scale $\mathrm{Re}^{-\frac{1}{5}}$, so as to not destroy the triple-deck system. Consequently, as $\Delta k \to \mathrm{Re}^{-\frac{2}{5}}$ by (3.5), the induced pressure gradient comes into action and the classical interaction region results are recovered. (See Section 3.1.)

Asymptotic series stream function solutions like (7.2) are found for the middle layer (region II in Figure 7.2) and the lower layer (region III) of the interaction region by the hierarchical principle and the method of matched asymptotic expansions, in Sections 3.2 and 3.3.

As a result of the condition of matching (3.28) between the middle layer and the lower layer, a necessary and sufficient *solvability condition* is found for the interaction region, with a negligible induced pressure gradient, to be consistent.[2] The solvability condition (3.48) is[3]

$$A^2(x,T) - x^2 + 2a(T) = -\frac{2^{\frac{3}{4}}}{\Gamma(\frac{5}{4})} \int_{-\infty}^{x} \frac{\partial A}{\partial T}(\xi, T) \, \frac{\mathrm{d}\xi}{(x-\xi)^{\frac{1}{4}}} . \tag{7.8}$$

(See Section 3.3 and in particular, Sections 3.3.5 and 3.3.6.)

The $A(x,T)$ term is directly proportional to the skin friction, defined as (4.2). If

[1] Sychev et al. (1998b).

[2] A change of variables and affine transformation (3.29); the subsequent Fourier transformation boundary value problem in Section 3.3.3; and the inverse Fourier transformation of the condition (3.45), follows the matching between the middle layer and lower layer!

[3] For simplicity, the bar and subscript notation is removed.

skin friction is positive then the fluid flow is attached and moving downstream. If skin friction is negative the flow is moving upstream against the current.

The parameter $a(T) \sim \Delta k$ is related to the change in angle of attack and comes from $a_1(T)$ in the viscous sublayer Ψ_1 component (7.3). For an airfoil with a slow change in angle of attack on the large time scale T that is also close to stall then $a(T)$ can be set to start close to but below the critical value $a_c = 1.33$, which then gently approaches the point of complex solution at $a = a_c$. For example, the angle of attack law (4.3) is

$$a(T) = 1.331 - (1.331 + 0.001)e^{-T}\,, \qquad T \geq 0\,. \tag{7.9}$$

(See the first part of Chapter 4.)

The interaction region problem is closed, with the derivation of the $A(x,T)$ solvability condition (7.8), because the induced pressure gradient is negligible. In other words, there is no need to consider an upper layer (region I in Figure 3.2) of the traditional triple deck theory for the interaction region. (See Section 3.4.)

7.2 A(x,T) Solvability Condition Analysis & the Nonlinear Breakdown

Chapter 4 is on the construction of the initial-boundary value problem and numerical solution for the solvability condition (4.1) of the interaction region:

$$A^2(x,T) - x^2 + 2a(T) = -\frac{2^{\frac{3}{4}}}{\Gamma(\frac{5}{4})} \int_{-\infty}^{x} \frac{\partial A}{\partial T}(\xi,T)\, \frac{\mathrm{d}\xi}{(x-\xi)^{\frac{1}{4}}} \tag{7.10}$$

with $a(T)$ given by (7.9). Far away from the local interaction, the boundary condition (4.4) is

$$A(x,T) = \left(|x|^2 + 2a(T)\right)^{\frac{1}{2}}\,, \qquad |x| \to \infty\,. \tag{7.11}$$

The thesis follows the theory of marginal separation from Stewartson et al. (1982). Hence, the class of far away attached flows is considered and the positive root of (7.11) is taken.

Initial conditions are based on but not identical to the initial conditions from Smith & Elliott (1985). An example initial condition applied at the start time $T = 0$ is "IC1" (4.25):

$$A(x,0) = \begin{cases} \frac{\sqrt{(2.5^2-2a(0))}}{\sqrt{(2.5^2-2a(0)+0.4)}} \cdot \sqrt{(x^2-2a(0)+0.4)}\,, & |x| \le 2.5 \\ \sqrt{(x^2-2a(0))}\,, & |x| > 2.5\,; \end{cases} \tag{7.12}$$

where the fluid flow is initially attached along the airfoil. It is similar to the boundary condition. (See Section 4.4.1.)

Solutions for the $A(x,T)$ equation are found based on the numerical treatment described by Smith & Elliott (1985). This numerical treatment is chosen because Smith & Elliott use the method to acquire solutions for a normalised quasi-steady version (4.5):

$$A^2(x,T) - x^2 + \bar{\Gamma} = \int_{-\infty}^{x} \frac{\partial A}{\partial T}(\xi,T)\,\frac{\mathrm{d}\xi}{(x-\xi)^{\frac{1}{4}}} \tag{7.13}$$

where $2a(T)$ is a constant $\bar{\Gamma} = -1$. Equation (7.10) is to be reformulated as a system of nonlinear equations on a uniform space x and time T grid. (See Section 4.1.) Ultimately, the nonlinear system of equations will be solved numerically using Newton's method, as described in Section 4.2. The treatment is tested in the Sections 4.3 and 4.4.

From IC1 (7.12), $A(x,T)$ has a positive minimum which increases as $T \to 1$ and shifts downstream from the origin to $x \simeq 0.1$, as shown at intervals of $\Delta T = 0.2$ in Figure 7.3. The flow structure is attempting to stabilise to a configuration with no separation. Figure 7.4 shows that between $T = 1.2$ and $T = 1.6$, the positive minimum levels out at $x \simeq 0.1$ where $A \simeq 0.45$. From $T = 1.6$, $A(x,T)$ decreases and shifts upstream until the minimum reaches zero at $x \simeq -0.1$, $T \simeq 3.0$, as shown at intervals of $\Delta T = 0.5$ in Figure 7.5. From thereon, $A(x,T)$ becomes negative

and a closed bubble of reversed flow forms on the surface. The region of reversed flow becomes more accentuated upstream towards $x = -1$ with time T until there is breakdown at end time $T_{\text{end}} \simeq 5.5$. (See Table 4.10 and in particular, Section 4.5.) The bubble erupts after a finite terminal time T_{end} and a singularity of $A(x, T)$ is reached.

From all initial conditions (4.24) to (4.27), the flow accelerates towards the breakdown despite the fact that change in angle of attack of the airfoil decelerates with time. This suggests the breakdown is a runaway process, occurring on even shorter time and length scales. (See Sections 4.4.1 and 4.5.2.)

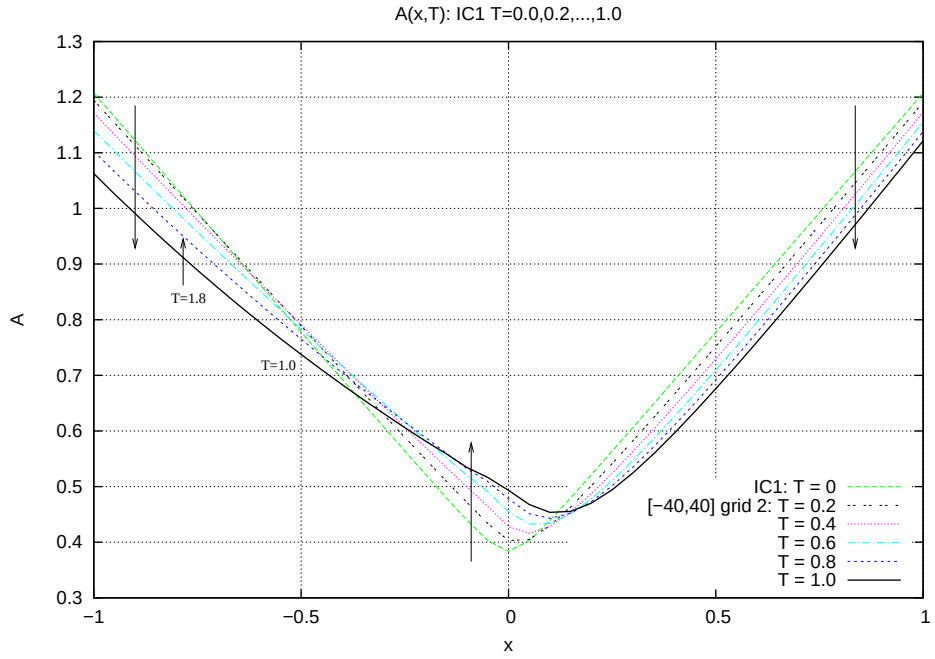

Figure 7.3: $A(x, T)$ from IC1 at $T = 0.0, 0.2, \ldots, 1.0$.

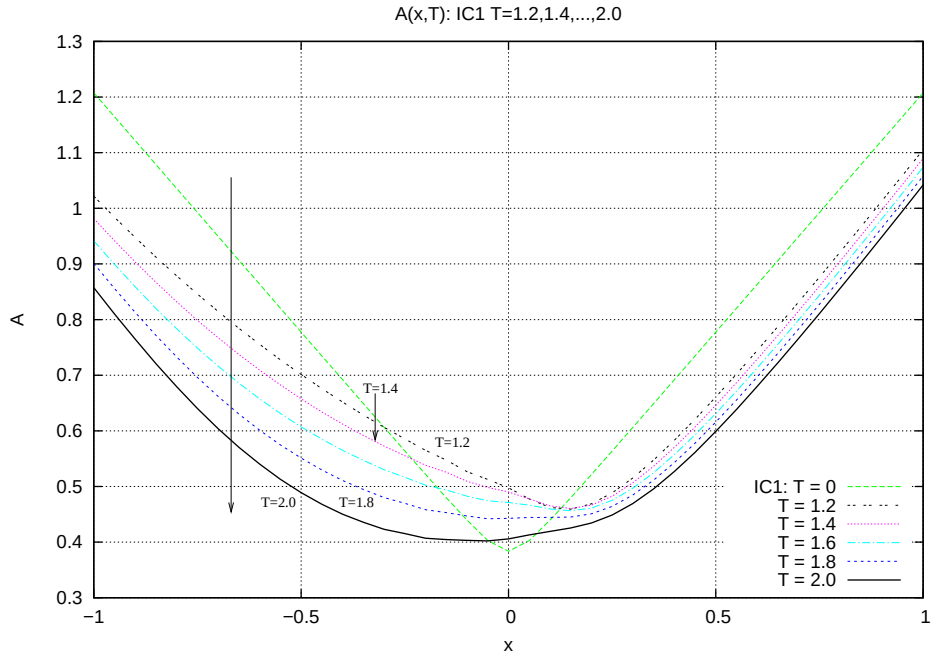

Figure 7.4: $A(x,T)$ from IC1 at $T = 1.2,\ 1.4,\ \ldots,\ 2.0$.

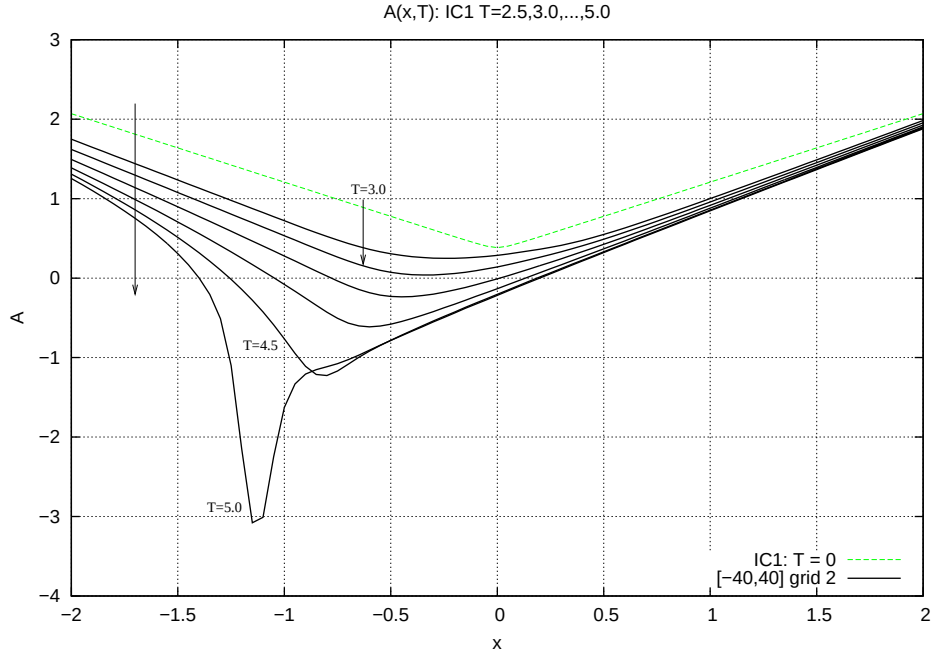

Figure 7.5: $A(x,T)$ from IC1 at $T = 2.5,\ 3.0,\ \ldots,\ 5.0$.

Prior to the singularity, nonlinear breakdown occurs. Nonlinear breakdown can be considered as a *second interactive stage* on an even smaller and faster time scale than the interaction region. The second interactive stage is the developing eruption of the bubble of reversed flow, which causes the boundary layer to thicken. Analysis of the second interactive stage shows that discontinuous skin friction solutions in the style of Heaviside function waves exist. (See the first part of Chapter 5.)

In short, the first interactive stage interaction region with coordinate x contains a second interactive region with coordinate X and within, a point of zero skin friction $x = x_s$ travels towards the terminal point of singularity at $X = X_s$ as $T \to T_s$:

$$x = x_s + C(T_s - T)^{\alpha} + (T_s - T)^{\beta} X \,, \tag{7.14}$$

$$X = O(1) \,, \qquad T \to T_s \,, \qquad \beta \geq \alpha > 0 \,. \tag{7.15}$$

The skin friction $A(x,T)$ series expansion of the second interactive region arises in the form (5.6):

$$A(x,T) = (T_s - T)^{\frac{3}{4}\beta - 1} \hat{A}(X) + \ldots \quad \hat{A}(X) = O(1) \,, \quad 0 < \beta < \frac{4}{3} \,. \tag{7.16}$$

where $|A(x,T)|$ is to be large during the nonlinear breakdown process. The constant C is arbitrary but related to the speed of travel of the point of zero skin friction and the direction of travel, depending on its sign. The constant α is also arbitrary except $0 < \alpha \leq \beta$ such that the point of zero skin friction is travelling towards the point of singularity at a slower rate than the second interactive region is decaying about it. The second interactive region is then an intact structure which does not destroy the interaction region from Chapters 3 and 4. (See Figure 7.6 and in particular, Sections 5.1 and 5.1.1.)

The solvability condition (7.10) of which the second interactive stage $\hat{A}(X)$ equation (7.17) originates, can be shown to admit discontinuous forms of $A(x,T)$ like

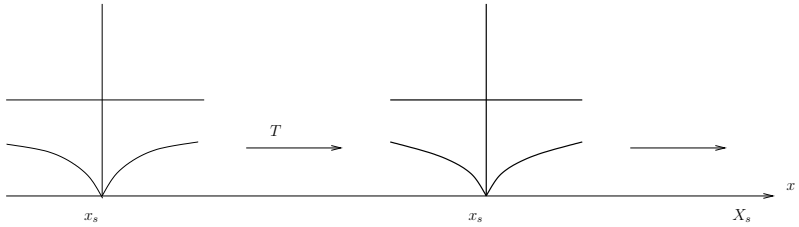

Figure 7.6: The point of zero skin friction $x = x_s$ and flow structure travelling towards the point of singularity $x = X_S$, when $\beta \geq \alpha > 0$.

(5.41):

$$A(x,T) = \bar{C}T^{\alpha}H\left[x - vT^{\beta}\right]$$

where $H\left[x - vT^{\beta}\right]$ denotes the Heaviside step function (5.42) (although they are not solved with boundary conditions). If discontinuous forms of $A(x,T)$ can exist for the solvability condition then discontinuous forms of $\hat{A}(X)$ can also exist.

The second interactive region eigenvalue β and $\hat{A}(X)$ boundary value problem coincides with the Smith & Elliott (1985) nonlinear breakdown problem. It consists of the nonlinear breakdown equation (5.21):

$$\hat{A}^2(X) = \int_{-\infty}^{X} \left[\left(\frac{3}{4}\beta - 1\right)\hat{A}(\xi) - \beta\xi\frac{\mathrm{d}\hat{A}}{\mathrm{d}\xi}(\xi)\right] \frac{\mathrm{d}\xi}{(X-\xi)^{\frac{1}{4}}}\,. \tag{7.17}$$

for $0 < \beta < \frac{4}{3}$ and $\beta \geq \alpha > 0$, with the boundary conditions (5.23):

$$\hat{A}(X) \sim \begin{cases} -|X|^{\frac{3}{4}-\frac{1}{\beta}}\,, & X \to -\infty \\ \lambda_2 X^{\frac{3}{4}-\frac{1}{\beta}}\,, & X \to \infty \end{cases} \tag{7.18}$$

where λ_2 is an arbitrary boundary value constant. (See Section 5.1.3.)

The boundary condition at $X = X_{m+1}$ can be satisfactorily achieved, with the constant λ_2 found, by implementation of a *minimising function* Φ (5.37). The $\hat{A}(X)$ solution must satisfy the minimising function to be a true solution. The value of the

true eigenvalue β is found from rearranging (5.37) to (5.38):

$$\beta = \left| X_m \cdot \left(\frac{\hat{A}_{m+1} - \hat{A}_m}{\mathrm{D}X \cdot \frac{1}{2}(\hat{A}_m + \hat{A}_{m+1})} \right) - \frac{3}{4} \right|^{-1} .$$

Furthermore, the value of constant λ_2 is found from rearranging the boundary condition (7.18) at $X = X_{m+1}$ (5.39), using the values for (5.37). (Section 5.2.1)

The problem (7.17), (7.18) is solved in MATLAB using the numerical shooting method and Newton's method for a system of nonlinear equations, both with minimising function Φ. The discretisation of the $\hat{A}(X)$ equation (7.17) is analogous to the numerical treatment of the $A(x,T)$ equation in Section 4.1. (See Section 5.2.) Both methods are tested in Section 5.3, 5.3.1 and 5.3.2.

The true eigenvalue $\beta \to 1.23$ and the boundary value constant $\lambda_2 \to 0.96$. Hence, the point of zero skin friction $x = x_s$ and the second interactive region X, behave like (5.64):

$$x = X_s + (T_s - T)^{1.23} X \,, \quad X_s = x_s + C(T_s - T)^{\alpha} \,, \quad 0 < \alpha \leq 1.23 \,; \tag{7.19}$$

whilst the first interactive stage skin friction $A(x,T)$ (7.16) and the second interactive stage $\hat{A}(X)$ analogy, behave like (5.65):

$$A(x,T) = (T_s - T)^{-0.0775} \hat{A}(X) + \ldots \qquad \hat{A}(X) = O(1) \,, \tag{7.20}$$

as the singularity at $X = X_s$, $T = T_s$ is approached during nonlinear breakdown.

The $\hat{A}(X)$ solution to the second interactive stage equation (7.17) exhibits a shock or discontinuity. There is an abrupt jump from a negative value $\hat{A}(X \simeq -1)$ to its modulus $\hat{A}(X \simeq +1)$ within a small number of grid points. Elsewhere, the numerical results show the existence of a smooth form of $\hat{A}(X)$ whenever $X \neq 0$. (See Figures 7.7a to 7.7c.)

The $\hat{A}(X)$ solution describes the three fluid flow configurations when the point of zero skin friction is either fixed; is travelling at a slower rate than the decay of the

second interactive region; or is travelling at the same rate as the decay of the second interactive region.[4] Furthermore, the flow structure is simply shifted with the point of zero skin friction, as illustrated in Figure 7.6. (See Section 5.1.1.)

Therefore, the shock at the point of zero skin friction shows a point of detachment or abrupt reattachment of a bubble or reversed flow to the airfoil.[5] The skin friction, being negative for $X < 0$, shows forward attached flow; and being positive for $X > 0$, shows reversed flow in the closed bubble. The shock can either be stationary or travelling along the airfoil towards a point of singularity. Coinciding with the decay of the second interactive region is the increasing accentuation of the bubble which thickens the boundary layer. Eventually, the flow regime returns to that of boundary layer thickness, as analysed in Chapter 6. (See Section 5.4.)

[4]This assertion is based on Moore (1958) for moving points of separation.
[5]Smith & Elliott (1985)

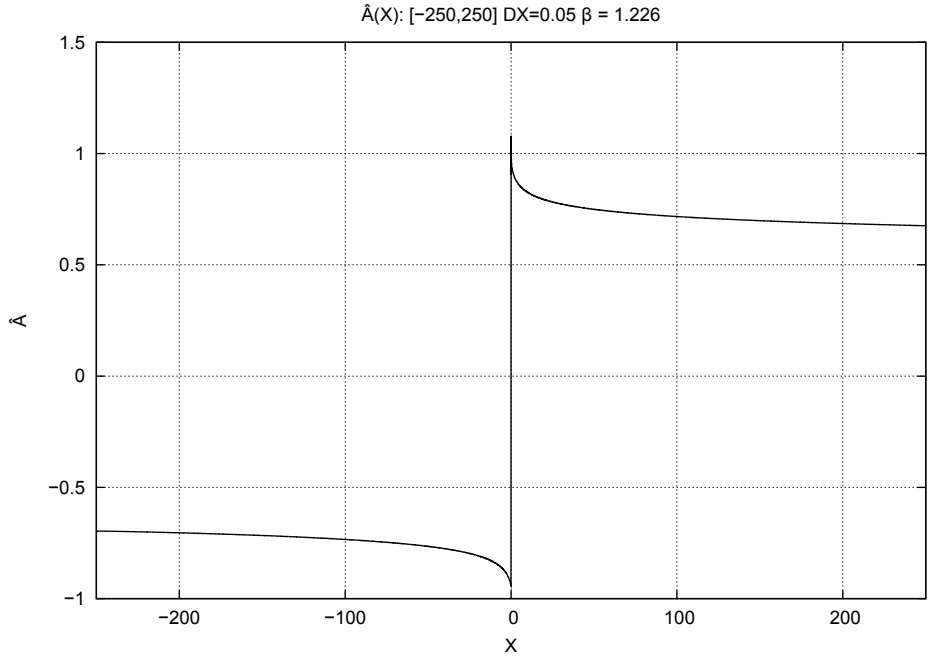

(a)

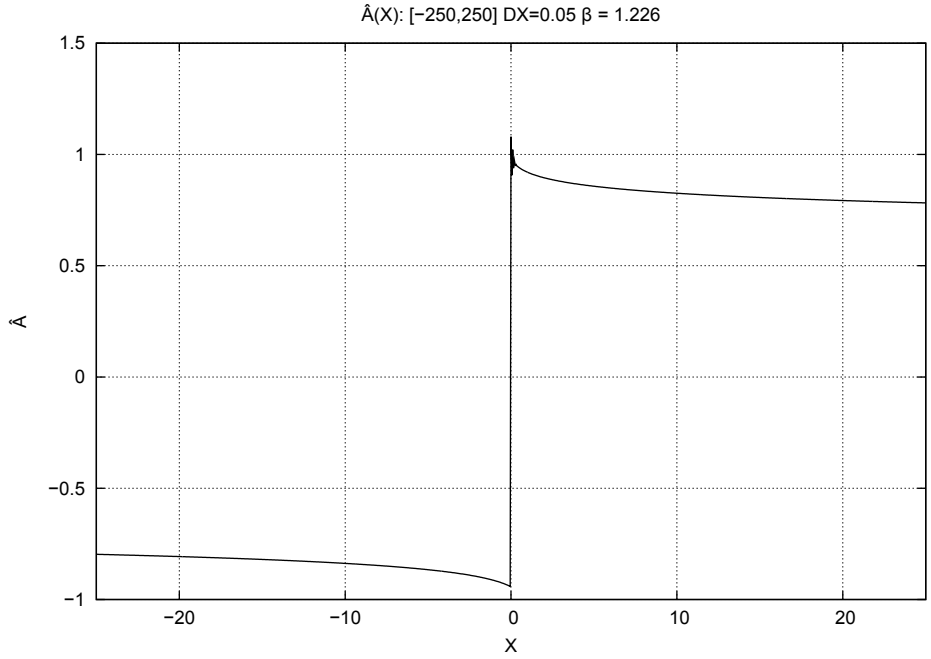

(b)

Figure 7.7: $\hat{A}(X)$ for domain $X \in [-250, 250]$, step size D$X = 0.05$; eigenvalue $\beta = 1.226$; boundary value constant $\lambda_2 = 0.96$, as shown in regions $X \in [-250, 250]$ and $X \in [-25, 25]$.

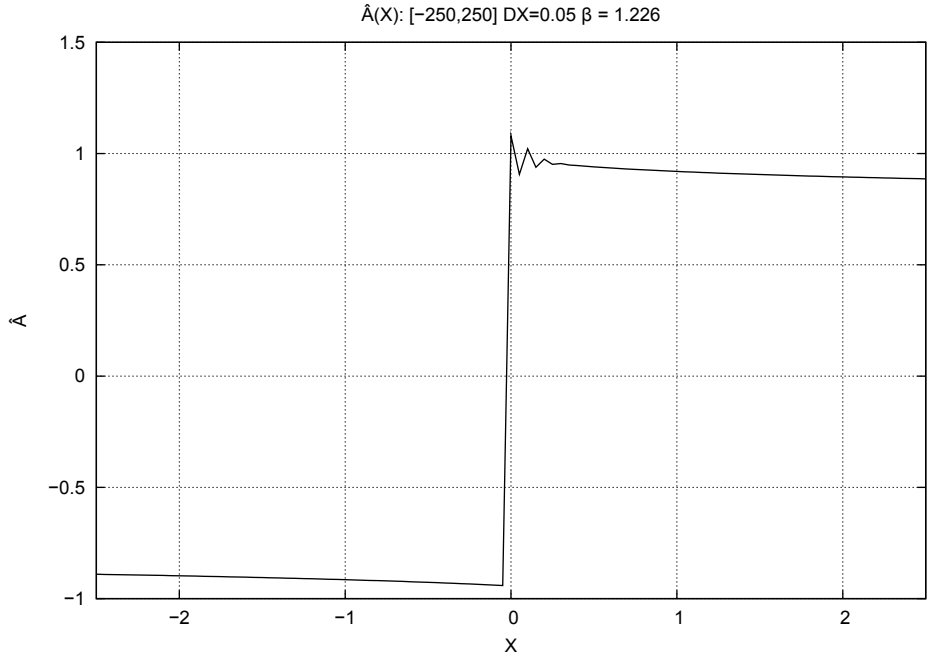

(c)

Figure 7.7: $\hat{A}(X)$, as shown in region $X \in [-2.5, 2.5]$. See Figures 5.33a and 5.33b.

The waning oscillations close to the discontinuity at $X = 0$, as shown closely in Figure 7.7c and seen in Figure 7.8 from Smith & Elliott (1985), appear in all $\hat{A}(X)$ solutions from Newton's method with Φ, regardless of size of domain or grid. The oscillations are assumed to appear in Newton's method solutions because there is discontinuity at $X = 0$ and the second interactive stage equation being solved is nonlinear. On the other hand, the oscillations are dampened with increase in size of domain and decrease in step size, as shown for example in the sequence of Figures 5.26 to 5.30 in Section 5.3.4. (See Section 5.4.)

On the other hand, the methods do not reproduce results from Smith & Elliott (1985) as shown when comparing any solution with the Figure 7.8 from Smith & Elliott (1985). One reason is that the shooting method and Newton's method with minimising function Φ happen to find another true $\hat{A}(X)$ solution as eigenvalue $\beta \to 1.23$ and $\lambda_2 \to 0.96$. (See Section 5.3.4.)

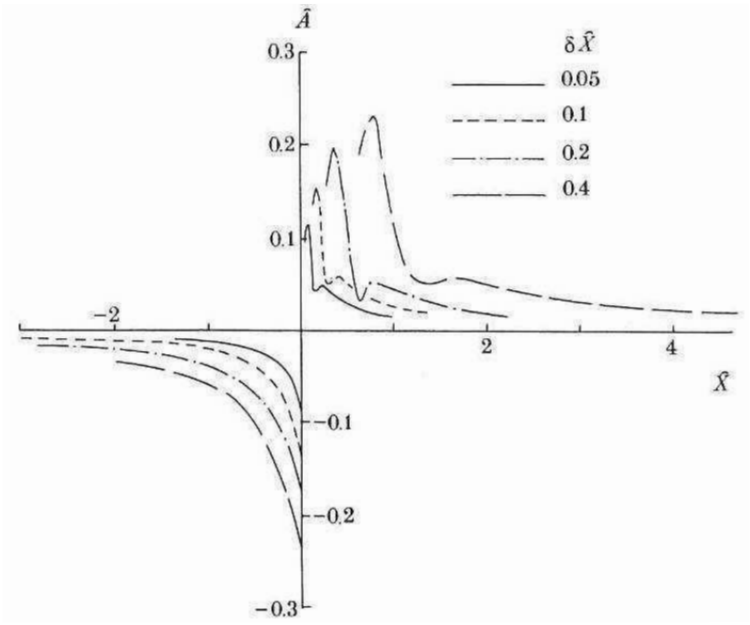

Figure 7.8: Smith & Elliott (1985), Figure 3, p. 18: "Numerical solutions... showing the shock-like (abrupt reattachment) trend near the origin."

7.3 Leading Edge Stall & Inviscid Euler Structure

The process of leading edge stall continues from the second interactive stage nonlinear breakdown (Chapter 5), where there is runaway growth of a bubble of reversed flow and discontinuous skin friction advancing towards a singularity. The induced pressure gradient (Section 3.1), that was made negligible in the interaction region by the slow perturbations to the airfoil on a large time scale T, exists in the unsteady interactive structure, regardless of the time scale on which the structure exists. Ultimately, the flow regime is that where time and length scales shorten to the scale of boundary layer thickness. The flow reaches a nonlinear Euler stage where the growth of the bubble spans the boundary layer. Evidence for the terminal flow is from analysis of the leading edge, starting with the boundary layer and its governing equations. The analysis follows from that of dynamic stall due to unsteady marginal separation by Elliott & Smith (1987), which has been adapted in Chapter 6.

According to the analysis, the terminal Euler flow regime is a short-scale breakdown with $|\bar{X}-\bar{X}_0| \sim |\bar{T}-\bar{T}_0|^{\frac{3}{5}}$, and with the viscous flow splitting into two.[6] There is an external inviscid part which erupts like $\bar{Y} \sim |\bar{T}-\bar{T}_0|^{-\frac{1}{5}}$ and a diminishing inner viscous region with $\bar{Y} \sim |\bar{T}-\bar{T}_0|^{-\frac{1}{2}}$. Eventually the external region will be indistinguishable from the majority of the boundary layer of thickness $O(\mathrm{Re}^{-\frac{1}{2}})$. This occurs when the Eulerian scalings:

$$\begin{aligned} t - \sigma T - \mathrm{Re}^{-\frac{1}{7}}\bar{T}_0 &= O\left(\mathrm{Re}^{-\frac{1}{2}}\right) \\ x - x_s - \mathrm{Re}^{\frac{1}{5}}x^* - \mathrm{Re}^{-\frac{2}{7}}\bar{X}_0 &= O\left(\mathrm{Re}^{-\frac{1}{2}}\right) \end{aligned} \tag{7.21}$$

are true. The velocity and pressure disturbances become increased to order unity and so the Euler equations come into operation across the entire boundary layer. A vortex starts to span the boundary layer and its evolution becomes a vortex sheet problem. (See Section 6.4.)

[6] See also Elliott & Smith (1987).

The effects described in Chapter 6 mark the end of the second interactive stage of the thickening of the boundary layer and the start of a third interactive stage where there is unsteady vortex development and ejection. The third interactive stage is the process of leading edge stall.

7.4 Further Work

Firstly, some further calculations need to be done to confirm error contributions from the integral (4.8) with the limits minus infinity to x_1 in the numerical treatment of the solvability condition $A(x,T)$ equation in Section 4.1 and from the analogous integral (5.25) with limits minus infinity to X_1 the second interactive stage nonlinear breakdown $\hat{A}(X)$ equation in Section 5.2.

The error contributions are found from the solution of the integrals with the next order terms of the integrands. The integral (4.8) for the $A(x,T)$ equation uses the derivative with respect to time T of the boundary condition (4.4):

$$A(x,T) = \left(|x|^2 + 2a(T)\right)^{\frac{1}{2}} , \qquad |x| \to \infty$$

as part of the integrand. The boundary condition itself is derived from (4.4):

$$A^2(x,T) = |x|^2 + 2a(T) + \frac{a^2(T)}{|x|^2} + \ldots \qquad |x| \to \infty$$

and hence, the next order term of the integrand involves the third term on the right hand side. The integral (5.25) for the $\hat{A}(X)$ equation also involves the boundary condition (5.23):

$$\hat{A}(X) \sim -|X|^{\frac{3}{4}-\frac{1}{\beta}} , \qquad X \to -\infty ;$$

however, its next order terms are not considered in the thesis and requires more work.

The original aim of the thesis was to bridge work on marginal separation with that steady flow over a downstream-moving surface, unsteady marginal separation

and dynamic stall. Slow perturbations from a slow change in angle of attack on a very large time scale are applied to the airfoil so as to weaken the induced pressure gradient in the interaction region. The slow perturbations can be applied to any airfoil problem mentioned in Recent Works (Chapter 1), for example, three-dimensional marginal separation theory, flows over obstacles, local suction flows, flows with severe pressure gradients or abruptly-started airfoils.

Bibliography

Abramovich, M. and Stegun, I. A. (1972). *Handbook of Mathematical Functions with Formulas, Graphs, and Mathematical Tables*, National Bureau of Standards, 9 edn, Wiley-Interscience.

Anderson, Jr, J. D. (1997). *The History of Aerodynamics and its Impact on Flying Machines*, Cambridge University Press.

Anderson, Jr, J. D. (2008). *Introduction to Flight*, 6 edn, New York: McGraw-Hill Higher Education.

Atkinson, K. and Han, W. (2003). *Elementary Numerical Analysis*, 3 edn, Wiley.

Batchelor, G. K. (2000a). *An Introduction to Fluid Dynamics*, Cambridge University Press, chapter 4.

Batchelor, G. K. (2000b). *An Introduction to Fluid Dynamics*, Cambridge University Press, chapter 6.

Batchelor, G. K. (2000c). *An Introduction to Fluid Dynamics*, Cambridge University Press, chapter 3.

Blasius, H. (1908). Grenzschichten in flüssigkeiten mit kleiner reibung., *Z. Math. Phys.* **56**(1): 1–37. English translation NACA TM 1256.

Braun, S. (2006). Recent developments in the asymptotic theory of separated flows. levenshulme lectures - lecture notes., Manchester Institute of Mathematics EPrints 2006.226. http://eprints.ma.man.ac.uk/656/.

Braun, S. and Kluwick, A. (2002). The effect of three-dimensional obstacles on marginally separated laminar boundary layer flows., *Journal of Fluid Mechanics* **406**: 57–82.

Braun, S. and Kluwick, A. (2004). Unsteady three-dimensional marginal separation caused by surface-mounted obstacles and/or local suction., *Journal of Fluid Mechanics* **514**: 121–152.

Braun, S. and Kluwick, A. (2005). Blow-up and control of marginally separated boundary layer flows., **363**: 1057–1067.

Brown, S. N. (1965). Singularities associated with separating boundary layers., *Philosophical Transactions of the Royal Society London A* **257**: 409–444.

Brown, S. N. and Stewartson, K. (1969). Laminar separation., *Annual Review of Fluid Mechanics* **1**: 45–79.

Brown, S. N. and Stewartson, K. (1983). On an integral equation of marginal separation., *SIAM Journal of Applied Mathematics* **43**(5): 1119–1126.

Cassel, K. W. (2000). A comparison of navier-stokes solutions with the theoretical description of unsteady separation., *Philosophical Transactions of the Royal Society London A* **358**: 3207–3227.

Cassel, K. W. and Obabko, A. V. (2010). A rayleigh instability in vortex-induced unsteady boundary layer., *Physica Scripta* **T142**: 1–14.

Cassel, K. W., Smith, F. T. and Walker, J. D. A. (1996). The onset of stability in unsteady boundary-layer separation., *Journal of Fluid Mechanics* **315**: 223–256.

Catherall, D. and Mangler, K. W. (1966). The integration of the two-dimensional laminar boundary-layer equations past the point of vanishing skin friction., *Journal of Fluid Mechanics* **26**(1): 163–182.

Chernyshenko, S. I. (1985). On the asymptotics of stationary solutions of the navier-stokes equations at large reynolds numbers., *Dokl. Akad. Nauk SSSR* **285**(6): 1353–1355. English translation.

Crabtree, L. F. (1959). The formation of regions of separated flow on wing surfaces. part i. low-speed tests on a two-dimensional unswept wing with a 10 per cent thick rae 101 section., *Reports and Memoranda, Part I 3122*, Aeronautical Research Council.

Degani, A. T., Li, Q. and Walker, J. D. A. (1996). Unsteady separation from the leading edge of a thin airfoil., *Physics of Fluids* **8**(3): 489–512.

Duck, P. W. (1990). Unsteady three-dimensional marginal separation including breakdown., *Journal of Fluid Mechanics* **220**: 85–98.

Elliott, J. W. and Smith, F. T. (1987). Dynamic stall due to unsteady marginal separation., *Journal of Fluid Mechanics* **179**: 489–512.

Elliott, J. W., Smith, F. T. and Cowley, S. J. (1983). Breakdown of boundary layers: (i) on moving surfaces; (ii) in semi-similar unsteady flow; (iii) in fully unsteady flow., *Geophysical and Astrophysical Fluid Dynamics* **25**: 77–138.

Goldstein, S. (1930). Concerning some solutions of the boundary layer equations in hydrodynamics., *Proceedings of the Cambridge Philosophical Society* **26**(1): 1–30.

Goldstein, S. (1948). On laminar boundary-layer flow near a position of separation., *Quarterly Journal of Mechanics and Applied Mathematics* **1**(1): 43–69.

Gorenflo, R. and Vessella, S. (2008). *Abel Integral Equations: Analysis and Applications*, Lecture Notes In Mathematics, Springer-Verlag New York.

Hackmüller, G. and Kluwick, A. (1990a). Effects of surface geometry and suction/blowing on marginal separation., *in* A. H. Nayfeh and A. Mobarak (eds), *Proc. 3rd Intl Congre. of Fluid Mechanics, Cairo*, Vol. 1, Cairo University, pp. 1–6.

Hackmüller, G. and Kluwick, A. (1990b). Effects of three-dimensional surface mounted obstacles on marginal separation., *in* V. V. Kozlov and A. V. Dovgal (eds), *Separated Flows and Jets*, Springer, pp. 55–65.

Hartree, D. R. (1939). A solution of the laminar boundary-layer equation for retarded flow., *A. R. C. R. & M.* **2426**.

Howarth, L. (1938). On the solution of the laminar boundary layer equations., *Proceedings of the Royal Society, London, A* **164**: 547–579.

Jones, B. M. (1933). An experimental study of the stalling of wings., *A. R. C. R. & M.* **1588**.

Jones, B. M. (1934). Stalling., *Journal of the Royal Aeronautical Society* **38**: 753–770.

Koromilas, C. A. and Telionis, D. P. (1980). Unsteady laminar separation: an experimental study., *Journal of Fluid Mechanics* **97**(2): 347–384.

Kuryanov, A. I., Stolyarov, G. I. and Steinberg, R. I. (1979). On the hysteresis of aerodynamic characteristics., *Uch. Zap. TsAGI* **10**(3): 12–15. in Russian.

Landau, L. D. and Lifshitz, E. M. (1944). *Mechanics of Continuous Media*, Gostekhizdat Moscow. English translation.

Lighthill, M. J. (1951). A new approach to thin airfoil theory., *Aeronautical Quarterly* **3**(3): 193–210.

Lighthill, M. J. (1953). On boundary layers and upstream influence. i. a comparison between subsonic and supersonic flows., *Proceedings of the Royal Society, London, A* **217**: 344–357.

Lighthill, M. J. (1958). On displacement thickness., *Journal of Fluid Mechanics* **4**(4): 383–392.

Lighthill, M. J. (1963). Introduction: Boundary layer theory, *in* L. Rosenhead (ed.), *Laminar Boundary Layers*, Oxford University Press, chapter 2.

McCroskey, W. J. (1982). Annual review of unsteady airfoils, *Fluid Mechanics* **14**: 285–311.

Messiter, A. F. (1979). Boundary-layer separation., *Proc. 8th U.S. Natl. Congr. Appl. Mech.* pp. 157–179. Western Periodicals, North Hollywood, CA.

Messiter, A. F. (1983). Boundary-layer interaction theory., *ASME Journal of Applied Mechanics* **50**(4b): 1104–1115.

Messiter, A. F. and Enlow, R. L. (1973). A model for laminar boundary-layer flow near a separation point., *SIAM Journal of Applied Mathematics* **25**(3): 655–670.

Moore, F. K. (1958). On the separation of the unsteady boundary layer., *in* H. Görtler (ed.), *Boundary Layer Research*, Springer Berlin, pp. 296–311.

Muskhelishvili, N. I. (1953). *Singular Integral Equations: Boundary problems of function theory and their application to mathematical physics.*, 2 edn, Groningen: P. Noordhoff. Translation from the Russian edited by J. R. M. Radok.

Neiland, V. Y. (1969). Theory of laminar boundary-layer separation in supersonic flow., *Fluid Dynamics* **4**(4): 33–35. English translation.

Obabko, A. V. and Cassel, K. W. (2002a). Detachment of the dynamic stall above a moving surface., *AIAA Journal* **40**(9): 1811–1822.

Obabko, A. V. and Cassel, K. W. (2002b). Navier-stokes solutions of unsteady separation induced by a vortex., *Journal of Fluid Mechanics* **465**: 99–130.

Obabko, A. V. and Cassel, K. W. (2005). On the ejection induced instability in navier-stokes solutions of unsteady separation., *Philosophical Transactions of the Royal Society London A* **363**: 1189–1198.

Prandtl, L. (1904). Motion of fluids with very little viscosity., *NACA Technical Memorandum* **452**. English translation.

Prandtl, L. (1935). The mechanics of viscous fluids, *in* W. F. Durand (ed.), *Aerodynamic Theory*, Vol. 3, Springer Berlin, pp. 34–208.

Rosenhead, L. (1963). *Laminar Boundary Layers*, Calrendon Press, Oxford, chapter 3.

Rott, N. (1956). Unsteady viscous flow in the vicinity of a stagnation point., *The Quarterly Journal of Mechanics and Applied Mathematics* **13**: 444–451.

Ruban, A. I. (1981). Singular solution of boundary layer equations which can be extended continuously through the point of zero surface friction., *Fluid Dynamics* **16**(6): 835–843.

Ruban, A. I. (1982a). Asymptotic theory of short separation regions on the leading edge of a slender airfoil., *Fluid Dynamics* **17**(1): 33–41.

Ruban, A. I. (1982b). Stability of preseparation boundary layer on the leading edge of a thin airfoil., *Fluid Dynamics* **17**(6): 860–867. English translation.

Ryzhov, O. S. and Smith, F. T. (1984). Short-length instabilities, breakdown and initial value problems in dynamic stall., *Mathematika: a Journal of Pure and Applied Mathematics* **31**(2): 163–177.

Samad, M. A. (2004). *Three Dimensional Marginal Separation Theory*, PhD thesis, University of Manchester, School of Mathematics.

Scheichl, S., Braun, S. and Kluwick, A. (2008). On a similarity solution in the theory of unsteady marginal separation., *Acta Mechanica* **201**: 153–170.

Sears, W. R. (1956). Some recent developments in airfoil theory., *Journal of Aeronautical Sciences* **23**(5): 490–499.

Sears, W. R. and Telionis, D. P. (1971). Unsteady boundary layer separation., *in* E. Eichelbrenner (ed.), *Recent Research on Unsteady Boundary Layers*, Vol. 1 of *Proc. Symposium of I. U. T. A. M.*, Laval University Press, Quebec, pp. 404–407.

Sears, W. R. and Telionis, D. P. (1975). Boundary-layer separation in unsteady flow., *SIAM Journal of Applied Mathematics* **28**(1): 215–235.

Smith, F. T. (1982a). Concerning dynamic stall., *Aeronautical Quarterly* **33**(4): 331–352.

Smith, F. T. (1982b). On the high reynolds number theory of laminar flows., *IMA Journal of Applied Mathematics* **28**: 207–281.

Smith, F. T. and Daniels, P. G. (1981). Removal of goldstein's singularity at separation, in flow past obstacles in wall layers., *Journal of Fluid Mechanics* **110**: 1–37.

Smith, F. T. and Elliott, J. W. (1985). On the abrupt reattachment downstream of leading-edge laminar separation., *Proceedings of the Royal Society, London A* **401**(1820): 1–27.

Stavrou, S. (2004). *Boundary Layer Separation Control and Receptivity Aspects in Marginal Separation Theory.*, PhD thesis, University of Manchester, School of Mathematics.

Stewartson, K. (1958). On goldstein's theory of laminar separation., *Quarterly Journal of Mechanics and Applied Mathematics* **11**(4): 391–410.

Stewartson, K. (1960). The theory of unsteady laminar boundary layers., *Advances in Applied Mechanics 6*, Academic Press, New York, pp. 1–37.

Stewartson, K. (1970). Is the singularity at separation removable?, *Journal of Fluid Mechanics* **44**(2): 347–364.

Stewartson, K., Smith, F. T. and Kaups, K. (1982). Marginal separation., *Studies in Applied Mathematics* **67**(1): 45–61.

Stewartson, K. and Williams, P. G. (1969). Self-induced separation., *Proceedings of the Royal Society, London A* **312**: 181–206.

Suli, E. and Mayers, D. (2003). *An Introduction to Numerical Analysis*, Cambridge University Press.

Sychev, V. V. (1972). Laminar separation., *Fluid Dynamics* **7**(3): 407–417. English translation.

Sychev, V. V., Ruban, A. I., Sychev, V. V. and Korolev, G. L. (1998a). *Asymptotic Theory of Separated Flows*, Cambridge University Press, chapter 1.

Sychev, V. V., Ruban, A. I., Sychev, V. V. and Korolev, G. L. (1998b). *Asymptotic Theory of Separated Flows*, Cambridge University Press, chapter 4.

Sychev, V. V., Ruban, A. I., Sychev, V. V. and Korolev, G. L. (1998c). *Asymptotic Theory of Separated Flows*, Cambridge University Press, chapter 5.

Sychev, V. V., Ruban, A. I., Sychev, V. V. and Korolev, G. L. (1998d). *Asymptotic Theory of Separated Flows*, Cambridge University Press, chapter 2.

Tani, I. (1964). Low speed flows involving bubble separations., *Progress in Aerospace Sciences* **5**: 70–103.

Telionis, D. P. and Werle, M. J. (1973). Boundary layer separation from downstream-moving boundaries., *Journal of Applied Mechanics* **40**(2): 369–374.

van Dyke, M. D. (1956). Second-order subsonic airfoil theory including edge effects., *NACA Technical Memorandum* **1274**.

van Dyke, M. D. (1975). *Perturbation Methods in Fluid Mechanics*, Parabolic Press.

Werle, M. J. and Davis, R. T. (1972). Incompressible laminar boundary layers on a parabola at an angle of attack: a study of the separation point., *ASME Journal Of Applied Mechanics* **39**(1): 7–12.

White, F. M. (2006). *Viscous Fluid Flow*, 3 edn, McGraw-Hill.

Appendix A

Derivation of the Navier-Stokes Equations

The Navier-Stokes equations are named after Claude-Louis Navier and George Gabriel Stokes who first derived the equations in the nineteenth century in accordance with the continuum hypothesis of fluids, Newton's Second Law and the principles of conservation of mass, momentum and energy.[1]

The fluid is assumed to be Newtonian in the thesis. The fluid motion is subsonic and within the framework of the traditional two-dimensional Cartesian coordinate system (x, y) with time t. Hence, the equations are described in this system also.

Newton's Second Law, when applied to a solid body is written as

$$m\mathbf{a} = \mathbf{f}$$

for the mass of the body m, acceleration $\mathbf{a}$ and the force applied to the body $\mathbf{f}$, such as gravity. When Newton's Second Law is formulated for fluid dynamics, the momentum equation

$$\rho\frac{\mathrm{D}\mathbf{v}}{\mathrm{D}t} = \rho\mathbf{f} + \nabla\cdot\boldsymbol{\Sigma} \tag{A.1}$$

holds for density ρ, velocity vector of the fluid $\mathbf{v} = (u, v)$ with tangential and normal

[1]See White (2006) and Batchelor (2000c) for more detailed derivations.

velocity components u and v; body force $\mathbf{f}$; and surface force stress tensor $\boldsymbol{\Sigma}$. The material derivative is defined as

$$\frac{\mathrm{D}}{\mathrm{D}t} = \frac{\partial}{\partial t} + u\frac{\partial}{\partial x} + v\frac{\partial}{\partial y}\,.$$

The divergence of stress tensor $\boldsymbol{\Sigma}$ is

$$(\nabla \cdot \boldsymbol{\Sigma})_i = \frac{\partial \Sigma_{ji}}{\partial x_j}\,, \qquad i = 1,\, 2 \tag{A.2}$$

in traditional tensor notation.[2] [3]

The principles of conservation require that the sum of changes of a property such as mass, momentum or energy over a controlled volume must be equal to what is gained or lost through the boundaries of the volume plus what is created or destroyed by sources or sinks respectively inside the volume. The conservation of mass density ρ can be written as:

$$\frac{\partial \rho}{\partial t} + \nabla \cdot (\rho \mathbf{v}) = 0$$

and in an incompressible fluid where ρ is a constant quantity, then

$$\nabla \cdot \mathbf{v} = \frac{\partial u}{\partial x} + \frac{\partial v}{\partial y} = 0\,. \tag{A.3}$$

[2]Equation (A.2) can be written as

$$(\nabla \cdot \boldsymbol{\Sigma})_i = \sum_{j=1}^{2} \frac{\partial \Sigma_{ji}}{\partial x_j}\,, \qquad i = 1,\, 2$$

where indices $i,\, j = 1,\, 2$ are representative of the components of the two-dimensional Cartesian coordinate system x, y respectively. For $i = 1$:

$$(\nabla \cdot \boldsymbol{\Sigma})_x = \frac{\partial \Sigma_{xx}}{\partial x} + \frac{\partial \Sigma_{yx}}{\partial y}$$

and for $i = 2$:

$$(\nabla \cdot \boldsymbol{\Sigma})_y = \frac{\partial \Sigma_{xy}}{\partial x} + \frac{\partial \Sigma_{yy}}{\partial y}$$

[3]The component Σ_{ji} is the stress on the j-th plane in the i-th direction. For example, for $i,\, j = 1$ both corresponding to the x coordinate then Σ_{xx} is the stress on the x-plane of an infinitesimal (cuboid) volume of fluid in the direction parallel to the x-axis.

A consequence of (A.3) for a Newtonian fluid is that the body forces and stress tensors are related by the constitutive equation:

$$\Sigma_{ji} = -p\delta_{ji} + \mu\left(\frac{\partial v_j}{\partial x_i} + \frac{\partial v_i}{\partial x_j}\right) \tag{A.4}$$

for pressure p, constant dynamic viscosity μ and the Kronecker delta δ_{ji}:

$$\delta_{ji} = \begin{cases} 1\,, & j = i \\ 0\,, & j \neq i\,. \end{cases}$$

The combination of Newton's Second Law (A.1), stress tensor (A.2), mass conservation law (A.3) and the constitutive equation (A.4) gives the Navier-Stokes equations for incompressible, Newtonian fluids (in coordinate decomposition):

$$\frac{\partial u}{\partial t} + u\frac{\partial u}{\partial x} + v\frac{\partial u}{\partial y} = f_x - \frac{1}{\rho}\frac{\partial p}{\partial x} + \nu\left(\frac{\partial^2 u}{\partial x^2} + \frac{\partial^2 u}{\partial y^2}\right),$$

$$\frac{\partial v}{\partial t} + u\frac{\partial v}{\partial x} + v\frac{\partial v}{\partial y} = f_y - \frac{1}{\rho}\frac{\partial p}{\partial y} + \nu\left(\frac{\partial^2 v}{\partial x^2} + \frac{\partial^2 v}{\partial y^2}\right),$$

$$\frac{\partial u}{\partial x} + \frac{\partial v}{\partial y} = 0\,,$$

with constant kinetic viscosity $\nu = \frac{\mu}{\rho}$.

Appendix B

The Integral of Small Perturbation Theory

The subsonic pressure-displacement relation (3.50) or (6.34) is obtained from the integral of small perturbation theory. The integral can be sought by considering the theory of separation from a smooth surface, adapted from Sychev, Ruban, Sychev and Korolev (1998a).

The independent variables and the stream function solutions for the boundary layer and interaction region in high Reynolds number flow across a smooth surface are found using the hierarchical process, similar to that for the boundary layer and interaction region in Chapters 2 and 3. The independent variables of the lower layer (region III) of the interaction region are

$$x^* = \mathrm{Re}^{\frac{3}{8}} x = O(1)\,, \qquad Y^* = \mathrm{Re}^{\frac{5}{8}} y = \mathrm{Re}^{\frac{1}{8}} Y = O(1)$$

where x, Y are the classical boundary layer coordinates and y is the normal coordinate of the external inviscid region. The displacement effect of the lower layer from flow over a smooth surface is transmitted across the middle layer (region II) of the interaction region without change, by (3.17). The angle of inclination θ of the

displaced streamlines is defined by the asymptotic expression:

$$\theta = \mathrm{Re}^{-\frac{1}{4}} G\left(x^*\right) + \ldots\,, \qquad G\left(x^*\right) = \lim_{Y^* \to \infty} \left\{ -\frac{\partial \Psi_0^*}{\partial x^*} \Big/ \frac{\partial \Psi_0^*}{\partial Y^*} \right\}. \tag{B.1}$$

The flow of the upper layer (region I) of the interaction region is determined by the method of small perturbations. From the order of magnitude of θ (B.1), a solution is sought in the form:

$$u = 1 + \mathrm{Re}^{-\frac{1}{4}} u_1\left(x^*, y^*\right) + \ldots\,, \qquad v = \mathrm{Re}^{-\frac{1}{4}} v_1\left(x^*, y^*\right) + \ldots\,,$$
$$p = p_{00} + \mathrm{Re}^{-\frac{1}{4}} p_1\left(x^*, y^*\right) + \ldots$$

The independent variables of the upper layer are

$$x^* = \mathrm{Re}^{\frac{3}{8}} x\,, \qquad y^* = \mathrm{Re}^{\frac{3}{8}} y\,. \tag{B.2}$$

If the longitudinal and transverse scales are not the same, degenerate equations are formed. The Navier-Stokes equations become a system of linearised Euler equations:

$$\frac{\partial u_1}{\partial x^*} + \frac{\partial p_1}{\partial x^*} = 0\,, \qquad \frac{\partial v_1}{\partial x^*} + \frac{\partial p_1}{\partial y^*} = 0\,, \qquad \frac{\partial u_1}{\partial x^*} + \frac{\partial v_1}{\partial y^*} = 0\,. \tag{B.3}$$

The streamline solutions must satisfy the Brillouin-Villat condition of smooth separation to define a unique solution and hence, the upper layer flow solution must match to the curvature of the free streamline:

$$\kappa = -k x^{-\frac{1}{2}} + \kappa_0 + O(x^{\frac{1}{2}})\,, \qquad x \to +0$$

where k is related to the point of zero skin friction and separation. The pressure gradient along the body surface is:

$$\frac{\mathrm{d}p_e}{\mathrm{d}x} = k(-x)^{-\frac{1}{2}} + \frac{16}{3}k^2 + O\left[(-x)^{\frac{1}{2}}\right], \qquad x \to -0\,,$$

$$\frac{\mathrm{d}p_e}{\mathrm{d}x} = 0\,, \qquad x > 0\,.$$

The solution is obtained using the classical small-disturbance theory by introducing the analytic function:

$$w(z) = p_1 + iv_1$$

of the complex variable $z = x^* + iy^*$. The analytic function can be represented in the form:

$$w(z) = \Phi(z) + i2c_1 z^{\frac{1}{2}}\,.$$

The condition of matching with that of the main external inviscid flow (region 1) as $|z| \to \infty$, is

$$\Phi \to 0\,, \qquad |z| \to \infty\,.$$

On the real axis:

$$\Im\Phi|_{y^*=0} = -2c_1 x^{*\frac{1}{2}} H\left(x^*\right) + G\left(x^*\right)\,,$$

where $H\left(x^*\right)$ is the Heaviside function. The analytic function $\Phi(z)$ in the upper half-plane under the matching conditions has the form:

$$\Phi(z) = \frac{1}{\pi}\int_{-\infty}^{\infty} \frac{G(t) - 2c_1 t^{\frac{1}{2}} H(t)}{(t-z)}\,\mathrm{d}t\,. \tag{B.4}$$

Using the Plemelj-Sokhotsky formula[1] and separating the real and imaginary parts, the pressure distribution is given (without the bookwork) as:

$$p_1\left(x^*, 0\right) = P_0^*\left(x^*\right) = -2c_1\left|x^*\right|^{\frac{1}{2}} H\left(-x^*\right) + \frac{1}{\pi}\int_{-\infty}^{\infty} \frac{G(t) - 2c_1 t^{\frac{1}{2}} H(t)}{(t-x^*)}\,\mathrm{d}t\,. \tag{B.5}$$

[1]The Plemelj-Sokhotsky formulae are used to solve singular integral equations, as shown in Muskhelishvili (1953).

Therefore, the formula for the pressure gradient has the form:

$$\left.\frac{\partial p_1}{\partial x^*}\right|_{y^*=0} = \frac{\mathrm{d}P_0^*}{\mathrm{d}x^*} = \frac{1}{\pi}\fint_{-\infty}^{\infty} \frac{G'(t)}{(t-x^*)}\,\mathrm{d}t\,. \tag{B.6}$$

This is the *integral of small-perturbation theory.*